

**INVESTIGATION OF THERMAL AND
ELASTIC PROPERTIES OF SELECTED
HIGH T_c SUPERCONDUCTORS**

THESIS

SUBMITTED TO THE
COCHIN UNIVERSITY OF SCIENCE AND TECHNOLOGY
FOR THE AWARD OF THE DEGREE OF
DOCTOR OF PHILOSOPHY

KALA M. S.

**DEPARTMENT OF PHYSICS
COCHIN UNIVERSITY OF SCIENCE AND TECHNOLOGY
COCHIN - 682 022, INDIA**


DECEMBER 1996

CERTIFICATE

Certified that the work presented in this thesis is based on the bona fide work done by Ms. Kala M. S. under my guidance in the Department of Physics, Cochin University of Science and Technology, Cochin - 22 and has not been included in any other thesis submitted previously for the award of any degree.

Cochin - 682 022
December 24, 1996




Dr. Jacob Philip
Dr. Jacob Philip
Supervising Guide
Professor & Head
Department of Instrumentation
COCHIN UNIVERSITY OF SCIENCE & TECHNOLOGY
KOCHI - 682 022

DECLARATION

Certified that the work presented in this thesis is based on the original work done by me under the guidance of Dr. Jacob Philip, Professor and Head, Department of Instrumentation, Cochin University of Science and Technology, Cochin - 22 and has not been included in any other thesis submitted previously for the award of any degree.

Cochin - 682 022
December 24, 1996


Kala M. S.

Preface

The discovery of high temperature superconductivity in the oxide system La-Ba-Cu-O by Bednorz and Muller in 1986, closely followed by the discovery of the famous "123" compound by Chu and his associates in 1987, raised exceedingly high hopes in the world scientific community. These new materials have generated tremendous excitement for the following two reasons. First, they open a new temperature realm for superconducting devices and components which should have widespread commercial applications and these potential benefits have attracted phenomenal attention from the public as well. Second, the conventional electron - phonon interaction appears not to be the origin of superconductivity in these materials, leaving the fundamental physics open to further investigations. Thus these exotic materials have been the subject of intense research by a large number of scientists from a wide range of fields of basic and applied research.

In this thesis we present the results of the investigations carried out by us on the thermal and elastic properties of some of the high T_c superconductors. The thermal properties investigated include the thermal diffusivity, specific heat and thermal conductivity of a set of $\text{YBa}_2\text{Cu}_3\text{O}_{7-\delta}$ samples added with different amounts of SnO_2 . The photoacoustic technique and differential scanning calorimetry have been employed to measure the thermal diffusivity and specific heat respectively and thermal conductivity is then evaluated from these parameters. The elastic properties investigated include measurement of ultrasonic velocity and attenuation in a set of Ga doped $\text{GdBa}_2\text{Cu}_3\text{O}_{7-\delta}$ samples using the ultrasonic technique, computation of elastic phase velocity, slowness and ray velocity surfaces from available elastic constant data for three major superconducting systems LSCO, YBCO and BSCCO and the evaluation of phonon enhancement factors for the first time in different directions for the above mentioned systems. The thesis is presented in eight chapters. A chapterwise description of the contents of the thesis is outlined below.

Chapter 1 is an introductory chapter which outlines the general aspects of the phenomenology of superconductivity. It gives a review of superconductivity, starting from the discovery of this spectacular phenomenon in 1911. The general features of

high T_c superconductors which include the structural features of major superconducting systems, various theoretical models that has been proposed to explain the normal state and superconducting properties and the general thermal and elastic properties of these materials are described in this chapter.

In chapter 2, we describe the experimental set-ups employed in carrying out the experimental investigations. The photoacoustic technique is employed to measure the thermal diffusivity of the superconducting samples. The details of the photoacoustic spectrometer used in the work is discussed with the help of a block diagram. For the specific heat measurements, a differential scanning calorimeter (Perkin - Elmer DSC - 7) has been used, the details of which are also given. The Matec model 7700 pulse modulator and receiver along with the necessary subsystems have been used for the measurement of ultrasonic velocity and attenuation. Details of this system and measurement technique are outlined with the help of a block diagram.

Though endowed with comparatively high transition temperatures, the prospects of application of the high T_c superconductors is severely limited due to various reasons. The addition of selected metals or oxides to a high T_c material, while retaining superconductivity, has been shown to change the other characteristic features drastically. This is of great technological importance because of the need for normal and stable materials to be used for various applications. The next two chapters (chapter 3 and 4) consist of the studies on the effect of various dopants on the properties of superconductors.

The effect of addition of SnO_2 on the thermal properties of $\text{YBa}_2\text{Cu}_3\text{O}_{7-\delta}$ is given in chapter 3. We have measured the thermal diffusivity of a set of YBCO - SnO_2 using the photoacoustic technique at different temperatures above and below T_c in the temperature range 85 - 300 K. Using the specific heat data obtained from the DSC measurement, the thermal diffusivity and density, the thermal conductivity of the samples have been calculated at room temperature. The details of the above measurements, the results and an analysis of these results are given in chapter 3. The results have been found to support the phonon mediated pairing mechanism as the possible reason for superconductivity.

In chapter 4, the effect of Ga doping on the elastic properties of $\text{GdBa}_2\text{Cu}_3\text{O}_{7-\delta}$ is outlined. The ultrasonic velocity of four different samples of GdBCO with varying amounts of Ga doping have been measured using the pulse echo overlap technique and the ultrasonic attenuation has been measured employing the pulse comparison technique in the temperature range 85 - 300 K. Apart from the anomalies observed near T_c , interesting features are found in the temperature range 180 - 220 K which has been observed by many workers in other experiments also. The results are explained taking into account the structural changes taking place in the compound with varying Ga doping levels.

In chapter 5, we present a detailed study of the elastic phase velocity surfaces of different high T_c superconductors. Starting from the Christoffel equation, the phase velocities are computed for the pure shear, quasishear and quasilongitudinal modes and the corresponding phase velocity surfaces are plotted as a function of propagation direction. The velocity surfaces are plotted for YBCO, BSCCO and LSCO either for single crystals, sinter - forged samples or polycrystalline specimens at temperatures above and below T_c subject to the availability of data, for propagation of waves in different planes. A comparative study of the wave surfaces of the three materials is given taking into account the structure of these compounds. The surfaces plotted at temperatures above and below T_c indicate that the nature of the surfaces do not change significantly as the sample undergoes the superconducting transition.

In an anisotropic solid, the group velocity, with which the energy is propagated, is generally different from the phase velocity with which the wave is propagated. A plot of group velocity as a function of propagation direction, also called the ray surface, can therefore provide, important information regarding the energy distribution in the crystal. In chapter 6, the ray velocity surfaces of three high T_c superconductors are plotted in different symmetry planes after deriving the corresponding equations. In addition, the slowness surfaces, which are the inverse phase velocity surfaces are also plotted, since they can explain many features of the ray surfaces which are much more complicated. The quasishear mode of all the superconductors investigated exhibit cuspidal edges at least in one symmetry plane, which are of great physical significance. The

computational details, results obtained and a discussion of the results are presented in this chapter.

When phonons are excited in a given region of an anisotropic crystal, the energy flow is found to be enhanced in certain directions and decreased in others even when the angular distribution of wave vectors is uniform. This amplification of phonons in certain directions of a crystal arises from elastic anisotropy of the crystal. The phonon enhancement factor, which is the ratio of the energy flux for a particular polarization and propagation direction to the corresponding flux in an isotropic solid, is calculated for the three superconducting systems - YBCO, BSCCO and LSCO - for the pure shear, quasi shear and quasi longitudinal modes and are plotted in pseudo 3D-representation as a function of the polar and azimuthal angles θ and ϕ in spherical coordinates. Sharp peaks are observed in the phonon intensity along specific directions in these plots. These are interpreted as not due to the real focussing of phonons, but due to caustic surfaces which are singularities occurring in the mathematical formulation of the theory of phonon focussing. The theoretical background, computational details, results obtained and an analysis of the results are given in chapter 7.

Chapter 8 is the concluding chapter in which the overall conclusions drawn from the work presented in the previous chapters are discussed. It also projects the scope for doing further work in the area of high temperature superconductivity.

The following papers have been published/ presented/ communicated for publication in different journals/ conferences during the course of this work.

1. Effect of SnO_2 addition on the thermal diffusivity of the high T_c superconductor $\text{YBa}_2\text{Cu}_3\text{O}_{7-\delta}$
M.S. Kala, J. Philip, M. T. Sebastian and A. D. Damodaran
Advances in Phonon Physics (Wiley Eastern, 1996).
2. Effect of Ga doping on the elastic properties of $\text{GdBa}_2\text{Cu}_3\text{O}_{7-\delta}$ high T_c superconductor : An ultrasonic study
M. S. Kala, R. Sreekumar, J. Philip and N. C. Mishra
Phys. Stat. Solidi **b158**, December 1996, (in press).

3. Anisotropy in elastic wave propagation in selected high T_c superconductors
M. S. Kala and J. Philip
Ind. J. Phys., (in press).
4. Slowness surfaces, ray velocity surfaces, phonon focussing and focussing catastrophes in high T_c superconductor crystals
J. Philip and M. S. Kala
Phys. Rev. B (submitted).
5. Phonon focussing in high T_c superconductors
M. S. Kala and J. Philip
Solid State Physics Symposium, December 27-31, 1996, Bhabha Atomic Research Centre, Bombay (accepted).
6. Investigation of thermal and elastic properties of selected high T_c superconductors
M. S. Kala
Solid State Physics Symposium, December 27-31, 1996, Bhabha Atomic Research Centre, Bombay (thesis presentation accepted).

In addition, the following papers, which are not included in this thesis, have also been published during the course of this work.

1. Spectral characteristics of the blood of streptozotocin diabetic rats using photoacoustic technique
T. T. Shreedevi, P. S. Padayatti, M. S. Kala, J. Philip and C. S. Paulose
Current Science, **66**, 763 (1994).
2. Specific heat of Al - based quasicrystal alloys
M. S. Kala, J. Philip, A. Srinivasan and E. S. R. Gopal
Proc. DAE SSP Symp., **36C**, 113 (1993).

Contents

Preface	i
Acknowledgements	vi
1 Introduction	1
1.1 Introductory remarks	1
1.2 High temperature superconductivity	3
1.3 General features of high T_c cuprate superconductors	7
1.3.1 $\text{La}_{2-x}\text{Sr}_x\text{CuO}_{4-\delta}$	8
1.3.2 $\text{YBa}_2\text{Cu}_3\text{O}_{7-\delta}$ and related 123 compounds	9
1.3.3 $\text{Bi}_2\text{Sr}_2\text{Ca}_{n-1}\text{Cu}_n\text{O}_{2n+4+\delta}$	11
1.3.4 $\text{Tl}_2\text{Ba}_2\text{Ca}_{n-1}\text{Cu}_n\text{O}_{2n+4+\delta}$	13
1.3.5 $\text{HgBa}_2\text{Ca}_{n-1}\text{Cu}_n\text{O}_{2n+2+\delta}$	14
1.4 Theoretical Developments	15
1.4.1 The BCS theory	15
1.4.2 The plasmon theory	17
1.4.3 The exciton theory	18
1.4.4 Spin fluctuations	19
1.4.5 The polaron, bipolaron theory	20
1.4.6 The Resonating Valence Bond (RVB) Theory	21
1.5 Thermal and elastic properties of high T_c superconductors	22
1.5.1 Specific heat	23
1.5.2 Thermal conductivity	28
1.5.3 Elastic properties - ultrasonic velocity and attenuation	32
1.6 A brief outline of the work presented in the thesis	37
1.7 References	38
2 Experimental Techniques	45
2.1 Introduction	45

2.2	Photoacoustics	45
2.2.1	The Photoacoustic setup	47
2.2.2	Thermal diffusivity measurements using PA technique	50
2.3	Differential Scanning Calorimetry	51
2.3.1	The experimental setup	53
2.3.2	Specific heat measurements using DSC	54
2.4	Ultrasonic Technique	57
2.4.1	Ultrasonic velocity and attenuation measurements in solids	57
2.4.2	Pulse Echo Overlap Method	59
2.4.3	The ultrasonic experimental setup	62
2.5	References	67
3	Effect of SnO₂ addition on the thermal properties of YBa₂Cu₃O_{7-δ}	69
3.1	Introduction	69
3.2	Experimental	74
3.3	Results and Discussion	75
3.4	Conclusions	83
3.5	References	84
4	Effect of Ga doping on the elastic properties of GdBa₂Cu₃O_{7-δ}	87
4.1	Introduction	87
4.2	Experimental	93
4.3	Results and Discussion	95
4.4	Conclusions	103
4.5	References	105
5	Elastic phase velocity surfaces of high T_c superconductors	109
5.1	Introduction	109
5.2	Elastic wave propagation in anisotropic solids	111
5.3	Wave propagation in orthorhombic and tetragonal systems	114
5.4	Elastic wave surfaces of selected high T _c superconductors	118

5.4.1	$\text{Bi}_2\text{Sr}_2\text{CaCu}_2\text{O}_{8-\delta}$ (BSCCO)	120
5.4.2	$\text{RBa}_2\text{Cu}_3\text{O}_{7-\delta}$ (RBCO) (R = Y or Gd)	124
5.4.3	$\text{La}_{2-x}\text{Sr}_x\text{CuO}_{4-y}$ (LSCO)	125
5.5	Discussion and conclusion	130
5.6	References	138
6	Slowness and ray velocity surfaces of high T_c superconductors	141
6.1	Introduction	141
6.2	The ray or group velocity in anisotropic solids - General aspects	143
6.3	Computation of group velocity for orthorhombic and tetragonal crystals	145
6.4	Slowness and ray surfaces for high T_c superconductors	149
6.5	Discussion and conclusions	162
6.6	References	165
7	Phonon focussing in high T_c superconductors	167
7.1	Introduction	167
7.2	Phonon focussing in orthorhombic and tetragonal crystals	170
7.3	Computation of phonon intensities in high T_c superconductor crystals	176
7.4	Phonon focussing catastrophes	185
7.5	Phonon enhancement along fold directions for the quasishear mode	186
7.6	Conclusions	192
7.7	References	193
8	Summary and conclusions	195
	Appendix A	199

Chapter 1

Introduction

1.1 Introductory remarks

The era of ‘superconductivity’ commenced in 1911 with the discovery of superconductivity in mercury by Kammerlingh Onnes; just three years after he liquified helium. Just like mercury, whose resistance drops to zero at 4.18 K, Onnes found that other materials like lead, tin, indium also undergo the same change at 7.2 K, 3.7 K and 3.4 K respectively. The temperature at which the transition to a zero resistance state takes place is the superconducting transition temperature (T_c) and is characteristic of the material. In 1913, Onnes himself found that superconductivity was destroyed in the presence of moderate current densities and ordinary magnetic fields of the order of 0.05 T. This disappearance of superconductivity above a critical magnetic field suggested that the phenomenon of superconductivity and magnetism are closely associated.

The research field was rather silent for more than a decade and in 1933, W. Meissner and R. Ochsenfeld came up with the second crucial discovery in the history of superconductivity. They reported that upon cooling, a magnetic field is expelled from a normal metal specimen when it passes through T_c and this effect was called the Meissner effect. Perfect diamagnetism was thus found to be an independent property of superconductors which suggested that superconductivity involves a change of the thermodynamic state and not just a change in the electrical resistance.

Later years witnessed theoretical attempts by many of the great physicists of the period, to characterise the nature of the superconducting state of matter. One such attempt was by Gorter and Casimir in 1934 with the ‘two-fluid’ model in which the superconducting state was considered as a result of a mixture of superconducting

and normal electrons. In 1935, the London brothers (F and H. London) came up with the electrodynamic equations who argued that superconductivity was a quantum mechanical phenomenon. Pippard modified this model to reduce the discrepancy between the theoretically predicted and the experimentally observed results. One of the other prominent theories is by Ginzburg and Landau (1950) which could not only account for the zero resistance and Meissner effect in fundamental terms, but could explain the second order nature of the superconducting phase transition in zero magnetic fields.

However, with the discovery of isotope effect, it became clear by the early 1950's that vibrations of the lattice are somehow involved in superconductivity. Frolich was able to show that two electrons in a metal could effectively attract each other, the attraction being mediated by lattice vibrations. In 1957, Bardeen, Cooper and Schrieffer developed a complete atomistic theory of superconductivity based on the formation of such electron pairs called the Cooper pairs and the coherent superposition of these pairs into a single quantum state. The possibility of such a state was foreshadowed in the work of Ginzburg and Landau. Bardeen, Cooper and Schrieffer were awarded the Nobel prize in 1972 for their work. Their theory which is known as the BCS theory made many detailed predictions which have been verified. A detailed discussion on BCS theory is given later in this chapter.

Another important event that took place in the history of superconductivity was the discovery of the Josephson effect in 1962. Earlier in 1959, Giaever had shown that single electron tunnelling was possible in superconductors. But Josephson showed theoretically that the Cooper pairs also can tunnel. 'Pair' tunnelling was carried out on very thin tunnel barriers which couple the superconducting materials to one another. These junctions have enormous technological applications and Josephson and Giaever received the Nobel prize for their work on tunnelling junctions.

At the same time, attempts were going on to find new materials which could superconduct. Many metals like Nb, Ru, Mo etc. have been found to be superconducting in the liquid helium range. Apart from these elements, a new class of superconductors which belong to the β -tungsten family, also called A-15 compounds, were developed. The first superconducting material of this structure was V_3Si with a T_c of 17.1 K. After

this discovery in 1953, several other A-15 compounds with higher T_c 's were discovered, the highest T_c being 23.2 K for the compound Nb_3Ge . This value remained the highest T_c for quite some years, till the discovery of 'high temperature superconductivity' in oxide systems.

Superconductivity was observed in some organic materials also. One of the early discoveries was the intercalation compounds of graphite (eg. C_8K) which becomes superconducting below 1 K. Organic metals such as the charge transfer compounds formed between strong electron accepting organic molecules (eg. tetra cyanoquinodimethane, TCNQ) and good electron donors (eg. derivatives of tetrathiofulvalene, TTF) also were found to be superconducting at low temperatures at ambient or high pressures.

Another class of superconductors worth mentioning is those that come under the family of 'heavy fermion superconductors'. UPt_3 , UBe_{13} , $CeCu_2Si_2$ etc. are a few examples of this class having T_c 's 0.54 K, 0.85 K and 0.65 K respectively. These heavy electron metals can be characterised by a low temperature specific heat that is two or three orders of magnitude larger than that of ordinary metals and usually are f - electron metals, having huge effective masses. In spite of the hectic search for higher T_c 's Nb_3Ge remained the material with the highest T_c for quite some years.

1.2 High temperature superconductivity

The second phase of the history of superconductivity began in 1986, with the discovery of 'high temperature superconductivity' in a class of cuprates by Bednorz and Muller [1] in the 30 K range. The material was La_2CuO_4 in which ions of Ba^{2+} had been introduced to replace some of the La^{3+} and the material is generally expressed by the formula $La_{2-x}Ba_xCuO_{4-\delta}$. Later it was found that these compounds have the general formula $La_{2-x}M_xCuO_{4-\delta}$ where M can be Ba, Sr or Ca and the T_c of the system is a function of x which reaches its maximum value of about 35 K for $x \approx 0.15$. Bednorz and Muller were awarded the 1987 Nobel prize in Physics for their discovery, making the time between a discovery and Nobel prize one of the shortest on record.

Chu and coworkers reported late in 1986 [2] that with increase in pressure,

T_c also increased in La-Ba-Cu-O, reaching 57 K at 12 kbar. Investigations of chemical pressure dependence on T_c followed and subsequently led to the substitution of Sr instead of Ba, increasing the T_c to 42.5 K. M.K.Wu and associates of the University of Alabama [3] could step up the T_c to 90 K by substituting both La and Sr with Y and Ba. The material was composed of two major phases - the green phase Y_2BaCuO_5 which was nonsuperconducting and the dark superconducting phase with the chemical formula $YBa_2Cu_3O_{7-\delta}$, also called the '123' compound. Further investigations indicated that $YBa_2Cu_3O_{7-\delta}$ was neither the most stable nor was the only superconductor in the Y-Ba-Cu-O family. $YBa_2Cu_4O_8$, also called the 124 compound is the most stable member which superconducts at ≈ 80 K. In addition, the 247 compound $Y_2Ba_4Cu_7O_{15}$, resulting from recurrent intergrowth of 123 and 124 units was also found to be superconducting. Later studies revealed that Y in the 123 compound can be replaced by any of the rare earths (R) with the exception of Sc, Ce, Pr and Tb [4,5] and the compound can be expressed by the formula $RBa_2Cu_3O_{7-\delta}$.

In 1988, another breakthrough followed. A new superconducting compound was discovered by H.Maeda's group in Japan [6]. They reported that the compound Bi-Sr-Ca-Cu-O superconducted at 110 K. However, the compound was found to contain many superconducting phases and it was not easy to separate the low T_c phases. Now this family of superconductors has been identified as having the general formula $Bi_2Sr_2Ca_{n-1}Cu_nO_{2n+4+\delta}$ with $n = 1, 2$ and 3 giving the Bi2201, Bi2212 and Bi2223 compounds with T_c 's 20 K, 85 K and 110 K respectively. These Bi based compounds were found to be far more stable than the YBCO compounds and had higher critical current densities.

Superconductivity was reported in compounds containing thallium in the same year by different groups. The superconducting oxides containing thallium fall into two main series, the single thallium - oxygen layer materials of the general formula $TlBa_2Ca_{n-1}Cu_nO_{2n+2+\delta}$ with $n = 1, 2, 3, 4$ [7] and the double layer materials having the general formula $Tl_2Ba_2Ca_{n-1}Cu_nO_{2n+4+\delta}$ with $n = 1, 2, 3, 4$ [8,9]. In each homologous series, as n increases the number of copper oxygen planes, which are separated by Ca ions, is incremented by one. It is generally found that with increase of n , T_c also increases,

at least upto $n = 3$. For example, the members of the first series, denoted by Tl1201, Tl1212, Tl1223 and Tl1234 (for $n = 1, 2, 3$ and 4) have T_c 's 50 K, 80 K, 110 K and 122 K respectively. The third member of the second series, namely $\text{Tl}_2\text{Ba}_2\text{Ca}_2\text{Cu}_3\text{O}_{10+\delta}$ (Tl2223) was the holder of the record of having the highest T_c of 125 K till 1993.

Putilin *et al.* [10] reported in 1993 that the mercury based compound $\text{HgBa}_2\text{CuO}_{4+\delta}$ superconducts at 94 K. This compound was later identified as the first member of the homologous series $\text{HgBa}_2\text{Ca}_{n-1}\text{Cu}_n\text{O}_{2n+2+\delta}$ with $n = 1$. Schilling *et al.* [11] in the same year reported the observation of superconductivity at 133 K in a Hg-Ba-Ca-Cu-O sample which consisted of both the $n = 2$ and $n = 3$ members of the above series. Other groups have since reported Schilling's results from different parts of the world and $\text{HgBa}_2\text{Ca}_2\text{Cu}_3\text{O}_{8+\delta}$ with $T_c = 133$ K remains as the compound with the highest T_c . The manner in which the superconducting transition temperature increased over the years is pictorially depicted in Fig. 1.1.

There are other materials also which were found to be superconducting, even though their T_c 's are not as high as that of the materials described above. One such material is $\text{Ba}_{0.6}\text{K}_{0.4}\text{BiO}_3$ [12], which belongs to the BaBiO_3 class of superconductors and found to be having a T_c of ≈ 30 K. This material aroused much interest among scientists because of the absence of Cu. Eventhough the T_c was low, the material exhibited 3D - superconductivity which was isotropic compared to Y, Bi or Tl based superconductors. Superconductivity has also been observed in alkali metal doped La_2CuO_4 with the structure $\text{La}_{2-x}\text{A}_x\text{CuO}_4$ with $\text{A} = \text{Na}$ or K [13]. Another compound which was found to be superconducting is $\text{Nd}_{2-x}\text{Ce}_x\text{CuO}_4$ with a T_c of 30 K which was obtained by replacing Nd^{3+} in Nd_2CuO_4 with Ce^{4+} .

Another important class of superconductors which have been the subject of intense research belongs to the family of fullerenes. In 1985, Kroto *et al.* [14] were successful in producing a remarkably stable cluster consisting of 60 carbon atoms by the vaporisation of graphite by laser irradiation. Six years later Hebard and his group [15] of AT and T Bell Labs reported that these C_{60} fullerenes when doped with potassium become superconducting with a T_c of 18 K. Later in the same year it was shown by the same group [16] that the transition temperature is raised to 28 K when C_{60} is doped

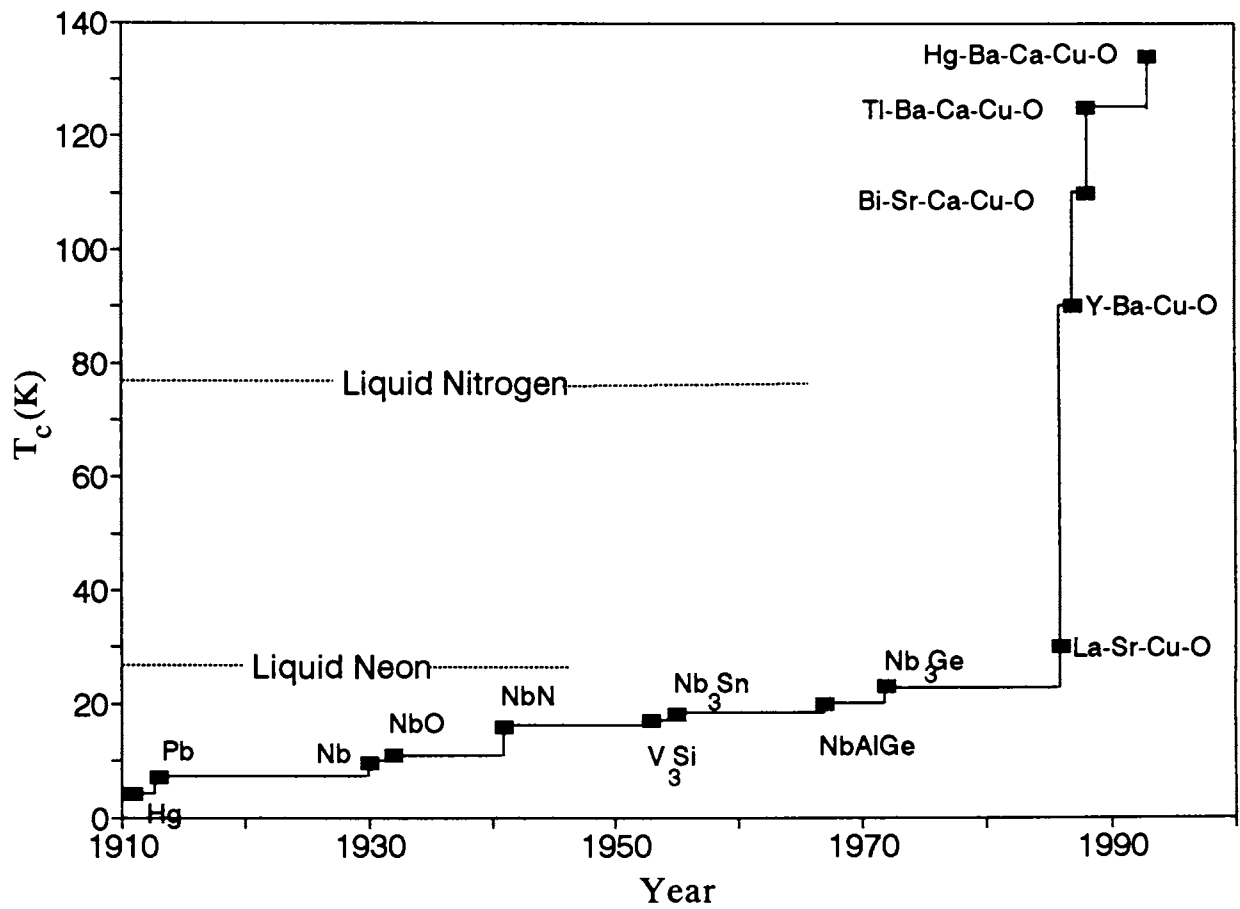


Fig. 1.1

Schematic representation of increase of T_c through the years.

with rubidium. Another report by Tanigaki *et al.* [17] indicated that when C_{60} is doped with cesium and rubidium ($Cs_xRb_yC_{60}$), the material has got a T_c of 33 K. This value of T_c is higher than that previously observed in any molecular, elemental or intermetallic superconductor and is surpassed only by the cuprate superconductors.

1.3 General features of high T_c cuprate superconductors

The different types of high T_c cuprates discussed above possess some unusual properties, when compared to the conventional superconductors. Extremely high values of T_c , linear d.c. resistivity in the normal state, unusual behaviour of the nuclear relaxation rate below T_c , extremely small coherence lengths, close analogy to antiferromagnetic phases etc. are a few characteristic properties common to these materials.

These materials can generally be described as consisting of rock-salt type metal-oxygen layers and defect perovskite layers. All of them have Cu-O sheets with a square-pyramidal or octahedral coordination of Cu with an apical oxygen. The Cu-O bond is quite covalent with an average distance around 1.9Å. Besides the two-dimensional Cu-O sheets which are primarily responsible for superconductivity, they have charge reservoirs in the form of Cu - O chains or TlO (BiO, HgO) layers. The superconducting cuprate families generally have parent members which are antiferromagnetic insulators (eg. La_2CuO_4 , $YBa_2Cu_3O_6$, $Bi_2CaSr_2LnO_8$ etc.).

Because of the presence of two-dimensional Cu-O sheets, properties of these materials are highly anisotropic. Accordingly these cuprates show very much higher normal state resistivity perpendicular to the ab plane compared to that in the plane. Another important feature common to these materials is that they are all hole superconductors containing oxygen holes. It has also been found that in the different series of cuprates, the T_c varies with the hole concentration, though not linearly.

Many of the unusual properties exhibited by these materials can be explained on the basis of their structure. The structure of the superconducting compounds and those of the related phases have been well studied by both X-ray and neutron diffraction

techniques. Single crystal studies have shed light into the dimensions of the unit cell, electronic charge distribution, location of atoms in the cell, possible presence of atomic irregularities etc. In the following section, the structure and properties of major high T_c superconducting systems are discussed.

1.3.1 $\text{La}_{2-x}\text{Sr}_x\text{CuO}_{4-\delta}$

The first cuprate superconductor discovered in 1986, $\text{La}_{2-x}\text{Sr}_x\text{CuO}_{4-\delta}$ (LSCO) has a body centred tetragonal K_2NiF_4 structure at room temperature [18, 19]. The parent compound, La_2CuO_4 is orthorhombic at room temperature and transforms to a tetragonal structure around 500 K. It is insulating and antiferromagnetic with a Neel temperature of ≈ 290 K. As La^{3+} is replaced with Sr^{2+} or Ba^{2+} in La_2CuO_4 , the doping of the cation lattice introduces holes into the conduction band and the compound becomes superconducting.

The value of T_c in the $\text{La}_{2-x}\text{Sr}_x\text{CuO}_{4-\delta}$ system is found to be a function of x and reaches its maximum value of about 35 K for $x \approx 0.15$. The La ion can be replaced by Pr, Nd, Gd and other rare earth ions upto a point without losing superconductivity, while substitution of Cu partly by Ni or Zn drastically lowers the T_c . High resolution neutron diffraction experiments done on a powder sample of LSCO showed that this material undergoes a tetragonal to orthorhombic transition in the vicinity of 180 K [20] together with further structural anomalies on approach of the superconducting transition at ≈ 35 K.

As mentioned earlier, LSCO possesses a K_2NiF_4 type structure which can be described as containing alternate layers of perovskite (ABX_3) and rock salt (AX) units. At all temperatures, the lanthanum and strontium cations are found to be distributed at random over the equivalent sites of the same position. The copper - oxygen layers perpendicular to the c axis are separated by the La/Sr oxygen planes with the rock salt type of arrangement. The copper atoms in one plane do not share oxygen atoms with copper atoms in other planes. Each oxygen atom of the perovskite layers O(2) is bonded to two Cu atoms in the same plane and to four R atoms ($R = 0.925\text{La} + 0.075\text{Sr}$) in adjacent planes, while each oxygen atom of the rock salt layers O(1) is

linked to five R atoms and one copper atom in a distorted octahedral configuration. The Cu-O distances within the perovskite type planes are short (1.889Å) and those in the perpendicular directions are rather long (2.411Å). The schematic representation of the unit cell of LSCO is shown in Fig. 1.2(a).

1.3.2 YBa₂Cu₃O_{7-δ} and related 123 compounds

All the superconducting oxides in this family have the general formula RBa₂Cu₃O_{7-δ} (RBCO) where R can be any rare-earth with the exception of Sc, Ce, Pr, Tb and have an orthorhombic structure with T_c in the range 90 - 95 K. In general, the R ion has little effect on T_c, but the T_c and the orthorhombic lattice parameters is markedly dependent on the oxygen content δ. The T_c is found to remain stable around 90 K upto δ = 0.2 and then shows a plateau at 60 K when δ = 0.3 - 0.4, T_c is 45 K when δ = 0.5 and the material becomes non-superconducting when δ = 0.6. The structure is orthorhombic over the entire range of δ = 0.0 - 0.6, but becomes tetragonal when δ ≥ 0.6.

Structural studies carried out by means of single crystal and powder X-ray diffraction techniques [21-26] indicate that the structure of YBCO can be obtained from that of perovskite by tripling the c axis, by eliminating all the oxygen atoms at (0 0 $\frac{1}{2}$) and half of those at (0 $\frac{1}{2}$ 0) and ($\frac{1}{2}$ 0 0), by ordering the metal atoms with yttrium at ($\frac{1}{2}$ $\frac{1}{2}$ $\frac{1}{2}$) and barium at ($\frac{1}{2}$ $\frac{1}{2}$ $\frac{1}{6}$) and ($\frac{1}{2}$ $\frac{1}{2}$ $\frac{5}{6}$) and by shifting some of the atoms from the ideal positions they occupy in perovskite. The structure of superconducting YBCO is schematically represented in Fig. 1.2(b).

The ordered elimination of some of the oxygen atoms from the atomic arrangement of perovskite has significant effects on the features of the resulting compound. The copper atoms are located on two inequivalent positions in the compound. The first, Cu(2) has a pyramidal, almost square - planar coordination and the second, Cu(1) located at the origin has square - planar coordination in which the near square Cu-O₂ units share one corner and form chains along the b axis of the unit cell. The atoms Cu(2) are strongly bonded to the four oxygen atoms O(2) and O(3), forming the basis of the pyramid, and are weakly bonded to the oxygen atom O(1) at the apex. Because of this feature, there exists in the structure two dimensional layers of copper and oxygen

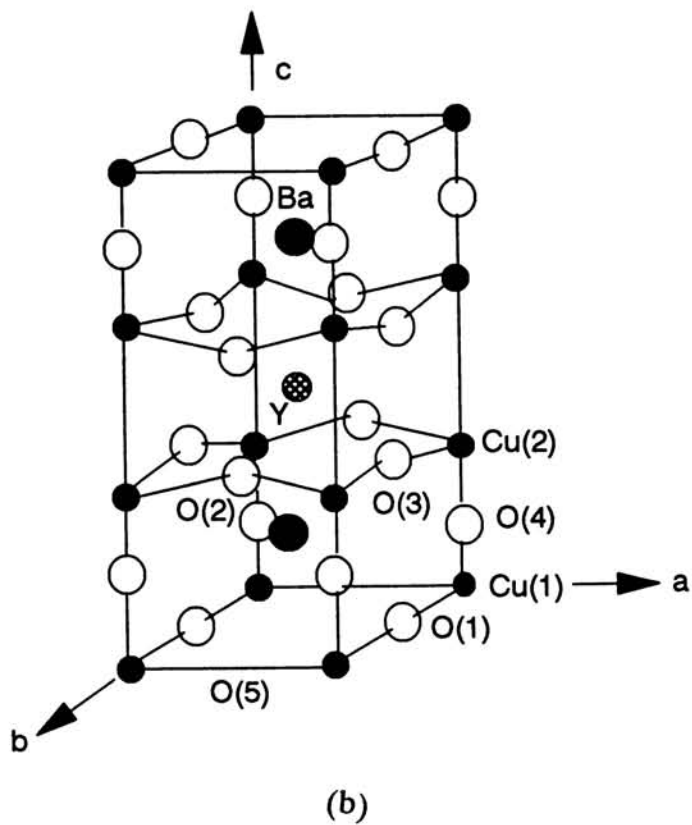
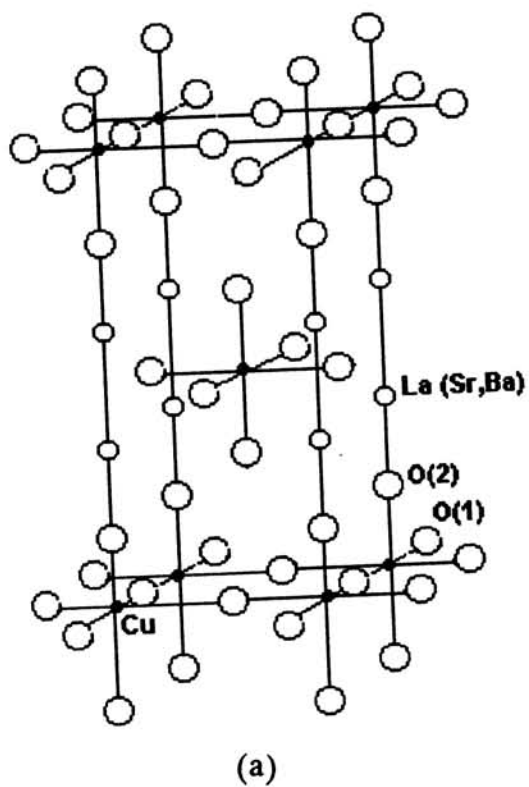


Fig. 1.2(a) : Structure of $\text{La}_{2-x}\text{Sr}_x\text{CuO}_{4-\delta}$.

Fig. 1.2(b) : Structure of $\text{YBa}_2\text{Cu}_3\text{O}_{7-\delta}$.

atoms perpendicular to the c axis. The oxygen atoms in these layers are slightly shifted from their ideal perovskite positions, producing the puckering of the layers indicated in the figure. The ordering of the oxygen vacancies also affects the coordination of other metal atoms. The yttrium atom is eight fold coordinated and the shape of the polyhedron is prismatic. The barium atoms, on the other hand, are tenfold coordinated and the coordination polyhedron can be described as a cubo octahedron with two oxygen atoms missing.

1.3.3 $\text{Bi}_2\text{Sr}_2\text{Ca}_{n-1}\text{Cu}_n\text{O}_{2n+4+\delta}$

In the $\text{Bi}_2\text{Sr}_2\text{Ca}_{n-1}\text{Cu}_n\text{O}_{2n+4+\delta}$ (BSCCO) series, the first three members with c parameters of 25, 31 and 38Å have been characterised; the T_c 's being 60, 90 and 110 K respectively. It has been found that T_c increases with the number of Cu-O₂ layers [27,28] and stabilises when Bi is partially substituted by Pb upto 25%. These cuprates are orthorhombic and consist of layer structures containing adjacent pairs of BiO planes that alternate along the c axis with perovskite like multilayers. Crystallites of these compounds have mica like morphology which is found to cleave readily between the layers. They show modulation in the ab plane, which is found to be related to the oxygen content and the structure of the Bi-O layers. One of the problems with these cuprates is the lack of single phase materials. Members with different n values are found to intergrow with each other, even at the unit cell level.

The structure of the second member of the family, $\text{Bi}_2\text{Sr}_2\text{CaCu}_2\text{O}_{8+\delta}$ (Bi2212) is shown in Fig. 1.2(c). In Bi2212, the perovskite like multilayer comprises two copper - oxygen sheets in the form of corner sharing CuO_5 pyramids separated on the base sides by calcium ions [29]. The Bi_2O_2 layers consist of two parallel, planar BiO sheets. The bismuth ion coordination is six with four oxygen atoms in the BiO plane, one oxygen on the adjacent BiO layer and one oxygen in the adjacent apex of a CuO_5 pyramid. These BiO octahedra are strongly distorted, having the typical oxygen coordination for Bi^{3+} with three short Bi-O bonds and three much longer Bi-O bonds in the direction of the lone pair electrons. These lone pairs are positioned in the interstitials between the pairs of BiO layers leading to a large interlayer spacing [30]. The lattice parameters of

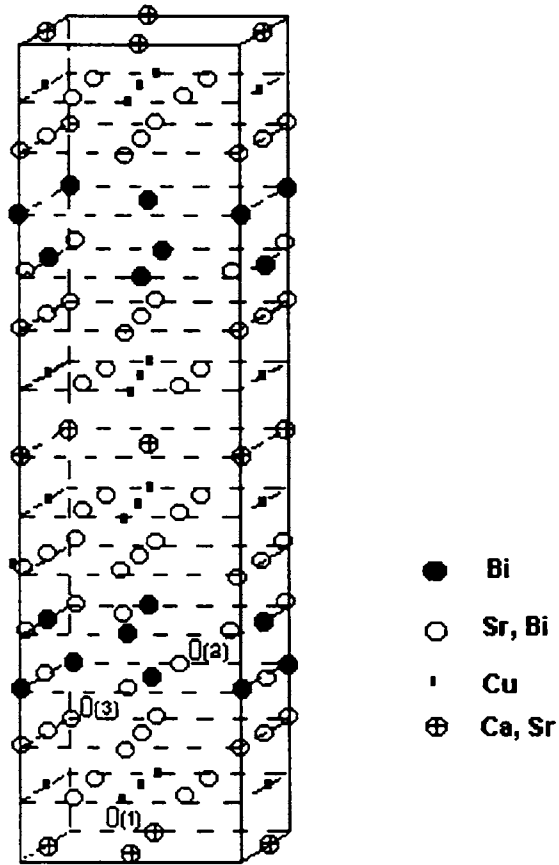


Fig. 1.2(c)
 Structure of $\text{Bi}_2\text{Sr}_2\text{CaCu}_2\text{O}_{8+\delta}$.

the Bi2212 compound is determined as $a = 5.4091\text{\AA}$, $b = 5.4209\text{\AA}$ and $c = 30.8445\text{\AA}$ which is very much larger than a and b .

One interesting aspect about these compounds is that the actual cationic composition is likely to be quite different from that given by the nominal formula. The most stable and easily reproducible composition is found to be the $\text{Bi}_2(\text{Sr,Ca})_3\text{Cu}_2\text{O}_{8+\delta}$ compound.

1.3.4 $\text{Tl}_2\text{Ba}_2\text{Ca}_{n-1}\text{Cu}_n\text{O}_{2n+4+\delta}$

The oxide superconductors containing thallium fall into two series depending on the number of Tl-O layers present in the structure, as mentioned earlier. Thallium cuprates of the general formula $\text{Tl}_2\text{Ba}_2\text{Ca}_{n-1}\text{Cu}_n\text{O}_{2n+4+\delta}$ (2-Tl) are tetragonal and contain two Tl-O layers and n Cu-O sheets. The T_c 's of these compounds are 80, 110 and 125 K respectively for $n = 1, 2$ and 3 . Members of the $\text{TlBa}_2\text{Ca}_{n-1}\text{Cu}_n\text{O}_{2n+2+\delta}$ family (1-Tl), having a primitive tetragonal structure, contain a single Tl-O layer. The T_c 's of these cuprates are slightly lower than those of the corresponding members of the 2-Tl series. Tl based cuprates with $n > 3$ have also been characterised, but it is seen that T_c does not increase beyond $n = 3$ [31, 32]. In the Tl family also, the problem of phasic inhomogeneity due to the intergrowth of different members of the series is encountered.

Due to high toxicity of thallium and the need for special hood chamber and related setups for preparation of Tl- based compounds, reports on the preparation and structural studies on these compounds are comparatively less in literature.

The synthesis and structural determination of the 2 - Tl family, have been carried out by Ogborne and group [33-35] by X - ray powder profile refinement. The structural features are found to be identical for all the members of the family. They are body centred tetragonal crystals and consist of n immediately adjacent Cu - O planes, with a Ca plane between each immediately adjacent Cu - O plane for $n \geq 2$. For example in the 2234 phase ($n = 4$), four such parallel layers exist, for the inner pair the copper coordination geometry is almost perfectly square planar with a slight buckling of the layers outwards from the calcium, whereas the outer sheets are formed from CuO_5 square pyramids, the coordination in the ab plane being almost perfectly square

planar. Separating the immediately adjacent Cu-O planes is a corrugated Ba-O plane, two Tl-O planes and another Ba-O plane before the next Cu-O plane is encountered. The distance between the Cu-O planes is rather large, $\approx 11\text{\AA}$ which is due to these four Ba-O and Tl-O isolation planes. The apical Cu-O distances are found to be typical for this family of materials, the value being 2.657\AA . The Tl-O layers show disordering of oxygen producing a complex coordination geometry around thallium with two short and two long in-plane Tl-O distances.

The structure of the single layer Tl compounds have also been determined from X-ray and neutron diffraction experiments. Here also the structure consists of n immediately adjacent Cu-O planes with a plane of Ca between the Cu-O planes for $n \geq 2$. For this structure there is only one Tl-O plane rather than two as in the 2-Tl family. Here the distance between Cu-O planes is just the c axis unit cell length and is equal to 9.7\AA .

1.3.5 $\text{HgBa}_2\text{Ca}_{n-1}\text{Cu}_n\text{O}_{2n+2+\delta}$

The members of the series $\text{HgBa}_2\text{Ca}_{n-1}\text{Cu}_n\text{O}_{2n+2+\delta}$ are structurally similar to the corresponding compounds of thallium, $\text{TlBa}_2\text{Ca}_{n-1}\text{Cu}_n\text{O}_{2n+2+\delta}$, the main difference between the two class of materials being the oxygen occupancy of the Tl and Hg layers which is almost complete in the case of thallium and less than 50% in the case of mercury. An increase of T_c is observed with increasing n until the third member of the series after which T_c is seen to be saturated. This behaviour also is quite similar to those of other homologous series such as those of Tl and Bi.

The crystal structure of these compounds have been well studied by X-ray and neutron powder diffraction [36-40]. Just like the single layer Tl compound, the structure of mercury compounds are based on the layer sequence in which blocks of Hg-O layers sandwiched between Ba-O layers having the rock-salt structure alternate with blocks of $(\text{Cu-O}_2)\text{-(}n\text{-1)Ca-(Cu-O}_2)$ having a perovskite structure. The third member of the series, $\text{HgBa}_2\text{Ca}_2\text{Cu}_3\text{O}_{8+\delta}$ (Hg1223) possesses a tetragonal structure with lattice parameters $a = 3.85\text{\AA}$ and $c = 15.85\text{\AA}$ [39]. There are two different kinds of CuO_2 layers - one in which the copper atoms have five-fold pyramidal coordination and one in which

the copper coordination is square planar. The in-plane Cu-O bond is almost identical for the two atoms. A comparison with the other members of the homologous series shows that this bond length is strongly dependent on the oxidation state of copper and varies from compound to compound. The apical Cu-O distance involving the copper atoms with pyramidal coordination is large when compared to other layered cuprate superconductors. The oxygen atoms of the CuO_2 planes containing the copper atoms in pyramidal coordination, are almost exactly coplanar with the copper atoms, a feature common to all members of this homologous series. The mercury atoms have two-fold dumbbell coordination in those unit cells in which the O(4) oxygen sites are empty, and they are coordinated by a third oxygen atom at much a larger distance when the sites O(4) are occupied. The coordination of Ba is also affected by the presence of O(4) atoms, being eight-fold when these sites are empty and nine-fold when they are full.

1.4 Theoretical Developments

Since the discovery of superconductivity, several theoretical models have been proposed to explain the normal state and superconducting properties of these materials. In the following sections, some of these prominent models are briefly outlined.

1.4.1 The BCS theory

The first successful microscopic theory of superconductivity, the BCS theory, was proposed by J. Bardeen, L. N. Cooper and J. R. Schrieffer in 1957 [41] which is based on the existence of a net attractive interaction between the electrons mediated by phonons. The idea was not entirely new ; the discovery of isotope effect earlier in the 1950's had suggested that lattice vibrations play a major role in the mechanism of superconductivity and in 1952 Frolich predicted that two electrons can attract each other via distortion of the lattice. This can be explained as follows. When an electron moves through a lattice of ions, it exerts forces on them and move them slightly from their equilibrium positions. The ions, being heavy, are set into slow forced oscillations, while the electrons being fast, would have already left this region. Another electron passing later through this region experiences a force due to the locally distorted oscillating lattice of

ions. This force is one of attraction. If this attractive interaction is greater than the coulomb repulsion, the two electrons pair up to form what is known as ‘Cooper pairs’. The coupling of the electrons into Cooper pairs marks the onset of superconductivity.

Theoretically, it is assumed that all the electrons in a superconducting body are paired into Cooper pairs at 0 K in the absence of an applied magnetic field and an electric current. The pairs break up when energy is supplied either by the application of an external magnetic field or by increasing the temperature. The population of unpaired electrons having energy E is proportional to $\exp(-E/k_B T)$ which explains the exponential temperature dependence of specific heat.

The Cooper pairs are governed by certain requirements of quantum mechanics, the most important of which is that for the Cooper pairs momentum is conserved. This property leads to the static electromagnetic properties of zero resistance and Meissner effect. The unpaired electrons coexisting with the Cooper pairs in the superconducting state are like the electrons in a normal metal. Currents carried by them are resistive and their contribution to the magnetic superconductivity are very small. A Cooper pair is more stable than two unpaired electrons by the amount of their binding energy, which is the energy of the superconducting ‘gap’.

The BCS theory makes predictions for the transition temperature T_c in terms of the parameters of the theory. The transition is governed by

$$k_B T_c = 1.134 \hbar \omega_D \exp\left(\frac{-1}{\lambda}\right) \quad (1.1)$$

where $\lambda = V N(E_F)$ is a dimensionless constant called the electron-phonon coupling constant in which V is the electron-electron interaction and $N(E_F)$ is the density of states at the Fermi level, and $\hbar \omega_D$ is the Debye energy for the phonons. Since the phonon frequency is inversely proportional to the square root of the mass for a simple metal, this prediction is in agreement with the isotope effect.

An expression for the energy gap (Δ) is also given by the BCS theory in terms of the above parameters as

$$\Delta = 2 \hbar \omega_D \exp\left(\frac{-1}{\lambda}\right) \quad (1.2)$$

This expression is for zero temperature. With increasing temperature, the energy gap monotonically decreases and approaches zero as $T \rightarrow T_c$. In the vicinity of T_c , the energy gap is expressed as

$$\Delta(T) = 1.74 \Delta(0) \left(1 - \frac{T}{T_c}\right)^{1/2} \quad (1.3)$$

The continuous approach of energy gap to zero is characteristic of a second order phase transition.

The theory also gives a relationship between the zero temperature energy gap and the transition temperature as

$$\frac{\Delta(0)}{k_B T_c} = 1.764 \quad (1.4)$$

This prediction is independent of the parameters of the theory and agrees quite well with many of the simple elemental superconductors.

Though the BCS theory was successful in explaining almost all the properties of conventional superconductors, many unusual properties of the high T_c materials could not be accounted for by this theory. The comparatively higher values of T_c , linear normal state d.c. resistivity, close proximity between superconductivity and antiferromagnetism, anisotropy of the superconducting energy gap etc. are a few examples of the properties of these new materials, which cast doubts on the applicability of the BCS theory to these materials. So new theoretical models invoking other possible excitations like plasmons, polarons, excitons etc. have been proposed for high T_c superconductors.

1.4.2 The plasmon theory

Based on electron-phonon interaction, the maximum value of T_c which a superconductor can have is less than 23 K. These low values of T_c may be due to the low energy of the phonon. This immediately suggests that a higher energy boson might act in place of or in addition to phonons, yielding a higher T_c .

When a test charge is inserted into a solid, three kinds of distortions occur : the lattice distorts which are the virtual phonons, the electrons can repopulate any partly filled band which are called 'the plasmons' or they can mix in components from

higher unfilled bands which are called ‘the excitons’. If the test charge is time dependent, then these distortions follow in time with a lag which is larger for a lattice distortion than electronic distortions. A second test charge will feel both the direct instantaneous repulsion of the first test charge and a time dependent attraction from these dynamical distortions. The usual phonon mediated coupling theory assumes that electronic polarisation serves only to cancel part of the direct coulomb repulsion and that only phonon polarisation is sufficiently strong and retarded to contribute to pair binding. But Rietschel and Sham [42] have shown that in the absence of phonons the plasmon mechanism can in principle, cause superconductivity. However, this solution is totally altered by Grabowski and Sham [43], who approximately included the effects of the lowest order vertex corrections and the graph with crossed coulombic interactions.

Experiments also suggested the possible existence of plasmon mechanism. X ray photoelectron spectroscopy (XPS) on single phase YBCO by Ihara *et al.* [44] has revealed a relatively high value of the density of states at Fermi level. The XPS $\text{Cu}^2\text{P}_{3/2}$ peak was divided into three peaks which were attributed to monovalent, bivalent and trivalent Cu ions with the concentration ratio of 1:2:1. These results and the lattice structure of YBCO lead to the T_c enhancement mechanism from the plasmon or exciton origin due to the Cu d-hole creation and annihilation resonating with vibrating modes of the CuO_5 and CuO_4 clusters.

1.4.3 The exciton theory

Two versions of the idea of excitons got developed during the past few years. Allender *et al.* [45] proposed getting a metal into such intimate contact with a polarisable, narrow gap semiconductor that the metallic electrons would be able to interact strongly with interband excitations of the semiconductor. Pairing would then occur by the exchange of these virtual excitations. Here the word ‘exciton’ is used loosely to describe the sort of virtual excitations involved in the polarisation of a valence band.

The exciton mechanism, like the plasmon mechanism, surely exists and helps in the sense that it weakens the direct coulomb repulsion of electrons. Unlike the plasmon in the free electron gas, there is no obvious simple model system which should

be subjected to rigorous theoretical investigations.

The other version of this idea was in the original paper by Little [46]. It is almost the same as that of the first version except that it is presumed that it is better not to have intimate contact between the electrons involved in pairing and the entity undergoing electronic polarisations. Separation eliminates exchange interactions between Cooper pairs and polarising electrons, which otherwise would reduce the attraction.

Though there are evidences for these excitons, a general difficulty with excitonic mechanisms is that the effective electron-electron interaction is required to be attractive over sizable electronic length and time scales, while we know it to be repulsive at long distances and times. Since there is no separation of energy scales as for phonons, these two requirements are difficult to reconcile.

1.4.4 Spin fluctuations

In a magnetic medium, a free electron can scatter off the spin system, emitting a spin wave. Superconducting systems are generally magnetically ordered, except perhaps at temperatures lower than T_c as in rare earth substituted $\text{YBa}_2\text{Cu}_3\text{O}_7$. An exception is the heavy fermion systems like URu_2Si_2 [47, 48] in which superconductivity may be caused by exchange of antiferromagnetic spin fluctuations. A more common situation for a metal to be close to magnetic ordering when becoming superconducting is in which one expects to have relatively long lived local spin fluctuations. This scattering of electrons from these fluctuations will alter the tendency to form pairs. Usually this alteration has been assumed to be harmful in the sense that a spin up electron will attract other electrons of up spin, creating a locally ferromagnetic region, and repelling the down spin electron needed for singlet Cooper pairing. This process is found to be helpful to triplet pairing, and is believed to be an important source of triplet pairing in liquid ^3He . So far there is no proof that any metal has a triplet pairing state, although UPt_3 and other heavy fermion systems as well as some organic superconductors are possible candidates. These materials all have low T_c values.

The experimental discovery of closely related antiferromagnetic and superconducting states in organometals and then in heavy fermion metals has raised the question

of the existence of antiferromagnetic spin fluctuations [49-51]. However, it is not obvious whether an up spin electron will create or destroy local antiferromagnetic polarisation or whether this will attract or repel other electrons of opposite or parallel spin. The discovery of antiferromagnetism in $\text{La}_2\text{CuO}_{4-y}$ [52] and $\text{YBa}_2\text{Cu}_3\text{O}_{7-\delta}$ [53] has raised further interest in this mechanism.

Schrieffer *et al.* [54] have proposed a simple scenario which suggest that free carriers in a material wanting commensurate antiferromagnetism will weaken the tendency to order. Thus an up spin electron repels local spin order. Other free carriers, with either spin orientation, will be attracted to the region of depleted spin giving a net attractive interaction.

1.4.5 The polaron, bipolaron theory

The polaron theory was first developed [55] on the basis of periodic lattice in molecular crystals where a polaron was defined as the combination of the metal atom with its extra charge plus its deformed oxygen coordination. This model could successfully explain the conduction mechanism in disordered systems like transition metal oxide glasses like Bi-Sr-Ca-Cu-O [56]. Later on this theory was applied to superconducting oxides [57] like SrTiO_3 , $\text{BaPb}_{1-x}\text{Bi}_x\text{O}_3$, $\text{La}_{2-x}\text{Sr}_x\text{CuO}_4$ etc. by treating them as doped semiconductors where conductivity is due to induced doping or self doping. Doping leads to mixed valence condition for the metal ions responsible for the formation of polarons, where the mobility of these polarons is ensured through the mixed valence charge transfer mechanism.

Under special circumstances, these polarons may combine to form ‘bipolarons’. The first idea of the existence of bipolarons came from Vinetskii [58,59]. Two polarons separated by a finite distance and bound by a common polarisation constitutes a bipolaron. A bipolaron may also be viewed as a quasi particle consisting of a self consistent state of two conduction electrons and the axially symmetric polarisation potential well which is produced by them and which binds them. There is no unambiguous evidence that bipolarons exists in any known solids, but a plausible case has been made [60] that the metal insulator transitions seen in Ti_4O_7 at 140 K and at 150 K could be described

as bipolaronic.

It is possibly accidental but nevertheless interesting that the idea of bipolaronic superconductivity, specifically in Jahn-Teller distorted systems, is part of what motivated Bednorz and Muller [1] to search for superconductivity in Cu-O based systems. Scalapino *et al.* [61] argued that Cu-O based superconductivity may be electron-phonon driven, and on the border between bipolaronic and BCS like.

1.4.6 The Resonating Valence Bond (RVB) Theory

According to P.W.Anderson [62], the oxide superconductors possess some peculiarities that suggest a common unique magnetic mechanism as responsible for superconductivity which is known as the resonating valence bond (RVB) model. The unique and extraordinary properties of these materials like - high T_c values, anomalous superconductor - normal metal tunnelling, indications of unstable superconductivity even at room and higher temperatures, strong sound attenuation, IR absorption different from that of the BCS materials etc. have led to the development of this theory.

Superconductivity in most of the cuprates occur near a metal to insulator transition known as the Mott transition into an odd electron insulator phase with peculiar magnetic properties. This insulating phase was proposed to be the 'Resonating Valence Bond' or 'quantum spin liquid' hypothesised in 1973. This insulating magnetic phase is favoured by low spin, low dimensionality and magnetic frustration. When doped sufficiently to become a metal, the insulating state magnetic-singlet pairs become charge superconducting pairs. Thus the pairing mechanism is proposed to be predominantly electronic and magnetic, although weak phonon interactions might favour the state.

The RVB model predicts and is compatible with many experimental findings such as the absence of an isotope effect, behaviour of low temperature specific heats, elastic properties dominated by electronic energies, the absence of an effective energy gap, the insulating and/or antiferromagnetic states of undoped or weakly doped copper oxide compounds, anomalous temperature dependence of the normal state resistivity etc..

1.5 Thermal and elastic properties of high T_c superconductors

The high T_c materials have been the subject of intense research by scientists from a wide range of fields of both basic and applied research since their discovery, not only because of the unusual properties exhibited by them, but also due to the prospects of applications of these materials. Since the discovery in 1986, nearly every conceivable measurement has been performed on this class of materials and innumerable reports concerning different aspects of superconductivity have appeared in literature.

The magnetic properties of these materials is an area of hectic research which include the Meissner effect, determination of both upper and lower critical fields, the interplay between long range magnetic order and superconductivity, the critical current density, compositional variation of the magnetic properties etc.. The preparation and substitutional studies of the ceramic oxides both in bulk polycrystalline and single crystal form has been another important area of research since these sort of studies could result in new superconducting materials with even higher T_c 's. The structural studies of these materials by X-ray and neutron diffraction experiments, thermal and transport properties, pressure and temperature dependent studies on various parameters of the system, elastic properties, energy gap determination from photoelectron spectroscopy (PES) etc. are important for the scientific community since they can provide valuable information about the mechanisms responsible for superconductivity. The development of thin and thick films of these materials, development of high field superconducting magnets to be used in electronic and radio frequency devices, nuclear magnetic resonance (NMR) spectrometers, fabrication of Josephson junctions with high T_c materials to be used in SQUIDS etc. are some of the challenges faced by scientists of the technical field where intense research is going on. A detailed review of all the experimental investigations probing different properties of these materials is beyond the scope of this chapter and hence is not attempted.

Among these different areas of research, the thermal and elastic properties of the high T_c oxides have attracted almost as much attention as the superconducting

properties, not only because of the technological importance of these types of investigations but also due to the information provided by these studies for the theoretical understanding of the mechanism. Since this thesis is the result of our investigations on the thermal and elastic properties of high T_c superconductors, an outline of the important properties coming under the thermal and elastic regime is given in the following sections.

1.5.1 Specific heat

The specific heat of a superconducting material is a true measure of its bulk properties which plays an important role in determining the volume fraction of superconductivity which cannot be determined by other measurements. The temperature dependence of the specific heat $C(T)$ can provide valuable information concerning the nature and energy dependence of many excitations like phonons, electrons, spin waves etc. in condensed matter systems [63,64]. Actually it was the exponential temperature dependence of the electronic contributions to the specific heat for $T < T_c$ in conventional superconductors along with the lack of a latent heat of transformation at T_c which revealed many major facts leading to the development of the BCS theory. Similarly specific heat studies of the oxide superconductors do provide valuable insight into both the normal and superconducting behaviour of these new and unusual systems.

In the normal state, there are several types of excitations which may contribute to the measured specific heat $C(T)$, where $C(T)$ here refers to the specific heat measured at constant pressure. In general ,

$$C(T) = C_e(T) + C_{ph}(T) + C_{sf}(T) + C_T + C_{sch}(T) \quad (1.5)$$

where $C_e(T)$ is the electronic contribution, $C_{ph}(T)$ is the phonon term, $C_{sf}(T)$ is due to spin or magnetic fluctuations, C_T is due to ionic tunnelling between nearly degenerate states and $C_{sch}(T)$ represents a contribution due to a Schottky anomaly resulting from a multilevel system.

$C_e(T)$, The electronic contribution

The electronic contribution to the specific heat $C(T)$, is given by γT for $T \ll T_F$, the

Fermi temperature characterising the electron gas. The electronic coefficient of $C(T)$, γ for nearly free electrons is proportional to the density of electronic states at the Fermi level, $N(E_F)$, and is given by

$$\gamma = \frac{2}{3} \pi^2 k_B^2 N(E_F) \quad (1.6)$$

The linear T dependence for $C_e(T)$ is found to be independent of the dimensionality of the system.

$C_{ph}(T)$, The phonon contribution

The phonon contribution to the specific heat has been derived in the Debye model and is given by

$$C_{ph}(T) = \frac{9nN_0k_B}{\nu_D^3} \int_0^{\nu_D} \frac{(h\nu/k_B T)^2 e^{(h\nu/k_B T)}}{(e^{(h\nu/k_B T)} - 1)^2} \nu^2 d\nu \quad (1.7)$$

where n is the number of ions per molecular units, N_0 is the Avogadro number and ν_D is the Debye frequency. At low temperatures ($k_B T \ll h\nu_D$) the above equation gets simplified to

$$C_{ph}(T) = \frac{12}{5} \pi^4 n N_0 k_B \left(\frac{T}{\theta_D} \right)^3 \quad (1.8)$$

where θ_D is the Debye temperature. Thus the Debye model predicts a T^3 law for $C(T)$ at low temperatures.

$C_{sf}(T)$, spin fluctuation contribution

The spin fluctuations, which are highly damped excitations of the spin degrees of freedom of the system, lead to an enhancement of magnetic susceptibility and a modification to $C(T)$ at low temperatures. These excitations lead to an enhancement of the electronic coefficient of the specific heat γ and introduces a $T^3 \ln T$ correction. Including this, the electronic specific heat becomes

$$C_e(T) = \left(\frac{m^*}{m} \right) \gamma_0 T + \delta T^3 \ln(T) \quad (1.9)$$

where $\frac{m^*}{m}$ is a mass enhancement due to spin fluctuations and δ depends on electronic parameters such as the exchange interaction, $N(E_F)$, T_F etc. The $T^3 \ln T$ term produces an upswing in $C(T)/T$ as $T \rightarrow 0$, which is observed for many of the high T_c oxide systems [65].

$C_T(T)$, two level tunnelling contributions

The anomalous thermal properties of the disordered systems have been modelled assuming a two-level excitation system representing the tunnelling of atoms or group of atoms from one potential well to a degenerate or nearly degenerate neighbouring well. If one includes a small distribution in the size of the potential barriers and energy splitting between the two levels, a density of the tunnelling states which is nearly constant over a limited range of energy is obtained. Then $C(T) = \beta T$ is obtained with β proportional to the density of tunnelling states. Thus two level tunnelling models lead to a nonelectronic contribution to $C(T)$ as $T \rightarrow 0$ which is linear in T , thus mimicking an electronic contribution.

$C_{sch}(T)$, Schottky contribution

A system of discrete excitations such as a two-level system with a ground state of degeneracy g_0 , an excited state of degeneracy g_1 and an energy splitting Δ will lead to an additional contribution, called the Schottky contribution to $C(T)$ given by

$$C_{sch}(T) = \frac{R(\Delta/T)^2 \frac{g_1}{g_0} e^{\Delta/T}}{1 + \frac{g_1}{g_0} e^{\Delta/T}} \quad (1.10)$$

where R is the universal gas constant. At low temperatures, a T^{-2} dependence for $C(T)$ has been observed for several high T_c oxides and has been associated with the Schottky contribution.

The Gibb's free energy difference between the normal and superconducting states in a magnetic field H can be written as

$$G_N - G_S = \left(\frac{H_c^2}{8\pi} - \frac{H^2}{8\pi} \right) V_s \quad (1.11)$$

where H_c is the thermodynamic critical field and V_s is the volume of the superconductor. Using this free energy difference, the difference in specific heat along the superconducting-normal state boundary is calculated as

$$C_N - C_S = - \left(\frac{V_s T}{4\pi} \right) \left[H_c \left(\frac{d^2 H_c}{dT^2} \right) + \left(\frac{dH_c}{dT} \right)^2 \right] \quad (1.12)$$

The observed temperature dependence of the thermodynamic critical field of many

superconductors is well represented by a parabolic relationship,

$$H_c(T) = H_c(0) \left[1 - \left(\frac{T}{T_c} \right)^2 \right] \quad (1.13)$$

Substituting in eqn.(1.12), the difference in specific heat becomes

$$C_N - C_S = \frac{H_c^2(0)}{2\pi T_c} \left[\left(\frac{T}{T_c} \right) - 3 \left(\frac{T}{T_c} \right)^3 \right] \quad (1.14)$$

The first term on the R.H.S. can be associated with the normal state contribution given by

$$C_N(T) = \left(\frac{H_c^2(0)}{2\pi T_c^2} \right) T = \gamma T \quad (1.15)$$

where the second term represents $C(T)$ of the electrons in the superconducting state, given by

$$C_S(T) = \frac{3 H_c^2(0)}{2\pi T_c} \left(\frac{T}{T_c} \right)^3 \quad (1.16)$$

This thermodynamic argument, along with the observed parabolic dependence of $H_c(T)$ predicts a T^3 dependence for $C_S(T)$ as $T \rightarrow 0$. However, both experiments and BCS theory indicate that $C_S(T)$ goes to zero more rapidly than T^3 , and this difference is due to the slight difference between the assumed parabolic T dependence of $H_c(T)$ and the actual dependence. But, near T_c this difference is found to be very small.

a. Conventional superconductors

One of the significant accomplishments of the BCS theory is that it provided a correct description of the thermodynamic properties of superconductors. The BCS theory predicts a second order transition to the superconducting state with a discontinuity in the specific heat at $T = T_c$, given by

$$\frac{C_S - C_N}{\gamma T_c} = \frac{\Delta C}{\gamma T_c} = 1.43 \quad (1.17)$$

where γ is the electronic specific heat coefficient in the normal state.

In most of the elemental superconductors like Al, Ga, Cd, V, Zn etc. $\Delta C/\gamma T_c$ is in good agreement with 1.43. However this ratio has been found to depend on the details of the pairing interactions. For example, in strong coupled superconductors like Pb, Hg, Nb etc. in which the superconducting pairing energy is not negligible

compared to the phonon energies, the value of $\Delta C/\gamma T_c$ is as high as 2.5. And, if an excitonic coupling is added phenomenologically to the electron-phonon coupling and modelled just by adding the effective electron-phonon and electron-exciton couplings, then $\Delta C/\gamma T_c$ has been found to decrease monotonically with increasing electron-phonon weight.

For $T \ll T_c$, the BCS theory predicts that $C_{es}(T)$, the electronic contribution to $C(T)$ in the superconducting state, will be proportional to $\exp(-\Delta/k_B T)$ where Δ is the superconducting gap in the electron density of states at E_F . Extensive studies have been reported in most of the elemental superconducting systems and the results are consistent with the weak coupling BCS theory or appropriate extensions of this theory to account for strong coupling corrections.

b. High T_c oxide superconductors

There are some distinct differences between specific heats of conventional and oxide superconductors. First, since T_c of these materials is high, the phonon specific heat dominates over electronic contribution which is opposite to the behaviour exhibited by conventional superconductors. Second, the critical field necessary to suppress superconductivity is too large in the oxide superconductors to obtain reliable normal state data on $T < T_c$. This coupled with the large phonon contribution to $C(T)$ for $T < T_c$ makes it nearly impossible to establish the temperature dependence of $C_{es}(T)$, the electronic contribution to $C(T)$ for $T < T_c$.

Specific heat measurements have been reported on all the major high T_c oxide systems [66-72], mainly using the adiabatic or quasi adiabatic calorimetric techniques. All of them exhibit a distinct anomaly in specific heat around T_c , though there is no general agreement on the magnitude of this anomaly. The possible reasons for this disagreement have been suggested to be the broad and possibly incomplete transition due to the lack of phase purity and an intrinsic broadening of the transition due to thermodynamic fluctuations of the order parameter. In spite of sample inhomogeneities and fluctuation effects, a discontinuity is obtained at T_c and is attributed to a mean field theory transition. Another interesting feature is the linear term and an 'upturn' in specific heat observed at low temperatures. The upturn has been found to be associated

with electronic magnetic moments that order at very low temperatures as shown by its magnetic field dependence.

There have also been attempts to calculate the ratio $\Delta C/\gamma T_c$ for these materials. Since an unambiguous determination of γ is not easy in these materials, the values show variation from sample to sample even for the same material. For YBCO and LSCO, this ratio is found to be close to or higher than the BCS value [66,67], suggesting these materials to be in the weak coupling or strong coupling limits respectively.

1.5.2 Thermal conductivity

The measurement of transport properties such as Hall effect, electrical resistivity, thermal conductivity, thermopower etc. of a superconducting system can yield valuable information regarding the nature of the charge carriers and their interactions. In addition, the strange normal state properties of high T_c materials, which are not characteristic of other materials, are most vividly displayed in their transport properties. For example, the electrical conductivity is found to be extremely anisotropic with metallic like behaviour along one direction and semiconducting or insulating like behaviour along the other.

The thermal conductivity K is a particularly useful transport coefficient in the sense that it can probe scattering processes in both normal and superconducting states. Since heat is conducted by both charge carriers and phonons, a measurement of thermal conductivity can give valuable information not only about the spectra of electrons and phonons, but also about the interactions between them.

The thermal conductivity K , like the specific heat, can be separated into different components as

$$K = K_e + K_{ph} \quad (1.18)$$

where K_e and K_{ph} refer to the electronic and phononic contributions to the thermal conductivity. The temperature dependence of each of these contributions is found to depend on the nature of the scattering processes.

K_e , the electronic contribution

Electrons in a material are scattered by other electrons, by phonons and by defects and

boundaries of the material. According to Matheissen's rule, K_e can be expressed as

$$K_e = \left[(K_{e,ph})^{-1} + (K_{e,e})^{-1} + (K_{e,d})^{-1} \right]^{-1} \quad (1.19)$$

where the additional subscripts ph , e , and d refer to phonon, electron and defect - limited thermal conduction.

The electronic thermal conductivity can be calculated from the Wiedmann - Franz law using the relation

$$K_e = L \sigma T \quad (1.20)$$

where $L = 2.45 \times 10^{-8} \text{ V}^2 \text{ K}^{-2}$, is the Lorenz number and σ is the electrical conductivity. Since σ is inversely proportional to the temperature T , K_e is a constant at high temperatures. As the temperature decreases phonon scattering becomes less and less effective, impurity scattering dominates and correspondingly K_e goes through a maximum value. The temperature at which K_e becomes maximum and the value of K_e at this temperature depend on the defect content. At very low temperatures, boundary or defect scattering limits the electron mean free path to a temperature independent value and the electronic thermal conductivity varies linearly with temperature.

K_{ph} , the phonon contribution

Here also, the thermal conductivity depends on the nature of the scattering processes, playing a dominant role in the temperature region of concern. K_{ph} can also be split into different components as

$$K_{ph} = \left[(K_{ph,ph})^{-1} + (K_{ph,e})^{-1} + (K_{ph,d})^{-1} \right]^{-1} \quad (1.21)$$

where the subscripts represent, as before, the phonon, electron and defect components.

At high temperatures, phonon - phonon scattering is dominant and the number of phonons excited at any frequency is proportional to the temperature T . In this range of temperatures, the corresponding mean free path is inversely proportional to temperature and hence the thermal conductivity. As the temperature decreases, the mean free path due to phonon - phonon interaction increases exponentially with $1/T$ and K_{ph} also follows such a temperature dependence. At very low temperatures, the primary scattering mechanism is the external boundaries of the specimen and K_{ph} varies

as T^3 . In metals, it is found that there can be an intermediate region in which phonon - electron scattering dominates and K_{ph} varies as T^2 .

The thermal conductivity of a material can show a complicated temperature variation depending on the relative strengths of the electronic and phononic contributions. In a pure metal the electronic contribution dominates while in an alloy or a compound with a relatively high resistivity both contributions may be important in certain temperature ranges.

a. Conventional superconductors

The variation of thermal conductivity with temperature in metallic superconductors has been well explained by the BCS theory, as follows. When a metal becomes superconducting, electrons form Cooper pairs. Such pairs of electrons do not carry entropy and hence cannot contribute to thermal conductivity, while the single particle Fermion excitations do transport heat. As the temperature decreases below T_c the number of such excitations decays exponentially as they form Cooper pairs. The electronic thermal conductivity therefore falls rapidly below T_c .

On the other hand, the phonon contribution K_{ph} will increase as the temperature falls because of the corresponding increase in the mean free path due to the rapid decrease in the number of single particle Fermion excitations in the superconductor. The ultimate temperature dependence of thermal conductivity below T_c will depend upon whether the material is clean or dirty. In ideal superconductors, with no trace of impurities, the phonon contribution is negligible down to the lowest temperature and the electron contribution decreases exponentially to zero. If the superconductor is in the dirty limit, the decreasing electronic contribution to the thermal conductivity will be compensated by the increasing phonon contribution at temperatures below T_c . So the thermal conductivity will show a peak at a certain temperature T_m below T_c . Below T_m , the phonon contribution is dominant and as T tends to zero, thermal conductivity will vary as T^3 .

b. High T_c oxide superconductors

Since in conventional superconductors the main heat carriers are electrons, the thermal conductivity followed by the Wiedmann - Franz relation gives the same information as

that which can be obtained from the more easily measured electrical resistivity. Only well below T_c are phonons the main heat carriers and different information can be extracted. However, phonon scattering in these low temperature regions is mainly due to boundary scattering and no intrinsic features of the sample can be observed. The uniqueness and importance of thermal conductivity measurements in high temperature superconductors become evident at this point. Electrons are not the principal heat carriers in these materials, they only contribute values that range from 3% of the thermal conductivity at 300 K to perhaps 30% in single crystals. In other words, the high transition temperatures get the electrons out of the way at temperatures where phonons can still probe intrinsic properties.

Eventhough there are numerous reports on the thermal conductivity of high T_c materials [73-81], the interpretation of the data is difficult because of a number of reasons. The thermal conductivity of the samples should be anisotropic, but since most of the measurements are made on sintered polycrystalline samples, the value averaged over all possible orientations of the individual grains is obtained. Secondly, the oxygen stoichiometry plays an important role on the superconducting properties and for a given oxygen stoichiometry, the distribution of oxygen atoms do play an important role in defect scattering. Further, the magnetic excitations which are likely to be present in some of the superconductors can play a part in scattering phonons and even in the transport of heat.

In spite of the complications mentioned above, thermal conductivity measurements in high T_c superconductors have revealed a uniformity in behaviour. Above T_c all superconducting samples follow an almost temperature independent behaviour, while at T_c an abrupt increase in K is reported, though the magnitude of this increase differs from one report to another. This behaviour is explained on the basis of electron pairing. The electron - phonon interaction is very strong in these materials and causes a reduction in the phonon mean free path in the normal state. When the material becomes superconducting, the electrons get paired and the phonons cannot be scattered against these pairs anymore and their mean free path and hence the thermal conductivity increases. When the temperature is further lowered, the scattering of phonons by defects,

grain boundaries etc. come into play, causing a reduction in thermal conductivity at low temperatures well below T_c .

1.5.3 Elastic properties - ultrasonic velocity and attenuation

One of the most important measurements for the study of superconducting phase transitions is the velocity and attenuation of ultrasound which probe the elastic properties of the material. Because the elastic moduli and therefore the sound velocities, are directly proportional to the second derivative of the Gibb's free energy with respect to stress, ultrasound provides a direct probe of phase transitions where strain is the order parameter. Additional information such as the coupling of phonons with electrons, relaxation mechanisms etc. can also be derived from the attenuation of ultrasound. Moreover, the measurement of sound velocity can not only provide results that are difficult to obtain by other methods, but also be used to confirm the results of other measurements.

If the elastic constants of a superconductor are measured as a function of temperature, certain features in the vicinity of the transition temperatures can be observed. Many nonoxide superconductors with high T_c 's have transitions that are accompanied by structural instabilities or structural transitions and in some cases the structural transition may be arrested by the onset of superconductivity. Such instabilities are important to the theory of superconductivity. For conventional BCS superconductors the increase of the superconducting transition temperature near a structural instability is understood because the electron pairing mechanism involves strong electron - phonon coupling. For the new oxide superconductors, the role of lattice is uncertain. In this context, the measurement of the elastic constants become important because, as a derivative of free energy, the elastic constants are a sensitive probe of the environment in which the electrons pair.

a. Conventional superconductors

Ultrasonic techniques have commonly been used to study normal metals and superconductors, since it is a very good tool to probe the bulk properties of materials. In conventional superconductors, sound propagation studies have primarily focussed on attenuation since it provides direct measurement of the superconducting energy gap

leading to direct confirmation of the BCS theory.

At high temperatures, the dominant attenuation mechanism is the scattering of the sound wave from dislocations in the lattice. As the temperature is lowered and the electron mean free path becomes longer, the interaction of electrons with the lattice also contributes to the attenuation.

In the limit $ql \ll 1$, where q is the sound wave vector and l is the electron mean free path, the expressions for attenuation α , of longitudinal (L) and transverse (T) sound are given by

$$\alpha_L = \frac{4}{15} \frac{Nm v_F}{\rho v_L} q^2 l \quad (1.22)$$

and

$$\alpha_T = \frac{1}{5} \frac{Nm v_F}{\rho v_T} q^2 l \quad (1.23)$$

where N , m , v_F are the number density, effective mass and Fermi velocity of the electrons, v_L and v_T are the longitudinal and transverse sound velocities and ρ is the density. The attenuation is proportional to the mean free path and the square of the frequency since $\omega = qv$. As the temperature falls, the electron mean free path increases and ultimately saturates because of scattering from imperfections in the crystal.

In the collisionless limit $ql \gg 1$, ie, for high purity samples and/or high frequencies, the attenuation becomes independent of l and is proportional to the frequency f , and the expressions get modified as

$$\alpha_L = \frac{\pi}{6} \frac{Nm v_F}{\rho v_L} q = \frac{\pi^2}{3} \frac{Nm v_F}{\rho v_L^2} f \quad (1.24)$$

and

$$\alpha_T = \frac{4}{3\pi} \frac{Nm v_F}{\rho v_T} q = \frac{8}{3} \frac{Nm v_F}{\rho v_T^2} f \quad (1.25)$$

In most superconducting materials, the electronic contribution to the attenuation drops sharply at T_c , approaching zero as the temperature is lowered. The superconducting state is characterised by the existence of a gap in the energy spectrum, which increases with decreasing temperature, approaching $\Delta = 1.764 k_B T_c$ at zero temperature. The existence of the energy gap implies that there are no unbound electrons to scatter the sound and therefore the attenuation at $T = 0$ should go to zero. At finite

T, thermally excited quasiparticles are present, the distribution of which is governed by the Fermi distribution, leading to an exponential temperature dependence for the attenuation. An expression for the temperature dependent attenuation is given by

$$\left(\frac{\alpha_S}{\alpha_N}\right) = \frac{2}{e^{\Delta(T)/k_B T} + 1} \quad (1.26)$$

where α_S and α_N are the attenuation coefficients in the superconducting and normal states respectively and $\Delta(T)$ is the temperature dependent energy gap.

Elastic measurements, either through sound propagation or through vibrating reed type techniques, are not routinely made in conventional superconductors for the simple reason that the condensation energy per particle is very small, approximately 10^{-6} times the typical elastic energy. The net effect in sound velocity is of the order of a few parts per million and can be studied only with the most precise techniques in the most carefully prepared single crystals. These measurements are used in conventional superconductors to test the thermodynamic relationships that exist among the various second derivatives of the free energy such as compressibility, specific heat and thermal expansion coefficient. These measurements have yielded information on the microscopic parameters involved in the BCS theory such as the strain dependence of the electronic density of states, electron - electron interactions etc.

The isothermal elastic modulus C_{ij} , obtained as the second derivative of the Helmholtz free energy (F) with respect to strain (ϵ) is given by

$$C_{ij} = \left(\frac{1}{V_0} \frac{d^2 F}{d\epsilon_i d\epsilon_j} \right)_T \quad (1.27)$$

where V_0 is the unstrained volume. Substituting the expression for the free energy, the velocity jump at the transition is obtained as

$$C_{ij}^S - C_{ij}^N = -\frac{\alpha^2}{4\pi} \frac{\partial T_c}{\partial \epsilon_i} \frac{\partial T_c}{\partial \epsilon_j} \quad (1.28)$$

where the superscripts S and N refer to the superconducting and normal states respectively.

b. High temperature superconductors

Unlike conventional superconductors, sound propagation in high T_c materials is complex and reflects the remarkably wide range of phenomena exhibited by multiconstituent

oxides. Several factors make the extraction of clear results from acoustic investigations difficult : large anisotropies arising from the 2-D planar structural elements, low crystalline symmetry, sensitivity to oxygen stoichiometry, impurities, magnetic interactions, structural instabilities etc. being a few examples.

The bulk of acoustic investigations of high T_c superconductors have been performed on ceramic samples comprising aggregated micron sized crystallites. Such experiments generally probe spherically averaged properties, which cannot provide any information regarding the anisotropy. Measurements on single crystals is a solution to this problem. However, the successful growth of single crystals is not easy, whereas ceramics have been easy to synthesize. The control of stoichiometry is generally more difficult in crystals as compared to microcrystalline ceramics. As a result there have been only a handful of acoustic studies on high T_c single crystals [82-86].

Extensive sound velocity and attenuation measurements have been reported in ceramic polycrystalline high T_c materials [87-95]. The velocity measurements generally give consistent results over a wide temperature range for both sintered polycrystalline ceramics and single crystals. The velocity generally increases with decreasing temperature and in the vicinity of T_c , there is a change of the derivative of velocity with respect to temperature, though reports vary on the magnitude of this change at T_c . The anomalies exhibited at temperatures above T_c , usually in the range 180 -220 K, the large hysteresis observed in heating - cooling cycles etc. are other interesting features characteristic of these materials.

The discontinuity of velocity at T_c can be explained thermodynamically by the jump in specific heat observed at T_c and by the pressure dependence of T_c . At zero magnetic field, the superconducting transition is a second order phase transition. Starting from one of the TdS equations,

$$TdS = C dT - TV\beta dP \quad (1.29)$$

and a differential equation for $V(P,T)$,

$$dV = \frac{\partial V}{\partial T} dT + \frac{\partial V}{\partial P} dP \quad (1.30)$$

an Ehrenfest's equation for a second order phase transition can be obtained. By using the fact that entropy and the specific volume are continuous across a second order phase transition, we have

$$\begin{aligned}\frac{dP}{dT} &= \frac{\Delta C}{TV\Delta\beta} \\ \frac{dP}{dT} &= \frac{\Delta\beta}{\Delta K}\end{aligned}\quad (1.31)$$

Here the thermal expansion coefficient β and compressibility K are defined as follows.

$$\begin{aligned}\beta &= \frac{1}{V} \frac{\partial V}{\partial T} \\ K &= -\frac{1}{V} \frac{\partial V}{\partial P}\end{aligned}\quad (1.32)$$

After simplification, eliminating $\Delta\beta$, one gets

$$\Delta K = \frac{1}{T_c V} \left(\frac{\partial T_c}{\partial P} \right)^2 \Delta C \quad (1.33)$$

Since the compressibility K is the reciprocal of the bulk modulus B , it follows that

$$\frac{\Delta B}{B} = -\frac{\Delta C}{T_c} B \left(\frac{\partial T_c}{\partial P} \right)^2 \quad (1.34)$$

Similarly the shear modulus G and the strain ϵ at the transition temperature can be written as

$$\begin{aligned}\frac{\Delta G}{G} &= \frac{T\Delta S}{T_c} G \left(\frac{\partial^2 T_c}{\partial \sigma_s^2} \right) \\ \Delta\epsilon_\alpha &= \frac{T\Delta S}{T_c} B \left(\frac{\partial T_c}{\partial \sigma_\alpha} \right)\end{aligned}\quad (1.35)$$

where ΔS is the entropy change at T_c , σ_s is the shear stress, ϵ_α is the generalised strain and σ_α is the conjugate stress.

Ultrasonic attenuation measurements in high T_c materials generally yield three attenuation maxima in the temperature range from 4 K to 300 K in zero magnetic field. One of the three maxima is around the superconducting transition temperature and the other two are located at higher temperatures. The positions of these maxima display considerable frequency and sample dependence. In addition, a peak is observed below

the superconducting transition in some systems. It has been suggested that the change in attenuation is too large to be produced by electron - phonon interaction alone in high T_c materials and the peak below T_c is not directly associated with the superconducting transition. Rather, this behaviour is characteristic of a relaxation process for sound wave attenuation. Anisotropy is another feature observed in attenuation when the measurements are performed in single crystals or sinter forged samples.

1.6 A brief outline of the work presented in the thesis

The following chapters of this thesis give a detailed account of the work carried out on high T_c superconducting samples and the experimental techniques employed for these investigations. The thermal properties such as thermal diffusivity, specific heat and the thermal conductivity of a set of $\text{YBa}_2\text{Cu}_3\text{O}_{7-\delta}$ - SnO_2 composites have been measured employing the photoacoustic technique and differential scanning calorimetry. The effect of Ga doping on the elastic properties of $\text{GdBa}_2\text{Cu}_3\text{O}_{7-\delta}$ superconducting samples is another investigation presented in the thesis. The ultrasonic velocity and attenuation as a function of temperature have been measured in this set of samples using the ultrasonic technique. In addition, the thesis contains numerical investigations carried out on selected superconducting systems. The phase and group velocities have been computed for superconducting LSCO, YBCO and BSCCO for waves propagating in different directions and the corresponding velocity surfaces have been plotted as a function of propagation direction, taking the single crystal elastic constant data available in literature. Another investigation carried out is the evaluation of phonon focussing and amplification for elastic waves of different polarisations propagating along different directions in the superconductors LSCO, YBCO and BSCCO again using the elastic constant data taken from literature. Phonon amplification factors have been plotted as function of the polar and azimuthal angles in a pseudo 3D representation.

1.7 References

- [1] J. G. Bednorz and K. A. Muller, *Z. Phys.* **B64**, 189 (1986).
- [2] C. W. Chu, P. H. Hor, R. L. Meng, L. Gao and Z. J. Huang, *Science* **235**, 567 (1987).
- [3] M. K. Wu, J. R. Ashburn, C. J. Torng, P. H. Hor, R. L. Meng, L. Gao Z. J. Huang, Y. Q. Wang and C. W. Chu, *Phys. Rev. Lett.* **58**, 908 (1987).
- [4] Z. Fisk, J. D. Thompson, E. Zirngiebl, J. L. Smith and S. W. Cheong, *Solid State Commun.* **62**, 743 (1987).
- [5] H. C. Ku, M. F. Tai, S. W. Hsu, K. H. Lii, H. D. Yang and R. N. Shelton, *Chin. J. Phys.* **26**, S99 (1988).
- [6] H. Maeda, Y. Tanaka, M. Fukutomi and T. Asano, *Jpn. J. Appl. Phys.* **27**, L209 (1988).
- [7] R. Sugise, M. Hirabayashi, N. Terada, M. Jo, T. Shimomura and H. Ihara, *Physica* **C157**, 131 (1989).
- [8] C. C. Torardi, M. A. Subramanian, J. C. Calabrese, J. Gopalakrishanan, K. J. Morrisey, T. R. Askew, R. B. Flippen, U. Chowdry and A. W. Sleight, *Science* **240**, 631 (1988).
- [9] T. Zetterer, H. H. Otto, G. Lugert and K. F. Renk, *Z. Phys.* **B73**, 321 (1988).
- [10] S. N. Putilin, E. V. Antipov, O. Chmaissem and M. Marezio, *Nature* **362**, 226 (1993).
- [11] A. Schilling, M. Cantoni, J. D. Guo and H. R. Ott, *Nature* **363**, 56 (1993).
- [12] R. J. Cava, B. Batlogg, J. J. Krajowski, R. Farrow, L. W. Rupp Jr., A. E. White, K. Short, W. F. Peck and T. Kometani, *Nature* **332**, 814 (1988).

- [13] M. A. Subramanian, I. Gopalakrishanan, C. Torardi, T. R. Askew, R. B. Flippen, A. W. Sleight, J. J. Lim and S. J. Poon, *Science* **240**, 495 (1988).
- [14] H. W. Kroto, J. R. Heath, S. C. O'Brien, R. E. Curl and R. E. Smalley, *Nature* **318**, 162 (1985).
- [15] A. F. Hebard, M. J. Rosseinsky, R. C. Haddon, D. W. Murphy, S. H. Glarum, T. T. M. Palstra, A. P. Ramirez and A. R. Kortan, *Nature* **350**, 600 (1991).
- [16] M. J. Rosseinsky, A. P. Ramirez, S. H. Glarum, D. W. Murphy, R. C. Haddon, A. F. Hebard, T. T. M. Palstra, A. R. Kortan, S. M. Zahurak and A. V. Makhija, *Phys. Rev. Lett.* **66**, 2830 (1991).
- [17] K. Tanigaki, T. W. Ebbesen, S. Saito, J. Mizuki, J. S. Tsai, Y. Kubo and S. Kuroshima, *Nature* **352**, 222 (1991).
- [18] S. Uchida, H. Tagaki, K. Kitazawa and S. Tanaka, *Jpn. J. Appl. Phys.* **26**, L1 (1987).
- [19] H. Tagaki, S. Uchida, K. Kitazawa and S. Tanaka, *Jpn. J. Appl. Phys.* **26**, L123 (1987).
- [20] D. M. Paul, G. Balakrishnan, N. R. Bernhoeft, W. I. F. David and W. T. A. Harrison, *Phys. Rev. Lett.* **58**, 1976 (1987).
- [21] P. M. Grant, R. B. Beyers, E. M. Engler, G. Lim, S. S. P. Parkin, M. L. Ramirez, V. Y. Lee, A. Nazzal, J. E. Vasquez and R. J. Savoy, *Phys. Rev.* **B35**, 7242 (1987).
- [22] D. G. Hinks, L. Soderholm, D. W. Capone, J. D. Jorgensen, I. K. Schuller, C. V. Segre, K. Zhang and J. D. Grace, *Appl. Phys. Lett.* **50**, 1688 (1987).
- [23] K. Kadowaki, Y. K. Huang, M. van Sprang and A. A. Menovski, *Physica* **B145**, 1 (1987).
- [24] P. Ganguly, R. A. Mohanram, K. Sreedhar and C. N. R. Rao, *J. Phys.* **28**, L321 (1987).

- [25] T. Siegrist, S. Sunshine, D. W. Murphy, R. J. Cava and S. M. Zahurak, *Phys. Rev.* **B35**, 7137 (1987).
- [26] Y. Syono, M. Kikuchi, K. Oh-ishi, K. Hiraga, H. Arai, Y. Matsui, N. Kobayashi, T. Sasaoka and Y. Muto, *Jpn. J. Appl. Phys.* **26**, L498 (1987).
- [27] C. N. R. Rao, P. Ganguly, R. A. Mohanram and K. Sreedhar, *Nature* **326**, 856 (1987).
- [28] J. L. Tallon, R. G. Buckley, P. W. Gilberd, M. R. Presland, I. W. M. Brown, M. E. Browden, L. A. Christiann and R. Goguel, *Nature* **333**, 153 (1988).
- [29] J. B. Torrance, Y. Tokura, S. J. LaPlaca, T. C. Huang, R. J. Savoy and A. I. Nazzal, *Solid State Commun.* **66**, 703 (1988).
- [30] P. Bordet, J. J. Capponi, C. Chaillout, J. Chenavas, A. W. Hewat, E. A. Hewat, J. L. Hodeau, M. Marezio, J. L. Tholence and D. Tranqui, *Physica* **C156**, 189 (1988).
- [31] M. R. Presland, J. L. Tallon, P. W. Gilberd and R. S. Liu, *Physica* **C191**, 307 (1992).
- [32] M. Hervieu, A. Maignan, C. Martin, C. Michel, J. Provost and B. Raveau, *Mod. Phys. Lett.* **B2**, 1103 (1988).
- [33] D. M. Ogborne and M. T. Weller, *Physica* **C201**, 53 (1992).
- [34] D. M. Ogborne, M. T. Weller and P. C. Lanchester, *Physica* **C200**, 167 (1992).
- [35] D. M. Ogborne, M. T. Weller and P. C. Lanchester, *Physica* **C200**, 207 (1992).
- [36] J. L. Wagner, P. G. Radaelli, D. G. Hinks, J. D. Georgensen, J. F. Mitchell, B. Dabrowski, G. S. Knapp and M. A. Beno, *Physica* **C210**, 447 (1993).
- [37] O. Chmaissem, Q. Huang, E. V. Antipov, S. N. Putilin, M. Marezio, S. M. Loureiro, J. J. Capponi, J. L. Tholence and A. Santoro, *Physica* **C217**, 265 (1993).

- [38] Z. J. Huang, R. L. Meng, X. D. Qiu, Y. Y. Sun, J. Kulik, Y. Y. Xue and C. W. Chu, *Physica C* **217**, 1 (1993).
- [39] H. M. Shao, K. Zhou, Y. Rui, J. C. Shen, X. N. Xu, H. L. Ji, X. X. Yao, L. J. Shen, Z. Wu, Z. J. Li, G. N. Zhang, G. C. Che and Z. X. Zhao, *Solid State Commun.* **92**, 595 (1994).
- [40] H. Schwer, J. Karpinski, L. Lense, C. Rossel, A. Morawski, T. Lada, A. Paszewin, *Physica C* **254**, 7 (1995).
- [41] J. Bardeen, L. N. Cooper and J. R. Schrieffer, *Phys. Rev.* **108**, 1175 (1957).
- [42] H. Rietschel and L. J. Sham, *Phys. Rev.* **B28**, 5100 (1983).
- [43] M. Grabowski and L. J. Sham, *Phys. Rev.* **B29**, 6132 (1984).
- [44] H. Ihara, M. Hirabayashi, N. Tenada, Y. Kimura, K. Seazaki, M. Akimoto, K. Bushida, F. Kawashima and R. Uzuka, *Jpn. J. Appl. Phys.* **26**, L460 (1987).
- [45] D. Allender, J. Bray and J. Bardeen, *Phys. Rev.* **B7**, 1020 (1973).
- [46] W. A. Little, *Phys. Rev.* **134**, A1416 (1964).
- [47] T. T. M. Palstra, A. A. Menovski, J. van den Berg, A. J. Dirkmaat, P. H. Kes, G. J. Nienwenhuys and J. A. Mydosh, *Phys. Rev. Lett.* **55**, 2727 (1985).
- [48] M. B. Maple, J. W. Chen, Y. Dalichaouch, T. Kohara, C. Rossel, M. Torikachvili, M. W. Elfresh and J. D. Thompson, *Phys. Rev. Lett.* **56**, 185 (1986).
- [49] M. T. Beal-Monod, C. Bourbonnais and V. J. Emery, *Phys. Rev.* **B34**, 7716 (1986).
- [50] D. J. Scalapino, E. Loh Jr. and J. E. Hirsch, *Phys. Rev.* **B34**, 8190 (1986).
- [51] K. Miyake, S. Schmitt-Rink and C. M. Varma, *Phys. Rev.* **B34**, 6554 (1986).
- [52] D. Vaknin, S. K. Sinha, D. E. Moncton, D. C. Johnston, J. M. Newsam, C. R. Safinya and H. E. King Jr., *Phys. Rev. Lett.* **58**, 2802 (1987).

- [53] J. M. Tranquada, D. E. Cox, W. Kunnmann, H. Moudden, G. Shirane, M. Suenaga, P. Zolliker, D. Vaknin, S. K. Sinha, M. S. Alvarez, A. J. Jacobson and D. C. Johnston, *Phys. Rev. Lett.* **60**, 156 (1988).
- [54] J. R. Schrieffer, X. G. Wen and S. C. Zhang, *Phys. Rev. Lett.* **60**, 944 (1988).
- [55] T. Holstein, *Annals of Phys. (N4)* **8**, 325 (1959).
- [56] S. Mollah, K. K. Som, K. Bose, A. K. Chakraborty and B. K. Chaudhuri, *Phys. Rev.* **B46**, 11075 (1992).
- [57] L. J. de Jongh, *Physica* **C152**, 1710 (1988).
- [58] V. L. Vinetskii and M. Sh. Giterman, *Sov. Phys. JETP* **6**, 560 (1958).
- [59] V. L. Vinetskii, *Sov. Phys. JETP* **13**, 1023 (1961).
- [60] B. K. Chakraverty and C. Schlenker, *J. de Physique* **37**, suppl.C4, 353 (1976).
- [61] D. J. Scalapino, R. T. Scalettar and N. E. Bickers, in *Novel Superconductivity* (eds. S. A. Wolf and V. Z. Kresin) Plenum, New York, (1987) p.475.
- [62] P. W. Anderson, *Science* **235**, 1196 (1987).
- [63] S. Doniach and S. Engelesberg, *Phys. Rev. Lett.* **17**, 750 (1966).
- [64] E. S. R. Gopal in *Specific Heats at Low Temperatures*, Plenum, New York, (1966).
- [65] R. A. Fisher, J. E. Gordon and N. E. Phillips, *J. Supercond.* **1**, 231 (1988).
- [66] S. E. Inderhees, M. B. Salamon, T. A. Friedmann and D. M. Ginsberg, *Phys. Rev.* **B36**, 2401 (1987).
- [67] M. V. Nevitt, G. W. Crabtree and T. E. Klippert, *Phys. Rev.* **B36**, 2398 (1987).
- [68] N. Wada, T. Obana, Y. Nakamura and K. Kumagai, *Physica* **B165 & 166**, 1341 (1990).

- [69] N. Okazaki, T. Hasegawa, K. Kishio, K. Kitazawa, A. Kishi, Y. Ikeda, M. Takano, K. Oda, H. Kitaguchi, J. Takada and Y. Miura, *Phys. Rev.* **B41**, 4296 (1990).
- [70] T. Atake, H. Kawaji, M. Itoh, T. Nakamura and Y. Saito, *Physica* **C162-164**, 488 (1989).
- [71] J. W. Loram, K. A. Mirza, J. R. Cooper and W. Y. Liang, *Phys. Rev. Lett.* **71**, 1740 (1993).
- [72] O. Jeandupeux, A. Schilling and H. R. Ott, *Physica* **C216**, 17 (1993).
- [73] D. T. Morelli, J. Heremans and D. E. Swets, *Phys. Rev.* **B36**, 3917 (1987).
- [74] C. Uher and A. B. Kaiser, *Phys. Rev.* **B36**, 5680 (1987).
- [75] B. Salce, R. Calemczuk, C. Ayache, E. Bonjour, J. Y. Henry, M. Raki. L. Forro, M. Couach, A. F. Khoder, B. Barbara, P. Burlet, M. J. M. Jurgens and J. Rossat-Mignod, *Physica* **C153-155**, 1014 (1988).
- [76] M. A. Izbizky, M. D. N. Regueiro, P. Esquinazi and C. Fainstain, *Phys. Rev.* **B38**, 9220 (1988).
- [77] M. F. Crommie and A. Zettl, *Phys. Rev.* **B41**, 10978 (1990).
- [78] M. D. N. Regueiro and D. Castello, *Int. J. Mod. Phys.* **5**, 2003 (1991).
- [79] S. T. Ting, P. Pernambucowise and J. E. Crow, *Phys. Rev.* **B50**, 6375 (1994).
- [80] A. V. Inyushkin, A. N. Taldenkov, L. N. Dem'yanets, T. G. Uvarova and A. B. Bykov, *Physica* **B194-196**, 479 (1994).
- [81] J. Isaac, J. Philip, M. T. Sebastian and A. D. Damodaran, *Physica* **C199**, 247 (1992).
- [82] Ming Lei, J. L. Sarrao, W. M. Visscher, T. M. Bell, J. D. Thompson and A. Migliori, *Phys. Rev.* **B47**, 6154 (1993).

- [83] P. Baumgart, S. Blumenroder, A. Erle, B. Hillebrands, G. Guntherodt and H. Schmidt, *Solid State Commun.* **69**, 1135 (1989).
- [84] M. Saint-Paul and J. Henry, *Solid State Commun.* **72**, 685 (1989).
- [85] J. Wu, Y. Wang, P. Guo, H. Shen, Y. Yan and Z. Zhao, *Phys. Rev.* **B47**, 2806 (1993).
- [86] A. Migliori, W. M. Visscher, S. Wong, S. E. Brown, I. Tanaka, H. Kojima and P. B. Allen, *Phys. Rev. Lett.* **64**, 2458 (1990).
- [87] D. J. Bishop, P. L. Gammel, A. P. Ramirez, R. J. Cava, B. Batlogg and E. A. Rietman, *Phys. Rev.* **B35**, 8788 (1987).
- [88] S. Hoen, L. C. Bourne, C. M. Kim and A. Zettl, *Phys. Rev.* **B38**, 11949 (1988).
- [89] J. Dominec, P. Vasek, P. Svoboda and V. Plechacek, *Mod. Phys. Lett.* **B6**, 1049 (1992).
- [90] J. Dong, T. Deng, F. Li and Y. Yao, *Phys. Rev.* **B42**, 301 (1990).
- [91] K. J. Sun, W. P. Winfree, M. F. Xu, M. Levy, B. K. Sarma, A. K. Singh, M. S. Osofsky and V. M. Le Tourneau, *Phys. Rev.* **B42**, 2569 (1990).
- [92] Y. Horie, T. Fukami and S. Mase, *Solid State Commun.* **63**, 653 (1987).
- [93] P. V. Reddy, S. Shekar and K. Somaiah, *Mat. Lett.* **21**, 21 (1994).
- [94] E. Biagi, E. Borchini, R. Garre, S. De Genaro, L. Masi and L. Masotti, *Phys. Status Solidi* **A138**, 249 (1993).
- [95] J. Dominec, *Acta Phys. Slovaca* **43**, 153 (1993).

Chapter 2

Experimental Techniques

2.1 Introduction

In this chapter, the different experimental techniques employed for the investigations presented in the thesis are described. Three different techniques have been used for these studies. They are

1. Photoacoustics
2. Differential scanning calorimetry
3. Ultrasonics

A description of each of the experimental methods and setups used for the measurements is given in the following sections.

2.2 Photoacoustics

The photoacoustic (PA) effect has its origin long back in 1880, when Alexander Graham Bell [1,2] discovered that when a periodically interrupted beam of sunlight falls on a solid in an enclosed cell, an audible sound could be heard. Subsequent studies by other scientists revealed that this effect was not exhibited by solids alone, but an acoustic signal was found to be produced when a liquid or gas in an enclosed cell was illuminated with chopped light. However, the potentialities of this technique in the study of thermal and optical properties of solids remained almost unexploited until the advent of the microphone. Since then this technique has evolved as a very powerful method for the investigation of solid samples.

The PA effect is the generation of an acoustic signal when the sample under

investigation, placed inside a closed cell, is irradiated by an intensity modulated beam of light. In the case of gas and liquid samples, the sample fills the entire volume of the cell, while the solid sample occupies only a portion of the cell and the remaining volume of the cell is filled with a nonabsorbing gas such as air. The internal energy levels of the sample are excited by the absorption of incident radiation and upon subsequent deexcitation, all or part of the absorbed photon energy is converted into heat through nonradiative deexcitation processes. In the case of solid samples, this periodic heating of the sample results in a periodic heat flow from the interior of the sample to the surrounding gas which in turn produces pressure fluctuations in the gas which can be detected as an acoustic signal by the microphone. In gas and liquid samples, the internal heating causes pressure fluctuations having the same frequency as that of the incident beam, which can be detected by an acoustic transducer.

Eventhough the PA effect was discovered more than a century ago, a proper theoretical understanding of this effect in solids was lacking until recently despite several attempts by many physicists. Though it was correctly deduced by Bell himself that the PA effect is due to the internal heating of the sample by the absorbed energy, the generation of the acoustic signal due to this heating could not be correctly explained. Many suggestions were put forward to explain the generation of the acoustic signal [3-5], but were found to be inadequate in explaining the experimental results.

The present understanding of the PA effect in solids is based on the general theory developed by Rosencwaig and Gersho (R-G theory) [6,7], which has been found to be very successful in interpreting most of the experimental observations. The theory predicts that in a gas - microphone PA cell, the signal depends both on the generation of an acoustic pressure wave at the sample - gas interface and on the transport of this pressure disturbance through the gas to the microphone. The pressure fluctuations at the sample - gas interface are caused by the periodic heat flow from the sample which is governed by thermal diffusion equations. Rosencwaig and Gersho solved the thermal diffusion equations for the sample, the backing material on which the sample is mounted and the gas in the cell and obtained exact expressions for the periodic temperature at the sample - gas interface. However, a detailed discussion of the theory is not presented

here since it is beyond the scope of this chapter.

2.2.1 The Photoacoustic setup

The photoacoustic method has been used extensively in the study of optical and thermal properties of solid samples. The essential modules of a PA spectrometer are a source of intensity modulated optical radiation, a PA cell which incorporates the microphone and the electronics for detecting the photoacoustic signal.

A block diagram of the PA setup used for the temperature dependent studies described in the next chapter is shown in Fig. 2.1. It consists of (i) a 1000 W Xe arc lamp, (ii) an electromechanical chopper, (iii) a variable temperature PA cell, (iv) a lock-in amplifier and (v) a temperature controller. A brief description of each of these components is given below.

The light source we have used, *i. e.*, the 1000 W high pressure Xenon arc lamp (Spectroscopy Instruments, Model SVX 1000) has got a continuous emission from 280 to 2500 nm with high intensity in the visible region. The power of the lamp can be varied from 600 to 1000 W and the intensity of the lamp is found to be highly stable.

Intensity modulation of the incident light beam is accomplished by an electromechanical chopper (Photon Technology International, Model OC 4000). Using two discs, the chopping frequency can be varied continuously from 4 to 4000 Hz. The chopper also provides appropriate reference signal to the lock-in amplifier with excellent phase stability.

The PA cell, which forms the central part of the PA spectrometer, can be used over a wide range of temperature, from 85 - 450 K. Fig. 2.2 shows the schematic diagram of the PA cell used for our studies. The sample compartment made out of a brass rod, is in the form of a cold finger, one end of which is in contact with a liquid nitrogen reservoir and is kept inside a vacuum chamber. The sample cell is sealed with a window against the vacuum outside using an 'O' ring made of indium wire. The liquid nitrogen reservoir has a double wall construction, with the vacuum extending throughout the interior of the walls. The microphone compartment is integrated with the other endside wall of the outer chamber and is acoustically coupled to the sample cell through a thin

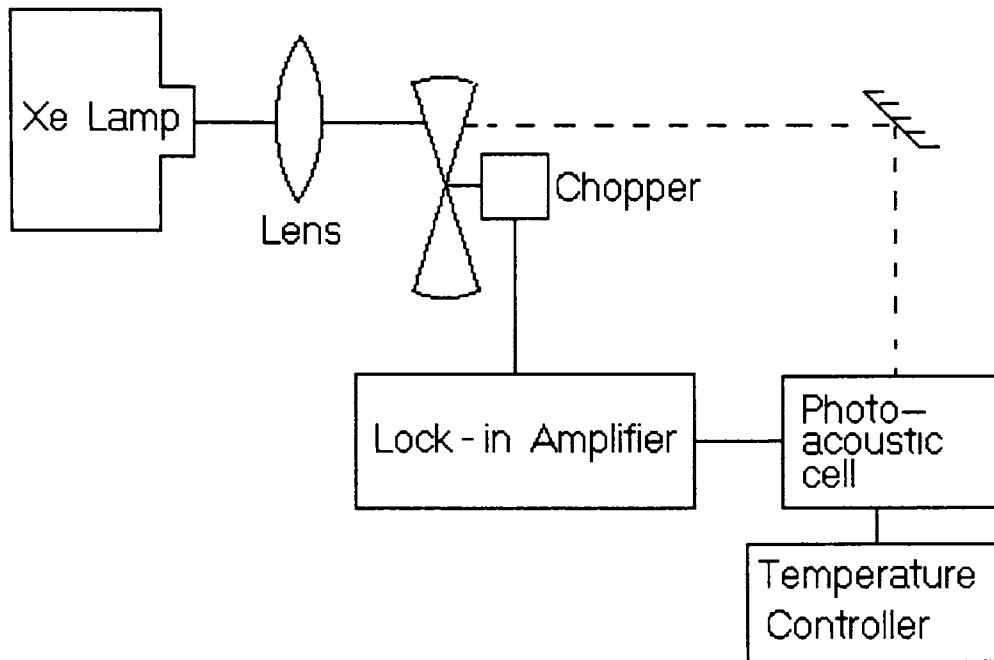
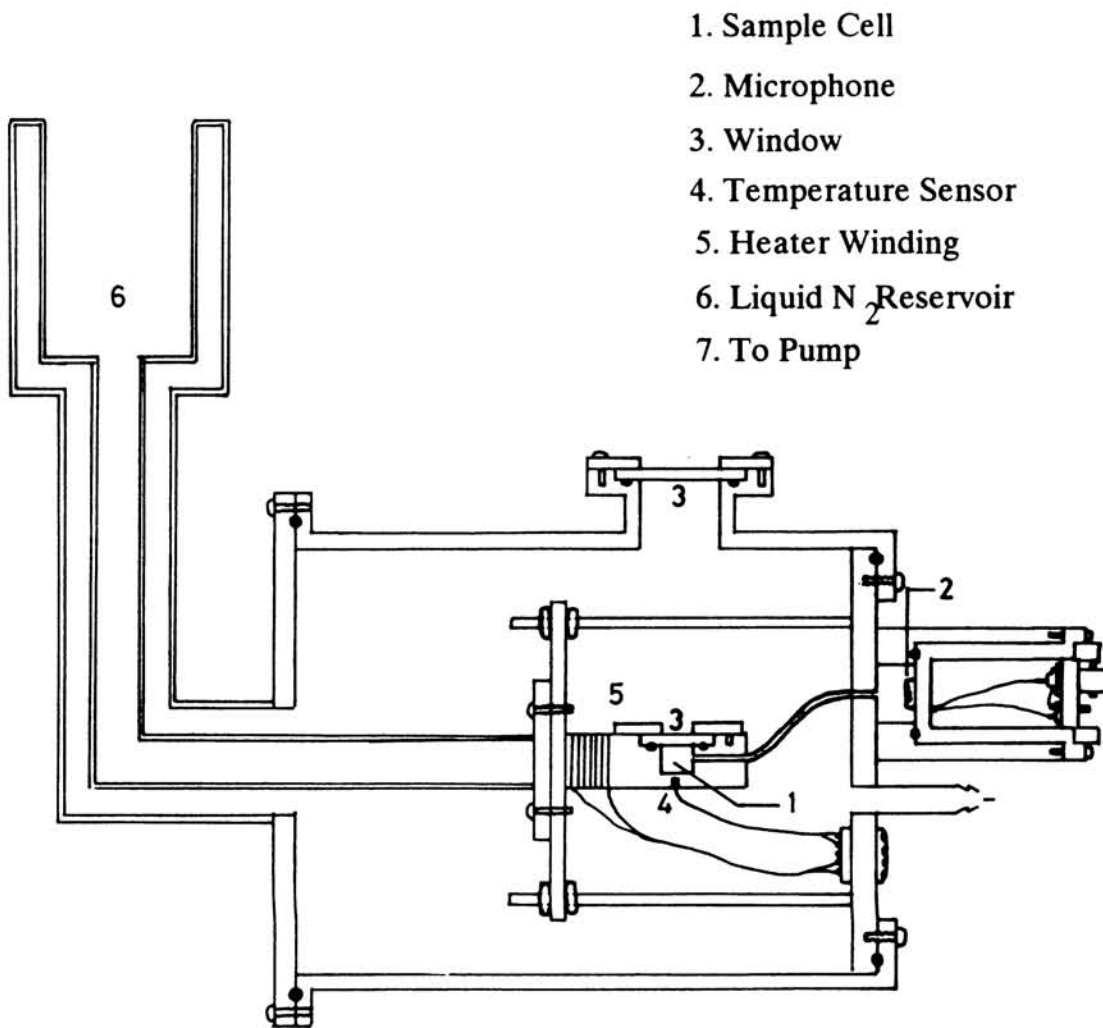


Fig. 2.1

Schematic representation of the photoacoustic setup.



1. Sample Cell
2. Microphone
3. Window
4. Temperature Sensor
5. Heater Winding
6. Liquid N₂ Reservoir
7. To Pump

Fig. 2.2

Schematic diagram of the variable temperature PA cell.

walled stainless steel tube. This configuration permits large variations in the sample temperature without altering the microphone temperature appreciably. The sample temperature is detected by a platinum resistance sensor and can be varied by the heater wound around the cold finger. Both the temperature sensor and heater are connected to a temperature controller. The modulation frequency and temperature dependence of the cell have been characterised using carbon black sample. The resonant frequency of the cell is determined to be around 310 Hz at room temperature.

A small size flat type electret microphone (Knowles, Model BT 1759) is used in the PA cell to pick up the generated acoustic signals. It has got a flat frequency response in the range 10 to 5000 Hz and a high sensitivity of 10 mV/Pascal.

The PA signal detected by the microphone is processed using a single phase lock-in amplifier (Stanford Research Systems, Model SR 510). The lock-in amplifier has a built in preamplifier providing a full scale sensitivity of 10 nV maximum. It has an operating frequency range from 0.5 Hz to 100 kHz. Phase can be adjusted in large steps of 90° and fine steps of 0.025°.

The temperature dependent studies have been carried out with the help of a temperature controller (Lakeshore Model DR 82C). This is a three mode controller utilizing the proportional, integral and derivative functions (PID). There are provisions to use two temperature sensors - one as control sensor and the other as sample sensor.

2.2.2 Thermal diffusivity measurements using PA technique

Using the photoacoustic technique, the thermal diffusivity of the superconducting samples have been measured at different temperatures. This has been done by measuring the amplitude of the PA signal as a function of the chopping frequency f . The amplitude of the PA signal is determined primarily by the amplitude of the temperature oscillations at the sample surface and it is governed by the thermal diffusivity (α) of the sample, which is related to other thermal parameters of the sample by

$$\alpha = \frac{K}{\rho C} \quad (2.1)$$

where K , ρ and C are the thermal conductivity, density and specific heat of the sample respectively.

The R-G theory predicts different quantitative relations between α and the PA signal depending upon the experimental conditions. One of the parameters which determine the amplitude of the PA signal is the thermal diffusion length μ , which is defined as

$$\mu = \sqrt{\frac{\alpha}{\pi f}} \quad (2.2)$$

where f is the chopping frequency. When the chopping frequency is varied, μ changes giving two different conditions according to the relative magnitudes of the thermal diffusion length μ as compared to the physical length l of the sample. For a sample thickness l , mounted on a suitable backing material, at low chopping frequencies when $\mu > l$, the acoustic signal varies as ω^{-1} (where $\omega = 2\pi f$) and depends on the thermal properties of the backing material and this condition of the sample is referred to as thermally thin regime. At higher chopping frequencies, μ becomes less than l and the PA signal reflects the thermal properties of the sample material and is independent of the properties of the backing material. In this condition the sample is said to be thermally thick and the acoustic signal varies as $\omega^{-3/2}$ in this regime. So for an appropriate sample thickness, one can obtain a crossover from the thermally thin regime to the thermally thick regime by increasing the chopping frequency. The amplitude versus chopping frequency plot hence shows a change in slope at the characteristic frequency f_c at which the crossover takes place. The characteristic frequency f_c is related to the thermal diffusivity of the sample by the relation [8]

$$\alpha = f_c l^2 \quad (2.3)$$

f_c can be determined from the amplitude versus chopping frequency plot and measuring the sample thickness l , α can be calculated using the above relation.

2.3 Differential Scanning Calorimetry

Whenever a material undergoes a change in its physical state such as melting or transition from one crystalline form to another, or whenever it reacts chemically, heat is either absorbed or liberated. In other words, thermal changes in a sample are due to endothermic or exothermic enthalpic transitions or reactions. Such enthalpic changes

can be caused by phase changes, fusion, crystalline inversions, boiling, sublimation, vapourisation, oxidation, reduction or other chemical reactions. Generally phase transitions, dehydration, reduction and some decomposition reactions are endothermic in nature, whereas crystallisation, oxidation etc. are exothermic.

In order to study the thermal behaviour of materials as they undergo physical and chemical changes during heat treatment, several experimental techniques have been developed over the past years. Differential Scanning Calorimetry (DSC), Differential Thermal Analysis (DTA), Thermogravimetry (TG), Thermo Mechanical Analysis (TMA), dilatometry etc. are a few examples of the techniques which can be used to detect the physical and chemical changes which are accompanied by a gain or loss of heat in a material as its temperature is varied.

Among these different techniques, the DSC and DTA are being used widely, since the thermal properties of a wide variety of materials can be investigated and are particularly useful tools in the characterisation of organic polymers, biological materials, inorganics, amorphous alloys etc. In addition, they find applications in qualitative and quantitative evaluation of phase transformations such as glass transition, melting, crystallisation etc., study of polymerisation, determination of thermal and processing histories etc.

In DSC, the thermal behaviour of the material is studied by measuring the differential heat flow required to maintain the sample material and an inert reference material at the same temperature, while in DTA the temperature difference arising between the sample and reference materials is measured as both are heated at a constant rate in the same environment. Although DSC yields data which are inherently more qualitative and more amenable to theoretical interpretation than the DTA data, it does not seem to have been used as widely as the latter. The DSC technique has been applied, however, to diverse types of compounds and reviews on the application of DSC to petroleum products, plastics, biological systems, metal complexes, polymers etc. have appeared in literature [9-13].

The term differential scanning calorimetry was first used by Watson *et al.* [14] to describe the instrumental technique developed by the Perkin - Elmer Corporation.

This technique, as mentioned earlier, maintains the sample and reference materials isothermal to each other by proper application of electrical energy, as they are heated or cooled at a linear rate. The curve obtained is a recording of heat flow dH/dt in mcal/sec as a function of temperature. In the true thermodynamic sense, an endothermic peak curve is indicated by a peak in the upward direction, indicating an increase in enthalpy, while an exothermic peak is recorded in the opposite direction. The area enclosed by the DSC curve peak is directly proportional to the enthalpy change, as in DTA.

Though this technique suffers from serious limitations such as relatively low accuracy and precision, inability to determine the enthalpy changes of overlapping reactions conveniently etc., it has got many advantages over conventional calorimetric techniques. Rapidity in the determination of thermal properties over a wide temperature range, small amounts sample required for measurements, easy data analysis procedure, ability to study many different types of reactions etc. are some of the unique features possessed by the DSC technique.

2.3.1 The experimental setup

Generally two different types of techniques - power compensated DSC and heat flux DSC - are used to obtain calorimetric data. In power compensated DSC, the sample and reference materials are heated by separate heaters in such a way that their temperatures are increased or decreased linearly. In heat flux method, the difference in heat flow into the sample and the reference material is measured as the sample is heated or cooled linearly. Although the two methods provide the same information, the instrumentation for these two is fundamentally different.

We have used the DSC-7 differential scanning calorimeter (Perkin - Elmer) for our measurements which operates in the power compensation design. With the 3700 Data station, the modular DSC-7 permits the direct calorimetric measurement, characterisation and analysis of thermal properties of materials. Under the control of the computer, the DSC-7 is programmed from an initial to a final temperature through transitions in the sample material.

Platinum resistance heaters and thermometers are used in DSC-7 to accom-

plish the temperature and energy measurements. The continuous and automatic adjustment of heater power necessary to keep the sample holder temperature identical to that of the reference holder provides a varying electrical signal equivalent to the varying thermal behaviour of the sample. This measurement is made directly in energy units (mW), providing true electrical energy measurements of peak areas.

For standard operation the DSC-7 is equipped with an insulated reservoir which allows the use of ice water coolant. In this configuration it can be operated from 25°C to 730°C. With additional accessories, the temperature can be lowered to liquid nitrogen temperature. The scanning rate, *i.e.*, the rate at which the sample is heated or cooled can be varied over a wide range from 0.1°C to 200°C/minute in steps of 0.1°C/minute.

Before any quantitative measurement is made, the calorimeter must be calibrated for the temperature and energy scales. High purity metals with accurately known enthalpies of fusion are generally used as calibration standards. Zinc and indium are the commonly used calibrants, using which the instrument can be calibrated over a wide temperature range.

2.3.2 Specific heat measurements using DSC

Determination of specific heat of a material is accomplished in two ways, depending on the temperature range in which the property is to be measured. From cryogenic temperatures to approximately 350 K, adiabatic calorimeters are usually used, while at higher temperatures, the drop calorimeter using the method of mixtures is generally preferred.

Though these techniques can provide fairly accurate results, there are some serious drawbacks too. For example, the analysis time is prohibitively long, large samples are required for the measurements and sample geometries must be carefully controlled for the accurate determination of the specific heat. Another objection to these techniques concerns their precision at transition temperatures of the sample material.

The differential scanning calorimetry can also be used for the direct measurement of the specific heat of materials. The basic principle involved is that when a sample

is subjected to a linear temperature increase, the rate of heat flow into the sample is directly proportional to the instantaneous specific heat of the sample. By measuring this heat flow rate as a function of temperature and comparing it with a standard material under the same conditions, one can obtain the specific heat as a function of temperature [15, 16].

The procedure to determine the specific heat of a material using DSC is briefly described below. Empty aluminium pans are placed in the sample and reference holders. An isothermal baseline is recorded which indicates the differential losses of the two sample holders caused by the thermal capacity mismatch between the two sample holders and their contents. The procedure is then repeated with a weighed amount of the sample placed in the sample holder. There is an offset from the baseline owing to the absorption of heat by the sample. The heat flow rate into the sample is then given by

$$\frac{dH}{dt} = m C_p \frac{dT}{dt} \quad (2.4)$$

where dH/dt is the heat flow rate, m is the sample mass, C_p is the specific heat and dT/dt is the programmed rate of temperature increase.

Eqn.(2.4) can be used for the specific heat calculation, but the ordinate calibration and the temperature program rate must be known with at least the precision required for the final result. However, these parameters can be eliminated from the calculation if a material with a known specific heat is used to calibrate the instrument. Such a material is α - aluminium oxide or synthetic sapphire, for which the specific heat has been determined to five significant figures in the temperature range 0 to 1200 K [17].

In order to avoid the errors, the above procedure is repeated with a known mass of sapphire, after the baseline and sample programs. Then at any temperature T , the following equations apply :

$$K y = m C_p \frac{dT}{dt} \quad (2.5)$$

$$K y' = m' C_p' \frac{dT}{dt} \quad (2.6)$$

where y and y' are the ordinate deflections due to the sample and the standard respectively, as is shown in Fig. 2.3. m' and C_p' are the mass and specific heats of the standard and K is the ordinate calibration factor.

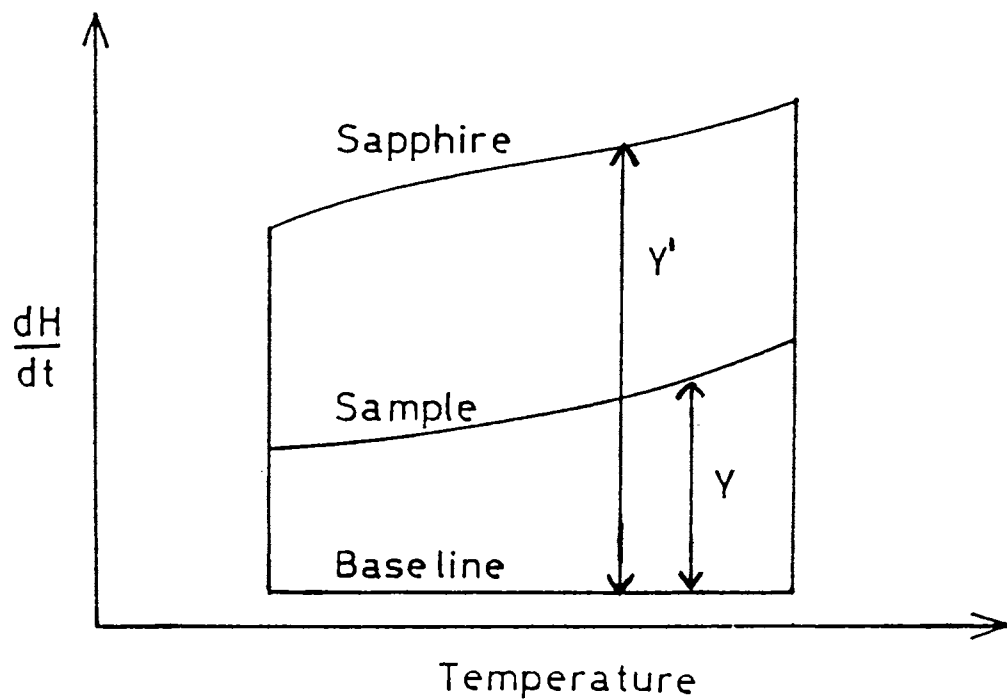


Fig. 2.3
Specific heat determination by ratio method.

Dividing eqn.(2.5) by (2.6) and rearranging terms,

$$\frac{C_p}{C_p'} = \frac{m'y}{my'} \quad (2.7)$$

Thus the determination of the specific heat requires only the comparison of two ordinate deflections at the same temperature and this method of determining the specific heat is referred to as the ratio method [15]. It has been observed that, in this method the calculation of specific heat would be correct even if the ordinate calibration and the program rate are temperature dependent.

2.4 Ultrasonic Technique

Study of elastic wave propagation through solids is very important both from scientific and technological points of view since it enables to probe the bulk elastic properties as well as microscopic lattice dynamical properties of materials. Since the measurement of elastic response can provide a lot of information about the nature of transition and the order parameter involved, they become very valuable in phase transition studies as well. While determination of elastic constants by measuring ultrasound velocities helps to locate transition points, to determine phase diagrams etc., ultrasound attenuation measurements provide direct information about the dynamic behaviour of the system.

2.4.1 Ultrasonic velocity and attenuation measurements in solids

As the measurement of acoustic parameters is very important in characterising materials, several experimental methods have been developed for the purpose, such as torsion pendulum, resonance - antiresonance, ultrasonics, hypersonics, Brillouin scattering etc. for different frequency ranges. Among these, ultrasonic techniques have been widely used in the study of elastic properties of solids because of the higher frequency range (1 MHz - 1 GHz), greater variability and sensitivity compared to other methods. Besides, the ultrasonic techniques enable one to make simultaneous velocity and attenuation measurements very accurately.

The ultrasonic techniques again can be broadly divided into two categories - continuous wave (cw) methods and pulse methods. In the cw method, a standing wave pattern is obtained in a specimen by applying an acoustic excitation such that an integral number of half wavelengths are set up between the opposite faces of the sample. Using frequency modulation techniques, one can measure changes in velocity and attenuation of the specimen. Though this technique provides results with high precision, there are several sources of error in this method and proper corrections are required. cw methods are seldom used for low temperature measurements because of sample heating due to the large input power into the sample.

The pulse methods are very popular and in its simplest form, an ultrasonic pulse of short duration is injected into the sample by a piezoelectric transducer made of materials like quartz, LiNbO_3 , BaTiO_3 , SrTiO_3 etc. This pulse sent into the sample is almost perfectly reflected at the opposite air - sample interface and it returns to the transducer - sample interface, where all but a small fraction of energy is again returned to the sample. By the time the first echo has arrived back at the transducer, the transducer has been turned off. The transducer converts a small amount of the energy of the returned pulse into electrical energy. This electrical signal is amplified by an appropriate receiver and the result is displayed on an oscilloscope. The other portion of the acoustic energy gets reflected at the transducer - sample interface and the process described above is repeated. The received signals can be seen on the oscilloscope screen as a series of echoes. Because of multiple reflections, each time the stress wave passes through the sample, a fraction of its energy is absorbed or scattered. The result is an exponentially decaying echo pattern. By measuring the time between two successive echoes and knowing the thickness of the sample, the ultrasonic velocity can be determined. Attenuation can be measured by observing the decay rate of these successive echoes.

Considering the plane attenuated wave as represented by

$$A(x, t) = A_0 e^{-\alpha x} e^{i(\omega t - kx)} \quad (2.8)$$

the attenuation factor α can be defined as the imaginary part of the complex propagation

vector, while the phase velocity v_p is given by the real part. Then the attenuation can be expressed as

$$\alpha = \frac{1}{(x_2 - x_1)} 20 \log_{10} \left(\frac{A(x_1)}{A(x_2)} \right) \quad dB/unitlength \quad (2.9)$$

where $A(x_1)$ and $A(x_2)$ are the amplitudes of the two echoes and $x_2 - x_1$ represent the distance between these echoes.

There are a number of pulse techniques used for accurate ultrasonic velocity and attenuation measurements, and among them the most important and widely used ones are the pulse superposition technique, sing - around technique and pulse echo overlap technique. Since we have used the pulse echo overlap technique in our measurements, it is discussed in some detail in the following section.

2.4.2 Pulse Echo Overlap Method

The Pulse Echo Overlap (PEO) method is a very versatile and highly accurate technique for measuring the velocity of ultrasonic waves in materials and structures [18-21]. The absolute accuracy of this method arises from the fact that the method is capable of measuring accurately from any cycle of one echo to the corresponding cycle of the next echo. In addition, the attenuation of the ultrasonic wave can be measured simultaneously in this technique.

In PEO method, the rf pulse is applied to the sample through a transducer which is bonded to the sample. A series of echoes is obtained on the oscilloscope screen as explained earlier. In order to measure the time between two echoes, the two echoes of interest are overlapped on the oscilloscope screen by driving the x - axis with a frequency whose period is the travel time between the signals of interest. Then one echo appears on one sweep and the other on the next sweep on the oscilloscope screen and thus echo overlap is effected optically on the screen. Instead of driving the x - axis directly using a cw, a trigger pulse generated from this can also be used to trigger the x - axis of the oscilloscope and this is more convenient. For jitter free overlap the signals of interest must be synchronised with the phase of the cw voltage. This condition is achieved by generating the repetition rate of the input rf pulse from the phase of the cw voltage by

a frequency divider. Division by a large integer of the order of 100 or 1000 allows all the echoes from one pulse to be attenuated before the next pulse is applied. The output of the frequency divider is a trigger signal synchronous with the cw voltage and it triggers a pulsed rf oscillator which is connected to the transducer. The echoes are amplified by an amplifier and a diode limiter circuit keeps the input pulse from overloading the amplifier. The trigger signal also triggers two intensifying pulses which are applied to the oscilloscope to select any pair of echoes of interest and to blank out all other signals.

To make a measurement, the oscilloscope is first set in the triggered mode of operation. The delays and widths of the intensifying pulses are then adjusted to cover the signals of interest. The frequency of the cw oscillator is then set approximately as the reciprocal of the travel time between the signals of interest. The oscilloscope is switched to the driven x - axis mode of operation and the intensity is adjusted so that only the two selected echoes are visible. Then the cw frequency is adjusted so that the two signals overlap as shown in Fig. 2.4.

In order to accomplish an overlap, any pair of echoes can be chosen. However, this may lead to a cycle mismatch relative to the true delay in the specimen and a proper correction has to be applied. To decide which cycle is the proper one in each echo for matching, a technique called Mc Skimin Δt criterion [22,23] is used. It was developed for the pulse superposition technique initially and later it was shown by Papadakis [19] that the same can be applied to the PEO method when run with rf pulses exciting transducers bonded to the specimen directly. A computer program written in BASIC [24] to make the corrections numerically has been used to make the Mc Skimin Δt criteria in our measurements.

Ultrasonic attenuation α is measured as the logarithm of the ratio of the amplitudes of the ultrasonic wave at two distances along its propagation path. For a plane wave and a linear sensor that could not perturb the wave, attenuation can be given by [25, 26]

$$\begin{aligned} \alpha &= \frac{\ln(A_1/A_2)}{x_2 - x_1} \text{ nepers/unitlength} \\ &= \frac{20 \log(A_1/A_2)}{x_2 - x_1} \text{ dB/unitlength} \end{aligned} \quad (2.10)$$

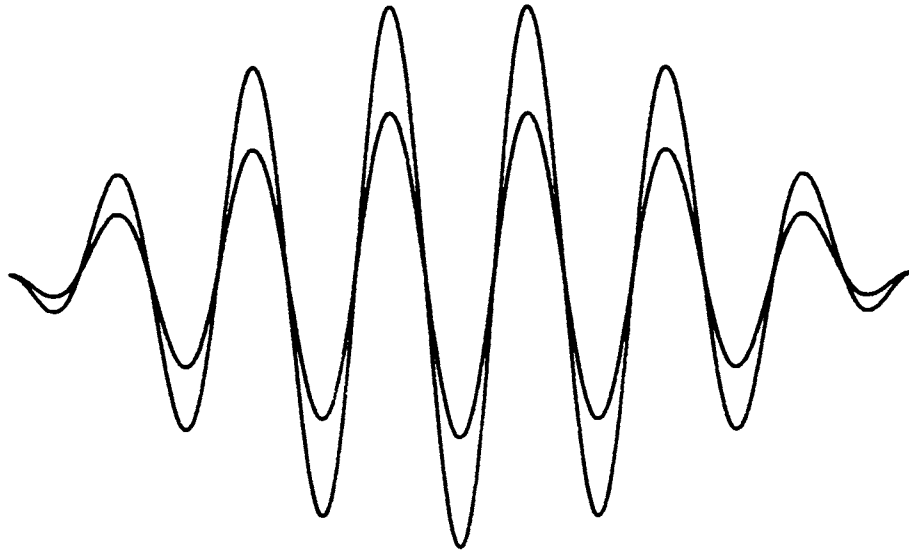


Fig. 2.4

Echo pair in the overlapped condition.

where A_1 and A_2 are the amplitudes of echoes sensed at positions x_1 and x_2 .

Various schemes have been developed to find the amplitudes of the echoes. MATEC has developed an automatic version of the attenuation measuring system, which has been used in our measurements. In this, two gates with variable delay are set on the two echoes of interest to sample them. The amplitude of the first echo is held constant by an AGC circuitry, and the amplitude of the second echo is sampled at its peak. A calibrated logarithmic amplifier converts the sample amplitudes to decibels relative to the constant amplitude of the first echo. The decibel level can be either recorded on a built-in strip chart recorder or can be read on a readout meter.

2.4.3 The ultrasonic experimental setup

The block diagram of the experimental setup used for measuring ultrasonic velocity using pulse echo overlap technique and attenuation by pulse comparison technique is given in Fig. 2.5. The system consists of the MATEC Model 7700 pulse modulator and receiver together with Model 760V rf plug-in, Model 122B decade divider and dual delay generator, Model 110 high resolution frequency source, Model 2470B attenuation recorder, Model 70 impedance matching network, HIL Model 2722 frequency counter and HIL Model 5022 oscilloscope. In order to carry out temperature dependent studies a cryostat and a temperature controller (Lakeshore Model DR 82C) have also been used.

The heart of the system is the pulse modulator and receiver with the RF plug-in. The pulse oscillator can be triggered either with an external sync pulse or with an internally produced one, which gives a peak power of 1 kW and a total receiver gain of 110 dB. It can provide rf frequency in the range 10 - 90 MHz. The cw signal from the high resolution frequency source is applied to the decade divider and dual delay generator, which is the key interfacing unit between the cw source and the pulsed oscillator in the PEO method. The output of the cw source is highly stable and can be varied from 0.5 Hz to above 50 MHz. The cw source is operated at a frequency whose period is equal to the round trip time in the sample under investigation. The trigger signal of the pulsed oscillator is obtained from the divided sync output of the decade divider and dual delay generator. The output of the cw source is applied to this decade

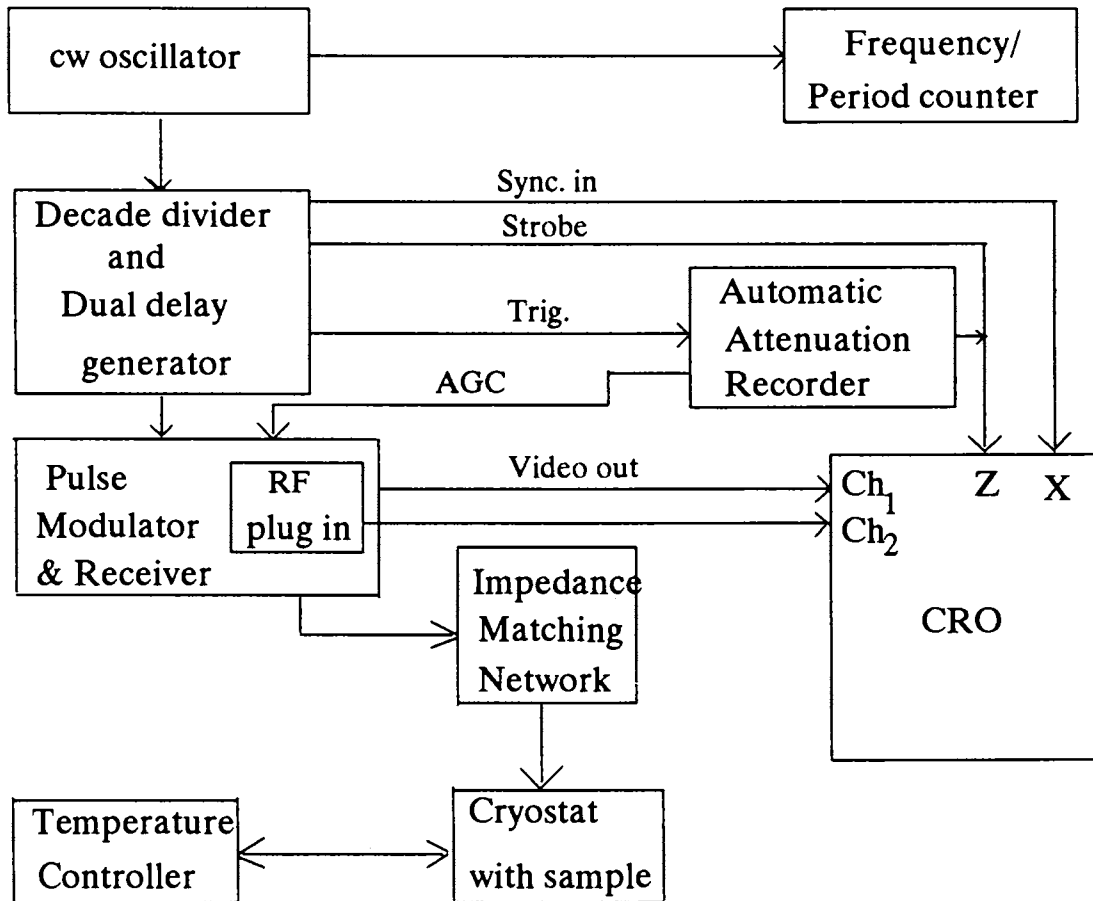


Fig. 2.5

Block diagram of the experimental setup for measuring ultrasonic velocity by Pulse Echo Overlap technique and attenuation by Pulse Comparison technique.

divider and dual delay generator and the divided sync output is obtained by dividing the cw signal by 10, 100 or 1000 which can be selected. Another output of this is the sweep sync out for the external trigger of the oscilloscope. This can be set in two modes, either equal to the divided frequency of the divided sync output or equal to the applied cw frequency itself. The first one is for getting a stable echo pattern on the oscilloscope and the latter is for overlapping purpose. It also provides two strobe outputs whose width and delay can be controlled, and it is applied to the z - axis of the oscilloscope for intensifying the desired echo pair. The frequency counter is directly connected to the high resolution frequency source to measure the frequency of the cw wave.

For attenuation measurements, the Model 2470B automatic attenuation recorder is incorporated in the setup. This also has a strobe output for selecting the desired echo pair for attenuation measurement. It provides the necessary AGC output to connect to the pulse modulator and receiver for keeping the amplitude of the first echo constant during the measurement. The attenuation value can be either recorded in a strip chart or can be seen on a panel meter. The sensitivity of the attenuation recorder can be varied from 0.01 dB to 20 dB/ division.

The transducer is bonded to the sample using a proper bonding medium. Silicone grease and Nonaq stopcock grease are found to be very good bond materials for longitudinal measurements at room temperature as well as at low temperatures, while for transverse waves silicone grease is found suitable for most samples.

The sample bonded to the transducer is connected to the pulse output of the system through an impedance matching network for optimum power transfer. Keeping the sweep sync out at the divided position, the echo pattern can be observed on the oscilloscope screen. Then, using the strobe signals from the decade divider and dual delay generator, any echo pair is selected and the approximate time difference between the two echoes are noted. The frequency of the high resolution frequency source is then fine adjusted so that its period is equal to this time difference. The sweep sync out is then changed to the direct position and the echoes are seen as approximately overlapped. By adjusting the cw source the echoes are overlapped exactly and the frequency is measured from the frequency counter. By determining the travel time from

this frequency, the velocity can be obtained.

In order to make temperature dependent studies, a bath type cryostat has been used in which liquid nitrogen is used as the cryogen. Fig. 2.6 gives a cross sectional view of the cryostat. The main parts are two stainless steel vessels. The first chamber is a double walled vessel A and the space between these walls can be evacuated through a port P1 by connecting it to a rotary vacuum pump, which reduces heat loss. The second vessel B is single walled and both the vessels are fixed to an upper annular flange F1. Liquid nitrogen can be poured to the space between the two vessels (C1) through two tubes T1. There is an upper flange F2 which rests over a rubber 'O' ring placed on the annular flange. One end of two stainless steel tubes T2 are fixed to the centre of this upper flange, while the other end is connected to the sample chamber C3. This can be evacuated or liquid nitrogen can be poured into it using the two ports P3. The stainless steel tube also houses all the electrical connections from the sample chamber to the appropriate connectors.

The sample chamber consists of small discs which acts as the platforms to place the sample (S) and the spring mechanisms for fixing the transducer. This arrangement is covered by a copper chamber on which a heater (H) is wound, and the sample chamber can be vacuum sealed using Wood's metal. Two temperature sensors (R) are used, one is placed very near the heater coil which is the control sensor and the other very close to the sample which is the sample sensor. The terminals of the sensors are taken out through a 9 pin D-type connector (E2) and the heater power from the temperature controller is applied through a 3 pin connector.

In ultrasonic experiments, it is most essential that the cooling rate of the sample be kept very small to avoid cracking of the sample. Moreover, if the cooling rate is not small, thermal gradients may be developed within the sample which can cause many undesired effects. Thus a slow and uniform heating (cooling) is necessary. In our setup a cooling rate of 1 K/ min. or less can be obtained and measurements can be made in the temperature range 80 - 300 K.

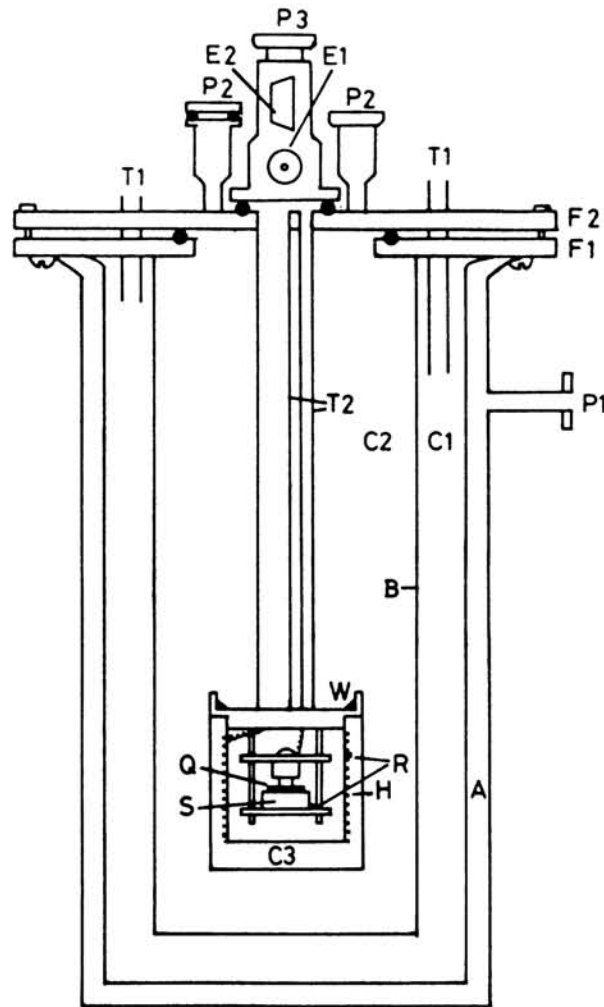


Fig. 2.6

Cross section of the cryostat.

(A - Double walled outer vessel, B - Single walled inner vessel, C1 - Chamber 1, C2 - Chamber 2, C3 - Sample chamber, E1, E2 - Electrical I/O, F1, F2 - Flanges, H - Heater coil, P1, P2, P3 - Evacuation ports, Q - Transducer, R - Temperature sensors, S - Sample, T1 - Liquid N₂ guide tube, T2 - Connection tube, W - Wood's metal joint)

2.5 References

- [1] A. G. Bell, *Amer. J. Sci.* **20**, 305 (1880).
- [2] A. G. Bell, *Phil. Mag.* **11**, 510 (1881).
- [3] Lord Rayleigh, *Nature* **23**, 506 (1881).
- [4] M. E. Mercardier and C. R. Hebd, *Serv. Acad. Sci.* **92**, 409 (1881).
- [5] W. H. Preece, *Proc. Royal. Soc.(Lond.)* **31**, 506 (1881).
- [6] A. Rosencwaig and A. Gersho, *Science* **190**, 556 (1975).
- [7] A. Rosencwaig and A. Gersho, *J. Appl. Phys.* **47**, 64 (1976).
- [8] P. Charpentier, F. Lepoutre and L. Bertrand, *J. Appl. Phys.* **53**, 608 (1982).
- [9] F. Pochetti, *Riv. Combust.* **25**, 461 (1971).
- [10] V. Era and A. Savolainen, *Suom. Kemi.* **A44**, 50 (1971).
- [11] J. M. Steim, in *Instrument News* Vol.19, Norwalk, Conn: Perkin - Elmer Corporation, (1968) p.12.
- [12] C. T. Mortimer, in *Calorimetry in Chemical and Biological Systems* **9** London : LKB Producer AB, (1969).
- [13] E. M. Barrall II and J. F. Johnson, *Tech. Methods, Polymer Eval.* **2**, 1 (1970).
- [14] E. S. Watson, M. J. O'Neill, J. Justin and N. Brenner, *Anal. Chem.* **36**, 1233 (1964).
- [15] M. J. O'Neill, *Anal. Chem.* **38**, 1331 (1966).
- [16] *Thermal Analysis Newsletter*, No.3 Norwalk, Conn : Perkin - Elmer Corporation.
- [17] D. C. Ginnings and G. T. Furukawa, *J. Amer. Chem. Soc.* **75**, 522 (1953).
- [18] J. E. May Jr., *IRE Natl. Conv. Rec.* **6**, 134 (1958).

- [19] E. P. Papadakis, *J. Appl. Phys.* **35**, 1474 (1964).
- [20] E. P. Papadakis, *J. Acoust. Soc. Am.* **42**, 1045 (1967).
- [21] D. H. Chung, D. J. Silversmith and B. B. Chick, *Rev. Sci. Instrum.* **40**, 718 (1969).
- [22] H. J. Mc Skimin, *J. Acoust. Soc. Am.* **33**, 12 (1961).
- [23] H. J. Mc Skimin and P. Andreath, *J. Acoust. Soc. Am.* **34**, 609 (1962).
- [24] L. Godfrey and J. Philip, *Acoust. Lett.* **19**, 11 (1995).
- [25] E. P. Papadakis, in *Physical Acoustics Vol.XII* (eds. W. P. Mason and R. N. Thurston), Academic Press, New York (1976).
- [26] R. Truell, E. Elbaum and B. B. Chick, in *Ultrasonic Methods in Solid State Physics*, Academic Press, New York (1969).

Chapter 3

Effect of SnO₂ addition on the thermal properties of YBa₂Cu₃O_{7- δ}

3.1 Introduction

One of the most exciting developments in modern physics has been the discovery of the oxide superconductors with T_c 's well above liquid nitrogen temperature. These materials have generated tremendous excitement for two basic reasons. First, in spite of the large variety of experimental techniques being employed to investigate these materials, the physical mechanisms responsible for the high T_c 's has not yet been identified, leaving the basic physics of these systems open to further investigations. Secondly they open a new temperature realm for superconducting devices and components which have got widespread commercial applications and this has attracted phenomenal popular interest in these materials. A number of devices have already been fabricated which make it clear that these oxide materials could have a substantial economic impact. They are also capable of supporting large critical currents and if high current devices can be successfully developed, then these materials should have a diversity of applications. And if, room temperature superconductivity ever becomes a reality, then superconductivity will have a profound influence on our every daylives which could rival developments such as the radio waves and the transistor.

However, it has soon been realised that the use of these materials for various applications and fabrication of various components and devices using these materials is not as easy as envisaged at the time of their discovery. Though endowed with comparatively high transition temperatures, the prospects of application of these materials

are severely limited due to a number of reasons. The brittle nature of these oxide superconductors, for example, is one of the drawbacks which prevents them from being used in the fabrication of wires and other useful forms. One of the main applications of these materials is in the form of thin and thick films to be used in electronic devices. But the high chemical reactivity of most of the oxide superconductors imposes severe restrictions on the availability of substrates for depositing thin films. Further, these superconducting oxides are found to interact with air, water, water vapour, moisture and other aqueous media, which deteriorates their superconducting properties. The aging effect, *i.e.*, the degradation of the superconducting samples in ordinary atmospheres with time, is another problem that is encountered, which makes the material unsuitable for investigations and various applications. In addition, the critical current density of high T_c materials are found to be smaller compared to the conventional superconductors. This has raised serious doubts about the use of these materials in various potential high magnetic field applications like superconducting machines, magnets and related systems.

So, commercially useful high T_c superconductors require enhancement of mechanical properties, critical current as well as thermal and environmental stability. Many reports indicate that addition of selected metals or oxides to high T_c superconductors retains the superconducting property, while changing the other features of the materials drastically. This suggests that practical applications of these materials are likely to be in their 'composite' form.

Numerous reports investigating the effects of various additives on the superconducting as well as the mechanical, electrical and magnetic properties of high T_c superconductors have appeared in literature [1-13] ever since the discovery of these materials. Among them the addition of various metal oxides like CdO, CeO₂, Cr₂O₃, Sb₂O₃ etc. and rare earth oxides [1,2] are found to be effective in increasing the microhardness and density of the superconductor, while the addition of Al₂O₃ is found to have a deteriorating effect on T_c [3]. The superconductor - silver composites have also been reported to possess many desirable properties. For example, addition of Ag₂O or Ag to a superconductor has been found to reduce the width of the superconducting transi-

tion, facilitate oxygen diffusion into bulk 123 compounds, improve the mechanical and fracture properties of materials like YBCO, BSCCO etc. [4-6] which enable them to be used in the fabrication of superconducting wires and tapes. Further, silver is found to be one of the few materials that does not degrade the properties of 123 compounds [7] and silver addition has been found to enhance the critical current density in high T_c materials [8, 9]. However, T_c is found to be depressed by partial replacement of Cu by Ag [10] and in one report, total replacement lowered the onset of T_c to 50 K [11]. A tremendous increase in the rate of oxygen absorption has been reported in ZrO_2 and Nb_2O_5 added YBCO system [12, 13] in which superconductivity is found to be obtained just by quenching the doped specimen in oxygen from sintering temperature, which makes the preparation much easier.

Though all the above mentioned additions are successful in improving any one of the properties, some other characteristic feature of the material has to be compromised. In this context, studies pertaining to the effect of SnO_2 addition on various superconductors have attracted considerable attention, as addition of SnO_2 is found to improve many properties of the superconductors and numerous reports can be found in literature on this [14-21].

A slight improvement in the T_c value has been reported with SnO_2 addition in YBCO and BSCCO systems [14, 15], the reasons for which is suggested to be the optimal carrier concentration and the possible increase in oxygen content. Osamura *et al.* [16] report an enhancement in critical current density with small amounts of SnO_2 , which is attributed to an increase in the pinning states. Increase in critical current density has also been reported in YBCO by Xu *et al.* [17] with $BaSnO_3$ addition and by Feng *et al.* [18] by the substitution of Sn for Cu.

The mechanical properties also show significant improvement with the addition of SnO_2 . An improvement in the microstructure and sintered density is reported in YBCO with SnO_2 addition which is found to reduce the porosity and distribute homogeneously among the YBCO grains [16, 19]. Another interesting feature that has been observed with SnO_2 added samples is the tremendous oxygen absorption [20], as has been found in the case of ZrO_2 and Nb_2O_5 added YBCO samples.

There have also been attempts to replace different elements of the superconductors with tin. These experiments, however, show conflicting results. Dubovitskii *et al.* [22] report that tin is contained in the lattice of 123 compounds and that it is present in two nonequivalent sites, replacing both the Cu(1) and Cu(2) sites, while the results of Mossbauer effect and positron annihilation spectra reported by Chen Ang *et al.* [14] show that Sn ions substitute only the Cu(1) sites. But other reports indicate that Sn does not substitute Cu or Ba but only Y upto 4% [23, 24]. Sn is reported to have a limited solubility in LSCO and substitutes for Cu upto 4 at.% [23, 24], while in BSCCO also, Sn ions are found to go to the Cu site rather than Sr or Ca. However, unlike the addition of SnO₂ which leads to an increase in T_c upto a certain concentration, substitution of Sn at the Cu site leads to a decrease in T_c [21, 25]. This indicates that the whole electronic structure of the system, or part of it, at the Cu - O planes may be changing with the partial replacement of Cu with Sn.

The thermal and transport properties of superconductors have attracted almost as much attention as their superconducting properties because of the valuable information they can provide about the superconducting mechanism, as has already been pointed out in chapter 1. Because of this reason, a large number of reports on these properties of superconductors such as thermal conductivity, specific heat etc. have been published, ever since the discovery of these materials, a review of which is also given in chapter 1.

The specific heat of a material is a bulk thermodynamic quantity determined uniquely for any material by its spectrum of excitations. The observation of a specific heat anomaly at T_c for a superconductor is, in principle, a proof of the bulk nature of its superconductivity. Since in high T_c superconductors, the electronic specific heat is only a few percentage of the total specific heat, the separation of the electronic component from the overwhelming lattice contribution is not easy. Further, the evaluation of $\Delta C/T_c$ is often hampered by considerable fluctuation effects.

The specific heat measurements in superconductors, in spite of these problems, show a distinct anomaly around T_c, though the magnitude of this anomaly is found to be sample dependent. Unlike the conventional superconductors, the ratio $\Delta C/\gamma T_c$ is also

found to vary from sample to sample, making it impossible to classify these materials as weak coupling or strong coupling superconductors.

Measurement of thermal conductivity in superconductors is another important probe to investigate the scattering mechanisms that comes into play in superconductivity. Heat is conducted by both electrons and phonons in a material and since electron - phonon scattering can limit the flow of heat in high T_c superconductors, thermal conductivity measurements can serve as a useful tool for investigating this important mechanism.

Though there are numerous reports on the measurement of thermal conductivity (K) of these materials, most of them have been on sintered polycrystalline specimens, mainly due to the non availability of large enough, crack free single crystals. In polycrystalline samples, the pores present and the grain size do impose serious limitations on the mean free path of phonons. However, thermal conductivity measurements show a uniformity in behaviour, despite these limitations, as mentioned earlier in chapter 1. It is found that thermal conductivity increases as the temperature drops below the transition, the amount of increase depending on the sample quality, purity and oxygen content. The consensus is that the increase is due to a drop in electron - phonon scattering as the charge carriers condense into superconducting pairs. Although the reduction of normal state carriers also lead to a loss of the electronic component of K , calculations indicate that the majority of heat is transported by the lattice. This interpretation has received theoretical support, applying the BCS theory to the phonon - scattering limited thermal conductivity. Thus by examining the shape and magnitude of the enhancement in K , it may be possible to estimate the electron - phonon coupling strength.

The thermal diffusivity (α) is another important thermal parameter of a material, that can provide similar information as that of the specific heat and thermal conductivity since it is related to these two quantities by the relation $\alpha = K/\rho C$ where ρ is the density of the material. Eventhough innumerable reports on the specific heat and thermal conductivity of high T_c superconductors are available in literature, only relatively few measurements on the thermal diffusivity of these materials have been reported which is usually measured using the photothermal or photoacoustic technique.

X.D.Wu *et al.* [26], for example, have reported the temperature variation of α along three axes of a $\text{Bi}_2\text{Sr}_2\text{CaCu}_2\text{O}_8$ single crystal using the photothermal technique, while the PA technique has been used by a few different authors [27-29] to study the temperature dependence of α of various polycrystalline superconductors like YBCO, BSCCO etc.

The PA technique has been used not only for the thermal diffusivity measurement, but also to detect the superconducting transition and for the measurement of specific heat. Y. S. Song *et al.* [30] have measured the relative values of specific heat for $\text{GdBa}_2\text{Cu}_3\text{O}_{7-\delta}$ and $\text{DyBa}_2\text{Cu}_3\text{O}_{7-\delta}$ using the technique, while the PA signal measurements on different 123 compounds [31, 32] indicate that it is possible to detect the superconducting transition from the temperature dependence of the PA signal amplitude and phase. In a review article, B. K. Chaudhury [33] explores the enormous possibilities of the PA technique for the characterisation of high T_c superconducting samples.

We have measured the temperature dependence of the thermal diffusivity of four samples of $\text{YBa}_2\text{Cu}_3\text{O}_{7-\delta}$ with different concentrations of SnO_2 added, using the PA technique. Measurements have been carried out on samples with varying SnO_2 concentration, above and below T_c . Details of the experiment and the results obtained are discussed in the following sections.

3.2 Experimental

The well established solid state reaction technique has been adopted for the preparation of $\text{YBa}_2\text{Cu}_3\text{O}_{7-\delta}$ (YBCO) samples used for the present investigations. High purity powders of Y_2O_3 , BaCO_3 and CuO are mixed in the appropriate stoichiometric ratios and calcined at 860°C for 12 hours. To the calcined powder, high purity SnO_2 powder is added in the range 0 - 8 wt% and mixed thoroughly. The pressed pellets are sintered at 940°C for 20 hours in flowing oxygen and slowly cooled to room temperature.

Four samples with different concentrations of SnO_2 are prepared. They are

Sample 1 : YBCO with 0.2 wt% of SnO_2

Sample 2 : YBCO with 0.5 wt% of SnO_2

Sample 3 : YBCO with 1.0 wt% of SnO₂

Sample 4 : YBCO with 8.0 wt% of SnO₂

Superconductivity of these samples have been verified by making electrical resistivity measurements. All these samples are found to undergo superconducting transition in the temperature range 92 - 94 K.

Thermal diffusivity of these samples have been measured using the photoacoustic technique in the temperature range 85 - 300 K. The method involves measurement of the amplitude of the PA signal as a function of the chopping frequency on a thin sample mounted on a suitable backing material, as has been described in the previous chapter. A log - log plot of the amplitude against chopping frequency shows a distinct change in slope at the characteristic frequency f_c above which the PA signal is independent of the properties of the backing material. In other words, the sample goes from a thermally thin regime to a thermally thick regime, as the chopping frequency is increased. Thermal diffusivity α can then be obtained using the relation $\alpha = f_c l^2$ where l is the sample thickness. Pellets of the YBCO samples have been thinned down to $\approx 200 \mu\text{m}$ by hand lapping and polishing. The thin sample is then mounted on a thick polished aluminium disc which acts as the thermally thick backing material, using silver epoxy to ensure good thermal contact. Using the photoacoustic experimental setup described in the last chapter, α of the samples are measured at different fixed temperatures in the range 85 - 300 K, where the temperature of the sample is kept constant within $\pm 0.5^\circ\text{C}$ during the measurement.

The specific heat of the samples have been measured at room temperature using the DSC - 7 differential scanning calorimeter described earlier, adopting the ratio method in which sapphire was used as the reference sample. Combining the thermal diffusivity and specific heat data with the density, the thermal conductivity has been calculated for all the samples at room temperature.

3.3 Results and Discussion

Fig. 3.1 shows a typical log - log plot of the amplitude of the PA signal measured as a function of the chopping frequency at 300 K for samples 1 to 4. The change in slope at

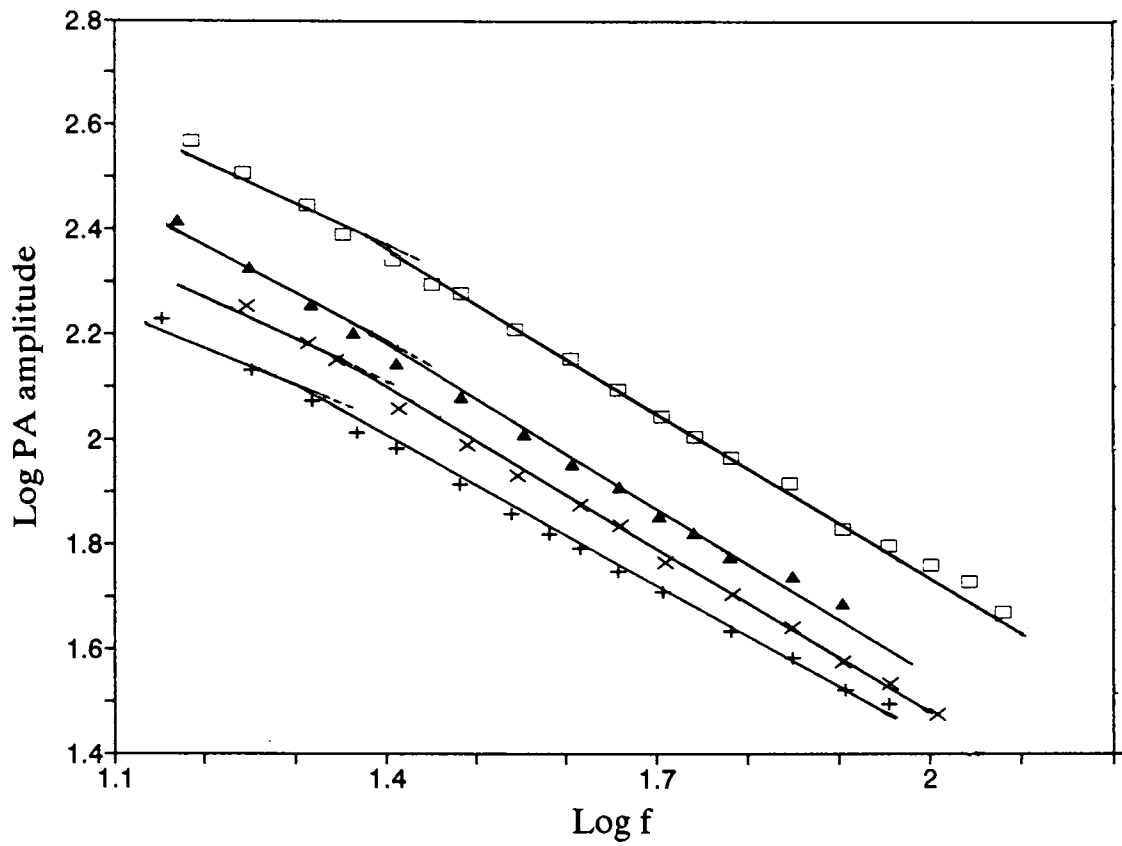


Fig. 3.1

Log - log plot of PA amplitude with chopping frequency at 300 K for YBa₂Cu₃O_{7-δ} - SnO₂ samples. (+ - sample 1, X - sample 2, □ - sample 3 and ▲ - sample 4).

the characteristic frequency f_c can be clearly seen in these figures from which the thermal diffusivity α can be determined using the relation $\alpha = f_c l^2$. The temperature variation of the thermal diffusivity of all the four samples in the temperature range 85 - 300 K are plotted in Fig. 3.2. As is evident from the figure, all samples show a uniform trend in the variation of α with temperature : there is a sharp increase in thermal diffusivity below T_c for all the samples. Fig. 3.3 shows the variation of density and specific heat with SnO_2 concentration at 300 K, while in Fig. 3.4 the thermal conductivity variation with the SnO_2 concentration is plotted at 300 K. The dependence of thermal diffusivity on the concentration of SnO_2 have been plotted at different temperatures above and below T_c . These curves are shown in Fig. 3.5. At all temperatures, the nature of variation of α is found to be the same with SnO_2 concentration.

It can be clearly seen from Fig. 3.2 that the thermal diffusivity suddenly increases just below T_c , which is similar to the behaviour exhibited by many high T_c superconductors in thermal conductivity measurements [34-40]. Eventhough α is related to both thermal conductivity (K) and specific heat (C) by $\alpha = K/\rho C$, the change in specific heat reported is not large enough to contribute to such a large increase in α , when compared to the increase in thermal conductivity near T_c . So an explanation for the observed thermal diffusivity variation near T_c can be given on the basis of the corresponding thermal conductivity variation.

The increase in thermal conductivity below T_c , which has been observed in all the high T_c superconductors, has been attributed to the condensation of free electrons into Cooper pairs below T_c . The electrons which are condensed into pairs do not carry entropy and hence do not contribute to thermal conductivity. Unpaired electrons in a superconductor can, however, transport heat, but as the temperature decreases below T_c , the number of such electrons decrease exponentially. The electronic contribution to thermal conductivity of a superconductor, therefore falls rapidly below T_c . On the other hand, since the paired electrons no longer scatter phonons, there will be an increase in the phonon mean free path below T_c , giving rise to a corresponding enhancement in the phononic contribution to thermal conductivity. The net temperature dependence of K below T_c will depend upon whether the electronic or phononic contribution dominates

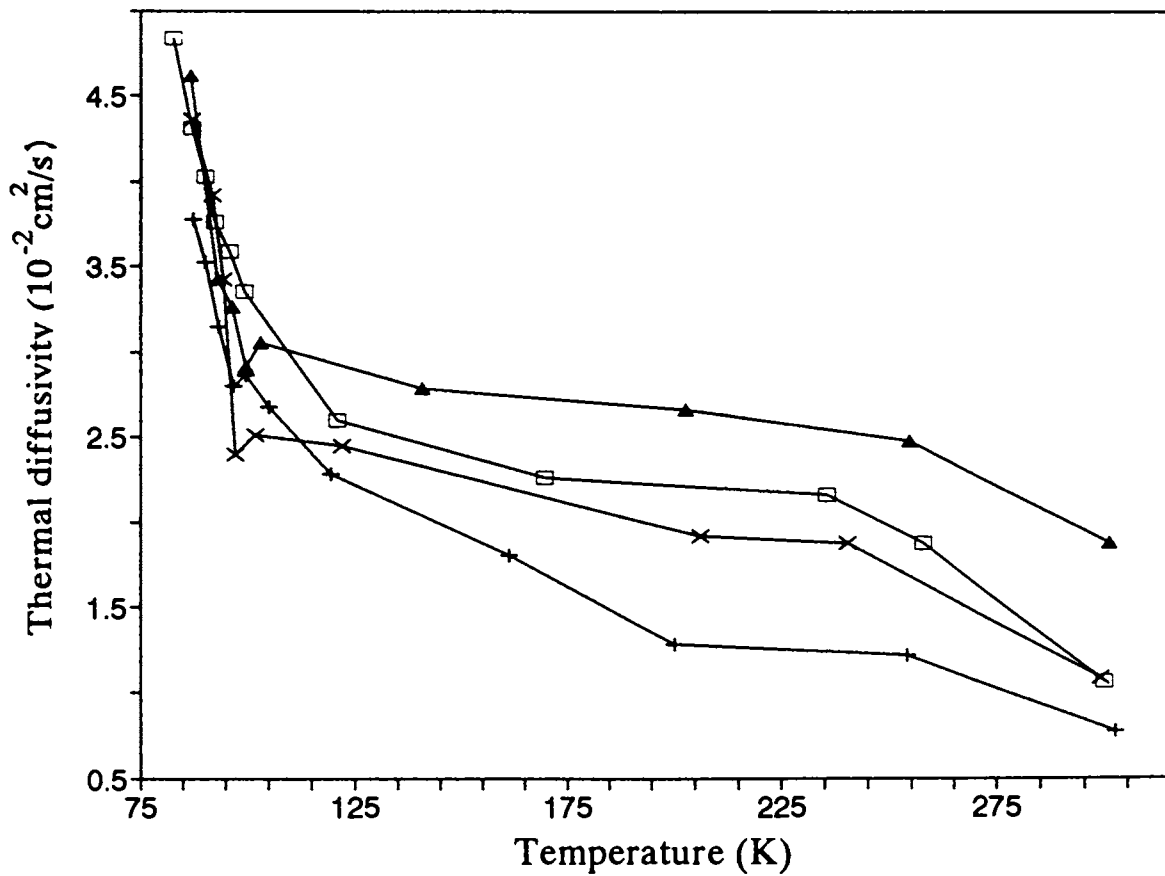


Fig. 3.2

Variation of thermal diffusivity (α) with temperature for $\text{YBa}_2\text{Cu}_3\text{O}_{7-\delta} - \text{SnO}_2$ samples. (+ - sample 1, X - sample 2, \square - sample 3 and \blacktriangle - sample 4).

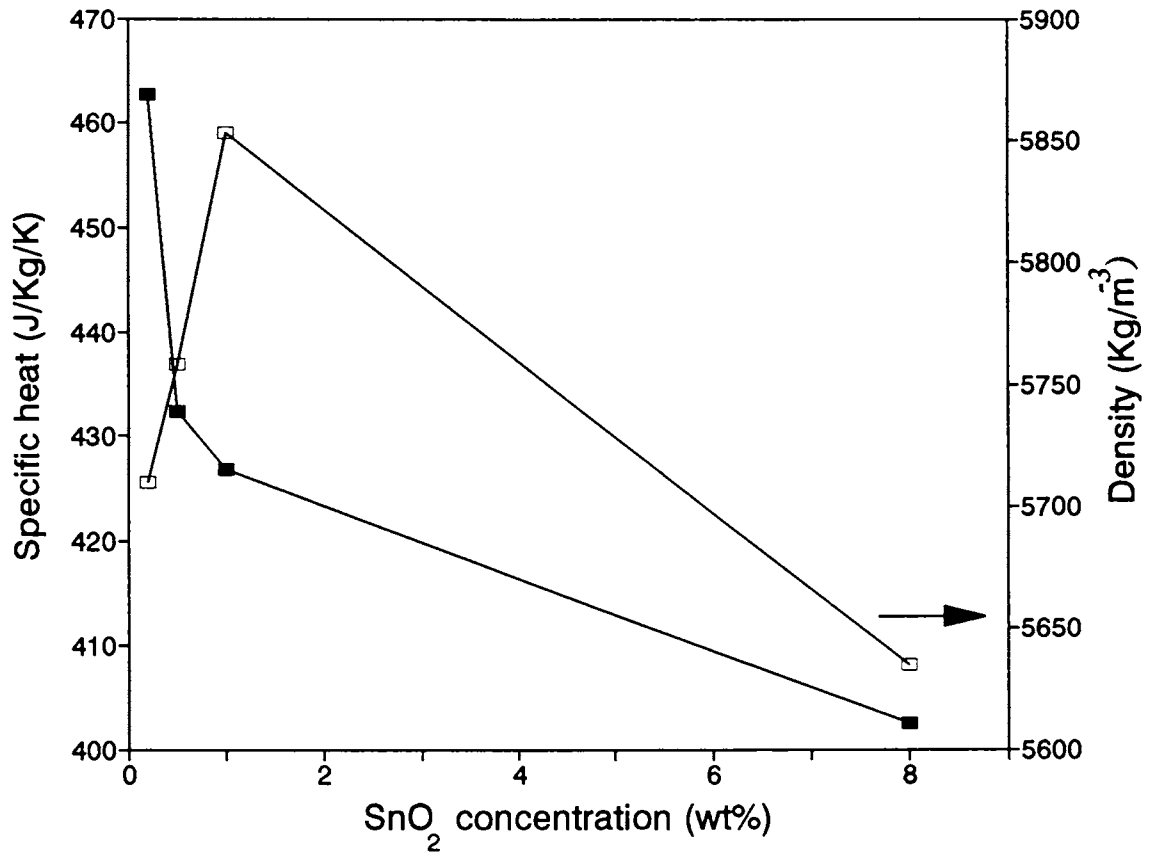


Fig. 3.3

Variation of density (ρ) and specific heat (C) with SnO₂ concentration at 300 K.

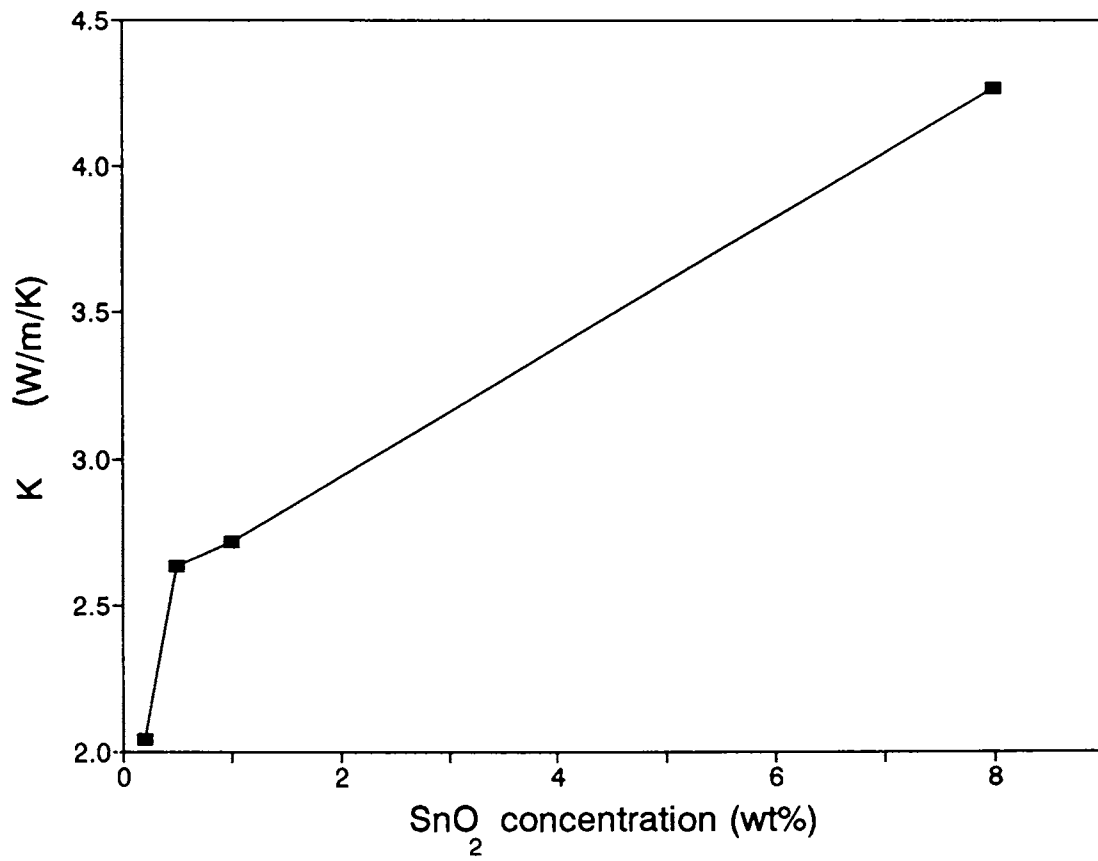


Fig. 3.4

Variation of thermal conductivity (K) with SnO₂ concentration at 300 K.

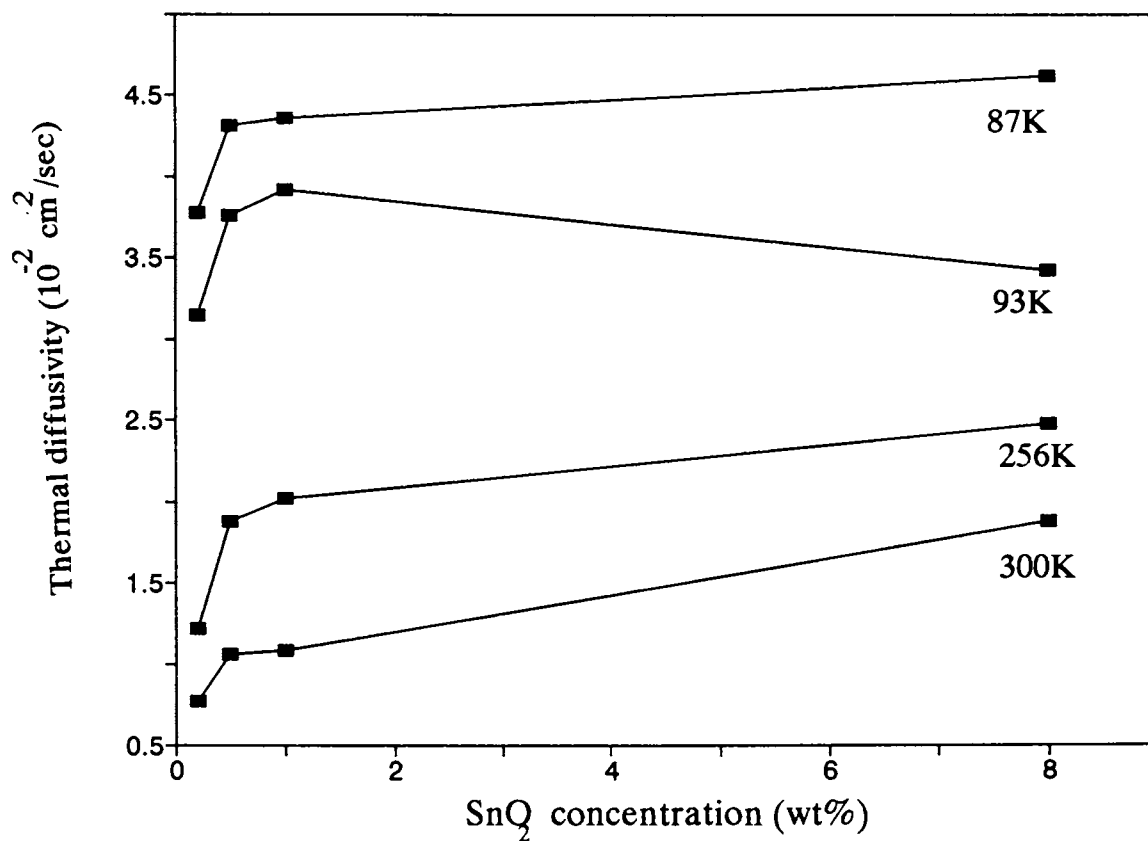


Fig. 3.5

Variation of thermal diffusivity (α) with SnO₂ concentration at different temperatures.

in the superconductor. The overall increase in K below T_c indicates that the major contribution to heat conduction in these materials is due to phonons.

These observations also indicate that thermal transport in the superconducting phase is limited primarily by phonon - defect scattering. Obviously, these arguments have their limitations owing to the fact that a quantitative deconvolution of thermal transport into its intrinsic electronic and phononic contributions is difficult due to the complexity of the polycrystalline system. The phonon - phonon umklapp processes can safely be ignored in these discussions as they are overshadowed by scattering from defects and electrons.

A small anomalous decrease in α can be noticed in Fig. 3.2 near T_c , which is absent in thermal conductivity measurements. This may be the consequence of the jump observed in heat capacity measurements near T_c [41, 42]. Another feature that can be observed is the very broadened peak or bump in α in the temperature range 200 - 260 K. However, no systematic variation with SnO_2 can be found in these curves. This also may be correlated to the anomaly observed in the specific heat of high T_c materials in the same temperature range [43, 44] due to the ordering of the Cu - O chains.

The curves in Fig. 3.5 represent the thermal diffusivity variation with SnO_2 concentration at different fixed temperatures. Generally speaking, α increase with concentration of SnO_2 , but the increase is not linear. The increase is rather sharp upto 0.5 wt% of SnO_2 , but after that it is at a slower pace. This behaviour is observed at all temperatures above and below T_c . These curves can be explained taking into account the density, specific heat and thermal conductivity variations of the samples with SnO_2 concentrations.

Many reports indicate an improvement in the density and microstructure of the samples with the addition of SnO_2 as mentioned earlier and the density is found to be closest to the theoretical value at 1 wt% of SnO_2 . Our samples also exhibit similar behaviour, *i.e.*, there is an increase in density upto 1 wt% eventhough the increase is small, after which the density decreases as is clear from Fig. 3.3. This decrease in density for sample 4, with 8 wt% of SnO_2 may have resulted due to the formation of impurity phases like CuO , BaSnO_3 etc. which also have been reported with higher concentrations

of SnO₂. The specific heat, on the other hand, shows a decrease throughout with increasing SnO₂. The decrease is rather sharp upto 0.5 wt% of SnO₂ after which the rate of decrease is low, which is evident from Fig. 3.3.

The improvement in the density and microstructure upto 1 wt% of SnO₂ may have caused a corresponding increase in thermal conductivity shown in Fig. 3.4. However, the decrease in density for sample 4 does not appear to have increased the porosity of the sample because the thermal conductivity is found to increase even above 1 wt%. Assuming that the variation of density and specific heat with SnO₂ concentration at room temperature is maintained at all temperatures, the variation in thermal diffusivity with SnO₂ concentrations at different temperatures, plotted in Fig. 3.5 can be explained. Taking into account the variations in density, specific heat and thermal conductivity, one can infer that the increase in density, which causes a corresponding increase in thermal conductivity and the sharp decrease in specific heat are responsible for the increase in thermal diffusivity upto 1 wt% SnO₂ added samples. The decrease in density and the slower decrease in specific heat above 1 wt% of SnO₂ may be the reasons for the comparatively lower rate of increase of α above 1 wt% of SnO₂.

3.4 Conclusions

Using the photoacoustic technique, we have measured the thermal diffusivity of a set of SnO₂ added YBa₂Cu₃O_{7- δ} samples. Like any other high T_c superconductor, these samples also show an abrupt increase in thermal diffusivity below T_c, owing to a corresponding increase in thermal conductivity. With increase in the amount of SnO₂, the thermal diffusivity also is found to increase, eventhough the increase is not linear. Taking into account the density, specific heat and thermal conductivity variation with the concentration of SnO₂, this behaviour has been explained.

The observation of enhancement of α below T_c is in accordance with the explanation that there is a reduction in the electron - phonon scattering below T_c due to the condensation of free electrons into Cooper pairs. In other words, these observations suggest that the BCS mechanism which is based on phonon mediated electron pairing is adequate to explain the thermal properties of high T_c materials.

3.5 References

- [1] C. J. Kim, H. C. Moon, K. B. Kim, S. C. Kwon, D. S. Suhr, I. S. Suh and D. Y. 'Won, *J. Mater. Sci. Lett.* **11**, 831 (1992).
- [2] I. N. Iveleva, A. P. Pivovarov, A. R. Rogachev and V. I. Rubstov, *Supercond. Phys. Chem. Tech.* **4**, 2090 (1991).
- [3] A. Srinivasa Rao, L. Arpigliano and O. P. Arora, in *Proc. 7th CIMTEC - World Ceramic Congress*, Trieste, Italy (1990), p.567.
- [4] P. Strobel, C. Paulsen and J. L. Tholence, *Solid State Commun.* **65**, 585 (1988).
- [5] D. Lee and K. Salama, *Jpn. J. Appl. Phys.* **29**, L2017 (1990).
- [6] B. R. Wienberger, L. Hynds, D. M. Potrepka, D. B. Snow, C. T. Burila, H. E. Eaton Jr., R. Cipolli, Z. Tan and J. I. Budnik, *Physica C* **161**, 91 (1989).
- [7] S. Jin, R. C. Sherwood, T. H. Tiefel, R. R. van Dover and D. W. Johnson Jr., *Appl. Phys. Lett.* **51**, 203 (1987).
- [8] B. Dwir, M. Affronte and D. Pavuna, *Appl. Phys. Lett.* **55**, 399 (1989).
- [9] N. Imanaka, F. Saito, H. Imai and G. Adachi, *Jpn. J. Appl. Phys.* **28**, L580 (1989).
- [10] C. V. Tomy, A. M. Umarji, D. T. Adroja, S. K. Malik, R. Prasad, N. C. Soni, A. Mohan and C. K. Gupta, *Solid State Commun.* **64**, 889 (1987).
- [11] K. K. Pan, H. Mathias, C. M. Rey, W. G. Moulton, H. K. Ng, L. R. Testardi and Y. L. Wang, *Phys. Lett.* **A125**, 147 (1987).
- [12] K.V.Paulose, J.Koshy and A.D.Damodaran, *Supercond. Sci. Tech.* **4**, 98 (1991).
- [13] K.V.Paulose, J.Koshy and A.D.Damodaran, *Jpn. J. Appl. Phys.* **30**, L458 (1991).
- [14] Chen Ang, Z. Yu, L. Biao-rong, W. Shao-jie and C. Yi-long, *J. Phys.* **C4**, 4981 (1992).

- [15] B. R. Sekhar, P. Srivastava, K. Asokan, N. L. Saini and K. B. Garg, *Int. J. Mod. Phys. B* **6**, 3079 (1992).
- [16] K. Osamura, N. Matsukura, Y. Kusumoto, S. Ochiai, B. Ni and T. Matsushita, *Jpn. J. Appl. Phys.* **29**, L1621 (1990).
- [17] Q. Xu, Z. Chen, D. Peng, Y. Chen, T. Wang, X. Pan and Y. Zhang, *J. Mater. Sci. Lett.* **12**, 799 (1993).
- [18] Y. Feng, L. Zhou, L. Shi, Y. F. Lu, X. Jin, Y. T. Zhang, J. R. Lin, X. X. Yao and Y. H. Zhang, *J. Appl. Phys.* **76**, 2954 (1994).
- [19] R. Chaim and Y. Ezer, *J. Mater. Sci.* **28**, 4205 (1993).
- [20] K. V. Paulose, J. Koshy and A. D. Damodaran, *Solid State Commun.* **79**, 815 (1991).
- [21] Y. L. Chen, B. R. Li, A. Chen and B. F. Xu, *Hyperfine Interactions* **55**, 1249 (1990).
- [22] A. V. Dubovitskii, N. V. Kireev, N. D. Kushch, E. F. Makarov, M. K. Markova, A. T. Mailybaev, V. A. Merzhanov, S. I. Pesotskii, R. A. Stukan, D. M. Shashkin, I. D. Datt and R. P. Ozerov, *Supercond. Phys. Chem. Tech.* **3**, 1030 (1990).
- [23] T. Satio, K. Mizuno, H. Watanabe and K. Koto, *Physica C* **171**, 167 (1990).
- [24] F. Licci, L. Raffo, T. Besagni, C. Frigeri and C. Paris, *Physica C* **196**, 307 (1992).
- [25] T. Yuen, C. L. Lin, J. E. Crow, G. N. Myer, R. E. Salomon, P. Schlottmann, N. Bykovetz and W. N. Herman, *Phys. Rev.* **B37**, 3770 (1988).
- [26] X. D. Wu, J. G. Fanton, G. S. Kino, S. Ryu, D. B. Mitzi and A. Kapitulnik, *Physica C* **218**, 417 (1993).
- [27] L. Gomes, M. M. F. Vieira, S. L. Baldochi, N. B. Lima, M. A. Novak, N. D. Vieira Jr., S. P. Morato, A. J. P. Braga, C. L. Cesar, A. F. S. Penna and J. M. Filho, *J. Appl. Phys.* **63**, 5044 (1988).

- [28] J. Isaac, J. Philip and B. K. Chaudhury, *Pramana* **32**, L167 (1989).
- [29] J. Isaac, J. Philip, M.T.Sebastian and A.D.Damodaran, *Physica* **C199**, 247 (1992).
- [30] Y. S. Song and N. S. Chung, *J. Appl. Phys.* **67**, 935 (1990).
- [31] J. Isaac, J. Philip and B. K. Chaudhury, *Pramana* **31**, L153 (1988).
- [32] Y. S. Song, H. K. Lee and N. S. Chung, *J. Appl. Phys.* **65**, 2568 (1989).
- [33] B. K. Chaudhury, *Ind. J. Phys.* **66A**, 713 (1992).
- [34] D. T. Morelli, J. Heremans and D. E. Swets, *Phys. Rev.* **B36**, 3917 (1987).
- [35] C. Uher and A. B. Kaiser, *Phys. Rev.* **B36**, 5680 (1987).
- [36] M. A. Izbizky, M. D. N. Regueiro, P. Esquinazi and C. Fainstein, *Phys. Rev.* **B38**, 9220 (1988).
- [37] M. F. Crommie and A. Zettl, *Phys. Rev.* **B41**, 10978 (1990).
- [38] M. D. N. Regueiro and D. Castello, *Int. J. Mod. Phys.* **5**, 2003 (1991).
- [39] S. T. Ting, P. Pernambucoise and J. E. Crow, *Phys. Rev.* **B50**, 6375 (1994).
- [40] A. V. Inyushkin, A. N. Taldenkov, L. N. Dem'yanets, T. G. Uvarova and A. B. Bykov, *Physica* **B194-196**, 479 (1994).
- [41] S. E. Inderhees, M. B. Salamon, T. A. Friedmann and D. M. Ginsberg, *Phys. Rev.* **B36**, 2401 (1987).
- [42] M. V. Nevitt, G. W. Crabtree and T. C. Klippert, *Phys. Rev.* **B36**, 2398 (1987).
- [43] R. Calemczuck, E. Bonjour, J. Y. Henry, L. Forro, C. Ayache, M. J. M. Jurgens, J. R. Mignod, B. Barbara, P. Burlet, M. Couach, A. F. Khoder and B. Salce, *Physica* **C153-155**, 960 (1988).
- [44] M. Slaski, T. Laegreid, O. M. Nes and K. Fossheim, *Mod. Phys. Lett.* **B3**, 585 (1989).

Chapter 4

Effect of Ga doping on the elastic properties of $\text{GdBa}_2\text{Cu}_3\text{O}_{7-\delta}$

4.1 Introduction

Substitutional studies have been found to be one of the interesting areas of research in high T_c superconductivity, in which one or more chemical constituents of the parent material are replaced either partially or completely by other elements. The importance of substitutional studies stems from their role as a probe of the chemical and structural environment which determines whether or not the system exhibits superconductivity. Besides, these studies may lead to new superconductors with higher T_c 's since all the major high T_c superconductors have shown their genesis in substitution at one or more cationic sites in the parental material.

Since the discovery of high T_c materials, numerous investigations have been carried out on substitution of each element of the copper oxide superconductors. These type of studies can be categorised into three major groups :- 1) those substitutions that have little or no effect on the CuO_2 planes 2) those that indirectly affect the planes by charge transfer and 3) those that directly affect the planes substituting for Cu in the planes. In the first case, there are no dramatic structural changes, the formal Cu valence is not affected and there is little or no suppression of T_c . In the second case, there exist significant structural changes as well as a change in the formal Cu valence and T_c drops in correlation with the structural changes. In the third case, there are no dramatic structural changes; the formal Cu valence does not change and the drop of T_c with doping level is the most severe.

Thus the chemical doping is a crucial investigative tool for the study of high T_c materials since the substituents can affect the structure including bond lengths and can also produce band filling in the parent compound. The determination of crystallographic structure and measurement of different properties of doped cuprate materials can provide valuable information regarding the correlation between superconducting and other physical properties. In addition, the sensitivity of superconducting and normal state properties to the electronic structure of the dopants will be very much useful for the confirmation of the theories of superconductivity.

Innumerable reports investigating the effects of various dopants on the superconducting and other properties of cuprate superconductors can be found in literature. In fact, it was this substitutional chemistry that led from the original report of superconductivity in the La-Ba-Cu-O system to the family of 90 K superconductors $\text{YBa}_2\text{Cu}_3\text{O}_{7-\delta}$. The Bi-, Tl- and Hg- based oxides with T_c 's well above 100 K were also discovered in a similar manner.

In $\text{YBa}_2\text{Cu}_3\text{O}_{7-\delta}$ (YBCO), which is the most thoroughly investigated high T_c superconductor, extensive substitution studies have been reported with virtually every element. Among them, the most successful substitution consists of replacing Y by other rare earth elements. With the exception of Sc, Ce, Pr and Tb, all rare earths are reported to substitute completely for Y, still retaining the high temperature superconductivity [1-4]. In the case of Sc, the Sc^{3+} ion is found to be too small to stabilize the structure. Substitution of Tb yields superconductivity, but with a relatively low T_c of 35 K [5]. In the compounds containing Ce, Pr and Tb, superconductivity may be weakened or destroyed through electronic effects originating with the valence state of the rare earth ion. Substitution of other nominally trivalent ions such as Al, Tl, In etc. are also reported [6, 7], but in the YBCO structure these elements do not raise the T_c value.

Partial or complete substitutions have been reported also for the alkaline earth Ba, which are found to result in a constant or declining transition temperature. The most common substitutions for Ba are other alkaline earths and some alkali metals [8-10]. Since Ba occupies one unique sublattice in the structure, most authors assume

partial substitutions occur statistically on this sublattice. In one report [11], the partial substitution of Ba by Pb and Y by Bi have shown that T_c remains unchanged while the normal state resistivity decreases by an order of magnitude. Both Bi and Pb oxides act as fluxes in the sintering process during the synthesis and changes in the morphology of the sintered grains take place.

Exciting results are reported for elemental substitution on the oxygen sublattices. Experiments replacing oxygen with isoelectronic sulfur atoms claim an increase in T_c upto 108 K [12]. This increase is attributed to the possible effects sulfur may have produced on the crystallographic stability. In another report, the partial substitution of fluorine for oxygen results in an increase in T_c upto 150 K [13]. But such compounds are found to be highly unstable and the results are often not reproducible.

Substitution at the copper site is considered to be the most important among all the cationic sites of YBCO, since Cu-O networks have been suspected to play the major role for the occurrence of superconductivity in these materials. Because of this reason, doping at the Cu site has been attempted with almost all the elements in the periodic table. Since Cu occupies two distinct sublattices in the orthorhombic unit cell of YBCO, there may be preferential site occupancy depending on the nature of the substituent.

Among these different dopants, substitution by the 3d transition elements have attracted considerable attention since they possess certain favourable features in respect of their compatible ionic sizes and closer orbital structure to that of copper. The 3d metallic dopants also provide interesting situation of interplay of superconductivity and magnetism. However, many of them exhibit multiple valencies varying from +2 to +4. Although some of the others like Co, Ni, Fe etc. substitute preferentially at one of the Cu sites, their large magnetic moments severely complicate the interpretation of superconducting mechanism. So the ideal dopants for Cu must have similar electronic configuration as that of Cu, must be non-magnetic and should substitute preferentially either at the Cu(1) or Cu(2) site. The post transition elements Zn and Ga, which are closed shell 3d non-magnetic ions with fixed valencies possess all these qualities and qualify themselves as the ideal candidates to replace Cu atoms.

Extensive studies have been made on the substitution of Zn and Ga in place of Cu, not in 123 compounds alone, but on other high T_c materials like LSCO, BSCCO, $\text{YBa}_2\text{Cu}_4\text{O}_8$ etc. [14-19]. In all these compounds, superconducting transition temperature is found to decrease with these dopants, though the T_c depression rates are different for Zn and Ga. In 123 compounds also, the behaviour is similar and it has been established beyond doubt that Zn, being divalent, substitutes preferentially at the Cu(2) site, while Ga, being trivalent, substitutes preferentially at the Cu(1) site in these compounds. When doped with Zn, T_c is found to decrease drastically and superconductivity disappears around 12 - 13 at.% of Zn. However, the samples remain orthorhombic throughout, indicating that the Cu-O chains remain intact in the Zn-doped system [20-24].

Substitution of the Cu site by Ga in 123 compounds has also been reported by many groups [22-33]. With Ga substitution also, T_c has been found to decrease, but the rate at which T_c decreases is much smaller than those due to Zn substitution. Reports vary on the T_c depression rates as well as on the exact solid solubility of Ga in 123 compound. While Xiao *et al.* [23] observe an initial rate of decrease of T_c of 1 K/atom.% and the solid solubility limit to be as high as $x = 0.2$ in $\text{YBa}_2(\text{Cu}_{1-x}\text{Ga}_x)_3\text{O}_{7-\delta}$, Xu *et al.* [25] report that Ga is incorporated into the compound only below $x = 0.05$. In a study of the ion size effect on T_c in Ga doped RBCO system (R - rare earth), Y.Xu *et al.* [26] have reported a T_c depression rate of ≈ 3 K/atom.% for YBCO and a decrease of T_c with increasing radius of R ions at a constant Ga concentration. The solid solubility limit reported by Mary *et al.* [27] in Ga doped NdBCO is as high as $x \approx 0.33$ while the rate of decrease of T_c is 12 K/atom.%.

Another interesting feature observed with Ga doping is that it induces an orthorhombic to tetragonal transition at a particular concentration of Ga. This effect has also been reported with other dopants like Al, Fe, Co etc. [24, 34]. However, there is no consensus on the exact doping concentration at which the transition takes place. While Hiratani *et al.* [28] observe that the concentration at which the transition takes place, x_{O-T} , to be as high as 0.1, Xiao *et al.* [23] report this transition value to be 0.06. However, the value of x_{O-T} , as observed by Maeno *et al.* [24], Xu *et al.*, [25], Mary

et al. [27], Suryanarayanan *et al.* [29] etc. is very low and is approximately 0.03. Y.Xu *et al.* [26] find that with increasing ionic radius of the rare earth ions, x_{O-T} is shifted to lower Ga concentration and in YBCO it is found to be 0.05.

Since the discovery of high T_c superconductivity in ceramic cuprates, nearly every conceivable measurement has been performed on this class of materials and ultrasonic studies are not an exception. In fact, sound velocity anomalies were among the first anomalous results obtained in these materials. In conventional superconductors, the results of sound attenuation has provided one of the first measurements of the energy gap and a direct confirmation of the BCS theory.

Extensive elastic measurements have been reported in cuprate superconductors using ultrasonic technique, since it is one of the standard methods in characterising the lattice dynamical properties of solids near phase transitions and critical points. Further, the measurement of sound velocity can provide informations that are difficult to obtain with other methods and it can also be used to confirm the results of other experiments. These types of measurements are generally made for two purposes - either to measure absolute values of velocities and elastic moduli or to study the general temperature dependence of velocity and attenuation.

In single crystals, the sound velocities depend on the direction of propagation and polarisation of sound, from which the elastic constants can be calculated. However, the successful growth of large single crystals required for these measurements have been found to be difficult. Available single crystals are usually in the form of thin platelets that do not allow the precise determination of the whole set of elastic constants. In addition, the control of stoichiometry is found to be more difficult in single crystals when compared to ceramic samples. Because of these reasons, the bulk of acoustic investigations on high T_c materials have been performed on ceramic specimens comprising aggregated micron sized crystallites, most of which involve measurement of the temperature dependence of velocity and attenuation.

When solid matter cools, it usually becomes stiffer. Consequently, the sound velocities and elastic constants increase. The normal change of sound velocity (v) can

be written as

$$\frac{\Delta v}{v} = \frac{\gamma^2 T^4}{\rho v^2} \frac{12 \pi^4}{5 \theta_D^3} k_B n \quad (4.1)$$

at low temperatures ($T < 10$ K)

and

$$\frac{\Delta v}{v} = \frac{-TC(T) \gamma^2}{\rho v^2} \quad (4.2)$$

at higher temperatures

Here C is the specific heat, k_B is the Boltzmann constant, n is the number of atoms per unit volume, θ_D is the Debye temperature and γ is the the effective Gruneisen parameter related to the modes of propagation of lattice waves.

The sound velocities in all high T_c materials are generally found to increase from room temperature to 4 K by 4 - 10%. Deviation from this standard behaviour is found in some materials like LCO, LSCO etc. which are caused by phase transitions and other effects in the material. The origin of attenuation consists of several components in these materials that can be treated as independent. These include diffraction losses, scattering from grain boundaries, interactions with thermal phonons and electrons, interaction with point defects and dislocations etc.

In 123 compounds, velocity measurements generally give consistent results over a wide temperature range for both polycrystalline ceramics and single crystals, when the porosity of the material is taken into consideration. The velocity, which increases with decreasing temperature, shows an anomalous jump in the vicinity of T_c in most of the measurements [35-38]. Below T_c , the velocity again increases, may be even more rapidly than above T_c . Attenuation measurements also exhibit anomalous changes near the superconducting transition. Various reasons have been attributed to these anomalies. The temperature variation of the first derivative of velocity has been related to the specific heat jump and the second stress derivative of T_c . Abd-Shukor [39] reports a change in the slope of the shear velocity with respect to temperature, which according to him, is expected of any volume preserving transition such as the superconducting transition.

Apart from these anomalies observed near T_c , anomalous changes are reported in both velocity and attenuation at temperatures above T_c in many measurements

[40-44]. Various explanations have been given for this behaviour also. While some reports suggest that the changes may be due to a phase transition [40,41], possibly of the martensitic type [42], some others stress the ferroelectric nature of the transition, which can explain changes in sound velocity and attenuation as well as sudden apparent changes in resistivity [43]. Regarding the peaks observed in attenuation at different temperatures above T_c , most of the authors agree that these peaks are of a relaxational character, since their position shifts with frequency and that they are in some way connected with the oxygen atoms [44].

Another interesting effect is the thermal hysteresis of the velocity, *i.e.*, the velocity is higher upon cooling than upon subsequent heating [40,43,45,46]. This effect appears in the temperature range 230 - 235 K in some samples and is found to be more pronounced in coarse grained samples than in fine grained ones. It depends on oxygen content and its origin is still unclear. While some authors suggest a phase transition as the possible reason for this effect [40,43], some others attribute it to twinning, twin boundary movement, reordering of oxygen atoms, relaxation of tension of grain boundaries etc. [45,46].

The work presented in this chapter is an attempt to study the effect of Ga doping on the elastic properties of superconducting $GdBa_2Cu_3O_{7-\delta}$ (GdBCO) samples. We have carried out ultrasonic velocity and attenuation measurements on pure and Ga doped GdBCO samples in an attempt to throw more light upon the mechanism of superconductivity in these materials.

4.2 Experimental

Samples investigated in this work have a general formula $GdBa_2(Cu_{1-x}Ga_x)_3O_{7-\delta}$ with $x = 0.0, 0.02, 0.04$ and 0.06 which are referred to as S1, S2, S3 and S4 respectively. They are prepared by the conventional solid state reaction method. Stoichiometric mixtures of Gd_2O_3 , $BaCO_3$, CuO and Ga_2O_3 powders are thoroughly mixed and calcined in the form of loosely packed pellets for about 80 hours with three intermediate grindings. Samples are then powdered and pelletised under a pressure of nearly 100 Kg cm^{-2} and sintered at $900 \text{ }^\circ\text{C}$ for 24 hours and then furnace cooled to room temperature. The T_c 's

of the samples are determined to be 92 K, 88 K, 83 K and 78 K respectively by dc resistivity measurements.

In order to study the variation of elastic properties with Ga doping, we have carried out ultrasonic velocity and attenuation measurements in all the four samples in the temperature range 85 - 300 K. Velocity and attenuation of longitudinal ultrasonic waves have been measured in all the samples as a function of temperature and transverse velocity was measured in S2 down to 85 K, using the ultrasonic PEO experimental setup already described in chapter 2.

Pelletised samples in the form of circular discs of diameter ≈ 10 mm and thickness ≈ 3.5 mm have been used for the measurements. The faces of the samples have been well polished so that they are plane and parallel to each other. An x-cut quartz transducer with resonant frequency 10 MHz is used to generate and detect ultrasonic waves of longitudinal polarisation while a y-cut transducer of the same resonant frequency is used for transverse waves. The transducer is bonded to the sample with nonaq stopcock grease for longitudinal waves while silicone grease is used as bond for transverse waves. The sample is then placed in the homemade stainless steel cryostat described earlier in chapter 2, in which liquid nitrogen is used as the cryogen. A temperature controller (Lakeshore DR 82C) is used to control the temperature of the sample in which the cooling rate is kept at approximately 0.5 K/min. Reasonably good echoes are obtained for all the samples at room temperature. For measuring the ultrasonic velocity, the pulse echo overlap technique is used, while the pulse comparison technique is employed to measure attenuation, as outlined in chapter 2.

From the measured velocities, the elastic constants are calculated at different temperatures for all the samples using the formula $C_{ij} = \rho v^2$. The Debye temperature θ_D is calculated for sample S2 from the measured longitudinal (v_l) and transverse (v_t) velocities as a function of temperature, using the relation [47]

$$\theta_D = \frac{h}{k_B} \left(\frac{9N}{4\pi V} \right)^{1/3} \left(\frac{1}{v_l^3} + \frac{2}{v_t^3} \right)^{-1/3} \quad (4.3)$$

where N is the Avogadro's number.

4.3 Results and Discussion

The absolute and relative ($\Delta v/v_{300}$) velocities of longitudinal ultrasonic waves for all the four samples as a function of temperature are shown in Figs. 4.1 and 4.2 respectively. Fig. 4.3 shows the variation of longitudinal attenuation with temperature for all the samples. The attenuation is plotted only down to 150 K for S1 because measurements could not be made below this temperature due to bad shape of the echoes. The variation in longitudinal elastic constant with Ga concentration at different fixed temperatures is depicted in Fig. 4.4. The temperature variation of the Debye characteristic temperature for S2, calculated from the longitudinal and transverse velocities, is plotted in Fig. 4.5.

As is evident from Figs. 4.1 and 4.2 there is a slope discontinuity in longitudinal ultrasonic velocity near T_c for S1 while S2 shows the onset of this anomaly, as has been observed in the case of most of the other high T_c superconductors. However, such an anomaly cannot be found in the curves for S3 and S4. The dip in velocity and the hardening of elastic modulus below T_c suggests that a structural instability is occurring at the transition point, while the hardening of the modulus below T_c may be due to the depletion of an excitation that cocondenses with the carriers, which couples strongly to the transverse acoustic phonons [39]. The anomalies near T_c are found to be more pronounced in transverse velocity measurements, since the order parameter has a stronger coupling with shear distortions than with compressive distortions, as suggested by Abd-Shukor [39]. Our observations also support this argument, since the anomaly near T_c is more pronounced in the transverse velocity for S2, which is reflected and is evident from the Debye temperature curve shown in Fig. 4.5. The absence of any anomaly in S3 and S4 may be due to the fact that their T_c 's are below 85 K, which is the lowest temperature at which we have made these measurements.

There is a much more pronounced anomaly in sound velocity far above T_c for all the samples, except S4, in the temperature range 150-200 K and is better seen in Fig. 4.2. Several reports reveal similar anomalies in high T_c materials above T_c , although the temperature at which these occur vary from sample to sample and there is no consensus on the reasons attributed to this behaviour. Structural measurements

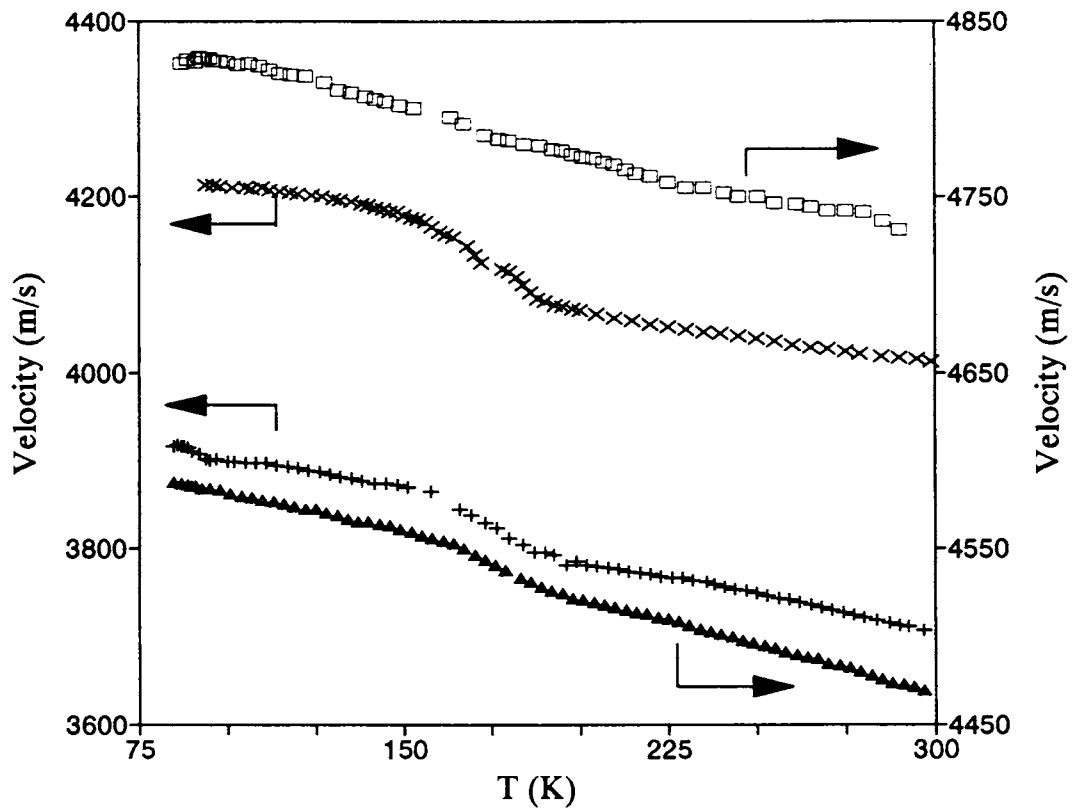


Fig. 4.1

Variation of longitudinal ultrasonic velocity with temperature for $\text{GdBa}_2(\text{Cu}_{1-x}\text{Ga}_x)_3\text{O}_{7-\delta}$

+ for $x = 0.00$ (S1), \square for $x = 0.02$ (S2), \times for $x = 0.04$ (S3) and \blacktriangle for $x = 0.06$ (S4).

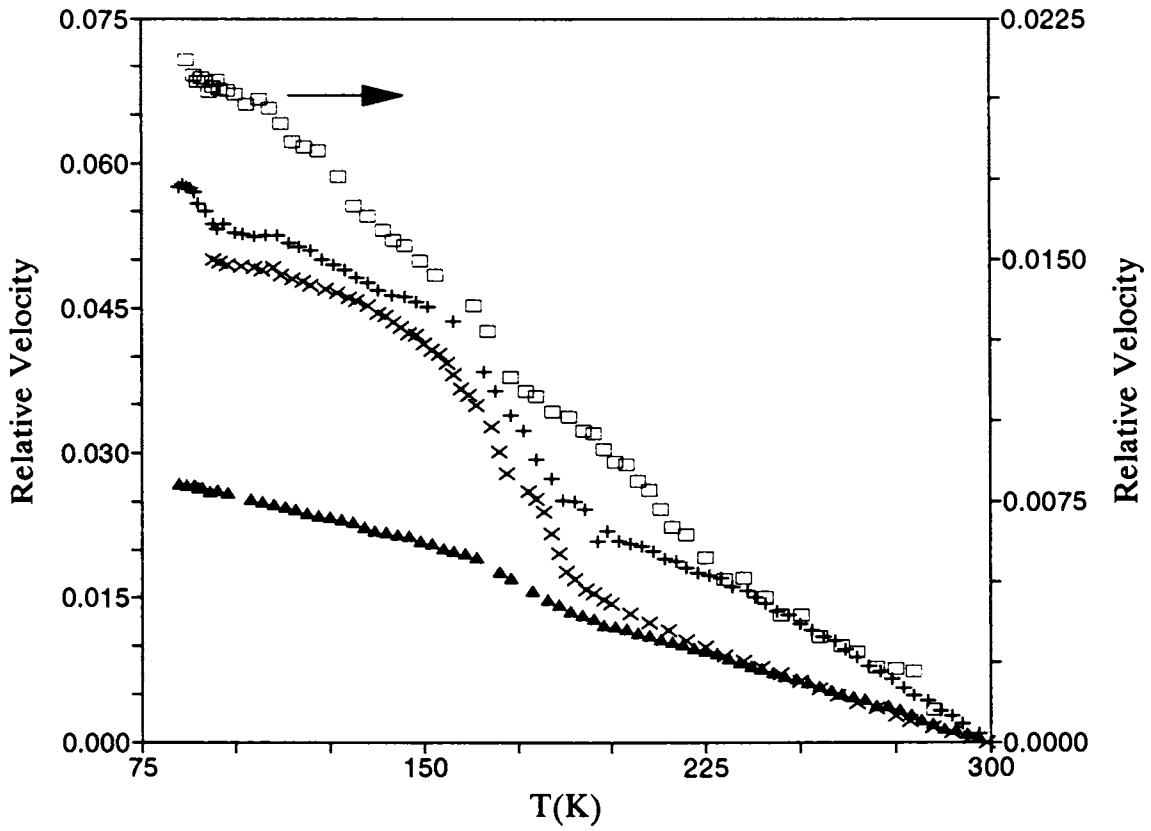


Fig. 4.2

Variation of relative longitudinal velocity ($\Delta v/v_{300}$) with temperature for $\text{GdBa}_2(\text{Cu}_{1-x}\text{Ga}_x)_3\text{O}_{7-\delta}$

+ for $x = 0.00$ (S1), \square for $x = 0.02$ (S2), X for $x = 0.04$ (S3) and \blacktriangle for $x = 0.06$ (S4).

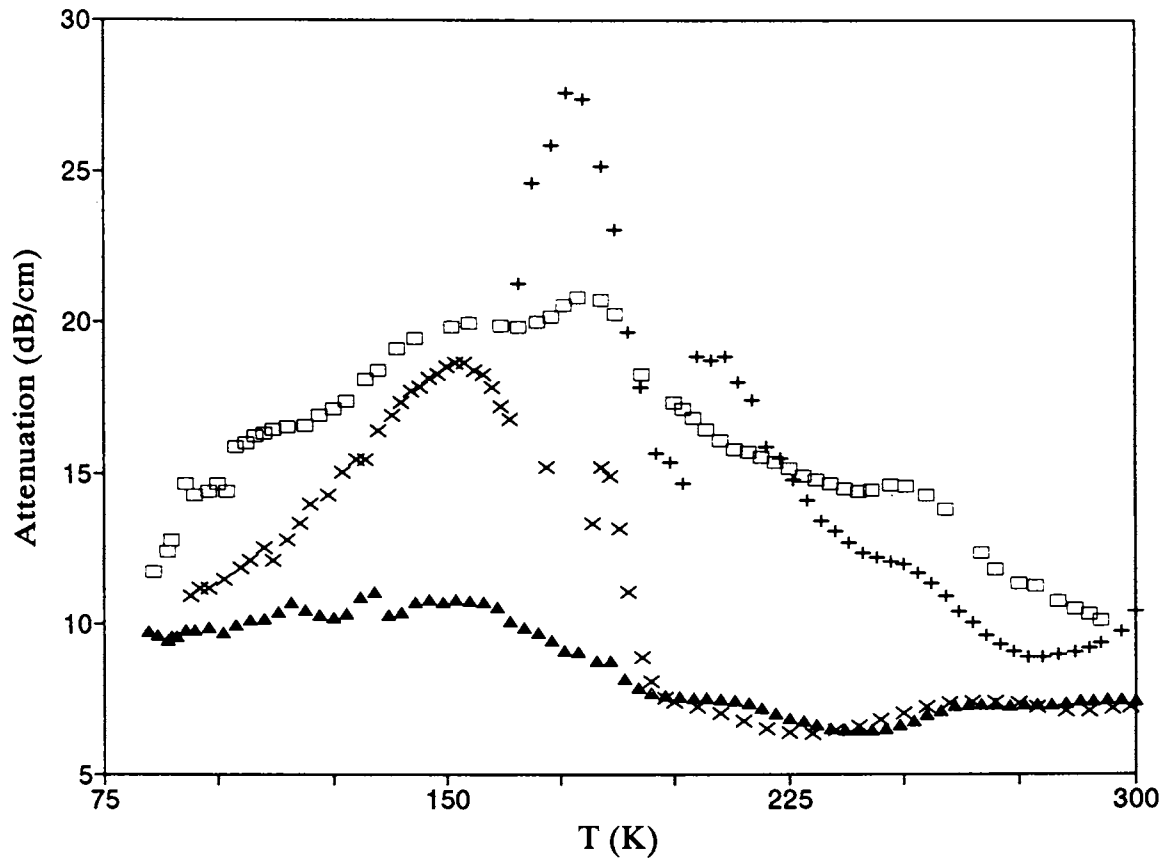


Fig. 4.3

Variation of ultrasonic attenuation with temperature for $\text{GdBa}_2(\text{Cu}_{1-x}\text{Ga}_x)_3\text{O}_{7-d}$
 + for $x = 0.00$ (S1), \square for $x = 0.02$ (S2), \times for $x = 0.04$ (S3) and \blacktriangle for $x = 0.06$ (S4).

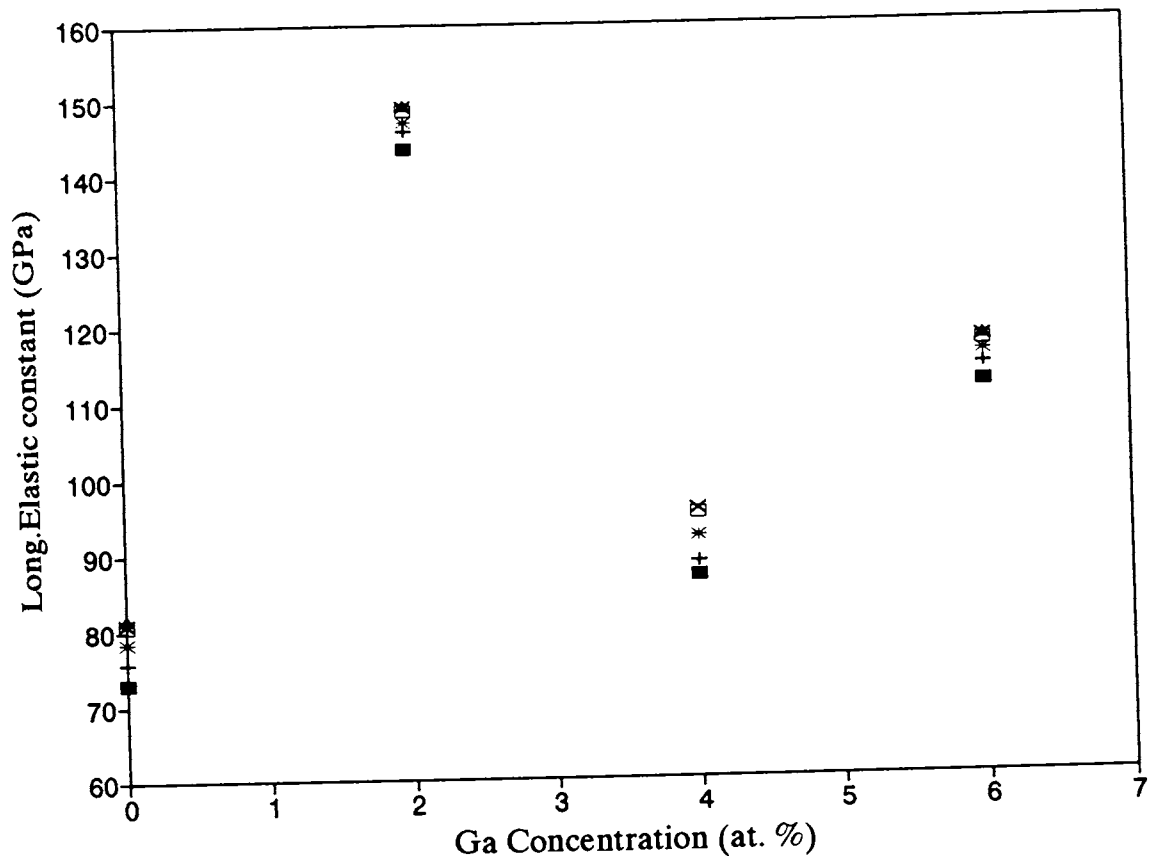


Fig. 4.4

Variation of longitudinal elastic constant with Ga concentration at different temperatures. □ at 300 K, + at 220 K, * at 170 K, □ at 120 K, X at 95 K and ▲ at 88 K.

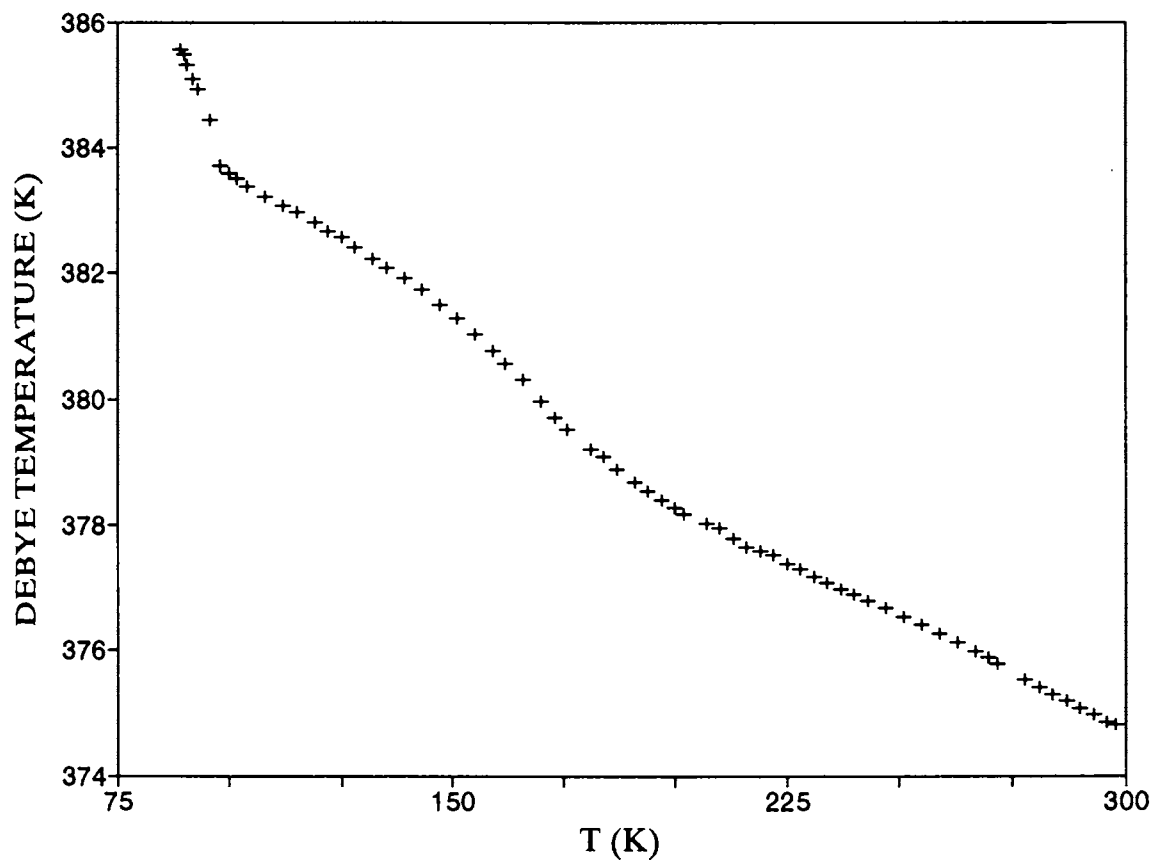


Fig 4.5
Variation of Debye temperature with temperature for S2.

have reported first order like transitions with changes in lattice constants, while calorimetric measurements reveal a large specific heat anomaly at this temperature. Oxygen vacancy ordering has also been suggested as one of the possible reasons. A comparative study of the ultrasonic characteristics of superconducting orthorhombic and nonsuperconducting tetragonal GdBCO is reported by Almond *et al.* [48]. The dominant feature of sound velocity, characteristic of superconducting GdBCO, is a step like change at temperatures around 200 K. Hysteresis is also found predominantly in the same temperature range. These features are absent in the characteristics of the sample in its nonsuperconducting tetragonal form. It is suggested that these phenomena may be due to the coexistence of superconducting and antiferromagnetic phases in the sample.

Similar behaviour is observed in our samples also, but all our samples are superconducting. In samples S1, S2 and S3 the step like increase in velocity is clearly visible in the temperature range 150-200 K whereas it is absent in S4 as is clear from Figs. 4.1 and 4.2.

In 123 compounds, there are two inequivalent positions for the Cu atoms; Cu(1) site or the so called chain Cu atom and the Cu(2) site which forms the two dimensional Cu-O planes. It has been established beyond doubt that the trivalent cations get substituted preferentially at the Cu(1) site and Ga is no exception. From neutron refinement studies it is found that with Ga doping, considerable disorder is induced on the chain Cu atom and in the limit of vanishing orthorhombic distortion the structure becomes tetragonal. The chain structure is fully disordered and the O(4) and O(5) sites become indistinguishable. Due to this distortion, a maximum difference in the lattice constants b and a is found to appear around the superconducting transition. This orthorhombic distortion does not result in changes of the volume of the unit cell or the area of the unit basal plane. There have been suggestions that the softening of sound velocity occurring near T_c also reflects this structural instability.

All our samples are superconducting with gradually decreasing T_c 's with increasing Ga doping concentration. So the superconductivity of the sample cannot be the possible reason for the anomaly since it is absent in S4 which has a T_c of 78 K. Instead of assuming the change in velocity to be caused by the superconductivity of the mate-

rial, it seems reasonable to assume that these changes are associated with the structure of the compound. So the possible conclusion that can be drawn is that the first three samples S1, S2 and S3 belong to the orthorhombic class while sample S4, even though superconducting, is in the tetragonal form. There are many reports which indicate that superconductivity can occur in the tetragonal form of YBCO, which supports this argument.

The attenuation measurements support the velocity curves which is evident from Fig. 4.3. Peaks or shoulders can be seen in attenuation in the same temperature range where the velocity anomaly occurs. The notable feature is that this maximum is absent in the case of S4 whereas it is very much pronounced in the case of the first three samples. The attenuation peaks around these temperatures have been observed by many groups and various possible reasons have been attributed to it, just as in the case of velocity measurements. The peaks are found to be highly sample dependent as well as frequency dependent. For example, Wolanski *et al.* [33] have reported attenuation measurements in pure and Ga doped YBCO. They observe attenuation maxima in the temperature range 175-200 K for both pure and doped samples. The positions of these peaks are found to be frequency dependent and they shift to higher temperatures as the frequency is increased. They attribute this to a thermally activated oxygen reorientation or a structural instability occurring in the samples in this temperature range.

Though reports vary on the exact reasons for this type of behaviour, most of them agree that the behaviour is characteristic of a relaxation process and various models have been suggested for the nature of the relaxation process. One of the reasons suggested is that of the orthorhombic distortion explained earlier. It is possible that this distortion also enhances the energy loss of sound at the same temperatures where there is anomalous change in velocity. The absence of any attenuation maximum in S4 may be due to the tetragonal structure of the sample. So from the velocity and attenuation measurements, it is safe to conclude that the structure of GdBCO remains orthorhombic upto a doping level of 4 at.% of Ga and at 6 at.% the structure is tetragonal.

From Fig. 4.4 it is clear that S2 has got the maximum value for elastic constant at all temperatures. Reports indicate that Ga can be incorporated into the lattice of

123 compounds only for low concentrations. This may be the reason for this behaviour and the decrease in elastic constant when the Ga concentration is greater than 2 at.% may be due to the deterioration of the single phase nature of the samples.

The Debye temperature is a very important physical parameter for a solid since it enters into a very large number of solid state phenomena such as temperature dependence of specific heat, electrical resistivity, diffuse X-ray reflection from lattice planes, scattering of thermal neutron by lattice vibrations etc. on account of its relationship with lattice vibrations. From the longitudinal and transverse velocities measured for sample S2, the Debye temperature is calculated and plotted as a function of temperature in Fig. 4.5. It essentially reflects the velocity variation; at T_c there is a pronounced slope change, much more pronounced than the one which is present in the longitudinal velocity in Fig. 4.1. This may be due to the fact that the anomaly near T_c is dominated by shear distortions, as explained earlier, which is reflected in Debye temperature.

4.4 Conclusions

A detailed study of the effect of Ga doping on the high T_c superconductor $\text{GdBa}_2\text{Cu}_3\text{O}_{7-\delta}$ has been carried out using ultrasonic technique. Longitudinal ultrasonic velocity and attenuation have been measured in samples with the general formula $\text{GdBa}_2(\text{Cu}_{1-x}\text{Ga}_x)_3\text{O}_{7-\delta}$ with $x = 0.0, 0.02, 0.04$ and 0.06 , as a function of temperature employing the pulse echo overlap technique and pulse comparison technique respectively in the temperature range 85 - 300 K. The longitudinal elastic constants are determined for all the samples at different temperatures and the Debye temperature is calculated for the sample with Ga concentration $x = 0.02$, for which the transverse velocity was also measured.

Apart from the anomalies observed near T_c , the samples exhibit pronounced anomalies in both velocity and attenuation in the temperature range 150 - 200 K. These changes are attributed to the structural changes taking place in the orthorhombic state due to Ga doping. The notable absence of anomalies in the sample with 6 at.% of Ga indicate that the structure has turned to tetragonal form at this concentration.

In summary, it can be concluded that the doping of Ga induces an orthorhom-

bic to tetragonal transition in GdBCO. The structure of GdBCO remains orthorhombic upto 4 at.% of Ga and it transforms into tetragonal form at 6 at.% of Ga. Our results reveal that this structural change can be detected from elastic measurements since they get reflected in the ultrasonic velocity and attenuation measurements.

4.5 References

- [1] H. C. Ku, M. F. Tai, S. W. Hsu, K. H. Lii, H. D. Yang and R. N. Shelton, *Chin. J. Phys.* **26**, S99 (1988).
- [2] P. H. Hor, R. L. Meng, Y. Q. Wang, L. Gao, Z. J. Huang, J. Bechtold, K. Forster and C. W. Chu, *Phys. Rev. Lett.* **58**, 1891 (1987).
- [3] K. N. Yang, Y. Dalichaouch, J. M. Ferreira, B. W. Lee, J. J. Neumeier, M. S. Torikachvili, H. Zhou, M. B. Maple and R. R. Hake, *Solid State Commun.* **63**, 515 (1987).
- [4] K. B. Lee, C. M. Park, H. S. Noh, C. K. Kim and K. Nahm, *J. Mater. Sci.* **28**, 6545 (1993).
- [5] Z. Fisk, J. D. Thompson, E. Zirngiebl, J. L. Smith and S. W. Cheong, *Solid State Commun.* **62**, 743 (1987).
- [6] J. P. Franck, J. Jung and M. A. K. Mohamed, *Phys. Rev.* **B36**, 2308 (1987).
- [7] Y. Saito, T. Noji, A. Endo, N. Higuchi, K. Fujimoto, T. Oikawa, A. Hattori and K. Furuse, in *Superconductivity in Highly Correlated Fermion Systems* (eds. M. Tachiki, Y. Muto and S. Maekawa), North Holland, Amsterdam (1987) p.336.
- [8] T. Wada, S. Adachi, O. Inoue, S. Kawashima and T. Mirhara, *Jpn. J. Appl. Phys.* **26**, L1475 (1987).
- [9] N. S. Raman and B. Viswanathan, *Bull. Mater. Sci.* **16**, 381 (1993).
- [10] Y. Tatsumi, F. Kimura and K. Fujiwara, *Jpn. J. Appl. Phys.* **33**, L219 (1994).
- [11] S. H. Kilcoyne and P. Cywinski, *J. Phys.* **D20**, 1327 (1987).
- [12] K. N. R. Taylor, D. N. Matthews and G. I. Russel, *J. Cryst. Growth* **85**, 628 (1987).

- [13] S. R. Ovshinsky, R. T. Young, D. D. Allred, G. Demaggio and G. A. Van der Leeden, *Phys. Rev. Lett.* **58**, 2579 (1987).
- [14] Y. Koike, A. Kobayashi, T. Kawaguchi, M. Kato, T. Noji, Y. Ono, T. Hikita and Y. Saito, *Solid State Commun.* **82**, 889 (1992).
- [15] J. Arai, S. Ogawa and K. Umezawa, *Physica* **C206**, 257 (1993).
- [16] N. Ishikawa, N. Kuroda, H. Ikeda and R. Yoshizaki, *Physica* **C203**, 284 (1992).
- [17] R. K. Nkum, A. Punnett and W. R. Datars, *Physica* **C202**, 371 (1992).
- [18] S. P. Pandey, M. S. Hegde, B. V. Kumaraswamy and A. V. Narlikar, *Physica* **C206**, 207 (1993).
- [19] S. K. Agarwal, V. N. Moorthy, G. L. Bhalla, V. P. S. Awana and A. V. Narlikar, *Ind. J. Pure & Appl. Phys.* **30**, 586 (1992).
- [20] A. Lanckbeen, P. H. Duvigneaud, P. Diko, M. Mehbod, G. Maessen and R. Deltour, *J. Mater. Sci.* **29**, 5441 (1994).
- [21] S. B. Ogale, D. D. Choughule, S. M. Kanetkar, P. Guptasharma and M. Multani, *Solid State Commun.* **89**, 1 (1994).
- [22] G. Xiao, M. Z. Cieplak, D. Musser, A. Gavrin, F. H. Streitz, C. L. Chien, J. J. Rhyne and J. A. Gotaas, *Nature* **332**, 238 (1988).
- [23] G. Xiao, M. Z. Cieplak, A. Gavrin, F. H. Streitz, A. Bakhshai and C. L. Chien, *Phys. Rev. Lett.* **60**, 1446 (1988).
- [24] Y. Maeno, T. Tomita, M. Kyogoku, S. Awaji, Y. Aoki, K. Hoshino, A. Minami and T. Fujita, *Nature* **328**, 512 (1987).
- [25] Y. Xu, R. L. Sabatini, A. R. Moodenbaugh and M. Suenaga, *Phys. Rev.* **B38**, 7084 (1988).
- [26] Y. Xu and W. Guan, *Physica* **C212**, 119 (1993).

- [27] T. A. Mary and U. V. Varadaraju, *Mat. Res. Bull.* **27**, 447 (1992).
- [28] M. Hiratani, Y. Ito, K. Miyauchi and T. Kudo, *Jpn. J. Appl. Phys.* **26**, L1997 (1987).
- [29] R. Suryanarayanan, G. T. Bhandage, M. Rateau, O. Gorochoy, H. Pankowska, A. M. Ghorayeb, G. Villers and C. Vard, *J. Less Common Metals* **151**, 109 (1989).
- [30] T. Den and T. Kobayashi, *Physica* **C196**, 141 (1992).
- [31] N. C. Mishra, A. K. Rajarajan, K. Patnaik, R. Vijayaraghavan and L. C. Gupta, *Bull. Mat. Sci.* **14**, 263 (1991).
- [32] S. A. Hoffman, M. A. Castro, G. C. Follis and S. M. Durbin, *Physica* **C208**, 59 (1993).
- [33] M. Wolanski, G. Savarino, T. Coyne and J. Trivisonno, *Proc. IEEE Ultrasonics Symposium* 445 (1989).
- [34] T. Siegrist, L. F. Schneemeyer, J. V. Waszczak, N. P. Singh, R. L. Opila, B. Batlogg, L. W. Rupp and D. W. Murphy, *Phys. Rev.* **B36**, 8365 (1987).
- [35] M. F. Xu, Y. J. Qian, K. J. Sun, Y. Zheng, Q. Ran, D. Hinks, B. K. Sarma and M. Levy, *Physica* **B165-166**, 1281 (1990).
- [36] D. J. Bishop, A. P. Ramirez, P. L. Gammel, B. Batlogg, E. A. Rietmann, R. J. Cava and A. J. Millis, *Phys. Rev.* **B35**, 8785 (1987).
- [37] Y. Horie and S. Mase, *Solid State Commun.* **69**, 535 (1988).
- [38] S. Bhattacharya, M. Higgins, D. Johnston, A. Jacobson, J. Stokes, J. Lewandowski and D. Goshorn, *Phys. Rev.* **B37**, 5901 (1988).
- [39] R. Abd-Shukor, *Jpn. J. Appl. Phys.* **31**, L1034 (1992).
- [40] G. Cannelli, R. Cantelli and F. Cordero, *Int. J. Mod. Phys.* **1**, 1157 (1988).

- [41] J. Jiang, H. Yin, X. Wang, Y. Sun, F. Zeng and J. Du, *Mater. Sci. Eng.* **B7**, 227 (1990).
- [42] J. Toulouse, X. M. Wang and D. J. L. Hong, *Phase Transitions* **23**, 35 (1990).
- [43] V. Muller and D. Maurer, *Phase Transitions* **22**, 211 (1990).
- [44] Y. Mi, R. Schaller, H. Berger, W. Benoit and S. Sathish, *Physica* **C172**, 407 (1991).
- [45] D. P. Almond, E. Lambson, G. A. Saunders and H. Wang, *J. Phys.* **F17**, L1221 (1987).
- [46] A. G. Ivanov and L. T. Tsymbal, *Physica* **B169**, 641 (1991).
- [47] G. A. Alers in *Physical Acoustics*, Vol.3, Part B, (ed. W. P. Mason), Academic Press, New York (1965).
- [48] D. P. Almond, Q. Wang, F. Freestone, E. F. Lambson, B. Chapman and G. A. Saunders, *J. Phys.* **C1**, 6853 (1989).

Chapter 5

Elastic phase velocity surfaces of high T_c superconductors

5.1 Introduction

The study of elastic properties of a material is very important since they are directly related to various fundamental solid state parameters such as specific heat, Debye temperature, phonon dispersion, thermal expansion, Gruneisen parameter etc. For superconductors, since the elastic constants can be linked explicitly to the superconducting transition temperature through the Debye temperature and the electron-phonon coupling parameter, their measurement become all the more important. In addition, the elastic constants directly determine the behaviour of long-wavelength acoustic phonons and provide a sensitive probe of structure related properties and phase transitions occurring in these materials. Because of these reasons, there have been a large number of studies on the elastic properties of these materials, aimed at getting some insight into the mechanisms responsible for superconductivity.

Extensive sound velocity measurements have been reported in high T_c superconducting cuprates, for a variety of reasons. First, as is obvious from their structures, they are extremely anisotropic, with a strong two-dimensional character. Therefore the coupling of superconductivity to structural distortions could also be highly anisotropic. Measurement of the sound velocity anomaly at the superconducting transition for sound waves with different polarizations propagating in different directions would, in principle, provide information on this particular aspect of superconductivity. Second, there are structural transitions in these systems, such as tetragonal to orthorhombic, that occur

above T_c , similar to the A-15 compounds, which get reflected in elastic measurements.

However, most of the early work on the elastic properties of these materials were performed on ceramic polycrystalline samples using ultrasonic or vibrating reed techniques. Since the synthesis of ceramic samples with dimensions large enough for the measurements is comparatively easy, numerous papers have appeared in literature reporting elastic measurements on such samples. Though these studies provide a very good tool to probe the bulk properties of these materials, they fail to give information about the elastic anisotropy, since such experiments generally probe the spherically averaged properties.

Elastic constant measurements on single crystals is the solution to the above problem. Growth of large and homogeneous single crystals of high T_c materials has proved to be extremely difficult when compared to the ceramic specimens and as a result there have been only a handful of elastic measurements reported on single crystals. Moreover, single crystals are usually in the form of thin platelets that do not allow the determination of the whole set of elastic constants and because of their small dimensions, precise measurement of elastic constants is rather difficult. Even by using the resonant ultrasound technique, which enables one to measure the elastic constants of small crystals of the size of even a few hundred microns, all the elastic constants of high T_c materials above and below T_c have not yet been reported due to various difficulties. Further, these systems and their superconducting properties are found to be extremely sensitive to their composition, such as oxygen stoichiometry. Moreover, since the superconducting coherence length is extremely short in these materials, one is not sure about the sample homogeneity even in small single crystals.

An alternative way to obtain information on the anisotropic elastic properties of high T_c superconducting materials is to make measurements on samples with preferentially aligned crystallites, or the so-called sinterforged samples. Large size samples are rather easy to obtain in this form as compared to single crystals and pulsed echoes in ultrasonic experiments can be separated owing to proper size of the samples. Oxygen content is usually more homogeneous because of the small size of the crystallites within them. Above all, these samples yield a nearly uniaxial symmetry, whereby the

behaviour in the Cu-O layers, as opposed to directions perpendicular to them, can be sorted out.

Eventhough elastic properties of these materials have been investigated thoroughly and elastic constants determined accurately for many of them, no serious attempt has been made so far to plot elastic wave surfaces and study elastic anisotropy in these materials in a systematic way. In this chapter, we have made an attempt to do this and analyse the results obtained on three popular high T_c superconductors, $\text{Bi}_2\text{Sr}_2\text{CaCu}_2\text{O}_{8-\delta}$, $\text{RBa}_2\text{Cu}_3\text{O}_{7-\delta}$ ($R = \text{Y}$ or Gd) and $\text{La}_{2-x}\text{Sr}_x\text{CuO}_{4-\delta}$. The details of this calculation of the phase velocity surfaces is presented after outlining the theory of elastic wave propagation in anisotropic solids and applying it to orthorhombic and tetragonal crystal symmetries to which most of the high T_c materials belong.

5.2 Elastic wave propagation in anisotropic solids

Elastic waves are generated by mechanical vibrations of material media, which are the result of collective vibrations of the atoms and molecules of the medium. The vibration characteristics of the atoms and molecules of the medium are determined by the magnitude of the interatomic forces, and the nature of these forces and hence their wave propagation characteristics are different for solids with different structures.

The elastic properties of a medium is understood in terms of its response to an applied stress. Under the application of an external stress the medium undergoes deformation and gets strained. The magnitude of the strain developed for a given stress is a characteristic of the medium. Under the assumption that stress is proportional to strain within the elastic deformation limit, the Hooke's law can be expressed as

$$\sigma_{ij} = \Sigma C_{ijkl} \epsilon_{kl} \quad (5.1)$$

Since the stress and strain are tensors of rank two, the proportionality constant connecting them is a fourth rank tensor, called the elastic stiffness C_{ijkl} . Its inverse is the elastic compliance S_{ijkl} which relates the strain to stress. Both C_{ijkl} and S_{ijkl} have 81 elements relating nine stress components to nine strain components. For convenience, a more compact two suffix notation is generally used to represent the elastic constants

in which the tensor for the C_{ijkl} ($i, j, k, l = 1, 2, 3$) is replaced by the matrix C_{ij} ($i, j = 1, 2, 3, 4, 5, 6$) according to the following equality

Tensor notation	11	22	33	23, 32	31, 13	12, 21
Matrix notation	1	2	3	4	5	6

which is called the Voigt notation [1,2].

When all the symmetries of the stress and strain components are taken into consideration, the number of independent elastic constants reduces to 21, which is the case for the most anisotropic system - the triclinic crystal. Further reduction in the number of independent elastic constants is possible when the structural symmetry of the crystals are considered and this number is different for the different crystal classes. For example, a cubic crystal has only 3 independent elastic constants, whereas an orthorhombic crystal has 9. An isotropic solid has only two independent elastic constants which are sometimes called the Lamé constants.

The propagation of acoustic waves in elastically anisotropic solids is governed by a set of three linear equations known as Christoffel equations. This characteristic equation relates the velocity v , the direction of wave propagation and the elastic constants of the medium and is cubic in v^2 . These equations play a central role in crystal acoustics, and their solutions are required for a wide variety of purposes [1-7]. Considerable simplification of these equations comes about when the wave normal lies along a crystal symmetry direction.

Consider an anisotropic medium which shows the ideal Hooke's law behaviour and in which dissipative, nonlinear and dispersive phenomena can be neglected. A disturbance in such a medium is governed by the equations of motion for an element of the medium. This, when expressed in the tensor format, will be

$$\rho \frac{\partial^2 u_i}{\partial t^2} = \frac{\partial \sigma_{ij}}{\partial x_j} \quad (5.2)$$

where ρ is the density of the medium. When the right hand side of this equation is expressed in terms of the deformation components u_i , the wave equation is obtained as

$$\rho \frac{\partial^2 u_i}{\partial t^2} = C_{ijkl} \frac{\partial^2 u_k}{\partial x_j \partial x_l} \quad (5.3)$$

In an unbounded medium this equation has basic solutions given by plane waves,

$$u_i = U_i \exp[i(\mathbf{k} \cdot \mathbf{r} - \omega t)] \quad (5.4)$$

Inserting this solution in the wave equation, one obtains, the following conditions on the wave amplitude U_i

$$(C_{ijkl} k_j k_l - \rho \omega^2 \delta_{ik}) U_k = 0 \quad (5.5)$$

The three homogeneous equations for U_i from the above equation are the Christoffel equations and they have a solution only if the secular equations of their coefficients is satisfied. This requirement leads to the familiar form of a determinantal equation for the propagation velocity $v = \omega/k$. If the propagation vector is written in terms of the direction cosines as $\mathbf{k} = k(l, m, n)$, the secular determinant becomes

$$|\lambda_{ij} - \rho v^2 \delta_{ij}| = 0 \quad (5.6)$$

where the λ 's are the elements of the Christoffel matrix whose values depend on the directions of wave propagation and the elastic constants. The expanded form of this determinantal equation for the most unsymmetric case is

$$\begin{vmatrix} (\lambda_{11} - \rho v^2) & \lambda_{12} & \lambda_{13} \\ \lambda_{12} & (\lambda_{22} - \rho v^2) & \lambda_{23} \\ \lambda_{13} & \lambda_{23} & (\lambda_{33} - \rho v^2) \end{vmatrix} = 0 \quad (5.7)$$

where the Christoffel coefficients are

$$\begin{aligned} \lambda_{11} &= l^2 C_{11} + m^2 C_{66} + n^2 C_{55} + 2mn C_{56} + 2nl C_{15} + 2lm C_{16} \\ \lambda_{22} &= l^2 C_{66} + m^2 C_{22} + n^2 C_{44} + 2mn C_{24} + 2nl C_{46} + 2lm C_{26} \\ \lambda_{33} &= l^2 C_{55} + m^2 C_{44} + n^2 C_{33} + 2mn C_{34} + 2nl C_{35} + 2lm C_{45} \\ \lambda_{12} &= l^2 C_{16} + m^2 C_{26} + n^2 C_{45} + mn(C_{25} + C_{46}) + nl(C_{14} + C_{56}) + lm(C_{12} + C_{66}) \\ \lambda_{13} &= l^2 C_{15} + m^2 C_{46} + n^2 C_{35} + mn(C_{36} + C_{45}) + nl(C_{13} + C_{55}) + lm(C_{14} + C_{56}) \\ \lambda_{23} &= l^2 C_{56} + m^2 C_{24} + n^2 C_{34} + mn(C_{23} + C_{44}) + nl(C_{36} + C_{45}) + lm(C_{25} + C_{46}) \end{aligned} \quad (5.8)$$

On evaluating the determinant and equating it to zero, the secular equation is obtained. This is a cubic equation in v^2 and hence has got three solutions. Thus in a given direction

there are three waves propagating with different velocities. The fastest of the three is the longitudinal wave or the quasilongitudinal wave, while the other two are the fast and slow shear waves or the pure and quasi shear waves. The waves are purely longitudinal or purely transverse only in the pure mode directions in the crystal and these directions are usually the symmetry directions or symmetry planes in the crystal.

5.3 Wave propagation in orthorhombic and tetragonal systems

The general expressions for elastic wave propagation presented in the previous section are required for the most unsymmetric triclinic crystal. Much simplified equations can be obtained for higher symmetry crystals since several elastic constants are zero for such crystals. Further simplification occurs when symmetry directions or planes are considered in which one or two of the direction cosines l , m , or n becomes equal to zero as shown in Fig. 5.1. Since all the superconductors for which the elastic wave surfaces are plotted in this chapter belong either to the orthorhombic or tetragonal symmetry, the necessary equations are given for these two crystal systems in the following paragraphs.

For orthorhombic crystals of all point groups the nonzero elastic constants are C_{11} , C_{22} , C_{33} , C_{44} , C_{55} , C_{66} , C_{12} , C_{13} and C_{23} . Retaining only those terms that contain the nonzero elements, the coefficients of the Christoffel matrix λ_{ij} can be written as

$$\begin{aligned}
 \lambda_{11} &= l^2 C_{11} + m^2 C_{66} + n^2 C_{55} \\
 \lambda_{22} &= l^2 C_{66} + m^2 C_{22} + n^2 C_{44} \\
 \lambda_{33} &= l^2 C_{55} + m^2 C_{44} + n^2 C_{33} \\
 \lambda_{12} &= lm (C_{12} + C_{66}) \\
 \lambda_{13} &= nl (C_{13} + C_{55}) \\
 \lambda_{23} &= mn (C_{23} + C_{44})
 \end{aligned} \tag{5.9}$$

Some of the off diagonal terms of λ_{ij} are still not equal to zero and so the characteristic equation cannot be factored and single term equations cannot be written for the velocity. So propagation of elastic waves in different symmetry planes are

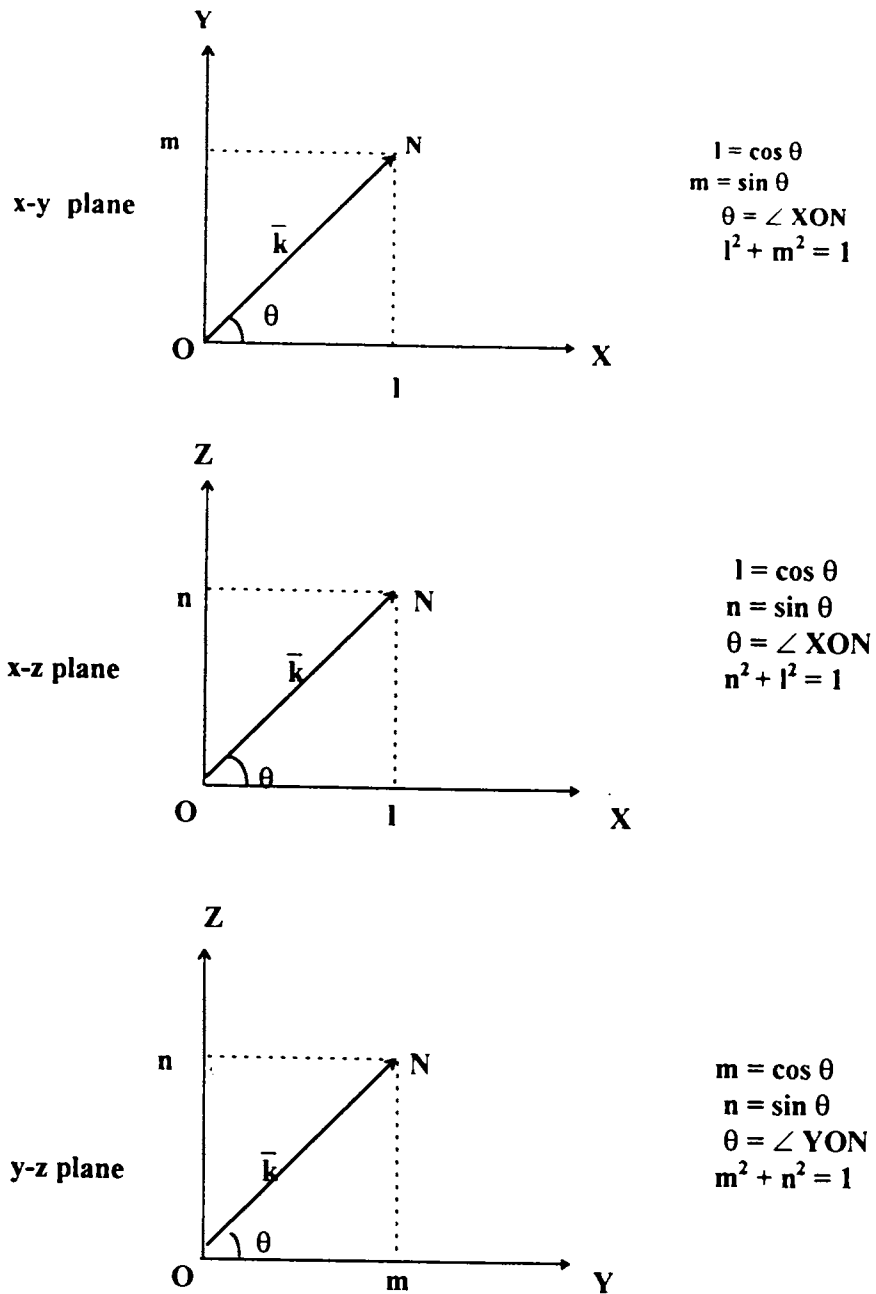


Fig. 5.1

Direction cosines to rotation angle conversion scheme in symmetry planes.

considered separately.

X-Y plane

Consider a wave propagating in the X-Y (a-b) plane, for which $n = 0$. The λ coefficients then become

$$\begin{aligned}
 \lambda_{11} &= l^2 C_{11} + m^2 C_{66} \\
 \lambda_{22} &= l^2 C_{66} + m^2 C_{22} \\
 \lambda_{33} &= l^2 C_{55} + m^2 C_{44} \\
 \lambda_{12} &= lm (C_{12} + C_{66}) \\
 \lambda_{13} &= 0 \\
 \lambda_{23} &= 0
 \end{aligned} \tag{5.10}$$

The determinantal equation can now be written as

$$\begin{vmatrix}
 (\lambda_{11} - \rho v^2) & \lambda_{12} & 0 \\
 \lambda_{12} & (\lambda_{22} - \rho v^2) & 0 \\
 0 & 0 & (\lambda_{33} - \rho v^2)
 \end{vmatrix} = 0 \tag{5.11}$$

Expanding this, one obtains

$$(\lambda_{33} - \rho v^2) [\rho^2 v^4 - \rho v^2 (\lambda_{11} + \lambda_{22}) + \lambda_{11} \lambda_{22} - \lambda_{12}^2] = 0 \tag{5.12}$$

Solving and substituting the values of λ , three solutions are obtained as

$$\begin{aligned}
 \rho v_0^2 &= C_{44} l^2 + C_{55} m^2 \\
 2\rho v_1^2 &= (C_{66} + C_{11} l^2 + C_{22} m^2) - \sqrt{(C_{66} + C_{11} l^2 + C_{22} m^2)^2 - 4C} \\
 2\rho v_2^2 &= (C_{66} + C_{11} l^2 + C_{22} m^2) + \sqrt{(C_{66} + C_{11} l^2 + C_{22} m^2)^2 - 4C}
 \end{aligned} \tag{5.13}$$

where

$$C = (C_{11} l^2 + C_{66} m^2) (C_{66} l^2 + C_{22} m^2) - (C_{12} + C_{66})^2 l^2 m^2$$

Here v_0 is the velocity of a pure shear wave with polarisation in the Z - direction, while v_1 is the velocity of a quasishear wave and v_2 that of a quasilongitudinal one.

X-Z plane

Consider the wave propagation in the X-Z (a-c) plane, for which $m = 0$. The λ_{ij}

coefficients are

$$\begin{aligned}
\lambda_{11} &= l^2 C_{11} + n^2 C_{55} \\
\lambda_{22} &= l^2 C_{66} + n^2 C_{44} \\
\lambda_{33} &= l^2 C_{55} + n^2 C_{33} \\
\lambda_{12} &= 0 \\
\lambda_{13} &= nl(C_{13} + C_{55}) \\
\lambda_{23} &= 0
\end{aligned} \tag{5.14}$$

The characteristic equation is then given by

$$(\lambda_{22} - \rho v^2) [\rho^2 v^4 - \rho v^2(\lambda_{11} + \lambda_{33}) + \lambda_{11} \lambda_{33} - \lambda_{13}^2] = 0 \tag{5.15}$$

Solving and substituting for λ 's as before,

$$\begin{aligned}
\rho v_0^2 &= C_{66} l^2 + C_{44} n^2 \\
2\rho v_1^2 &= (C_{55} + C_{11} l^2 + C_{33} n^2) - \sqrt{(C_{55} + C_{11} l^2 + C_{33} n^2)^2 - 4C'} \\
2\rho v_2^2 &= (C_{55} + C_{11} l^2 + C_{33} n^2) + \sqrt{(C_{55} + C_{11} l^2 + C_{33} n^2)^2 - 4C'}
\end{aligned} \tag{5.16}$$

where

$$C' = (C_{11} l^2 + C_{55} n^2)(C_{55} l^2 + C_{33} n^2) - (C_{13} + C_{55})^2 l^2 n^2$$

Y-Z plane

Considering the wave propagation in the Y-Z (b-c) plane for which $l = 0$, the coefficients are obtained as

$$\begin{aligned}
\lambda_{11} &= m^2 C_{66} + n^2 C_{55} \\
\lambda_{22} &= m^2 C_{22} + n^2 C_{44} \\
\lambda_{33} &= m^2 C_{44} + n^2 C_{33} \\
\lambda_{12} &= 0 \\
\lambda_{13} &= 0 \\
\lambda_{23} &= mn(C_{23} + C_{44})
\end{aligned} \tag{5.17}$$

The characteristic equation is then obtained as

$$(\lambda_{11} - \rho v^2) \left[\rho^2 v^4 - \rho v^2 (\lambda_{22} + \lambda_{33}) + \lambda_{22} \lambda_{33} - \lambda_{23}^2 \right] = 0 \quad (5.18)$$

The solutions of this equation are

$$\begin{aligned} \rho v_0^2 &= C_{66} m^2 + C_{55} n^2 \\ 2\rho v_1^2 &= (C_{44} + C_{22} m^2 + C_{33} n^2) - \sqrt{(C_{44} + C_{22} m^2 + C_{33} n^2)^2 - 4C''} \\ 2\rho v_2^2 &= (C_{44} + C_{22} m^2 + C_{33} n^2) + \sqrt{(C_{44} + C_{22} m^2 + C_{33} n^2)^2 - 4C''} \end{aligned} \quad (5.19)$$

where

$$C'' = (C_{22} m^2 + C_{44} n^2) (C_{44} m^2 + C_{33} n^2) - (C_{23} + C_{44})^2 m^2 n^2$$

The above analysis has provided three sets of equations corresponding to the three orthogonal symmetry planes of the orthorhombic crystal. It can be seen that when the wave propagation is in a symmetry plane there is always a pure shear mode which is polarised normal to the plane. These equations can be used to compute the velocities in any direction in these symmetry planes if the elastic constants are known.

For tetragonal crystals, the number of elastic constants can be 7 or 6 depending on the symmetry of the point group. The superconductor having tetragonal symmetry considered here comes under the second category and the six nonzero elastic constants for it are C_{11} , C_{33} , C_{44} , C_{66} , C_{12} and C_{13} . The equations for the wave propagation in a tetragonal crystal are very easily obtained from the equations for the orthorhombic crystal, by making the substitutions $C_{11} = C_{22}$, $C_{44} = C_{55}$ and $C_{13} = C_{23}$ and hence these equations are not rewritten. Further, it can be seen that these simplifications yield the same expressions for the velocities of waves propagating in the XZ and YZ planes.

5.4 Elastic wave surfaces of selected high T_c superconductors

The elastic wave propagation is highly anisotropic in many crystals in the sense that waves with different polarisations propagate with different velocities in different directions. Except in certain special directions, waves are not strictly transverse or longitudinal in crystals, as is clear from the above analysis. The velocities calculated from

the elastic constants as a function of θ (defined in Fig. 5.1) can be plotted for different propagation directions lying in different planes for each polarisation mode which give the corresponding phase velocity surfaces. The inverse of phase velocities also can be plotted for various propagation directions which are referred to as slowness surfaces. The pictorial representation of the wave velocities give a much better understanding of the anisotropic nature of elastic wave propagation in different directions in a crystal.

In this work, we have studied the anisotropy in elastic wave propagation in selected high T_c superconducting samples, by plotting the phase velocity surfaces in different symmetry planes. The surfaces have been plotted for three major superconductors - $\text{Bi}_2\text{Sr}_2\text{CaCu}_2\text{O}_{8-\delta}$, $\text{RBa}_2\text{Cu}_3\text{O}_{7-\delta}$ and $\text{La}_{2-x}\text{Sr}_x\text{CuO}_{4-\delta}$ - and for the nonsuperconducting La_2CuO_4 , at temperatures above and below T_c , either for single crystals, sinterforged samples or ceramic polycrystalline specimens subject to the availability of elastic constant data.

All the three systems studied belong either to the orthorhombic or tetragonal symmetry. The expressions for the velocities of acoustic waves in the symmetry planes of orthorhombic and tetragonal lattice are derived in the above section, using which the velocities have been computed and plotted for the superconducting systems. The velocities have been calculated using the elastic constant data taken from literature, as a function of θ varying from 0 to 2π in steps of 2° . For plotting the surfaces the calculated velocity v and the angle θ is converted into the x and y coordinates. If θ is measured from the x-axis, the x and y components are given by

$$\begin{aligned} x &= v \cos\theta \\ y &= v \sin\theta \end{aligned} \tag{5.20}$$

and if θ is measured from the y-axis, the corresponding relations are

$$\begin{aligned} x &= v \sin\theta \\ y &= v \cos\theta \end{aligned} \tag{5.21}$$

The work done on different systems are separately outlined in the following sections.

5.4.1 $\text{Bi}_2\text{Sr}_2\text{CaCu}_2\text{O}_{8-\delta}$ (BSCCO)

This compound is the second member of the superconductor family having the general formula $\text{Bi}_2\text{Sr}_2\text{Ca}_{n-1}\text{Cu}_n\text{O}_{4+2n-\delta}$ with $n = 1, 2, 3$ and is often referred to as the Bi2212 phase. The structure of BSCCO is orthorhombic with $c = 30.8445 \text{ \AA}$ which is much larger than the lattice parameters $a = 5.4091 \text{ \AA}$ and $b = 5.4209 \text{ \AA}$ which are nearly equal.

Eventhough there are many reports on the elastic properties of this material, none of them give the complete set of elastic constants, numbering nine, even at room temperature. The major work in this regard is by Wu *et al.* [8] who have determined the temperature variation of several of the constants by ultrasonic measurements, but do not give all the constants even at room temperature. There are other reports also which give only one or two constants [9-11].

However, a clear picture of the anisotropy in elastic wave propagation and their variation with temperature can be obtained since Saunders *et al.* [12] have determined all the elastic constants from ultrasonic measurements on a textured sample of BSCCO both above and below T_c . In this sample, a high proportion of the grains are found to be aligned preferentially with the c -axis along the forging direction, while it is isotropic in the plane normal to the forging axis. So the sample is assumed to have a cylindrical symmetry and the five independent elastic constants are given at 290 K and 20 K. In addition, they have plotted the velocity surfaces for the XZ plane at 290 K. Another important work in this direction is by Boekholt *et al.* [13], who have reported room temperature elastic constants measured from Brillouin light scattering experiments on a single crystal. Here also cylindrical symmetry is assumed and the five independent elastic constants have been determined. The elastic constants reported by different authors for this material are tabulated in Table 5.1.

We have computed the phase velocity surfaces above and below T_c using eqns. (5.13) and (5.16) using the elastic constants reported by Saunders *et al.* [12]. Because of the cylindrical symmetry of the sample, the surfaces are the same in the XZ and YZ planes. Figs. 5.2(a) and 5.2(b) gives the plots at 290 K while Figs. 5.2(c) and 5.2(d) are those at 20K where the symbols ps, qs and ql refer to the pure shear,

Table 5.1

Elastic constants of BSCCO (values in GPa)

C_{11}	C_{22}	C_{33}	C_{44}	C_{55}	C_{66}	C_{12}	C_{13}	C_{23}	T (K)	Reference
123.2	110.8	-	-	-	50.4	67.3	-	-	250	[8]
133.1	119.6	-	-	-	50.4	65.8	-	-	200	[8]
137.2	127.6	-	-	-	50.3	75.9	-	-	150	[8]
141.9	134.4	-	-	-	50.5	83.8	-	-	100	[8]
144.9	136.0	-	-	-	50.7	77.4	-	-	80	[8]
130.0	110.0	-	-	-	51.0	72.0	-	-	260	[9]
143.0	-	-	-	-	-	-	-	-	-	[10]
165.0	-	-	-	-	-	-	-	-	-	[11]
118.5		44.2	19.0		37.70	43.1	7.3		290	[12]
124.0		45.2	20.2		40.20	43.7	7.5		20	[12]
125.2		75.8	15.8		23.15	78.9	56.0		300	[13]

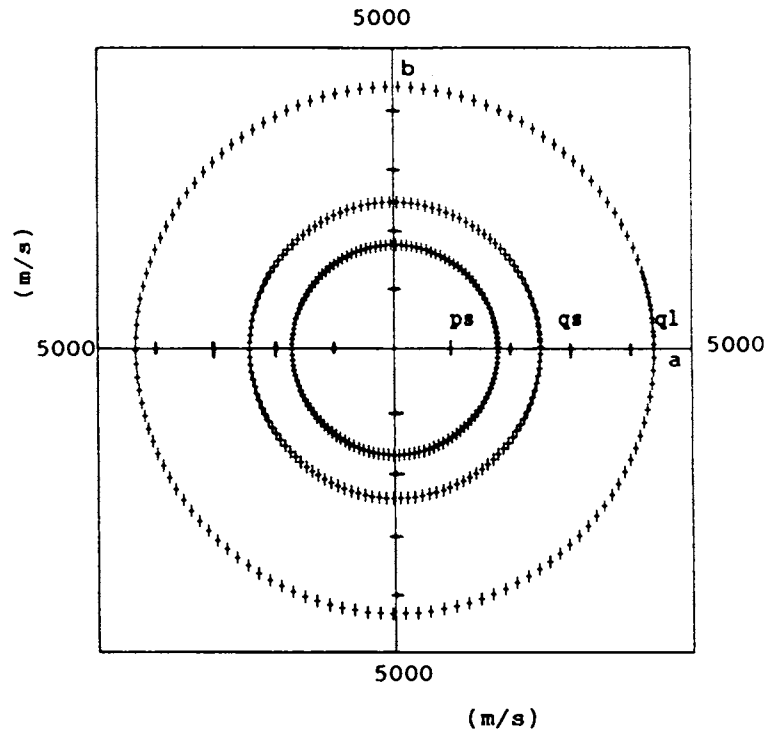


Fig. 5.2(a) Phase velocity surfaces in the ab (XY) plane for BSCCO at 290 K.

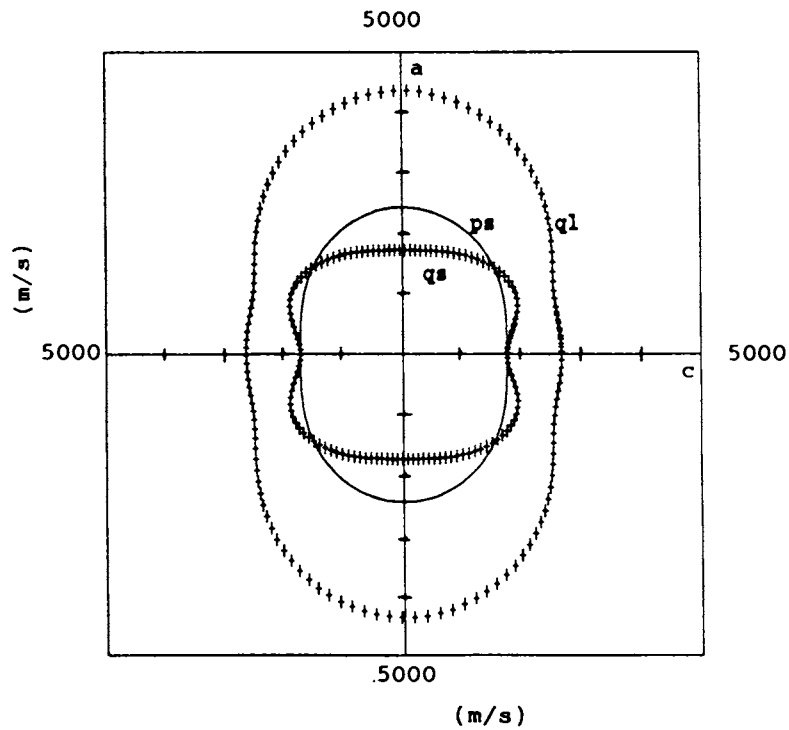


Fig. 5.2(b) Phase velocity surfaces in the ac (XZ) plane for BSCCO at 290 K.

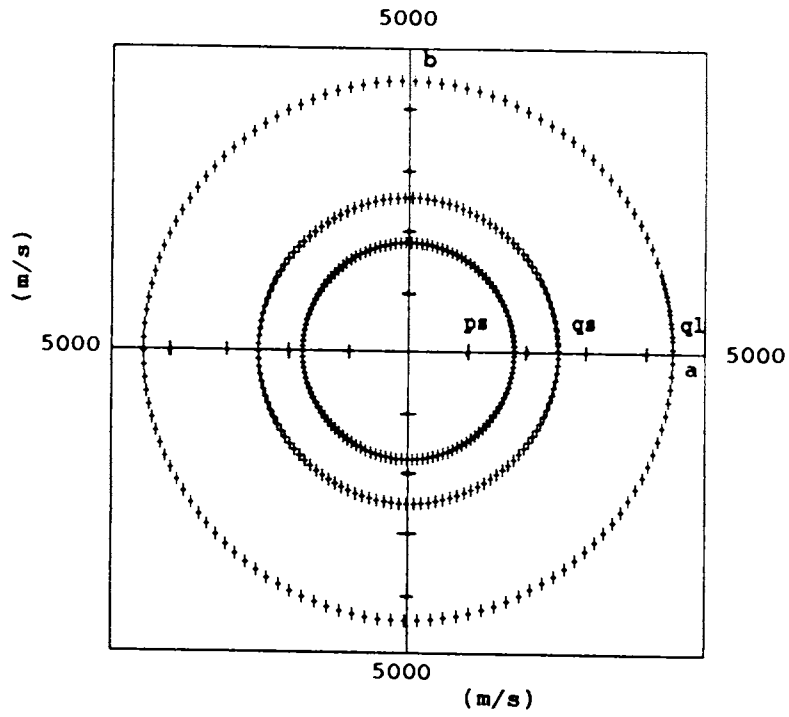


Fig. 5.2(c) Phase velocity surfaces in the ab (XY) plane for BSCCO at 20 K.

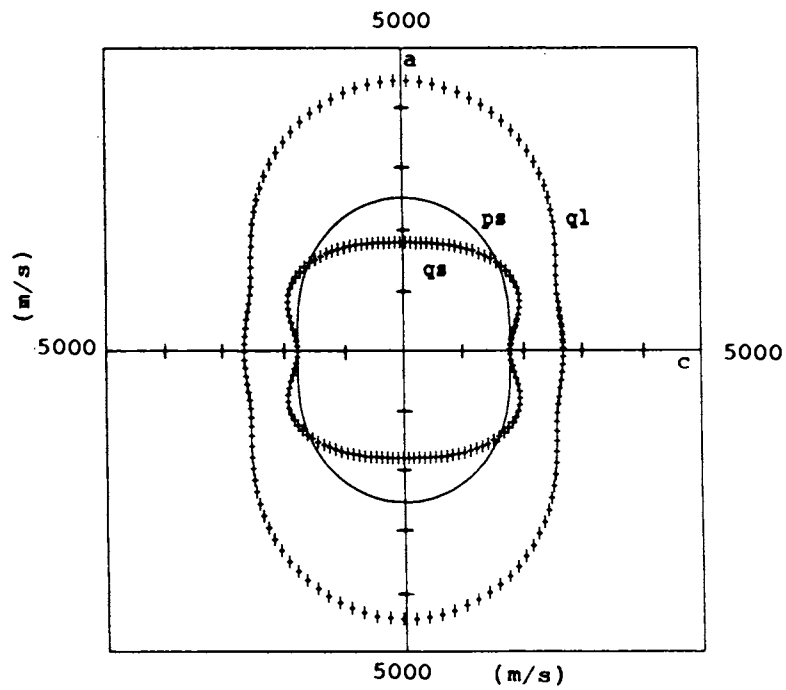


Fig. 5.2(d) Phase velocity surfaces in the ac (XZ) plane for BSCCO at 20 K.

quasishear and quasilongitudinal modes respectively.

5.4.2 $\text{RBa}_2\text{Cu}_3\text{O}_{7-\delta}$ (RBCO) (R = Y or Gd)

These compounds, also called the '123' compound have been investigated very thoroughly owing to their relatively high T_c values and straight forward method of synthesis. The structure of RBCO at room temperature is orthorhombic and is a tripled perovskite with a unit cell containing two Cu-O₂ layers (planes) and one Cu-O chain.

The elastic properties of this material have been investigated extensively. There exists several ultrasonic and other measurements of elastic constants on samples in the single crystal form [14-23]. The elastic constants reported for this material are summarised in Table 5.2.

The complete set of elastic constants for YBCO at room temperature are available from three different groups. Ming Lei *et al.* [14] have measured the complete set of elastic constants by the resonant ultrasound technique, while Ledbetter and Lei [15] have given the complete set from a semi-theoretical estimate. The third set by Reichardt *et al.* [16] is from inelastic neutron scattering and since they assume tetragonal symmetry only six constants are reported by them. Incomplete set of elastic constant data is available from many groups [17-23] which also are given in the table.

The phase velocity surfaces for YBCO have been plotted at room temperature using the elastic constant data reported by Ming Lei *et al.* [14]. Results obtained for propagation in the XY, XZ and YZ planes are plotted in Figs. 5.3(a), 5.3(b) and 5.3(c), where the symbols ps, qs and ql have the usual meaning. Though there are a number of measurements reported at low temperatures, for example Golding *et al.* [18] give two constants C_{11} and C_{33} measured at 80 K, no data giving complete set of elastic constants at low temperatures could be found.

As mentioned earlier, one of the alternative ways to shed light on the anisotropic nature of the elastic properties of these materials is to study the sinter forged materials when data on single crystals is lacking. Sinterforged YBCO samples show preferential orientation [24] with 80% of the *c*-axis of the crystallites aligned within 20° of the forging axis. Since in the direction perpendicular to the forging axis, the *a*

and b axes of the crystallites are randomly oriented, such samples show rotational symmetry and hence there are five different propagation modes for elastic waves. The major works are by Xu *et al.* [25] and Zhao *et al.* [26] who have reported incomplete sets of elastic constants at room temperature but no data at low temperatures could be found in literature for these type of samples.

Since a comparison of the wave surfaces above and below T_c has not been possible for YBCO due to the lack of data at low temperatures, we have plotted the surfaces for a polycrystalline 123 sample - GdBCO. For a polycrystalline material, the phase velocity is independent of direction and has only two values; v_l for the longitudinal wave and v_s for the shear wave. Many reports can be found in literature which give the longitudinal and transverse velocities of 123 compounds. The elastic constants taken from some of these reports for GdBCO are tabulated in Table 5.3, along with the values we have measured for a superconducting GdBCO at 300 K and 90 K using the ultrasonic pulse echo overlap technique. Figures 5.3(d) and 5.3(e) depict the surfaces at 300 K and 90 K plotted using the values measured by us where the symbols s and l refer to the shear and longitudinal modes respectively.

5.4.3 $\text{La}_{2-x}\text{Sr}_x\text{CuO}_{4-y}$ (LSCO)

This superconducting compound is derived from the stoichiometric compound La_2CuO_4 (LCO) by replacing La^{3+} with Sr^{2+} (or Ba^{2+}) partially. The parent LCO is a semiconductor which exhibits tetragonal symmetry of $I4/mmm$ space group at high temperatures (above 530 K), which distorts to a lower symmetry orthorhombic state on cooling. Since most of the measurements reported are at and below room temperature, the structure is invariably orthorhombic in all these. As La^{3+} is replaced by Sr^{2+} , the temperature at which the tetragonal - orthorhombic transition takes place decreases and LSCO is found to undergo the transition around 180 K for $x = 0.15$. So the superconducting LSCO has a tetragonal structure at room temperature and it transforms to the orthorhombic state at ≈ 180 K.

Though the parent compound LCO is not a superconductor, the elastic properties of this compound has also been measured. Migliori *et al.* [30] have measured all

Table 5.2

Elastic constants of YBCO (values in GPa)

C_{11}	C_{22}	C_{33}	C_{44}	C_{55}	C_{66}	C_{12}	C_{13}	C_{23}	T (K)	Reference
231	268	186	49	37	95	132	71	95	295	[14]
223	244	138	61	47	97	37	89	93	295	[15]
230	230	150	50	50	85	100	100	100	295	[16]
211	-	159	35	-	-	-	-	-		[17]
234	-	145	-	-	-	-	-	-	80	[18]
-	-	160	25	-	82	66	-	-		[19]
-	-	-	42	33	57	-	-	-		[21]
207	-	63	31,36	-	85	-	-	-	220	[22]
315	275	279	-	-	-	-	-	-		[23]

Table 5.3The longitudinal (C_l) and shear (C_s) elastic constants of polycrystalline GdBCO (values in GPa)

C_l	C_s	T(K)	References
143.5	49.4	300	[27]
149.1	52.4	90	[27]
158.2	52.0	-	[28]
170.6	64.5	4	[29]

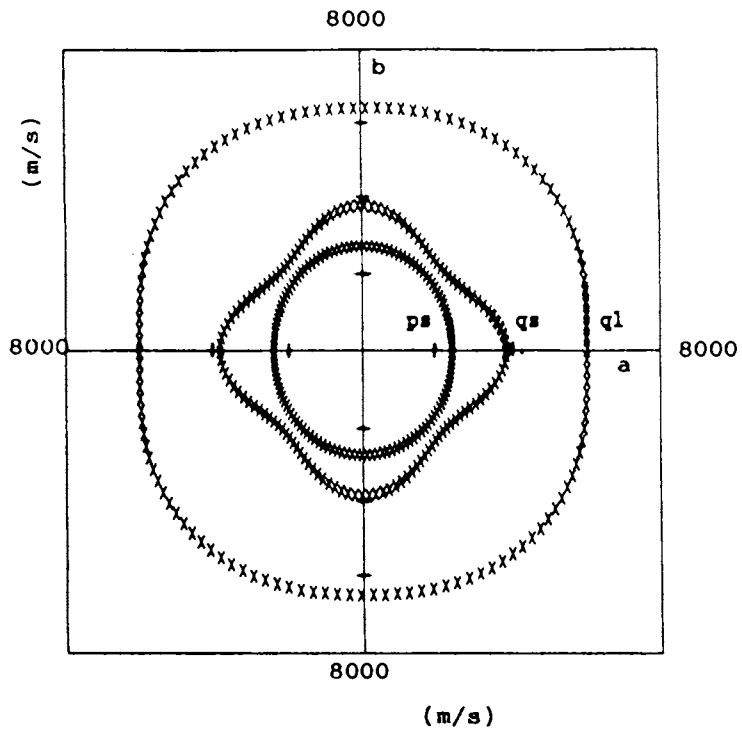


Fig. 5.3(a) Phase velocity surfaces in the ab (XY) plane at room temperature for YBCO.

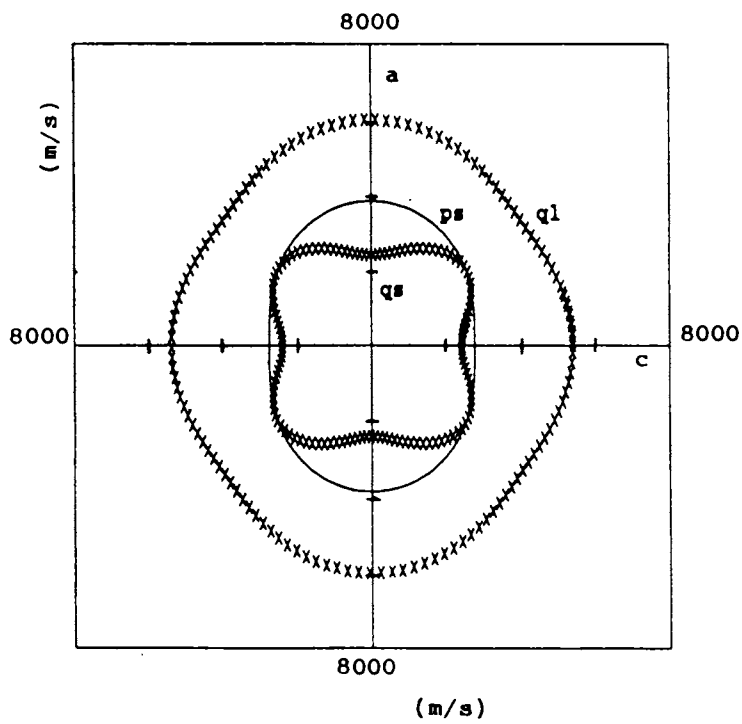


Fig. 5.3(b) Phase velocity surfaces in the ac (XZ) plane at room temperature for YBCO.

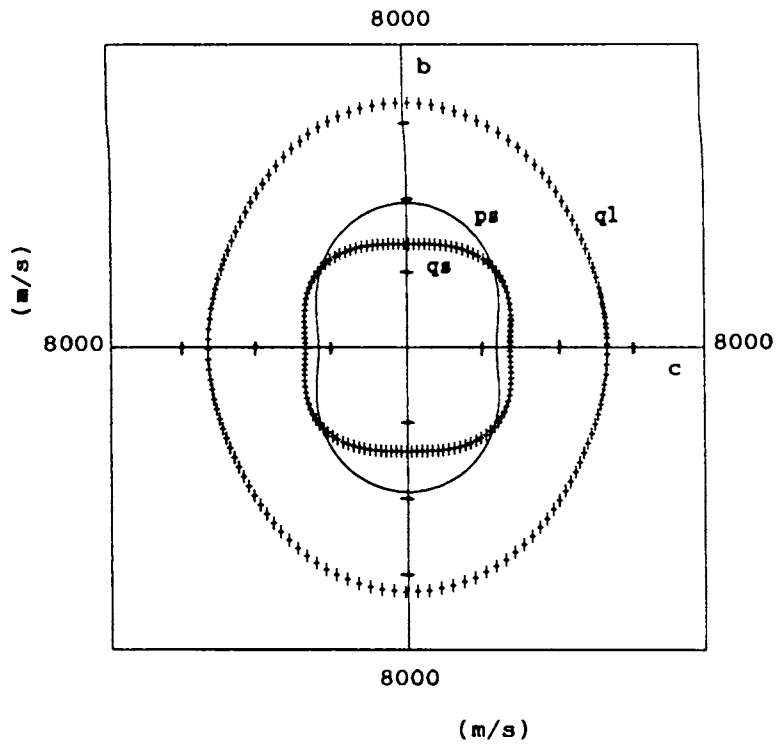


Fig. 5.3(c) Phase velocity surfaces in the bc (YZ) plane at room temperature for YBCO.

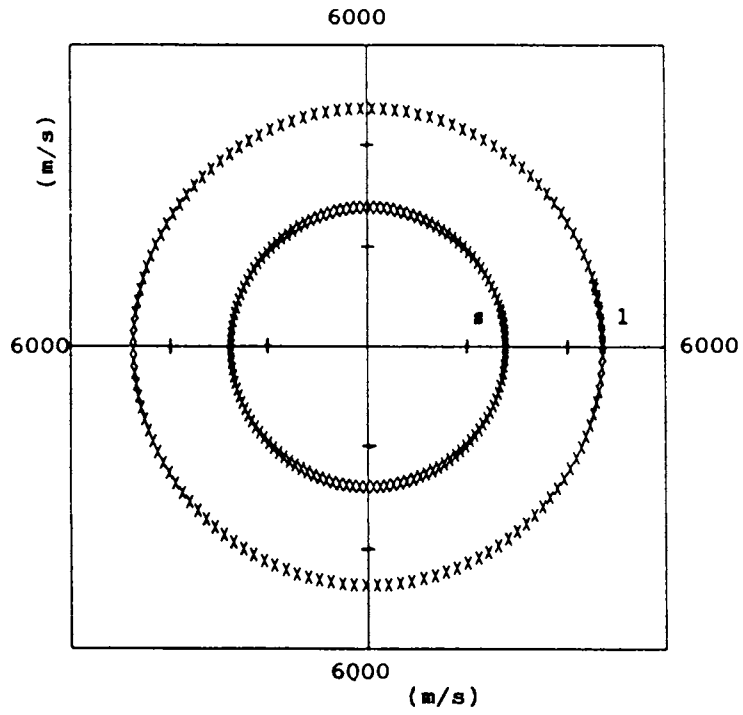


Fig. 5.3(d) Phase velocity surfaces for polycrystalline GdBCO at 300 K.

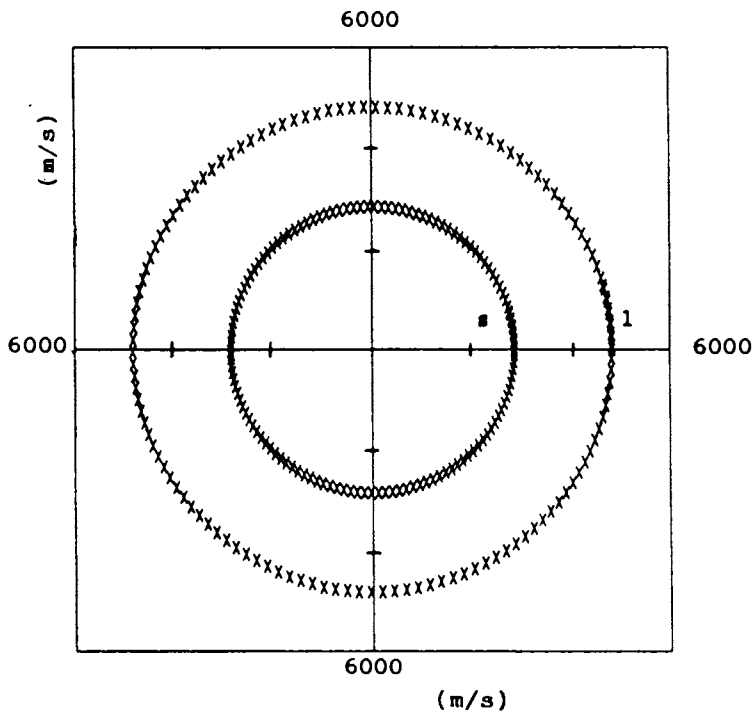


Fig. 5.3(e) Phase velocity surfaces for polycrystalline GdBCO at 90 K.

the nine constants of LCO at three different temperatures using the resonant ultrasound technique. Allan and Mackrodt [31] also give the complete set at room temperature which is the result of a molecular dynamic simulation. Incomplete data is available from different groups [32,33] and the results are tabulated in Table 5.4.

The velocity surface plots for LCO at 297 K, plotted using the data given by Migliori *et al.* [30] are given in Figs. 5.4(a), 5.4(b) and 5.4(c) for wave propagation in the XY, XZ and YZ planes respectively. The surfaces are more or less the same at 44 K and so the figures are not reproduced here.

Superconducting LSCO has tetragonal structure at room temperature, with the space group D_{4h}^{17} , and transforms into an orthorhombic state at 180 K with further structural anomalies on approach of the superconducting transition. Although the first member of the high T_c superconductor family, data is comparatively less on LSCO compared to other superconductors. Migliori *et al.* [34] have reported the complete set of elastic constants at 297 K measured using the resonant ultrasound technique. However, no data could be found which give all the six independent elastic constants at temperatures around or below T_c . The data which could be found in literature are given in Table 5.5.

Figs. 5.4(d) and 5.4(e) give the velocity surfaces plotted for wave propagation in the XY and XZ (YZ) planes respectively for LSCO at 297K using the elastic constants reported by Migliori *et al.* [34]. Though there are many reports on the temperature variation of sound velocity, the absolute values of longitudinal and transverse velocities at two temperatures (one above and the other below T_c) could not be found for the same sample and hence they are not plotted.

5.5 Discussion and conclusion

The velocity surfaces plotted for the superconducting compounds for the propagation of elastic waves in different planes clearly depict the elastic anisotropy in these materials.

For BSCCO, the three surfaces for the shear, quasishear and quasilongitudinal waves are circles in the XY plane (Fig. 5.2(a)) indicating that the phase velocity is independent of direction for all the waves. The compound possesses a layer structure

Table 5.4

Elastic constants of LCO (values in GPa)

C_{11}	C_{22}	C_{33}	C_{44}	C_{55}	C_{66}	C_{12}	C_{13}	C_{23}	T (K)	Reference
172.2	171.6	200	65.2	65.8	97.1	89.2	72.8	73.2	310	[30]
171.9	171.2	200	65.6	65.8	96.8	90.4	72.2	73.1	297	[30]
168.8	166.8	200	70.5	66.0	103.6	100.0	71.4	72.8	44	[30]
199.0	184.0	190	65.0	64.0	66.0	65.0	65.0	70.0	298	[31]
131.0	-	327.0	-	-	-	-	-	-	4	[32]
223.0	-	272.0	68.0	-	105.0	132.0	96.0	-	77	[33] +
						$C_{16} = -19.0,$	$C_{36} = -7.0$			

+ In the last set, the structure is treated as monoclinic and the additional constants are given.

Table 5.5

Elastic constants of LSCO (values in GPa)

C_{11}	C_{33}	C_{44}	C_{66}	C_{12}	C_{23}	T (K)	Reference
248.0	205.0	67.4	58.3	48	65	297	[34]
263.4	246.5	-	-	-	-	50	[35]

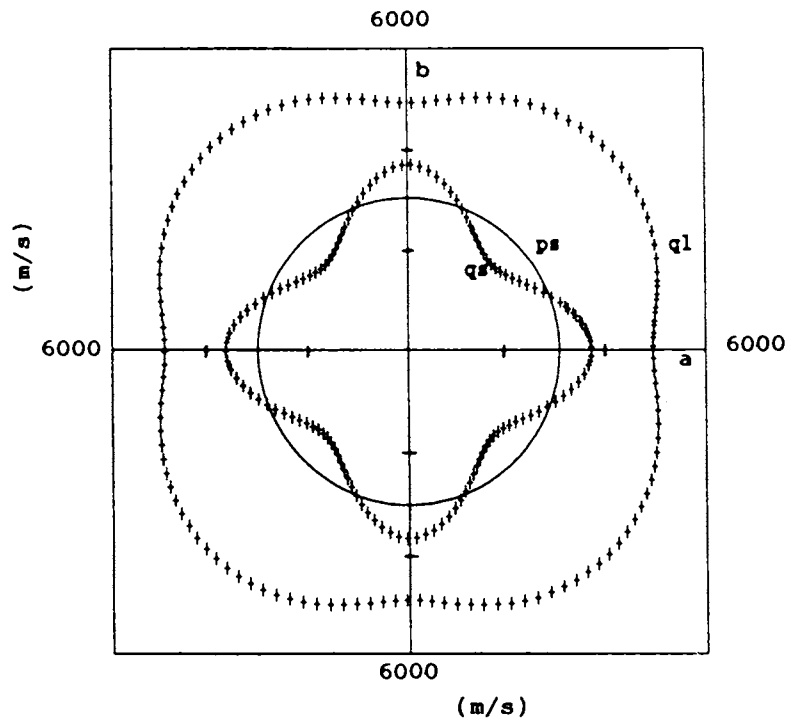


Fig. 5.4(a) Phase velocity surfaces in the ab (XY) plane for LCO at 297 K.

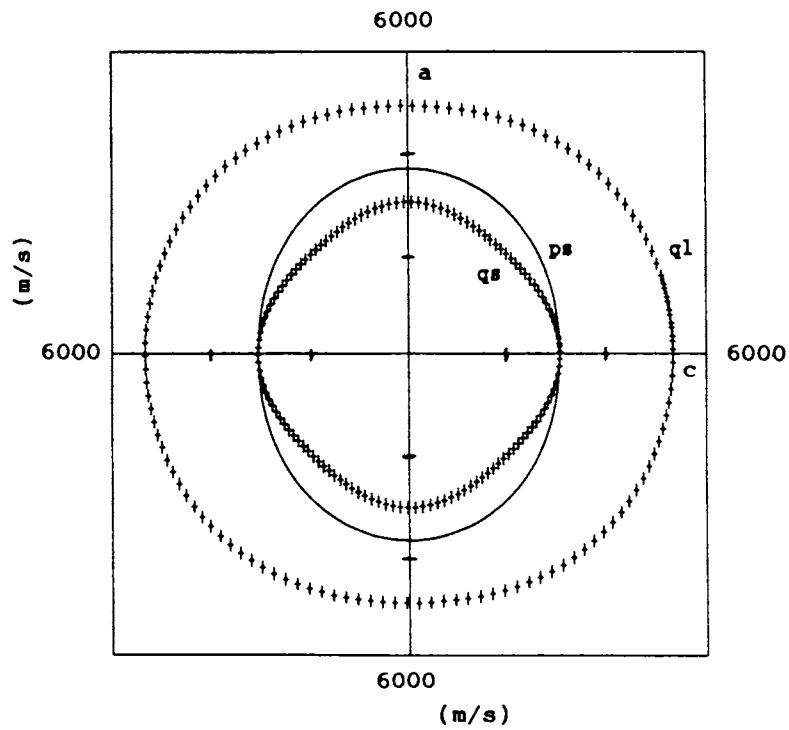


Fig. 5.4(b) Phase velocity surfaces in the ac (XZ) plane for LCO at 297 K.

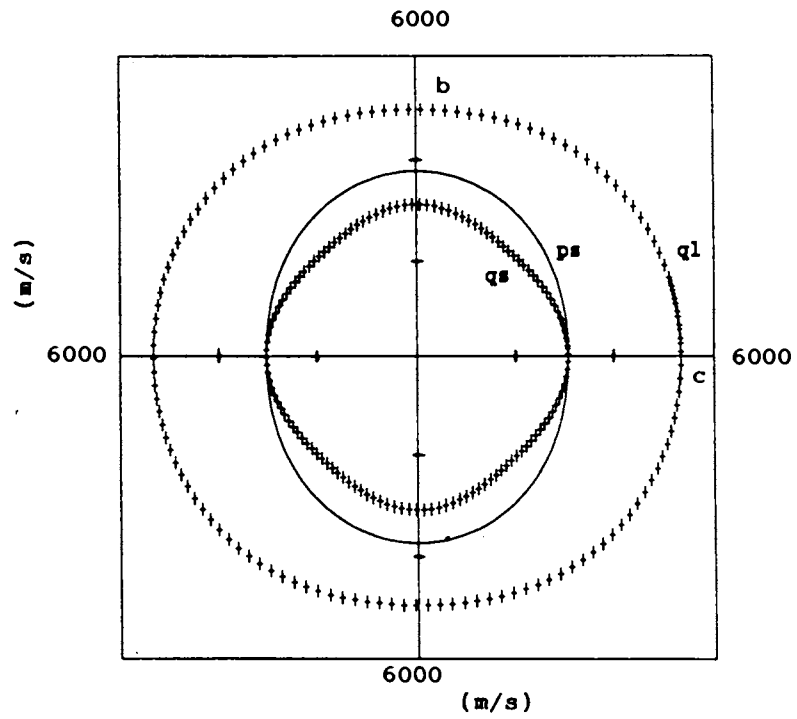


Fig. 5.4(c) Phase velocity surfaces in the bc (YZ) plane for LCO at 297 K.

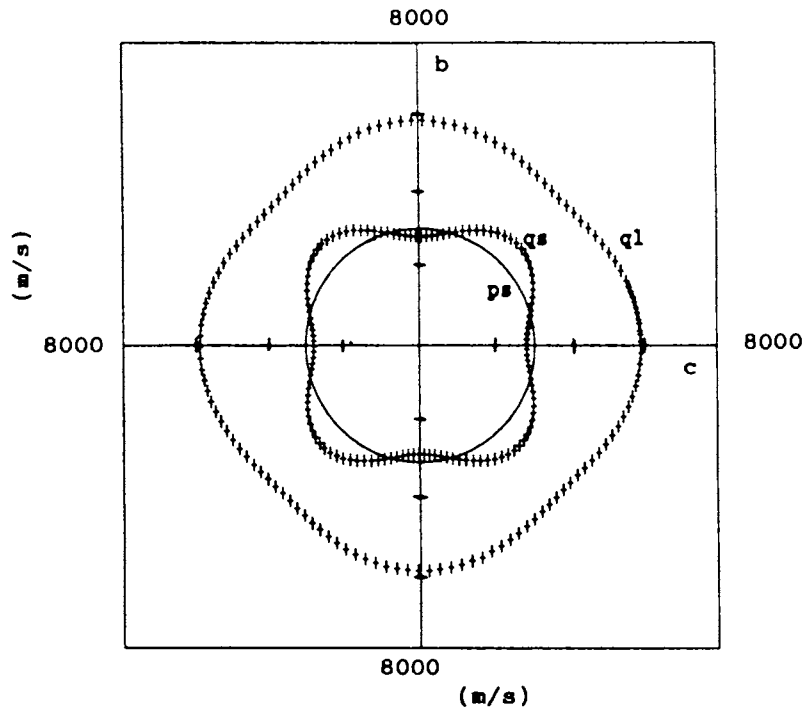


Fig. 5.4(d) Phase velocity surfaces in the ab (XY) plane for LSCO at 297 K.

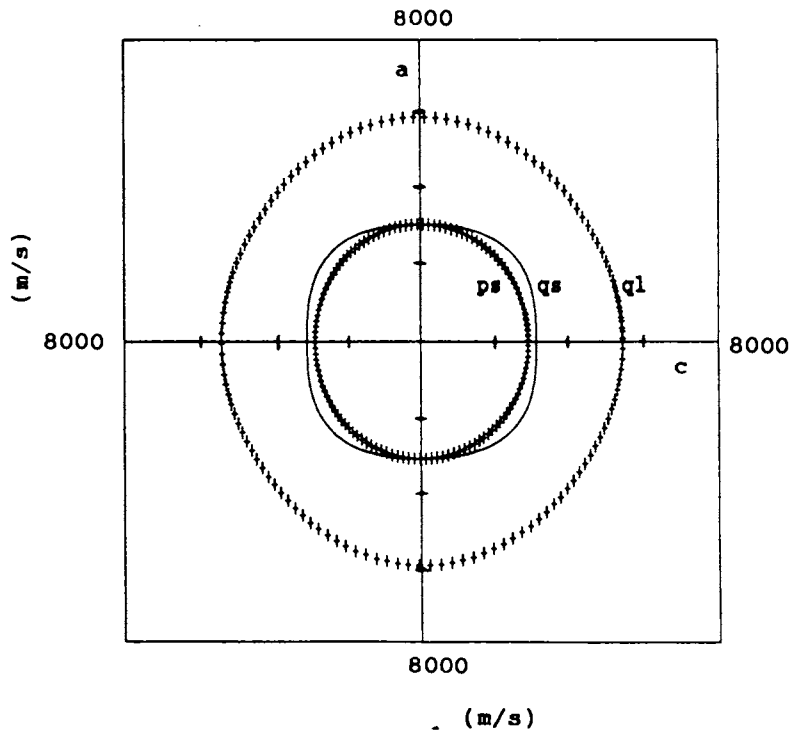


Fig. 5.4(e) Phase velocity surfaces in the ac (XZ) plane for LSCO at 297 K.

which consists of adjacent pairs of Bi-O planes that alternate along the c axis with perovskite like multilayers. The Bi_2O_2 layers consist of two parallel, planar Bi-O sheets while the perovskite multilayers comprise two Cu-O sheets in the form of corner sharing CuO_5 pyramids separated on the base sides by Ca ions. Crystals of BSCCO compounds have a mica-like morphology which indicates that the interlayer binding forces are very weak, while strong interatomic binding forces exist within the Cu-O planes.

The direction independent velocities in the XY plane may be explained on the basis of the structure. It is possible that the strong interatomic forces within the Cu-O layers are responsible for the ab (XY) plane rigidity and therefore control the wave propagation within this plane so that these waves have velocities which are essentially independent of direction.

In the XZ (YZ) plane the wave surfaces plotted for the three waves clearly indicate the anisotropy in this plane. The velocity of the longitudinal elastic wave propagating within the layer *i.e.*, along X (Y) direction is much greater than that of the waves propagating along the Z direction. The shear waves also have more or less the same behaviour. This behaviour is consistent with weak interlayer binding forces mentioned earlier.

The nature of the wave surfaces in YBCO should be similar to those in BSCCO since YBCO also possesses a layer structure. The unit cell of YBCO consists of two Cu-O_2 planes and one Cu-O chain with the Cu atoms located at two inequivalent positions. The first, Cu(2) has a pyramidal coordination while the Cu(1) located at the origin has a square planar coordination in which the near square Cu-O units share one corner and form chains along the b axis of the unit cell. The Cu(2) atoms are strongly bonded to the four oxygen atoms O(2) and O(3) forming the basis of the pyramid and are weakly bonded to the oxygen atom O(1) at the apex. Because of these features, there exists in the structure, two dimensional layers of Cu and O almost perpendicular to the c axis.

Just like BSCCO, the anisotropy is more in the XZ and YZ planes compared to the XY plane as is clear from Figs. 5.3(a), 5.3(b) and 5.3(c), though the velocities for the different modes are not independent of direction in the XY plane. In the XZ plane the velocities are higher along the Z direction. In other words, the elastic waves

propagating within the layers are faster than those perpendicular to the layer or in the direction of weak coupling which is again similar to that of BSCCO. The nature of the wave surfaces in the YZ plane is more or less similar to that in the XZ plane since both X and Y axes are within the layer and the Z axis normal to the layer.

Comparing BSCCO and YBCO it can be found that BSCCO is more anisotropic elastically. For example, the longitudinal velocity along the X axis is nearly double of that along the Z axis in BSCCO while the ratio of velocities along X and Z axes is not that high. This may be due to the larger number of layers present in the unit cell of BSCCO.

Though a nonsuperconductor, the interest in the elastic properties of LCO lies in the fact that the Cu-O planes present in the compound produce anisotropic elastic effects just as in a superconductor. Moreover, elastic and specific heat anomalies appear in this material at temperatures near T_c in the superconductor LSCO [36].

It is interesting to note that the anisotropy is more in the XY plane for both LCO and LSCO, contrary to what has been seen in the other two superconductors. The Cu-O perovskite layer perpendicular to the c axis are present in these materials also, which are separated by La/Sr-O₂ planes with a rock salt type of arrangement. Each O atom of the perovskite layers O(2) is bonded to two Cu atoms in the same plane and to four R atoms ($R = 0.925 \text{ La} + 0.075 \text{ Sr}$ in LSCO and La in LCO) in adjacent planes, while each O atom of the rock salt layers O(1) is linked to five R atoms and one Cu atom in a distorted octahedral configuration. In other words, the R atoms are strongly bonded to both the O atoms located on the same plane and those of the perovskite layers and the nature of the atoms forming R can strongly influence the Cu-O bonding [37]. So it is likely that wave propagation in the XY plane is not controlled by interatomic bonds within the layer alone, as in the case of the other two superconductors, but the La/Sr-O₂ bonds also have some influence on wave propagation in this plane. So the combined influence of these two interatomic bonds may be responsible for the anisotropy in this plane as is clear from the figures 5.4(a) and 5.4(d).

Comparing LCO and LSCO it is seen that velocities are higher in LSCO which indicate that doping with Sr makes the material stiffer. This is contrary to the usual

trend where charge carriers are found to soften elastic waves by screening. This stiffening has been attributed to the suppressed onset of the low temperature orthorhombic phase in the doped material [34].

Not much information can be expected to be obtained regarding the anisotropy by plotting the wave surfaces for polycrystalline samples for which just two elastic constants exist. However, for the 123 compound GdBCO the velocity surfaces have been plotted at two temperatures in order to check for any relative variations in the two velocity surfaces above and below T_c . It is found that the curves are exactly similar at these two temperatures indicating that there is no relative changes in velocity as the sample undergoes a superconducting transition. In the case of the velocity surfaces obtained above and below T_c for the sinterforged BSCCO sample also, the wave surfaces are quite similar at the two temperatures. These results indicate that the anisotropic nature of wave propagation does not change significantly upon superconducting transition.

5.6 References

- [1] R. Truell, C. Elbaum and B. B. Chick, in *Ultrasonic Methods in Solid State Physics*, Academic Press, New York (1969).
- [2] E. Schreiber, O. L. Anderson and N. Soga, in *Elastic Constants and their Measurements*, Mc Graw Hill, New York (1973).
- [3] B. A. Auld, in *Acoustic Fields and Waves in Solids*, Vol.1, John Wiley & Sons New York (1973).
- [4] M. J. P. Musgrave, in *Crystal Acoustics*, Holden Day, San Fransisco (1970).
- [5] H. J. Mc Skimin, in *Physical Acoustics*, Vol.1, Part A, (ed. W. P. Mason), Academic Press, New York (1964).
- [6] F. I. Federov, in *Theory of Elastic Waves in Crystals*, Plenum Press, New York (1968).
- [7] A. G. Every, *Phys. Rev* **B22**, 1746 (1980).
- [8] J. Wu, Y. Wang, P. Guo, H. Shen, Y. Yan and Z. Zhao, *Phys. Rev.* **B47**, 2806 (1993).
- [9] J.Wu, Y. Wang, H.Shen, J.Zhu, Y.Yan and Z.Zhao, *Phys. Lett.* **A148**, 127 (1990).
- [10] P. Baumgart, S. Blumenroder, A. Erle, B. Hillebrands, P. Splittgeiber, G. Guntherodt and H. Schmidt, *Physica* **C162-164**, 1073 (1989).
- [11] M. Saint-Paul, J. L. Tholence, H. Noel, J. C. Levet, M. Potel and P. Gougeon, *Physica* **C166**, 405 (1990).
- [12] G. A. Saunders, C. Fanggao, L. Jiaqiang, Q. Wang, M. Cankurtaran, E. F. Lambson, P. J. Ford and D. P. Almond, *Phys. Rev.* **B49**, 9862 (1994).
- [13] M. Boekholt, J. V. Harzer, B. Hillebrands and G. Guntherodt, *Physica* **C179**, 101 (1991).

- [14] Ming Lei, J . L. Sarrao, W. M. Visscher, T. M. Bell, J. D. Thompson and A. Migliori, *Phys. Rev.* **B47**, 6154 (1993).
- [15] H. Ledbetter and M. Lei, *J. Mater. Res.* **6**, 2253 (1991).
- [16] W. Reichardt, L. Pintschovius, B. Hennion and F. Collin, *Supercond. Sci. Tech.* **1**, 173 (1988).
- [17] P. Baumgart, S. Blumenroder, A. Erle, B. Hillebrands, G. Guntherodt and H. Schmidt, *Solid State Commun.* **69**, 1135 (1989).
- [18] B. Golding, W. H. Haemmerle, L. F. Schneemeyer and J. V. Waszczak, in *Proc. IEEE Ultrasonic Symp.*, (ed. B.R. Mc Avoy) IEEE, Piscataway (1988) p.1079.
- [19] M. Saint-Paul, J. L. Tholence, H. Noel, J. C. Levet, M. Potel and P. Gougeon, *Solid State Commun.* **69**, 1161 (1989).
- [20] M. Saint-Paul and J. Henry, *Solid State Commun.* **72**, 685 (1989).
- [21] E. Zouboulis, Sudha Kumar, U. Welp, C. H. Chen, S. K. Chan, M. Grimsditch J. Downey and L. Mc Neil, *Physica* **C190**, 329 (1992).
- [22] T. J. Kim, J. Kowalewski, W. Assmus and W. Grill, *Z. Phys.* **B78**, 207 (1990).
- [23] H. C. Gupta, *Mod. Phys. Lett.* **B2**, 811 (1988).
- [24] Q. Robinson, P. Georgopoulos, D. L. Johnson, H. O. Marcy, C. R. Kannewurf, S. -J. Hwu, T. J. Marks, K. R. Poepfelmeier, S. N. Song and J. B. Ketterson, *Adv. Ceram. Mater.* **2**, 380, (1987).
- [25] M. F. Xu, Y. J. Qian, K. J. Sun, Y. Zheng, Q. Ran, D. Hinks, B. K. Sarma and M. Levy, *Physica* **B165-166**, 1281 (1990).
- [26] A. Zhao, S. Adenwalla, A. Moreau, J. B. Ketterson, Q. Robinson, D. L. Johnson, S. -J. Hwu, K. R. Poepfelmeier, M. -F. Xu, Y. Hong, R. F. Wiegert, M. Levy and B. K. Sarma, *Phys. Rev.* **B39**, 721 (1989).

- [27] M. S. Kala, R. Sreekumar, J. Philip and N. C. Mishra, *Phys. Stat. Solidi b* (Dec. 1996) (in press).
- [28] M. Cankurtaran, G. A. Saunders, D. P. Almond, A. Al-Kheffaji, E. F. Lambson and R. C. Draper, *J. Phys. C1*, 9067 (1989).
- [29] D. P. Almond, Q. Wang, J. Freestone, E. F. Lambson, B. Chapman and G. A. Saunders, *J. Phys. C1*, 6853 (1989).
- [30] A. Migliori, W. M. Visscher, S. E. Brown, Z. Fisk, S. -W. Cheong, B. Alten, E. T. Ahrens, K. A. Kubat-Martin, J. D. Maynard, Y. Huang, D. R. Kirk, K. A. Gillis, H. K. Kim and M. H. W. Chan, *Phys. Rev. B41*, 2098 (1990).
- [31] N. L. Allan and W. C. Mackrodt, *Mat. Res. Soc. Symp. Proc.* **99**, 797 (1988).
- [32] N. V. Zavaritsky, A. V. Samoilov, A. A. Yurgens, V. S. Klochko and V. I. Makarov, *Physica C162-164*, 562 (1989).
- [33] N. G. Burma, A. L. Gaiduk, S. V. Zherlitsyn, I. S. Kolobov, V. D. Fil', A. S. Panfilov, I. V. Svechkarev, A. P. Ges', S. N. Barilo and D. I. Zhigunov, *Fiz. Nizk. Temp.* **18**, 247 (1992).
- [34] A. Migliori, W. M. Visscher, S. Wong, S. E. Brown, I. Tanaka, H. Kojima and P. B. Allen, *Phys. Rev. Lett.* **64**, 2458 (1990).
- [35] M. Nohara, T. Suzuki, Y. Maeno, T. Fujita, I. Tanaka and H. Kojima, *Physica C185-189*, 1397 (1991).
- [36] J. D. Maynard and M. J. Mckenna, in *Physical Acoustics*, Vol. XX (ed. M. Levy) Academic Press Inc., San Diego (1992).
- [37] A. Santoro, in *High Temperature Superconductivity*, (ed. J. W. Lynn), Springer-Verlag, New York, (1990).

Chapter 6

Slowness and ray velocity surfaces of high T_c superconductors

6.1 Introduction

The propagation characteristics of elastic waves in crystals are strongly affected by the elastic anisotropy of the lattice. As a result, elastic waves with different polarisations travel with different velocities in different directions and these waves are neither strictly transverse nor longitudinal except in specific directions of the crystal, as has been pointed out in the previous chapter. The phase velocity with which the wave propagates can be calculated from the elastic constants and can be plotted as a function of the propagation direction and is referred to as the phase velocity or simply velocity surfaces. Various aspects of these surfaces drawn for high T_c superconductor crystals have been discussed in detail in chapter 5.

Eventhough the phase velocity surfaces can provide information regarding the anisotropy in elastic wave propagation, it is common practice to plot the inverse of these phase velocities as a function of the propagation direction. Such surfaces are referred to as the slowness or inverse velocity surfaces and denotes the locus of the end points of the radius vectors whose lengths are proportional to the refractive indices. It is also known as the refraction or index surface, and apart from a factor of scale is identical to the surface of constant frequency ω or phonon energy $\hbar\omega$ in \mathbf{k} space. The slowness surface is often preferred over the phase velocity surface since one can trace all the features of the group velocity surface from the former. Further, the slowness surface is found to be of great importance in treating reflection and refraction processes at boundaries and is

a valuable aid in unravelling the complexities of the group velocity surface. Just like the velocity surface, it is also a surface of three sheets and possesses the same degeneracies as the phase velocity surface.

Another remarkable feature of elastic wave propagation in anisotropic solids, in contrast to those of isotropic ones, is that the direction of energy flow given by the group velocity vector is not collinear with the phase velocity vector which is parallel to the wave vector. Consequently, a plot of the group velocity as a function of direction, called the ray surface, cannot be obtained simply by inverting the slowness surface. However, it can be seen that the group velocity vector is always normal to the slowness surface. In other words, the ray surface can be defined as the envelope of plane wavefronts with respect to the slowness surface and is one of the important aspects in the understanding of elastic wave propagation in anisotropic solids.

Hence the velocity, slowness and ray surfaces are valuable aids to the understanding of the nature of acoustic wave propagation in elastically anisotropic solids. Some of the areas of interest where these surfaces find application are ballistic heat pulse propagation and phonon focussing effects, relaxation of paramagnetic and paraelectric centres, charge density waves, vibrational effects on x - rays, second sound, Akhiezer damping of sound waves, Kapitza resistance and measurement of elastic constants using nonaligned crystals [1-8]. In fact, these surfaces play a crucial role in every effect connected with long wavelength phonons or acoustic waves in crystalline media.

The ray surface is physically the most meaningful among these three surfaces in that it represents the wave front or surface of equal phase for an oscillating disturbance a unit time interval after it has been created at the origin. It also happens to be the most complicated of the three. The analytical techniques for generating these surfaces are well established and the group velocity surfaces for a large number of substances have been investigated by many previous workers [9-12]. For example, Musgrave [11] has plotted the ray surfaces for different substances belonging to different symmetry classes such as cubic, hexagonal, trigonal, tetragonal, orthorhombic etc. Philip *et al.* [12] have plotted the slowness and ray surfaces for over 65 cubic crystals including the superconducting A-15 compounds at temperatures below the transition.

There have been several papers of general nature also in this area and most of them focus on issues such as conditions for the existence of cuspidal edges in symmetry planes [13-16] and phonon enhancement factors in specific directions [16-18]. When a cuspidal edge occurs in the ray surface there exist two or three wave vectors corresponding to a single group velocity vector. The conditions for the existence of cuspidal edges have been derived by different authors [11, 13, 19]. McCurdy [19] has pointed out that the directions along which cuspidal edges occur might give rise to high phonon amplification. Every [20] has shown that the results of phonon imaging and other ballistic phonon experiments can be interpreted in terms of the shape of the acoustic ray surfaces of cubic crystals.

In this chapter, an attempt has been made to compute and plot the ray and slowness surfaces for three major high T_c superconductors, taking elastic constant data from literature. The details of the calculation and the results are presented after giving an outline of the theory behind computing the group velocity values for orthorhombic and tetragonal crystal systems and the necessary equations used in the calculations.

6.2 The ray or group velocity in anisotropic solids - General aspects

The ray velocity is an important physical attribute of any acoustic wave. This is the velocity with which energy is transported in the wave and is necessary to interpret different phenomena associated with ultrasonic wave propagation, thermal conductivity, phonon transport etc. Except in special circumstances the ray velocity does not coincide either in magnitude or direction with the phase velocity, as has been mentioned earlier.

The group velocity is the velocity of the modulation envelope of a wave packet composed of waves of slightly differing values of \mathbf{k} and ω and is given by

$$\mathbf{S} = \frac{\partial \omega}{\partial \mathbf{k}} \quad (6.1)$$

whereas the ray velocity is obtained from the acoustic Poynting vector. However, in the absence of dissipation the distinction between these velocities disappear and eqn.(6.1) provides a computational route for obtaining the velocity.

Though the ray surface cannot be obtained simply by the inversion of the slowness surface because of the noncollinearity of \mathbf{k} and \mathbf{S} , there exists an interesting and useful relationship between these surfaces. It has been shown that the group velocity must always be perpendicular to the slowness surface. In other words, the wave vector \mathbf{k} must always be normal to the ray surface. An important physical interpretation of this result can be made by expressing it as

$$v_p = \mathbf{S} \cos \psi \quad (6.2)$$

where ψ is the angle between the group velocity \mathbf{S} and the wave vector \mathbf{k} . This leads to a useful relation between the phase velocity and ray surfaces. It follows that the ray surface must be the envelope of planes normal to \mathbf{v}_p . Since the phase fronts of a plane wave are normal to \mathbf{k} , it is seen that each portion of the ray surface corresponds to the phase front for a plane wave with energy travelling in that direction.

The equation for \mathbf{S} , given by eqn. (6.1), is convenient to calculate the group velocity only if the dispersion relation is given explicitly as $\omega = f(k_x, k_y, k_z)$. But in section 5.2 of the previous chapter, it was seen that the dispersion relation for plane acoustic waves is obtained in the implicit form

$$\Omega(\omega, k_x, k_y, k_z) = |k^2 \lambda_{ij} - \rho \omega^2| = 0 \quad (6.3)$$

and this cannot always be transformed into an explicit equation for ω . In such cases, the different components of group velocity are obtained by implicit differentiation of eqn. (6.3) as shown below.

$$\left(\frac{\partial \Omega}{\partial \omega} \delta \omega + \frac{\partial \Omega}{\partial k_x} \delta k_x \right)_{k_y, k_z} = 0 \quad (6.4)$$

from which the x component of \mathbf{S} is obtained as

$$S_x = \left(\frac{\partial \omega}{\partial k_x} \right)_{k_y, k_z} = - \left(\frac{\partial \Omega}{\partial k_x} \right) / \left(\frac{\partial \Omega}{\partial \omega} \right) \quad (6.5)$$

Similarly the y and z components of group velocity can be written as

$$\begin{aligned} S_y &= - \left(\frac{\partial \Omega}{\partial k_y} \right) / \left(\frac{\partial \Omega}{\partial \omega} \right) \\ S_z &= - \left(\frac{\partial \Omega}{\partial k_z} \right) / \left(\frac{\partial \Omega}{\partial \omega} \right) \end{aligned} \quad (6.6)$$

Therefore the group velocity can always be evaluated as

$$\mathbf{S} = \frac{-\nabla_{\mathbf{k}} \Omega}{(\partial\Omega/\partial\omega)} \quad (6.7)$$

Since the group and ray (energy) velocity are identical for acoustic waves in a lossless medium, eqn.(6.7) provides an alternative to the Poynting vector calculation of ray velocity and this provides a significant computational advantage. The group velocity also has a directly measurable physical meaning that is not apparent in the definition of energy velocity (\mathbf{v}_e). If a pulse of acoustic energy is radiated by a plane wave transducer, the wavepacket is limited in two dimensions by the size of the transducer and in the third dimension by the pulse length. The wave fronts travel along the direction of \mathbf{k} , which is normal to the transducer surface; but the wavepacket modulation envelope travels in the direction $\mathbf{S} = \mathbf{v}_e$, which may be inclined at an angle to \mathbf{k} . This means that the receiving transducer must be offset in order to intercept the acoustic pulse. Experimental evidence of this effect is reported in single crystal quartz [21] where the path of the acoustic beam has been made visible by means of optical scattering. When the quartz crystal is oriented with \mathbf{k} parallel to the y crystal axis, it was seen that the quasilongitudinal wave should be deflected upwards and the quasishear waves deflected downwards by an angle of approximately 25° .

6.3 Computation of group velocity for orthorhombic and tetragonal crystals

The expression for the group velocity given by eqn.(6.7) can be used for crystals of any symmetry to calculate the group velocity in any direction. However, the general expressions for \mathbf{S} are formidably large and is essentially required for the triclinic system only. The expressions get much simplified when applied to higher symmetry crystals since several elastic constants become zero for these crystals. As has been seen in the case of phase velocity expressions, further simplification occurs when symmetry planes and directions are considered where one or two of the direction cosines l , m or n also becomes equal to zero. Since the superconductors for which the ray surfaces are drawn in this chapter belong either to the orthorhombic or tetragonal system, the expressions

for the group velocity are derived for these crystal classes in the following paragraphs.

For the orthorhombic symmetry, the coefficients of Christoffel matrix are given by eqn.(5.9) in chapter 5. However, since some of the off-diagonal terms are retained, the characteristic equation given by eqn.(6.3) cannot be factored. The equations are hence derived for the symmetry planes, as has been done for the phase velocities.

XY plane

For the XY (ab) plane, the direction cosine $n = 0$ and the dispersion relation can be written as

$$\Omega = (\lambda_{33} - \rho v^2) [(\lambda_{11} - \rho v^2)(\lambda_{22} - \rho v^2) - \lambda_{12}^2] = 0 \quad (6.8)$$

where the Christoffel coefficients are given by eqn.(5.10). Substituting the values of λ and expressing the equation in terms of k_x , k_y , k_z and ω where $k_x/k = l$, $k_y/k = m$, $k_z/k = n$ and $\omega = kv$, the dispersion relation for the pure shear mode works out to be

$$\Omega = C_{55} k_x^2 + C_{44} k_y^2 - \rho \omega^2 = 0 \quad (6.9)$$

from which the necessary derivatives are evaluated as

$$\begin{aligned} \frac{\partial \Omega}{\partial k_x} &= 2 C_{55} k_x \\ \frac{\partial \Omega}{\partial k_y} &= 2 C_{44} k_y \\ \frac{\partial \Omega}{\partial k_z} &= 0 \\ \frac{\partial \Omega}{\partial \omega} &= -2 \rho \omega \end{aligned} \quad (6.10)$$

from which the x, y and z components of \mathbf{S} can be obtained and hence the group velocity can be evaluated.

For the quasishear and quasilongitudinal modes, Ω is given by

$$\Omega = (C_{11} k_x^2 + C_{66} k_y^2 - \rho \omega^2)(C_{66} k_x^2 + C_{22} k_y^2 - \rho \omega^2) - (C_{12} + C_{66})^2 k_x^2 k_y^2 = 0 \quad (6.11)$$

from which the derivatives are obtained as

$$\begin{aligned} \frac{\partial \Omega}{\partial k_x} &= 2 C_{11} k_x (C_{66} k_x^2 + C_{22} k_y^2 - \rho \omega^2) + 2 C_{66} k_x (C_{11} k_x^2 + C_{66} k_y^2 - \rho \omega^2) \\ &\quad - 2(C_{12} + C_{66})^2 k_x k_y^2 \end{aligned}$$

$$\begin{aligned}
\frac{\partial \Omega}{\partial k_y} &= 2 C_{66} k_y (C_{66} k_x^2 + C_{22} k_y^2 - \rho \omega^2) + 2 C_{22} k_y (C_{11} k_x^2 + C_{66} k_y^2 - \rho \omega^2) \\
&\quad - 2(C_{12} + C_{66})^2 k_x^2 k_y \\
\frac{\partial \Omega}{\partial k_z} &= 0 \\
\frac{\partial \Omega}{\partial \omega} &= -2 \rho \omega (C_{66} + C_{11} k_x^2 + C_{22} k_y^2 - 2 \rho \omega^2)
\end{aligned} \tag{6.12}$$

from which the components of the group velocity can be obtained after substituting the appropriate values of phase velocity given by eqn. (5.13).

The deviation ψ of the ray from the wave normal can be calculated in this plane as

$$\tan \psi = \frac{S_y}{S_x} \tag{6.13}$$

XZ plane

For the XZ (ac) plane, the direction cosine $m = 0$ and the dispersion relation can be expressed as

$$\Omega = (\lambda_{22} - \rho v^2) [(\lambda_{11} - \rho v^2)(\lambda_{33} - \rho v^2) - \lambda_{13}^2] = 0 \tag{6.14}$$

where the λ 's are given by eqn.(5.14). Substituting the values of λ and rewriting the equation in terms of k_x , k_y , k_z and ω , the dispersion relation for the pure shear mode is obtained as

$$\Omega = C_{66} k_x^2 + C_{44} k_z^2 - \rho \omega^2 = 0 \tag{6.15}$$

The derivatives are calculated as

$$\begin{aligned}
\frac{\partial \Omega}{\partial k_x} &= 2 C_{66} k_x \\
\frac{\partial \Omega}{\partial k_y} &= 0 \\
\frac{\partial \Omega}{\partial k_z} &= 2 C_{44} k_z \\
\frac{\partial \Omega}{\partial \omega} &= -2 \rho \omega
\end{aligned} \tag{6.16}$$

from which the group velocity can be obtained after substituting for the phase velocity.

For the quasishear and quasilongitudinal modes, the dispersion relation is

$$\Omega = (C_{11} k_x^2 + C_{55} k_z^2 - \rho \omega^2) (C_{55} k_x^2 + C_{33} k_z^2 - \rho \omega^2) - (C_{13} + C_{55})^2 k_x^2 k_z^2 = 0 \tag{6.17}$$

and the derivatives are

$$\begin{aligned}
\frac{\partial \Omega}{\partial k_x} &= 2 C_{11} k_x (C_{55} k_x^2 + C_{33} k_z^2 - \rho \omega^2) + 2 C_{55} k_x (C_{11} k_x^2 + C_{55} k_z^2 - \rho \omega^2) \\
&\quad - 2(C_{13} + C_{55})^2 k_x k_z^2 \\
\frac{\partial \Omega}{\partial k_y} &= 0 \\
\frac{\partial \Omega}{\partial k_z} &= 2 C_{55} k_z (C_{55} k_x^2 + C_{33} k_z^2 - \rho \omega^2) + 2 C_{33} k_z (C_{11} k_x^2 + C_{55} k_z^2 - \rho \omega^2) \\
&\quad - 2(C_{13} + C_{55})^2 k_x^2 k_z \\
\frac{\partial \Omega}{\partial \omega} &= -2 \rho \omega (C_{55} + C_{11} k_x^2 + C_{33} k_z^2 - 2 \rho \omega^2)
\end{aligned} \tag{6.18}$$

The group velocity is obtained from the different components after substituting the values of phase velocity given by eqn. (5.16).

The angle of deviation ψ of the ray from the wave normal in this plane is

$$\tan \psi = \frac{S_x}{S_z} \tag{6.19}$$

YZ plane

For the YZ (bc) plane, the direction cosine $l = 0$ and the dispersion relation can be written as

$$\Omega = (\lambda_{11} - \rho v^2) [(\lambda_{22} - \rho v^2)(\lambda_{33} - \rho v^2) - \lambda_{23}^2] = 0 \tag{6.20}$$

where the Christoffel coefficients λ 's are given by eqn.(5.17). Substituting the values of λ and expressing the equation in terms of k_x , k_y , k_z and ω , the dispersion relation for the pure shear mode is obtained as

$$\Omega = C_{66} k_y^2 + C_{55} k_z^2 - \rho \omega^2 = 0 \tag{6.21}$$

from which the derivatives are evaluated as

$$\begin{aligned}
\frac{\partial \Omega}{\partial k_x} &= 0 \\
\frac{\partial \Omega}{\partial k_y} &= 2 C_{66} k_y \\
\frac{\partial \Omega}{\partial k_z} &= 2 C_{55} k_z \\
\frac{\partial \Omega}{\partial \omega} &= -2 \rho \omega
\end{aligned} \tag{6.22}$$

from which the x, y and z components of \mathbf{S} can be obtained and hence the group velocity can be calculated.

For the quasishear and quasilongitudinal modes, Ω is given by

$$\Omega = (C_{22} k_y^2 + C_{44} k_z^2 - \rho \omega^2) (C_{44} k_y^2 + C_{33} k_z^2 - \rho \omega^2) - (C_{23} + C_{44})^2 k_y^2 k_z^2 = 0 \quad (6.23)$$

from which the derivatives are obtained as

$$\begin{aligned} \frac{\partial \Omega}{\partial k_x} &= 0 \\ \frac{\partial \Omega}{\partial k_y} &= 2 C_{22} k_y (C_{44} k_y^2 + C_{33} k_z^2 - \rho \omega^2) + 2 C_{44} k_y (C_{22} k_y^2 + C_{44} k_z^2 - \rho \omega^2) \\ &\quad - 2(C_{23} + C_{44})^2 k_y k_z^2 \\ \frac{\partial \Omega}{\partial k_z} &= 2 C_{44} k_z (C_{44} k_y^2 + C_{33} k_z^2 - \rho \omega^2) + 2 C_{33} k_z (C_{22} k_y^2 + C_{44} k_z^2 - \rho \omega^2) \\ &\quad - 2(C_{23} + C_{44})^2 k_y^2 k_z \\ \frac{\partial \Omega}{\partial \omega} &= -2 \rho \omega (C_{44} + C_{22} k_y^2 + C_{33} k_z^2 - 2 \rho \omega^2) \end{aligned} \quad (6.24)$$

from which the components of the group velocity can be obtained by substituting the values of phase velocity given by eqn. (5.19).

The angle of deviation ψ of the group velocity vector from the wave normal can be calculated in this plane as

$$\tan \psi = \frac{S_y}{S_z} \quad (6.25)$$

For the superconductor which belong to the tetragonal symmetry, the corresponding equations for the group velocity can be obtained by making the substitutions $C_{11} = C_{22}$, $C_{44} = C_{55}$ and $C_{13} = C_{23}$ as seen in the case of the phase velocity calculations and they are not reproduced here as they can be obtained by making the above substitutions in the equations derived above.

6.4 Slowness and ray surfaces for high T_c superconductors

As is well known, even ten years after the first report of high T_c superconductivity in ceramic cuprates, the mechanism of superconductivity and the role played by phonons

in superconducting transition are not clear. Every possible experiment has been done on these materials and every conceivable theoretical model has been applied to explain experimental findings with varying degrees of success. Of late, with the success of growing single crystals of most of the high T_c oxide superconductors, it has become possible to get a better insight into these materials, with the aid of fine experiments.

A thorough knowledge of the elastic properties of these materials is necessary to understand the mechanism of superconductivity since these properties are closely related to a large number of fundamental solid state parameters. Actually the behaviour of long wavelength acoustic phonons is directly determined by the elastic constants of the material. In spite of these facts, elastic constant measurements on single crystals of all high T_c superconductors are not reported due to various technical difficulties involved in growing single crystals and making measurements. Even now, all the independent elastic constants are available only for a few high T_c materials, that too only at room temperature. The elastic constant measurements on high T_c superconductors have already been reviewed in chapter 5.

In this chapter we have plotted the slowness and ray surfaces for three superconducting systems $\text{Bi}_2\text{Sr}_2\text{CaCu}_2\text{O}_{8-\delta}$ (BSCCO), $\text{YBa}_2\text{Cu}_3\text{O}_{7-\delta}$ (YBCO) and $\text{La}_{2-x}\text{Sr}_x\text{CuO}_{4-\delta}$ (LSCO) for which the phase velocity surfaces have already been plotted in chapter 5. Eventhough the slowness surfaces, which are the inverse of the phase velocity surfaces plotted earlier, may not seem to give any more information than given by the phase velocity surfaces, they have a direct correlation with the ray surfaces and being the polar reciprocals of ray surfaces can explain many of the features of ray surfaces.

The three systems studied here have either orthorhombic or tetragonal symmetry. In order to plot the slowness surfaces, the inverse of the expressions derived for phase velocities in various symmetry planes in chapter 5 have been used, while the expressions for the group velocity given in the above section have been used to plot the ray surfaces. The inverse velocities and the group velocities have been calculated using the elastic constant data taken from literature. The calculated values have been plotted as a function of the propagation direction varying from 0 to 360 degrees in steps

of 2° after determining the x and y components of the velocities using the procedure described in chapter 5. The computations have been performed on a PC employing MATHCAD software.

For BSCCO, the surfaces have been plotted at two different temperatures - one above and the other below T_c - using the elastic constant data of Saunders *et al.* [22] determined from ultrasonic measurements. Since the measurements are performed on a sinterforged sample of BSCCO, the samples has a cylindrical symmetry and hence there are only five independent elastic constants. Consequently the surfaces are the same in the XZ and YZ planes. Figs. 6.1(a) and 6.1(b) give the slowness surfaces for this compound at 290 K in the XY and XZ (YZ) planes, which are plotted using the same expressions for phase velocity given in chapter 5. The corresponding surfaces at 20 K are plotted in Figs. 6.1(c) and 6.1(d). The ray surfaces in the XY and XZ (YZ) planes for BSCCO are plotted in Figs. 6.2(a) and 6.2(b) at 290 K while the plots in Figs. 6.2(c) and 6.2(d) depict the ray surfaces at 20 K, which are drawn using the expressions derived in the previous section. The symbols ps, qs and ql in all these plots represent the pure shear, quasishear and quasilongitudinal modes respectively.

In YBCO, since the complete set of elastic constants are reported only at room temperature, the surfaces have been plotted only at room temperature. The elastic constant data is taken from Ming Lei *et al.* [23] who have measured all the nine independent elastic constants for this material having orthorhombic symmetry by the resonant ultrasound technique. Plots given in Figs. 6.3(a), 6.3(b) and 6.3(c) are the slowness surfaces for YBCO in the XY, XZ and YZ planes respectively, while those in Figs. 6.4(a), 6.4(b) and 6.4(c) depict the ray surfaces in the same planes and the symbols in the figures have the usual meaning.

For LSCO also, complete set of elastic constants are available only at room temperature. The structure of this compound is tetragonal at room temperature and the six independent elastic constants have been determined by the resonant ultrasound technique by Migliori *et al.* [24]. Because of tetragonal symmetry, the surfaces are the same in the XZ and YZ planes. Figs. 6.5(a) and 6.5(b) are the slowness surfaces for this compound in the XY and XZ (YZ) planes and Figs. 6.6(a) and 6.6(b) are the

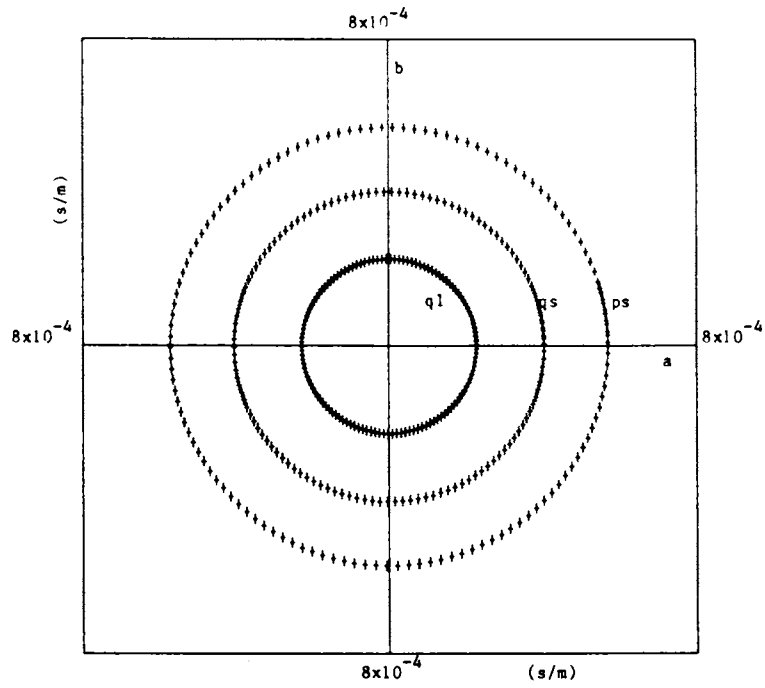


Fig. 6.1(a) Slowness surfaces in the ab (XY) plane for BSCCO at 290 K.

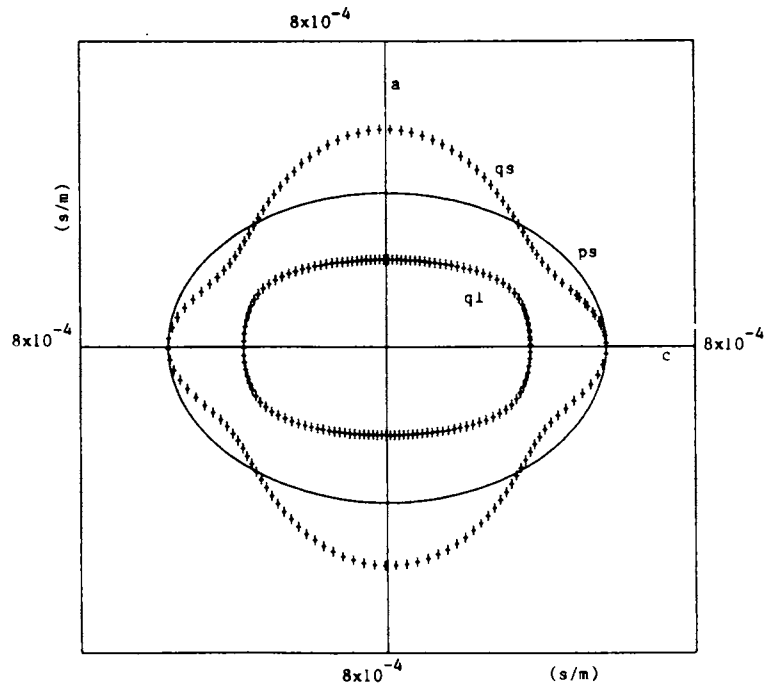


Fig. 6.1(b) Slowness surfaces in the ac (XZ) plane for BSCCO at 290 K.

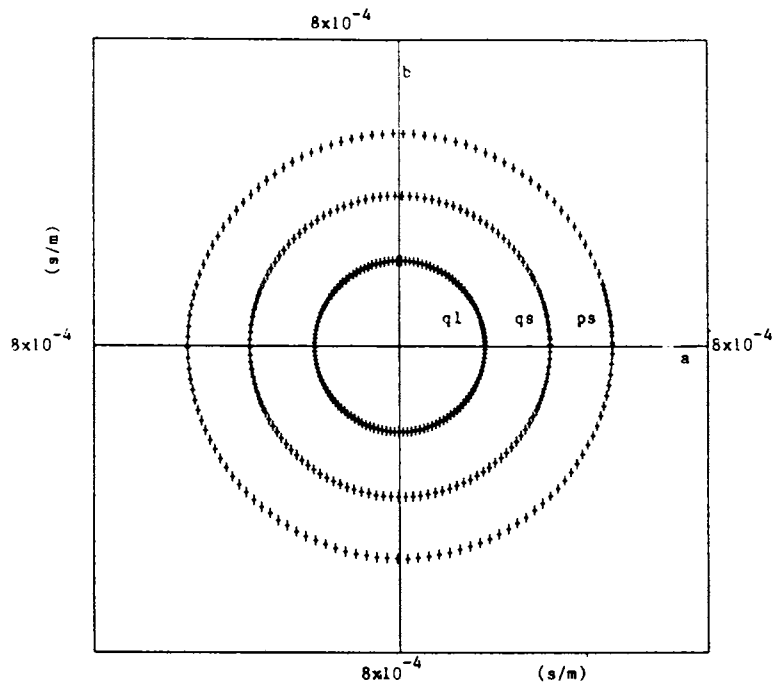


Fig. 6.1(c) Slowness surfaces in the ab (XY) plane for BSCCO at 20 K.

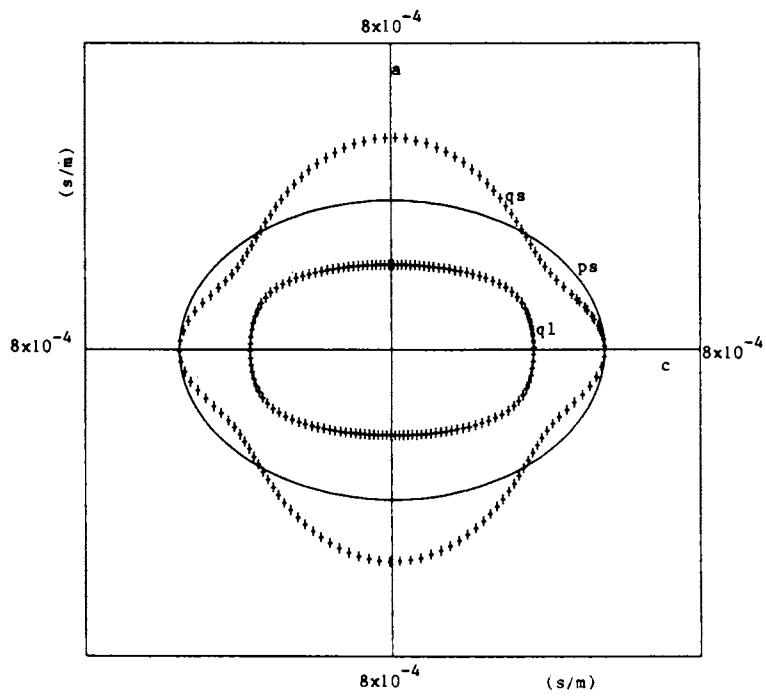


Fig. 6.1(d) Slowness surfaces in the ac (XZ) plane for BSCCO at 20 K.

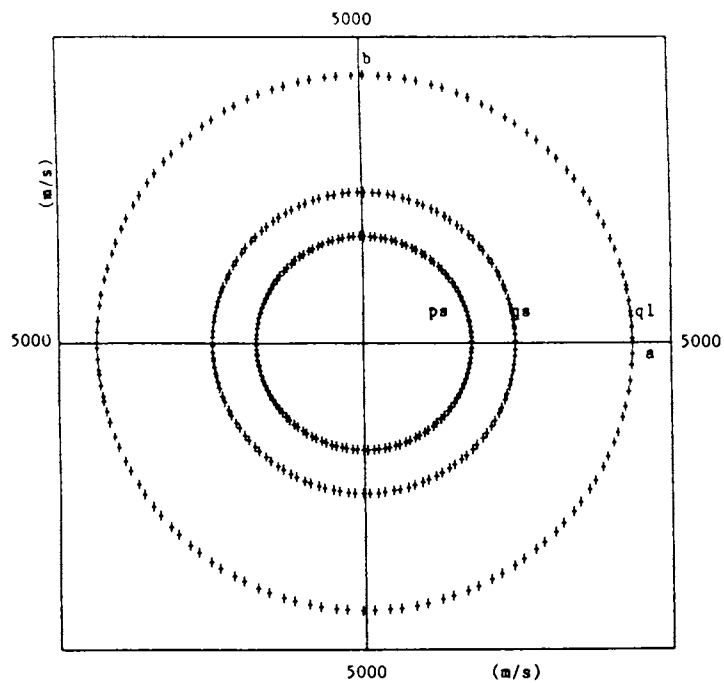


Fig. 6.2(a) Ray velocity surfaces in the ab (XY) plane for BSCCO at 290 K.

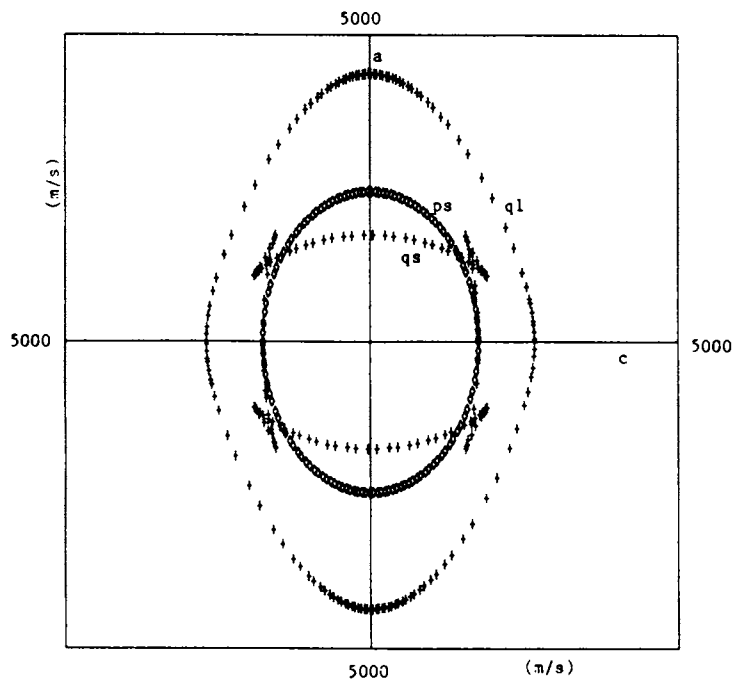


Fig. 6.2(b) Ray velocity surfaces in the ac (XZ) plane for BSCCO at 290 K.

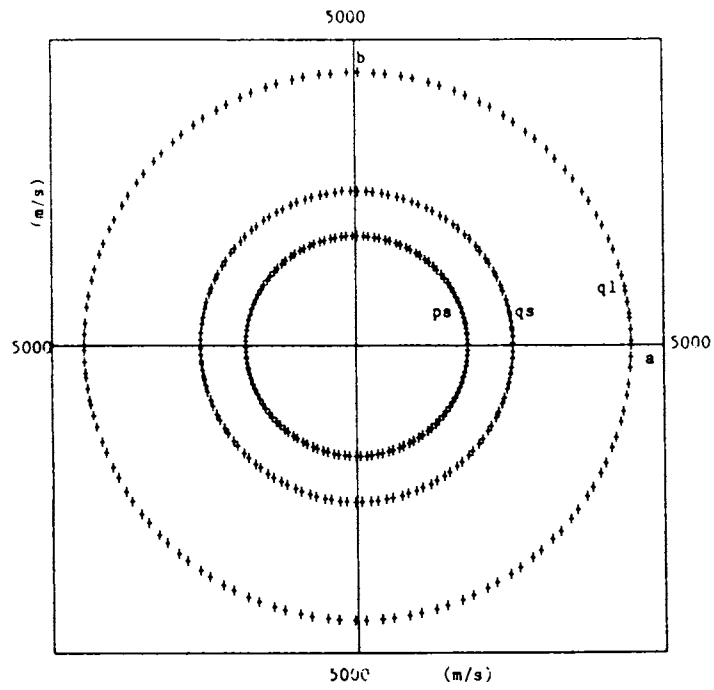


Fig. 6.2(c) Ray velocity surfaces in the ab (XY) plane for BSCCO at 20 K.

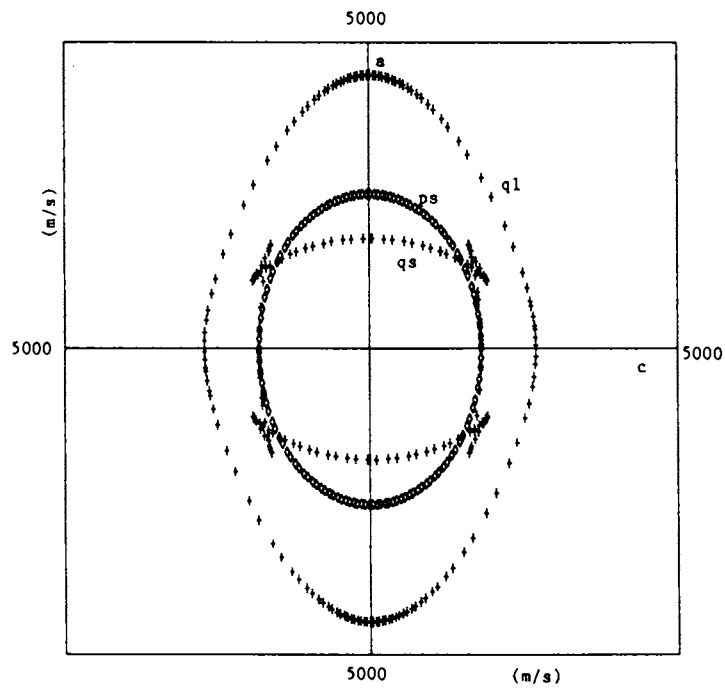


Fig. 6.2(d) Ray velocity surfaces in the ac (XZ) plane for BSCCO at 20 K.

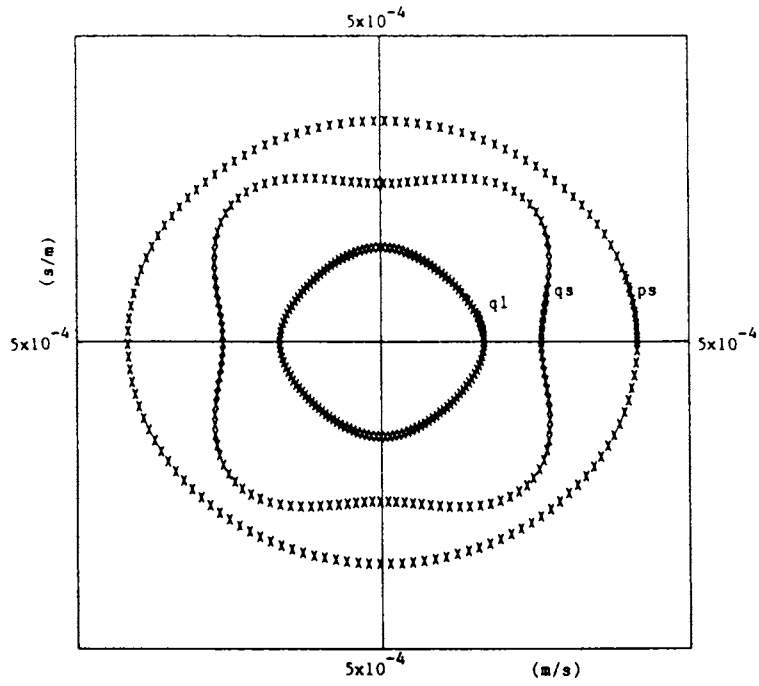


Fig. 6.3(a) Slowness surfaces in the ab (XY) plane for YBCO at room temperature.

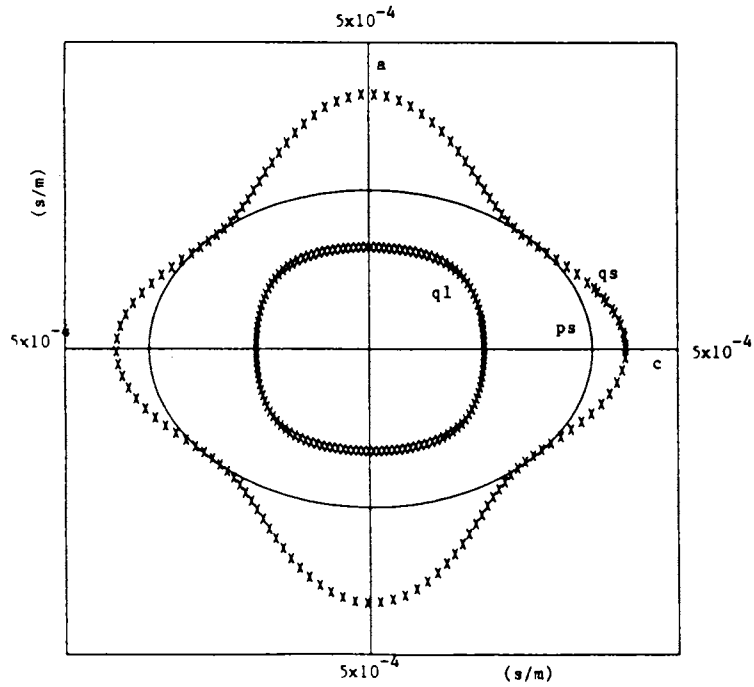


Fig. 6.3(b) Slowness surfaces in the ac (XZ) plane for YBCO at room temperature.

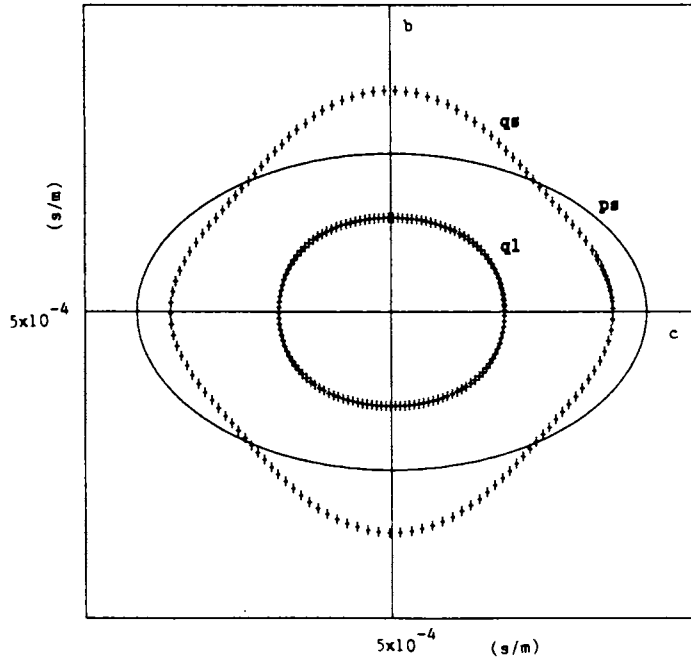


Fig. 6.3(c) Slowness surfaces in the bc (YZ) plane for YBCO at room temperature.

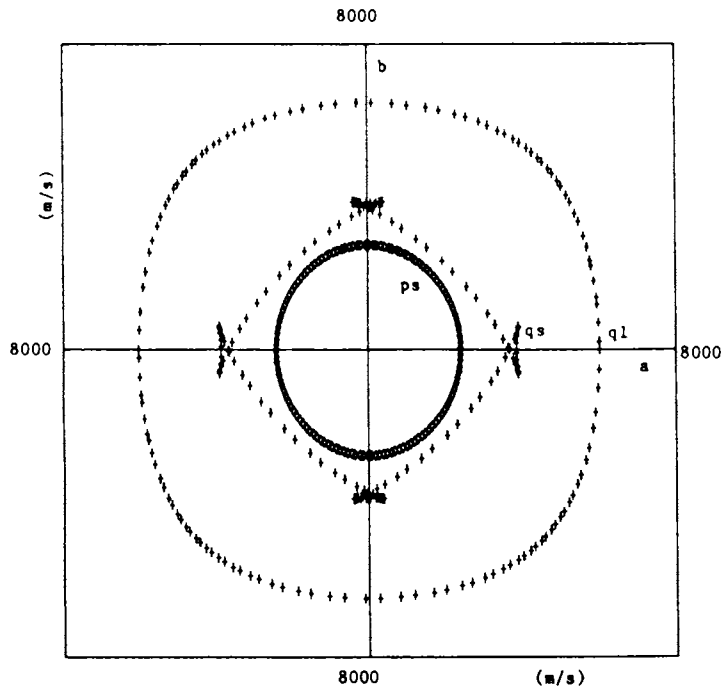


Fig. 6.4(a) Ray velocity surfaces in the ab (XY) plane for YBCO at room temperature.

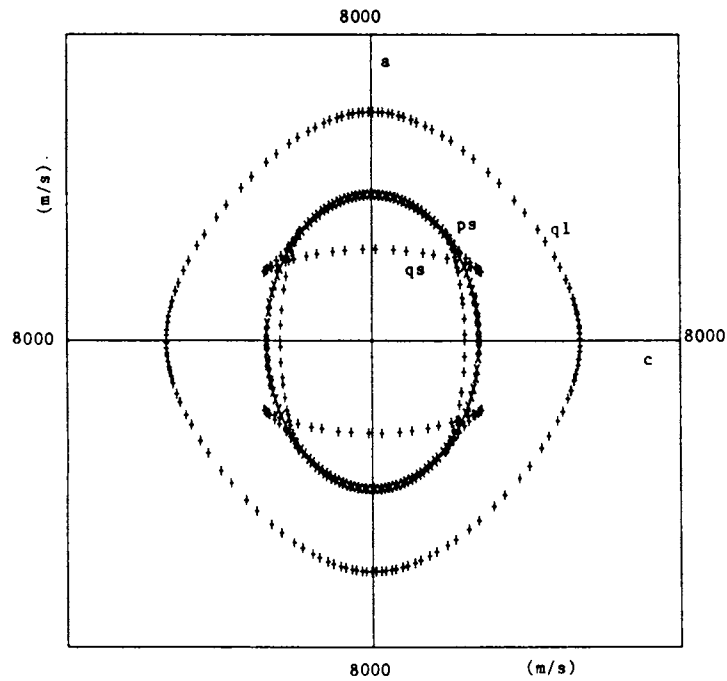


Fig. 6.4(b) Ray velocity surfaces in the ac (XZ) plane for YBCO at room temperature.

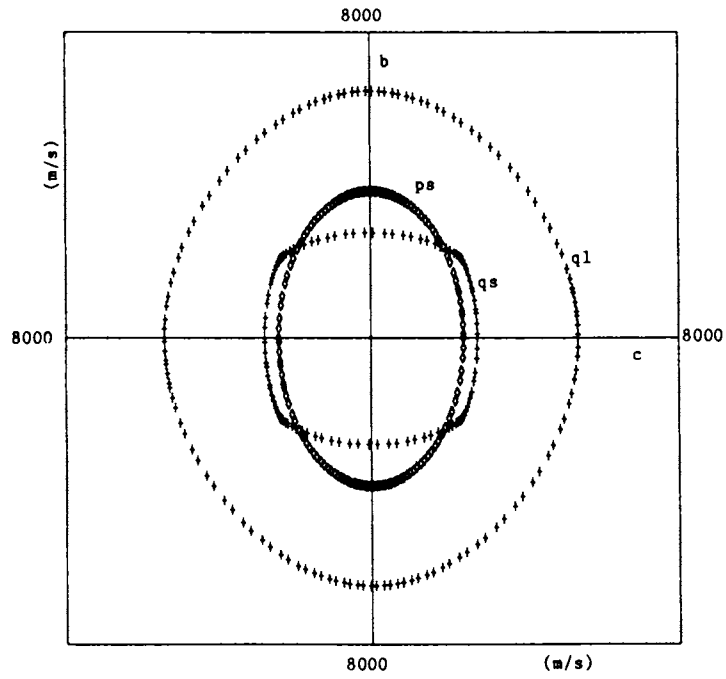


Fig. 6.4(c) Ray velocity surfaces in the bc (YZ) plane for YBCO at room temperature.

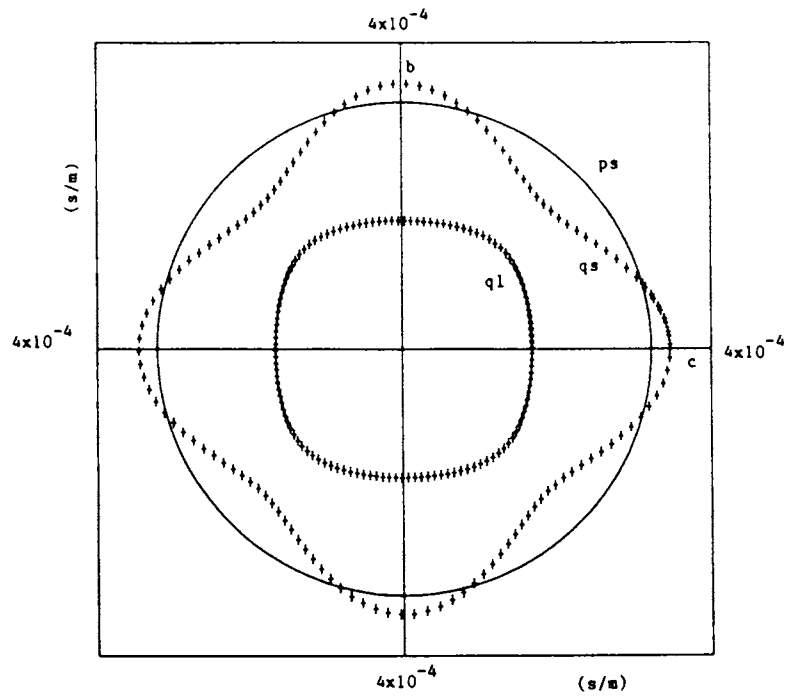


Fig. 6.5(a) Slowness surfaces in the ab (XY) plane for LSCO at 297 K.

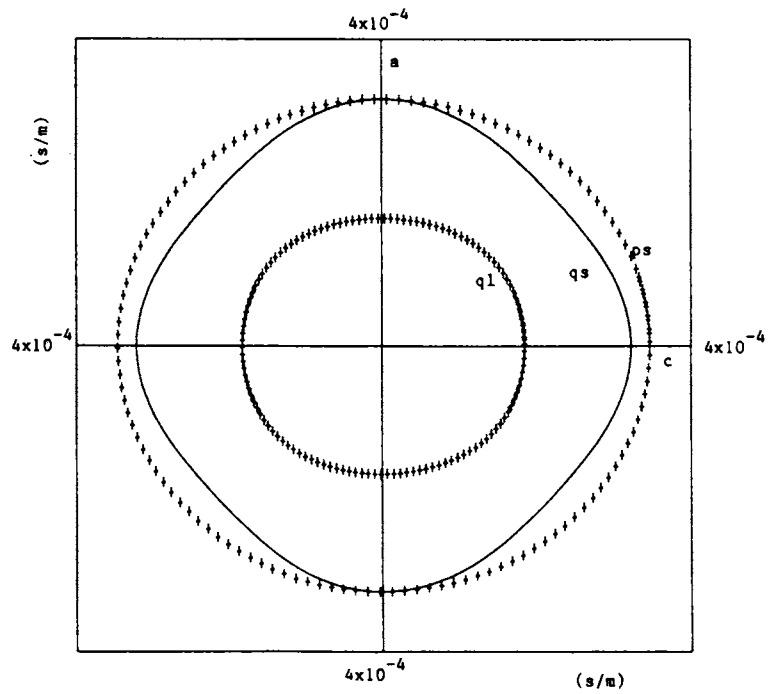


Fig. 6.5(b) Slowness surfaces in the ac (XZ) plane for LSCO at 297 K.

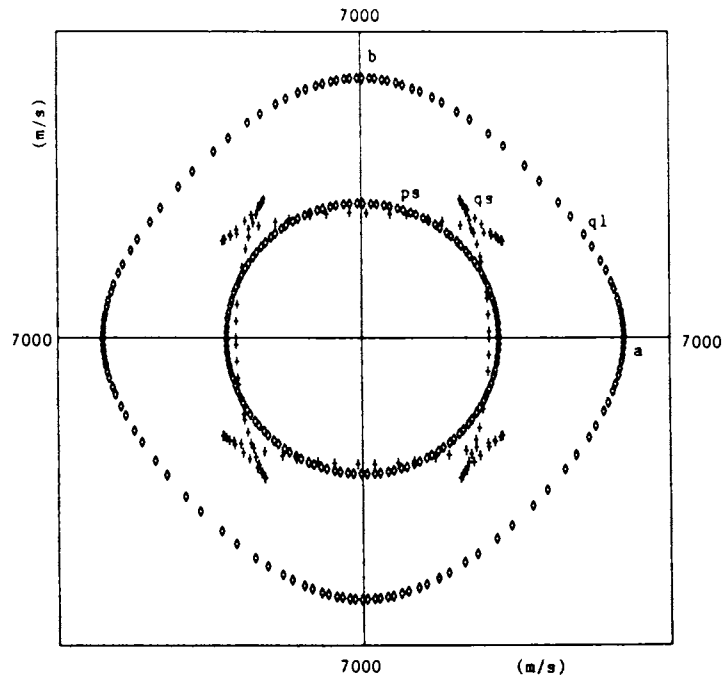


Fig. 6.6(a) Ray velocity surfaces in the ab (XY) plane for LSCO at 297 K.

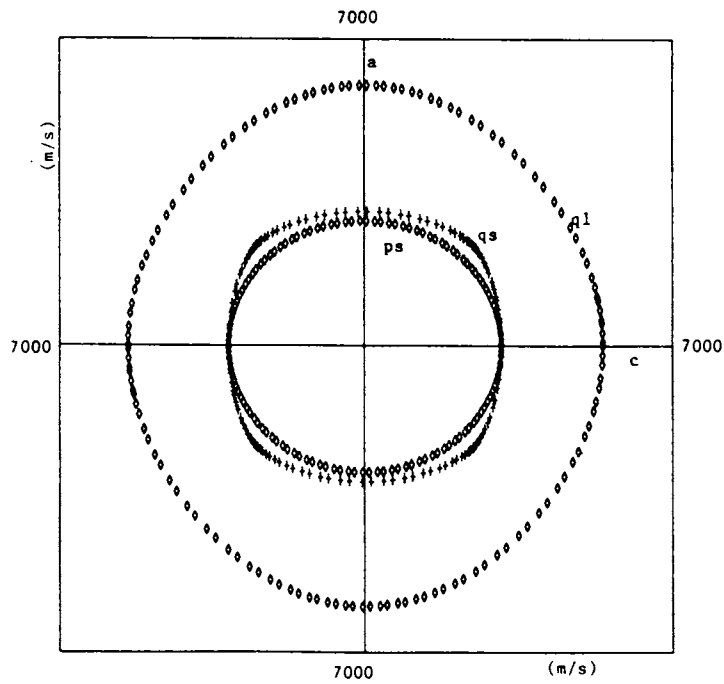


Fig. 6.6(b) Ray velocity surfaces in the ac (XZ) plane for LSCO at 297 K.

corresponding ray surfaces.

6.5 Discussion and conclusions

The slowness and ray velocity surfaces plotted for the three superconductors in different symmetry planes give a clear picture of the anisotropy in elastic wave propagation in these materials.

The slowness surfaces, as mentioned before, are the inverse phase velocity surfaces and are the polar reciprocals of the ray surfaces. The nature of elastic anisotropy exhibited by the phase velocity has been discussed in detail in chapter 5. It has been found that the anisotropy is more in the XZ (YZ) planes for the superconductors BSCCO and YBCO whereas in the XY plane the elastic waves are found to propagate with velocities that are essentially independent of direction. However, in LSCO the anisotropy is seen to be more in the XY plane. The difference in results are also discussed in chapter 5, taking into account the structure of these compounds.

The ray surface, as mentioned earlier represents the direction of propagation of phonon energy flux and is much more complex than the corresponding slowness surface. However, all the features of the ray surface can be traced from the shape of the slowness surface. It is found that if the slowness surface is circular, the group velocity is parallel to \mathbf{k} and the ray surface is simply another circle inverse to the slowness surface and is true in our plots also. For example, in BSCCO, the slowness and ray surfaces for all the three modes are circles in the XY plane as is evident from Figs. 6.1(a) and 6.2(a), indicating that the energy flow is distributed uniformly in the plane. For the other two superconductors one or two modes of the slowness and hence the corresponding ray surfaces are circles. For example, the slowness surfaces for the pure shear mode and quasilongitudinal mode in the XY plane of YBCO, pure shear mode in the XY and XZ planes of LSCO etc. are circles and hence the corresponding ray surfaces are also circles as is evident from Figs. 6.3(a), 6.4(a), 6.5(a), 6.6(a), 6.5(b), 6.6(b) etc.

As is well known, whenever the slowness surface is nonspherical in shape the ray surface is found to exhibit interesting features such as folds or cusps. Several papers have appeared in literature indicating that many crystals exhibit cuspidal edges in ray

velocity surfaces along specific directions for selected modes. When a cuspidal edge occurs in the ray surface there exist more than one wave vector corresponding to a single group velocity vector. All crystals do not give rise to cusps and the conditions under which a cusp occurs in the ray surface can be predicted from the shape of the slowness curve.

The cusps on the ray surface arises from the convoluted form of the corresponding slowness curve. In other words, the folds in the group velocity surface correspond to zero curvature of the slowness surface. At the point where a cusp is seen in the ray surface, there is an inflection in the curvature of the slowness surface.

The quasishear waves of all the superconductors investigated exhibit cuspidal edges in one or two planes in the ray surfaces. For example, cuspidal edges are clearly seen along the X and Y directions of YBCO in the XY plane, along 45° from the X direction in the XZ plane of YBCO, along 40° from the X axis in the XZ plane of BSCCO and along 45° from the X axis in the XY plane of LSCO etc. in the quasishear mode, as is clear from Figs. 6.2(b), 6.2(d), 6.4(a), 6.4(c), 6.6(a) etc. The point of zero inflection or a point of zero curvature is seen in the slowness surfaces exactly along the same directions where these cusps occur.

These cuspidal edges are of great physical significance in the light of the fact that many authors have suggested that the directions along which these edges occur might give rise to high phonon amplification. This effect, also called the phonon focussing is found to occur when an isotropic distribution of \mathbf{k} vectors, such as that emanating from an ideal point heat source, transforms into a distinctly anisotropic distribution of group velocities. Then the phonon energy is found to be concentrated or focussed along directions for which the curvature of the constant frequency slowness surface is small. And the folds in the ray surfaces define the real space directions of the singularities and are found to form boundaries between strong and weak focussing directions. This effect and various aspects associated with it are discussed in more detail in the next chapter.

A comparison of the energy distribution above and below T_c is also possible, since the ray surfaces have been plotted for BSCCO at two temperatures - one above and

the other below T_c in the XY and XZ planes. From these figures it is found that the ray surfaces do have the same shape at 290 K and 20 K. For example, from the figures 6.2(b) and 6.2(d) , it can be seen that the folds in the ray surface occur in the same direction in the crystal above and below T_c . This indicates that the nature of anisotropy associated with elastic energy propagation do not change with the superconducting transition, which is in accordance with the conclusions drawn from the phase velocity surfaces.

6.6 References

- [1] B. Taylor, H. J. Maris and C. Elbaum, *Phys. Rev.* **B3**, 1462 (1971).
- [2] A. K. McCurdy, H. J. Maris and C. Elbaum, *Phys. Rev.* **B2**, 4077 (1970).
- [3] H. B. Shore and L. M. Sander, *Phys. Rev.* **B12**, 1546 (1975).
- [4] G. F. Giuliani and A. W. Overhauser, *Phys. Rev.* **B20**, 1328 (1979).
- [5] V. A. Savastenko and A. V. Shelog, *Phys. Status Solidi* **A48**, K135 (1978).
- [6] S. S. Jaswal and R. J. Hardy, *Phys. Rev.* **B5**, 753 (1972).
- [7] R. Nava, M. P. Vecchi, J. Romero and B. Fernandez, *Phys. Rev.* **B14**, 800 (1976).
- [8] W. S. Gornall and B. P. Stoicheff, *Phys. Rev.* **B4**, 4518 (1971).
- [9] G. F. Miller and M. J. P. Musgrave, *Proc. R. Soc. London Ser.* **A236**, 352 (1956).
- [10] F. Rosch and O. Weis, *Z. Phys.* **B25**, 101 ; **B25**, 115 (1976).
- [11] M. J. P. Musgrave, in *Crystal Acoustics*, Holden Day, San Fransisco (1970).
- [12] J. Philip and K. S. Viswanathan, *Pramana* **8**, 348 (1977).
- [13] M. J. P. Musgrave, *Proc. Cambridge Philos. Soc.* **53**, 897 (1957).
- [14] M. J. P. Musgrave, *J. Elastic.* **9**, 105 (1979).
- [15] S. R. P. Nayar and K. S. Viswanathan, *Can. J. Phys.* **50**, 1903 (1972).
- [16] H. J. Maris, *J. Acoust. Soc. Am.* **50**, 812 (1971).
- [17] J. Philip and K. S. Viswanathan, *Phys. Rev.* **B17**, 4969 (1978).
- [18] C. G. Winterheimer and A. K. McCurdy, *Phys. Rev.* **B18**, 6576 (1978).
- [19] A. K. McCurdy, *Phys. Rev.* **B9**, 466 (1974).
- [20] A. G. Every, *Phys. Rev.* **B24**, 3456 (1981).

- [21] J. H. Staudt and B. D. Cook, *J. Acoust. Soc. Am.* **41**, 1547 (1967).
- [22] G. A. Saunders, C. Fanggao, L. Jiaqiang, Q. Wang, M. Cankurtaran, E. F. Lambson, P. J. Ford and D. P. Almond, *Phys. Rev.* **B49**, 9862 (1994).
- [23] Ming Lei, J. L. Sarrao, W. M. Visscher, T. M. Bell, J. D. Thompson and A. Migliori, *Phys. Rev.* **B47**, 6154 (1993).
- [24] A. Migliori, W. M. Visscher, S. Wong, S. E. Brown, I. Tanaka, H. Kojima and P. B. Allen, *Phys. Rev. Lett.* **64**, 2458 (1990)

Chapter 7

Phonon focussing in high T_c superconductors

7.1 Introduction

The propagation of long wavelength phonons in a crystalline solid is characterised by anisotropic velocities due to the direction dependent elasticity of the medium. Even in a highly symmetric cubic crystal, anisotropy in elastic properties are found to be significant. On the other hand, the thermal conductivity of a crystal, is usually represented by a second rank tensor, which for a crystal of cubic symmetry implies isotropic propagation of heat. The apparent discrepancy arises because the theory of thermal conductivity involves diffusion of high energy acoustic phonons with mean free paths much shorter than crystal dimensions.

However, if a localised pulse of high energy acoustic phonons or a heat pulse is introduced into an otherwise cold crystal, such phonons may travel ballistically over macroscopic distances, displaying anisotropies directly associated with the elastic tensor. Unlike the coherent plane waves produced at RF frequencies by a quartz transducer, a heat pulse consists of incoherently generated phonons with a near planck energy distribution characterised by the heater temperature. This heat pulse method, originally demonstrated in crystals by von Gutfeld *et al.* [1] generally utilises a resistive film to produce the heat pulse and a fast superconducting bolometer to detect the slight temperature rise when the ballistic phonons arrive at the opposite face of the crystal. The time of flight of these phonons across a crystal of known dimensions is well characterised by the corresponding sound velocities.

Shortly after these experiments it was observed that, in addition to the sound velocity, the phonon energy flux is dependent on the propagation direction. At low temperatures, where phonon mean free paths are comparable to crystal dimensions, which is called the ballistic regime, it was observed that there is an anisotropic channeling of phonon energies emanating from a localised heat pulse. The phenomenon was first explicitly demonstrated by Taylor *et al.* [2, 3], who have explained the 'phonon focussing' effect as a consequence of the noncollinearity of the phase and group velocities. They presented statistical calculations of the angular dependent flux enhancement which roughly explained their data.

In subsequent years there has been considerable activity in the area of ballistic phonon propagation in solids [4-9]. This was supported by the development of experimental techniques for generating and detecting acoustic phonons of frequencies upto several THz. In such heat pulse experiments, phonons are generated in a thin metallic film on one face of a crystal by means of short duration electrical, microwave or laser pulses. The phonons are detected, after propagating through the crystal, by means of a suitable bolometer. Metallic films which undergo superconducting to normal transition when the phonon flux arrives are very effective detectors. For heat pulse experiments, a crystal with phonon mean free path comparable to its linear dimensions is required so that the phonons will propagate ballistically rather than diffusively. Pulses due to phonons of different polarisations then arrive at the detector at different times and therefore can be studied independently. These experiments have considerable advantages over thermal conductivity studies as a means of investigating phonon - phonon and phonon - defect interactions. For example, the scattering of phonons by crystal defects may be studied by introducing the defects into the crystal and determining the fraction of phonons of a given polarisation which travel unscattered from the generator to the detector. Heat pulse studies thus make it possible to investigate the scattering of phonons of different polarisations separately. This is in contrast to thermal conductivity measurements, which only give some average scattering rate for all phonons. Another advantages of heat pulse studies is that the propagation of groups of phonons with wavelengths lying in different directions can be investigated, whereas, again, thermal

conductivity involves a complicated average over the k space.

The phonon focussing effect, as mentioned earlier, is one of the consequences of elastic anisotropy. The phonons generated by the film are assumed to have an approximately uniform distribution of wave vectors. However, since the wave vector and the group velocity vector are not collinear, a uniform distribution of directions in k space does not lead to a uniform distribution of energy flux. The amount of energy and hence the heat pulse amplitude received thus depend on the crystallographic direction between the detector and the generator. The energy received varies for the different phonon polarisations since the deviation of the group velocity direction from the wave vector direction is different for each polarisation.

The phonon focussing effect has been well studied both experimentally and theoretically. Heat pulse experiments carried out in ultrapure single crystals of Ge [10-13], GaAs [14], Si [15,16] etc. revealed sharp features in the phonon flux along specific directions for transverse acoustic modes. Large differences have also been observed by Taylor *et al.* [3] in the intensity of phonons of different polarisations propagating ballistically in LiF, KCl and Al₂O₃. Most of these experiments exploit temporal analysis of heat pulse intensity. Results of ballistic phonon imaging experiments, which offer a geometric visualisation of anisotropic phonon propagation in crystals, carried out on Ge [10,11], GaAs [14] and KDP [17] also show striking differences in the intensity of phonons propagating along different directions and found to have correspondence with phonon enhancement calculations in these crystals.

On the theoretical side also, there have been several attempts to study phonon focussing and to calculate the phonon enhancement factor employing various analytical techniques. Rosch *et al.* [7], for example have calculated the phonon focussing parameter for several crystals, which showed immense variations in phonon intensity within a given phonon mode. Philip *et al.* [8] have proposed a method to evaluate the phonon amplification factor for any general direction inside a cubic crystal. Northrop *et al.* [11] have explained the origin of complex intensity patterns observed in Ge in ballistic phonon imaging experiment, by calculating the complete locus of points on the slowness surface for which the enhancement factor diverges.

Eventhough the phonon focussing effect has been investigated thoroughly using various analytical techniques, the approach has always relied on the geometrical optics concept of a ray. And it has been found that in most crystals there exists certain directions, known in classical wave theory as caustics, where the geometrical optics approximation yield infinities in the displacement amplitude. These infinities are non-physical and violate the assumptions of linear elastic theory. The standard analysis of phonon focussing breaks down along these singular directions and catastrophe theory has been applied to the phenomenon [18, 19, 21].

In this chapter, an attempt has been made to calculate the phonon enhancement factor along different directions for three high T_c superconductors. The effect of caustics as well as the results obtained are discussed taking into account the slowness and ray surfaces of these materials, which are given in chapter 6. The results are presented after giving the details of computation of the phonon enhancement factor.

7.2 Phonon focussing in orthorhombic and tetragonal crystals

The phonon focussing, as has been mentioned already, is the amplification of phonons in certain directions of the crystal and the enhancement factor (A) is defined the ratio of energy flux for a particular polarisation and propagation direction to the corresponding flux in an isotropic solid. Mathematically it is equivalent to the ratio of the \mathbf{k} space solid angle $\Delta\Omega_k$ to the corresponding \mathbf{S} space (group velocity) solid angle $\Delta\Omega_s$. Thus the enhancement factor $A = |\Delta\Omega_k/\Delta\Omega_s|$ is proportional to the phonon energy flux and is equal to unity for an isotropic medium. The physical idea is contained in Fig. 7.1, plotted for Ge [11]. Fig. 7.1(a) represents the constant frequency slowness surface for Ge in the XY plane for the quasishear mode. For a given wavevector \mathbf{k} , terminating on this surface, the group velocity is normal to the slowness surface and is in general, not collinear with \mathbf{k} . Fig. 7.1(b) gives the plot of group velocities corresponding to the \mathbf{k} vectors in 7.1(a). Two equal solid angle sections along different group velocity directions are shown on the left side of the diagram. A mapping of these two real space sections

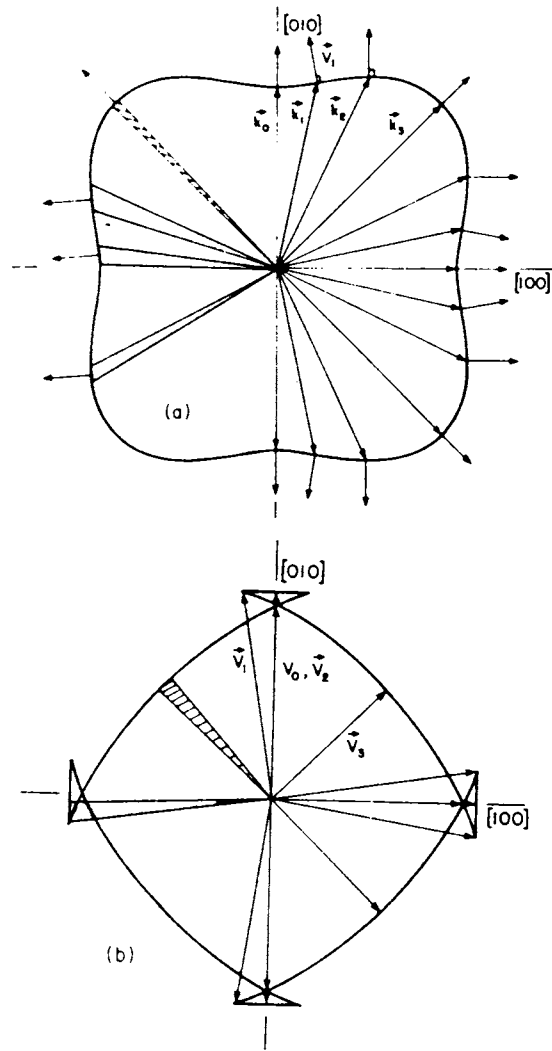


Fig. 7.1

(a) : Intersection of a constant frequency surface with the ab plane for the quasishear mode in Ge.

(b) : Plot of the group velocities corresponding to the \vec{k} vectors in (a).

into \mathbf{k} space is shown on the left half of Fig. 7.1(a). A constant real space solid angle $\Delta \Omega_s$, subtended by a detector corresponds to one or more \mathbf{k} space solid angles $\Delta \Omega_k$, differing in magnitude and location and flux enhancement along this group velocity direction is large. In other words, phonon energy is concentrated or focussed along group velocity directions for which the curvature of the constant frequency surface is small.

It has been shown that the phonon enhancement factor A can be expressed in spherical polar coordinates in terms of the Jacobian J of the transformation relating the variables (θ_k, ϕ_k) in \mathbf{k} space to the corresponding variables (θ_s, ϕ_s) in the group velocity space, and is given by [8]

$$A = \left| \frac{\Delta \Omega_k}{\Delta \Omega_s} \right| = \frac{1}{|J|} \quad (7.1)$$

where the Jacobian J is found to be proportional to the Gaussian curvature of the slowness surface and is dimensionless. Since J is expressed as a function of (θ_k, ϕ_k) and the energy propagation is along the corresponding (θ_s, ϕ_s) , calculation of the enhancement factor A requires the mapping of one two dimensional space (θ_s, ϕ_s) into another two dimensional space (θ_k, ϕ_k) . This mapping is generally not unique, there are cases where one (θ_s, ϕ_s) results from several different (θ_k, ϕ_k) as illustrated in Fig. 7.1

In this chapter, we have evaluated the phonon enhancement for high T_c superconductors, by evaluating the Jacobian of the transformation between these variables, taking the elastic constant data from literature. Since the superconductors investigated belong either to the orthorhombic or tetragonal symmetry, the details of the computation of A in these crystal classes is discussed. Previous workers have done the computation only in cubic crystals.

The dispersion equation for the propagation of an elastic wave of frequency ω and wavevector $\mathbf{k}(k_x, k_y, k_z)$ is given by

$$\Omega(\omega, k_x, k_y, k_z) = \begin{vmatrix} \lambda_{11} - \rho \omega^2 & \lambda_{12} & \lambda_{13} \\ \lambda_{12} & \lambda_{22} - \rho \omega^2 & \lambda_{23} \\ \lambda_{13} & \lambda_{23} & \lambda_{33} - \rho \omega^2 \end{vmatrix} \quad (7.2)$$

where the Christoffel coefficients λ for the orthorhombic symmetry is given by eqn.(5.9).

Expanding the determinant in eqn.(7.2), a cubic equation in $\rho\omega^2$ is obtained, which can be expressed as

$$\Omega = A_3 x^3 + A_2 x^2 + A_1 x + A_0 \quad (7.3)$$

where $x = \rho\omega^2$ and the coefficients are given by

$$\begin{aligned} A_3 &= 1 \\ A_2 &= -[l^2 J_x + m^2 J_y + n^2 J_z] \\ A_1 &= l^4 K_x + m^4 K_y + n^4 K_z + l^2 m^2 L_{xy} + l^2 n^2 K_{xz} + m^2 n^2 K_{yz} \\ A_0 &= -[l^6 L_x + m^6 L_y + n^6 L_z + l^4 m^2 L_{xy} \\ &\quad + l^4 n^2 L_{xz} + l^2 m^4 L_{yx} + m^4 n^2 L_{yz} \\ &\quad + l^2 n^4 L_{zx} + m^2 n^4 L_{zy} + l^2 m^2 n^2 L_{xyz}] \end{aligned} \quad (7.4)$$

where J 's, K 's and L 's are expressed in terms of the elastic constants as

$$\begin{aligned} J_x &= C_{11} + C_{55} + C_{66} \\ J_y &= C_{22} + C_{44} + C_{66} \\ J_z &= C_{33} + C_{44} + C_{55} \end{aligned} \quad (7.5)$$

$$\begin{aligned} K_x &= C_{11} C_{66} + C_{11} C_{55} + C_{55} C_{66} \\ K_y &= C_{22} C_{66} + C_{44} C_{66} + C_{22} C_{44} \\ K_z &= C_{33} C_{44} + C_{33} C_{55} + C_{44} C_{55} \\ K_{xy} &= C_{11} C_{22} + C_{11} C_{44} + C_{55} C_{66} + C_{44} C_{66} + C_{22} C_{55} - C_{12}^2 - 2 C_{12} C_{66} \\ K_{xz} &= C_{11} C_{44} + C_{11} C_{33} + C_{55} C_{66} + C_{33} C_{66} + C_{44} C_{55} - C_{13}^2 - 2 C_{13} C_{55} \\ K_{yz} &= C_{22} C_{33} + C_{22} C_{55} + C_{33} C_{66} + C_{44} C_{55} + C_{44} C_{66} - C_{23}^2 - 2 C_{23} C_{44} \end{aligned} \quad (7.6)$$

$$\begin{aligned} L_x &= C_{11} C_{55} C_{66} \\ L_y &= C_{22} C_{44} C_{66} \\ L_z &= C_{33} C_{44} C_{55} \\ L_{xy} &= C_{11} C_{22} C_{55} + C_{11} C_{44} C_{66} - C_{55} C_{12}^2 - 2 C_{12} C_{55} C_{66} \end{aligned}$$

$$\begin{aligned}
L_{xz} &= C_{11} C_{44} C_{55} + C_{11} C_{33} C_{66} - C_{66} C_{13}^2 - 2 C_{13} C_{55} C_{66} \\
L_{yz} &= C_{22} C_{55} C_{66} + C_{11} C_{22} C_{44} - C_{44} C_{12}^2 - 2 C_{12} C_{44} C_{66} \\
L_{yz} &= C_{22} C_{44} C_{55} + C_{22} C_{33} C_{66} - C_{66} C_{23}^2 - 2 C_{23} C_{44} C_{66} \\
L_{zx} &= C_{11} C_{33} C_{44} + C_{33} C_{55} C_{66} - C_{44} C_{13}^2 - 2 C_{13} C_{44} C_{55} \\
L_{zy} &= C_{22} C_{33} C_{55} + C_{33} C_{44} C_{66} - C_{55} C_{23}^2 - 2 C_{23} C_{44} C_{55} \\
L_{xyz} &= 4 C_{44} C_{55} C_{66} + C_{11} C_{22} C_{33} - C_{11} C_{23}^2 - C_{33} C_{12}^2 - C_{22} C_{13}^2 - 2 C_{11} C_{44} C_{23} \\
&\quad - 2 C_{12} C_{33} C_{66} - 2 C_{13} C_{22} C_{55} + 2 C_{12} C_{13} C_{44} + 2 C_{12} C_{13} C_{23} + 2 C_{13} C_{23} C_{66} \\
&\quad + 2 C_{12} C_{44} C_{55} + 2 C_{12} C_{23} C_{55} + 2 C_{13} C_{44} C_{66} + 2 C_{23} C_{55} C_{66} \tag{7.7}
\end{aligned}$$

In spherical polar coordinates, the direction cosines can be represented as

$$\begin{aligned}
l &= \frac{k_x}{k} = \sin \theta_k \cos \phi_k \\
m &= \frac{k_y}{k} = \sin \theta_k \sin \phi_k \\
n &= \frac{k_z}{k} = \cos \theta_k \tag{7.8}
\end{aligned}$$

To derive the expressions for phonon focussing, it is found necessary to have explicit expressions for the roots of the cubic equation (7.3). Let

$$\begin{aligned}
q &= \frac{A_1}{3} - \frac{A_2^2}{9} \\
\gamma &= \frac{1}{6} (A_1 A_2 - 3 A_0) - \frac{A_2^3}{27} \tag{7.9}
\end{aligned}$$

Since the roots of eqn.(7.3) are real, the discriminant $(q^3 + \gamma^3)$ is negative and hence we can write [21]

$$(q^3 + \gamma^3)^{1/2} = i B^{1/2} \tag{7.10}$$

where

$$B = |q^3 + \gamma^3|$$

Let

$$(\gamma + i B^{1/2}) = R e^{i\psi} \tag{7.11}$$

where

$$R^2 = \gamma^2 + B$$

and

$$\tan \psi = \frac{B^{1/2}}{\gamma}$$

Then the roots of eqn.(7.3) can be written as

$$\begin{aligned} x_1 &= 2 R^{1/3} \cos\left(\frac{\psi}{3}\right) - \frac{A_2}{3} \\ x_2 &= -R^{1/3} \cos\left(\frac{\psi}{3}\right) - \frac{A_2}{3} - \sqrt{3} R^{1/3} \sin\left(\frac{\psi}{3}\right) \\ x_3 &= -R^{1/3} \cos\left(\frac{\psi}{3}\right) - \frac{A_2}{3} + \sqrt{3} R^{1/3} \sin\left(\frac{\psi}{3}\right) \end{aligned} \quad (7.12)$$

Of these, x_1 denotes the pure shear mode whereas x_2 and x_3 denote the quasishear and quasilongitudinal modes respectively.

As stated earlier, the group velocity \mathbf{S} of the wave is not in the same direction as that of the wavevector \mathbf{k} . The cartesian components of \mathbf{S} can then be expressed in spherical polar coordinates as

$$\begin{aligned} S_x &= -\frac{D_x}{\partial\Omega/\partial\omega} = \mathbf{S} \sin \theta_s \cos \phi_s \\ S_y &= -\frac{D_y}{\partial\Omega/\partial\omega} = \mathbf{S} \sin \theta_s \sin \phi_s \\ S_z &= -\frac{D_z}{\partial\Omega/\partial\omega} = \mathbf{S} \cos \theta_s \end{aligned} \quad (7.13)$$

where the derivatives D_x , D_y and D_z can be evaluated from eqn.(7.3), after substituting for A_3 , A_2 , A_1 and A_0 and the direction cosines. The expression for D_x is given in terms of k_x , k_y and k_z as

$$\begin{aligned} D_x = \frac{\partial\Omega}{\partial k_x} &= -2(\rho\omega^2)^2 k_x J_x + 2(\rho\omega^2) [2k_x^3 K_x + k_x k_y^2 K_{xy} + k_x k_z^2 K_{xz}] \\ &\quad -2[3k_x^5 L_x + 2k_x^3 k_y^2 L_{xy} + 2k_x^3 k_z^2 L_{xz} + k_x k_y^4 L_{yx} \\ &\quad + k_x k_z^4 L_{zx} + k_x k_y^2 k_z^2 L_{xyz}] \end{aligned} \quad (7.14)$$

The other two derivatives can be obtained by a cyclic rotation of the coordinates. However, the values of k_x , k_y and k_z have to be substituted in spherical polar coordinates given by eqn.(7.8). Also, we have from eqn.(7.13)

$$\tan \theta_s = \frac{(S_x^2 + S_y^2)^{1/2}}{S_z} = \frac{(D_x^2 + D_y^2)^{1/2}}{D_z} \quad (7.15)$$

and

$$\tan \phi_s = \frac{S_y}{S_x} = \frac{D_y}{D_x} \quad (7.16)$$

The above equations show that θ_s and ϕ_s are functions of θ_k and ϕ_k and from these the Jacobian of the transformation relating the variables (θ_s, ϕ_s) and (θ_k, ϕ_k) can be written as

$$J = \frac{d\theta_s d\phi_s}{d\theta_k d\phi_k} = \frac{\partial\theta_s}{\partial\theta_k} \frac{\partial\phi_s}{\partial\phi_k} - \frac{\partial\theta_s}{\partial\phi_k} \frac{\partial\phi_s}{\partial\theta_k} \quad (7.17)$$

If the Jacobian of the transformation is evaluated, the phonon enhancement factor (A) can be written as

$$A^{-1} = \frac{d\Omega_s}{d\Omega_k} = \frac{\sin \theta_s}{\sin \theta_k} \frac{d\theta_s}{d\theta_k} \frac{d\phi_s}{d\phi_k} = J \frac{\sin \theta_s}{\sin \theta_k} \quad (7.18)$$

To evaluate the Jacobian, it is necessary to obtain the four partial derivatives $\frac{\partial\theta_s}{\partial\theta_k}$, $\frac{\partial\theta_s}{\partial\phi_k}$, $\frac{\partial\phi_s}{\partial\theta_k}$, and $\frac{\partial\phi_s}{\partial\phi_k}$ and these can be obtained by direct partial differentiation of eqns. (7.15) and (7.16) with respect to θ_k and ϕ_k . The procedure involves considerable algebraic work and formidably long expressions are obtained and are not reproduced here. However, in obtaining the equations, it must be remembered that the expressions for D_x , D_y and D_z involves ρv^2 and the partial derivatives of ρv^2 with respect to θ_k and ϕ_k should be evaluated in each case.

For tetragonal symmetry, the expressions for phonon enhancement factor can easily be obtained by imposing the equalities $C_{11} = C_{22}$, $C_{44} = C_{55}$ and $C_{13} = C_{23}$.

7.3 Computation of phonon intensities in high T_c superconductor crystals

The importance of studies probing the different aspects of elastic wave propagation in high T_c superconductors have been discussed in the previous chapters. However, literature is short of such reports due to the technical difficulties in growing single crystals of these materials. The elastic constant measurements reported on high T_c superconducting crystals have been thoroughly reviewed in chapter 5.

We have calculated the phonon enhancement factors for three superconducting systems - BSCCO, YBCO and LSCO - for which the phase velocity, slowness and ray surfaces have been plotted in chapters 5 and 6. Eventhough phonon focussing may

not have any direct bearing on the superconducting transition, it would be of great interest to understand the anisotropic nature of phonon propagation in these materials. A computer program written in FORTRAN has been used to evaluate the phonon enhancement factors for the shear, quasishear and quasilongitudinal modes for the three superconductors. Computations have been performed in each crystal, varying θ_k and ϕ_k and from 0 to $\pi/2$, each in steps of 2° , resulting in performing the computation at 2025 points in the wave vector space. The phonon intensities are then plotted in a pseudo 3D representation as a function of θ_k and ϕ_k . A print out of the program is given in Appendix A. The elastic constant values used for these computations are the same as the ones used to compute the phase velocity surfaces in chapter 5 and the ray velocity and slowness surfaces in chapter 6.

The phonon enhancement factors have been computed and plotted for BSCCO for the shear, quasishear and quasilongitudinal modes at two temperatures - one above and the other below T_c , taking the elastic constant data of Saunders *et al.* [22]. Figs. 7.2(a), 7.2(b) and 7.2(c) represent pseudo 3D plots of the phonon intensities for the shear, quasishear and quasilongitudinal modes respectively of BSCCO at 290 K. The plots in Figs. 7.3(a), 7.3(b) and 7.3(c) depict the corresponding pseudo 3D plots for the three modes at 20 K. Plots of one particular mode at 290 K and 20 K are given together so that a comparison of the distribution of the intensities at temperatures above and below T_c is possible.

For the two superconductors studied, *i. e.*, YBCO and LSCO, such a comparison is not possible since the complete set of elastic constant data is lacking for these materials at low temperatures as has been mentioned already. Figs. 7.4(a), 7.4(b) and 7.4(c) represent the pseudo 3D plots of the phonon intensities for shear, quasishear and quasilongitudinal modes for YBCO computed using the elastic constant data reported by Ming Lei *et al.* [23] at room temperature. In Figs. 7.5(a), 7.5(b) and 7.5(c), we have shown the pseudo 3D plots of the phonon intensities for the shear, quasishear and quasilongitudinal modes respectively for LSCO at 297 K, computed using the elastic constant data reported by Migliori *et al.* [24].

In these figures, sharp features are visible in phonon enhancement factors in

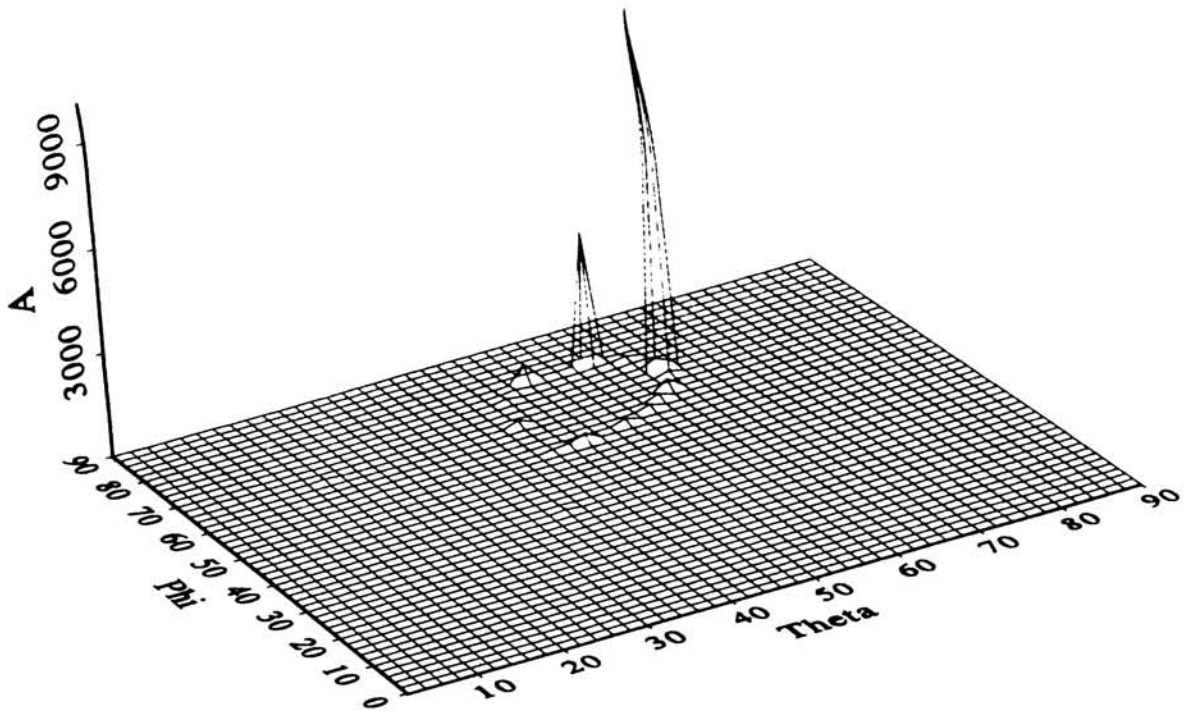


Fig. 7.2(a) Pseudo 3D representation of the distribution of phonon intensity (A) for the shear mode of BSCCO at 290 K.

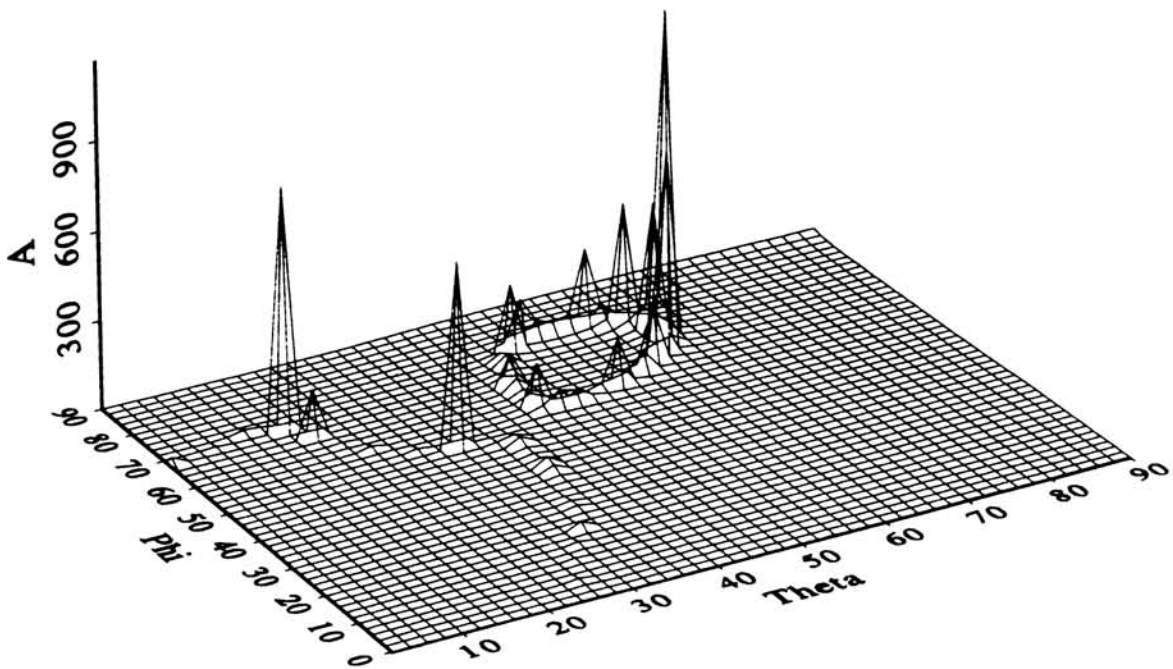


Fig. 7.3(a) Pseudo 3D representation of the distribution of phonon intensity (A) for the shear mode of BSCCO at 20 K.

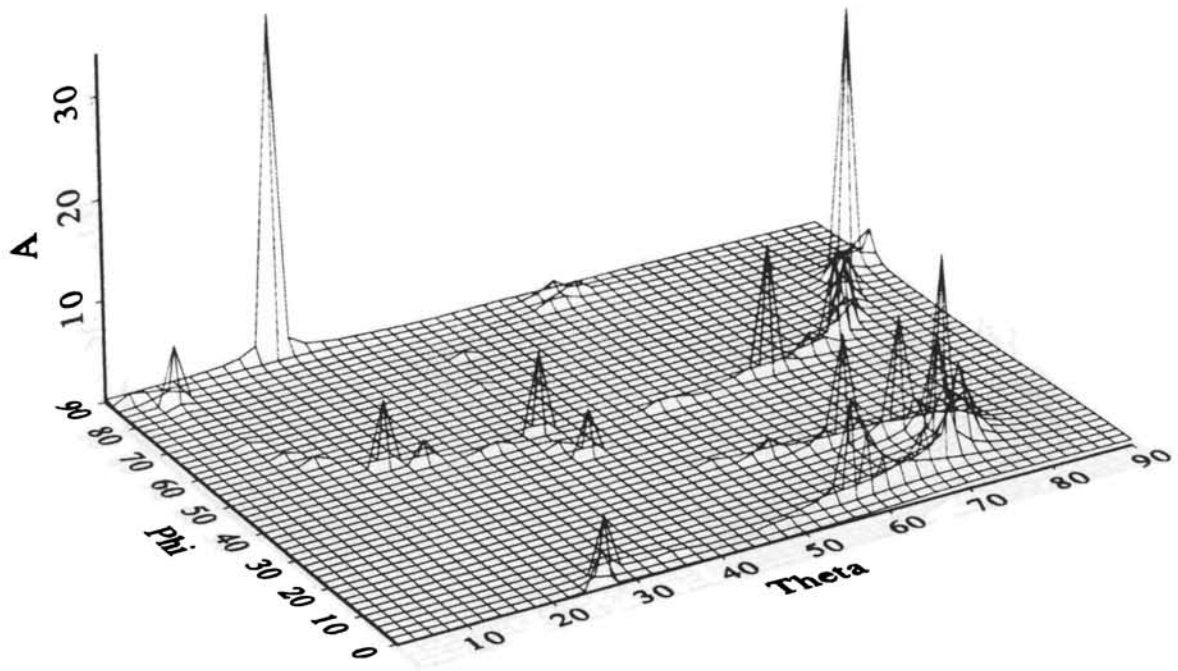


Fig. 7.2(b) Pseudo 3D representation of the distribution of phonon intensity (A) for the quasishear mode of BSCCO at 290 K.

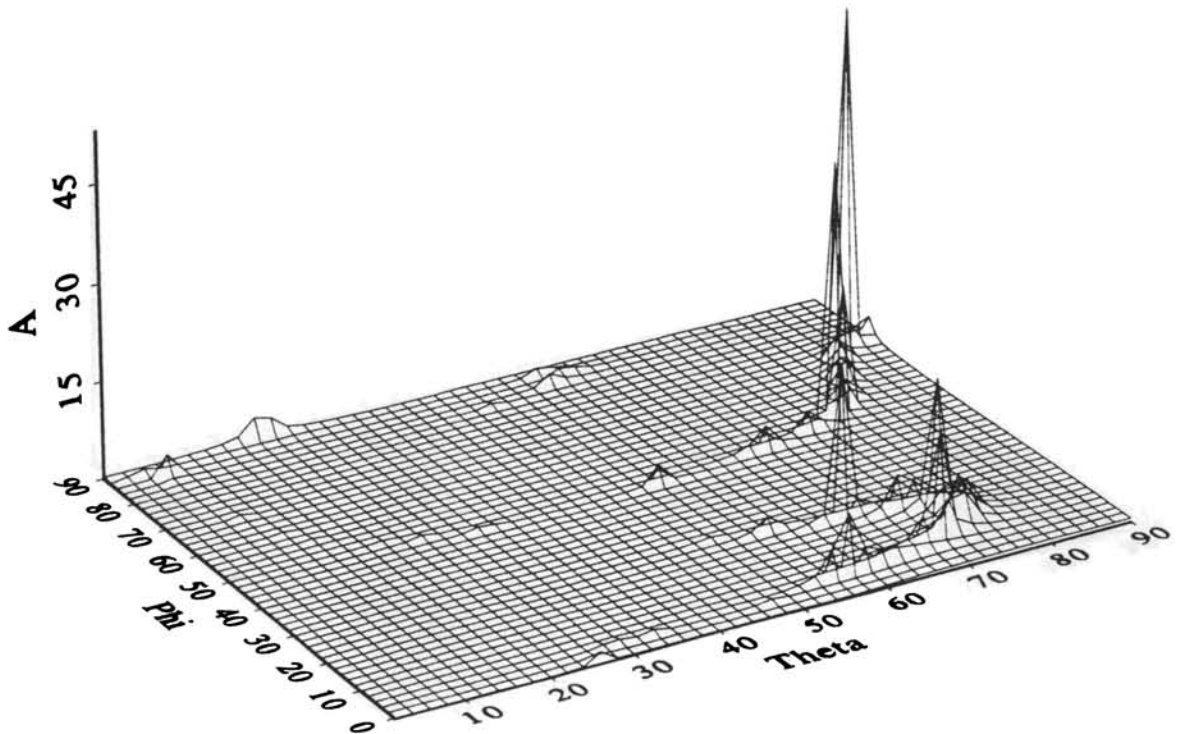


Fig. 7.3(b) Pseudo 3D representation of the distribution of phonon intensity (A) for the quasishear mode of BSCCO at 20 K.

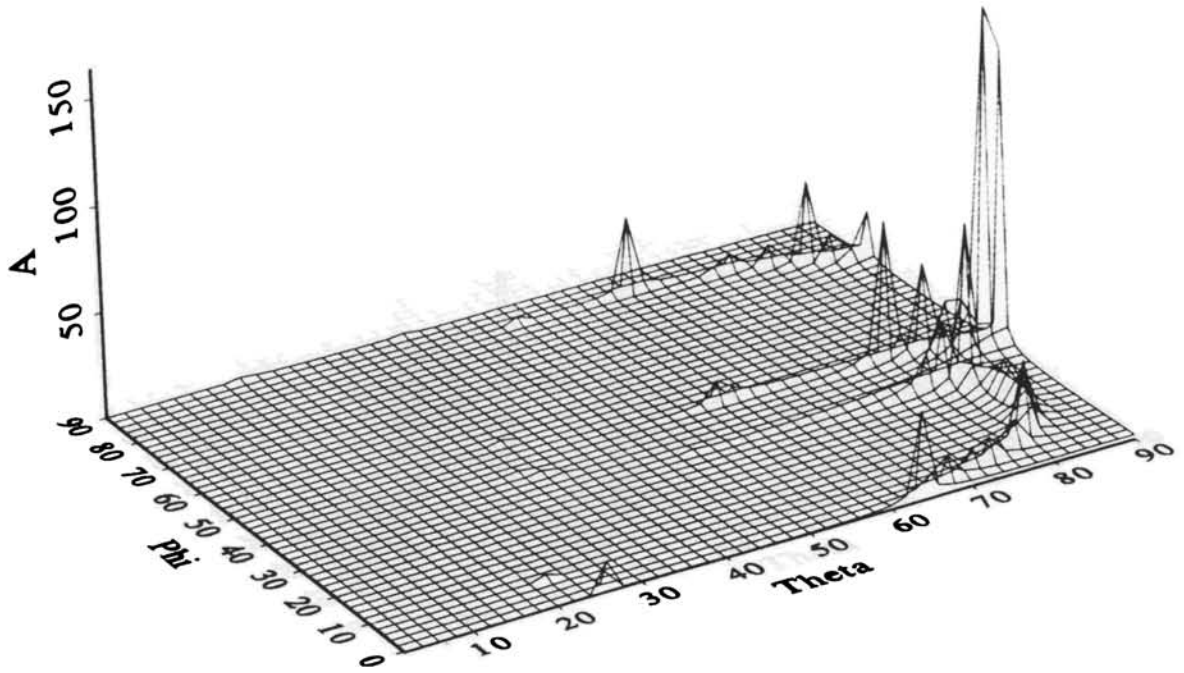


Fig. 7.2(c) Pseudo 3D representation of the distribution of phonon intensity (A) for the quasilongitudinal mode of BSCCO at 290 K.

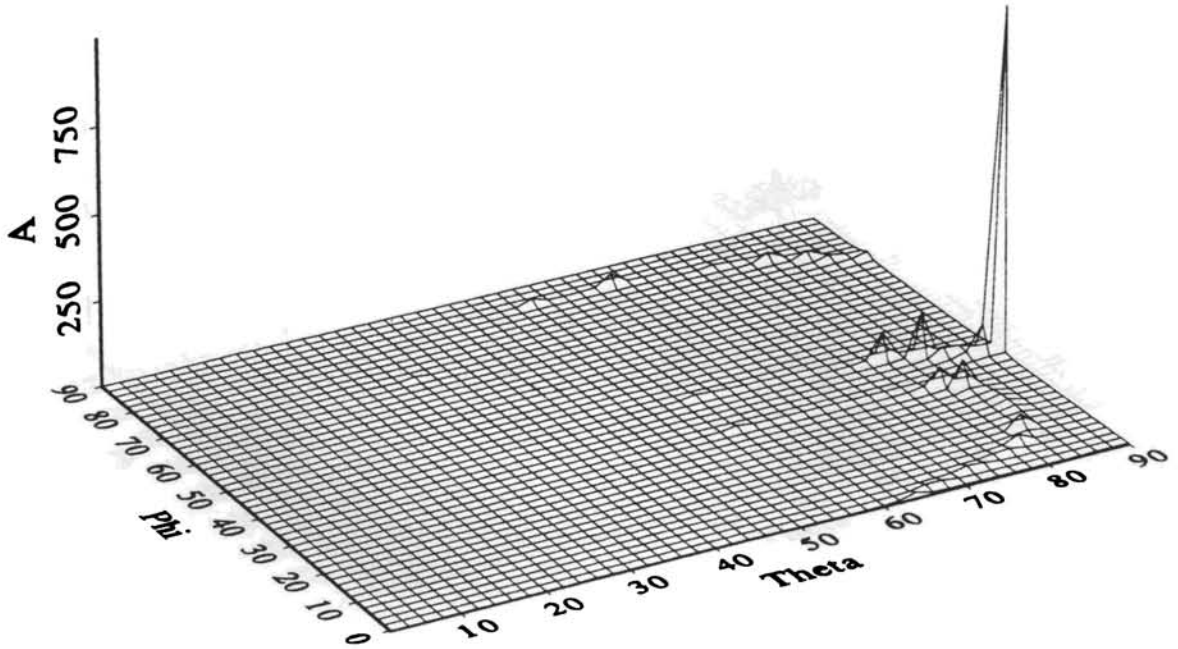


Fig. 7.3(c) Pseudo 3D representation of the distribution of phonon intensity (A) for the quasilongitudinal mode of BSCCO at 20 K.

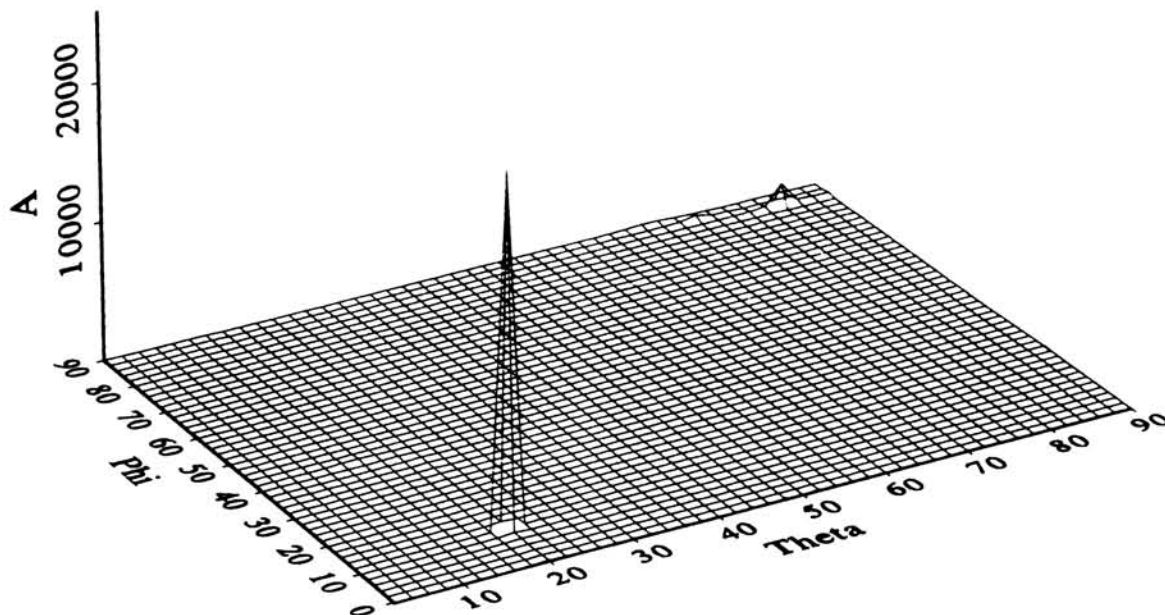


Fig. 7.4(a) Pseudo 3D representation of the distribution of phonon intensity (A) for the shear mode of YBCO at room temperature.

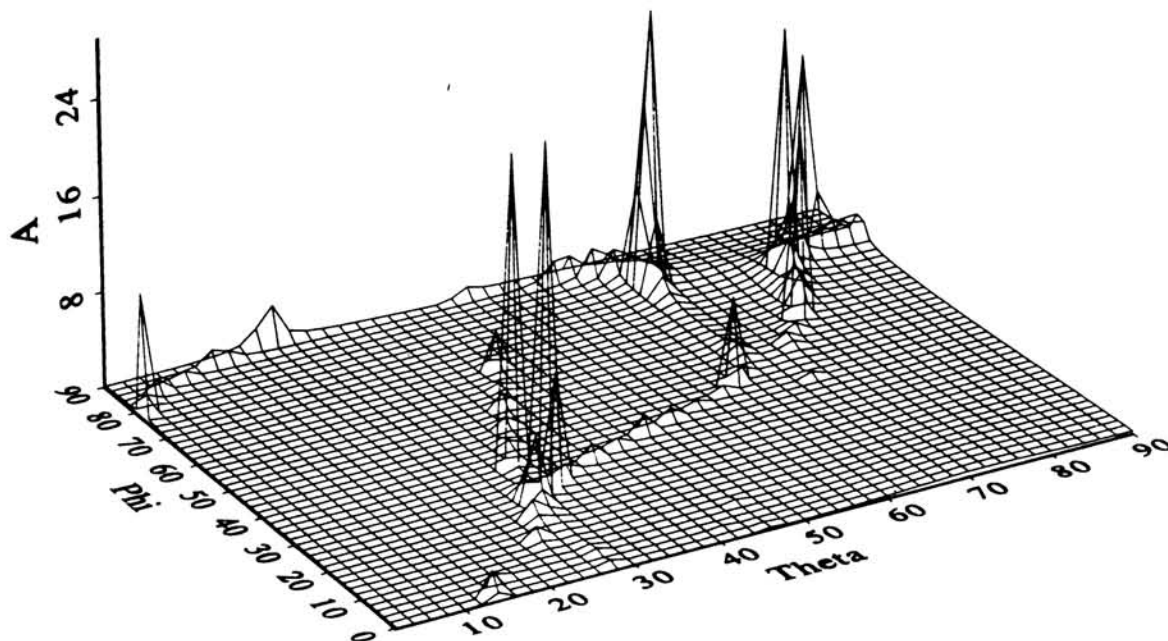


Fig. 7.4(b) Pseudo 3D representation of the distribution of phonon intensity (A) for the quasishear mode of YBCO at room temperature.

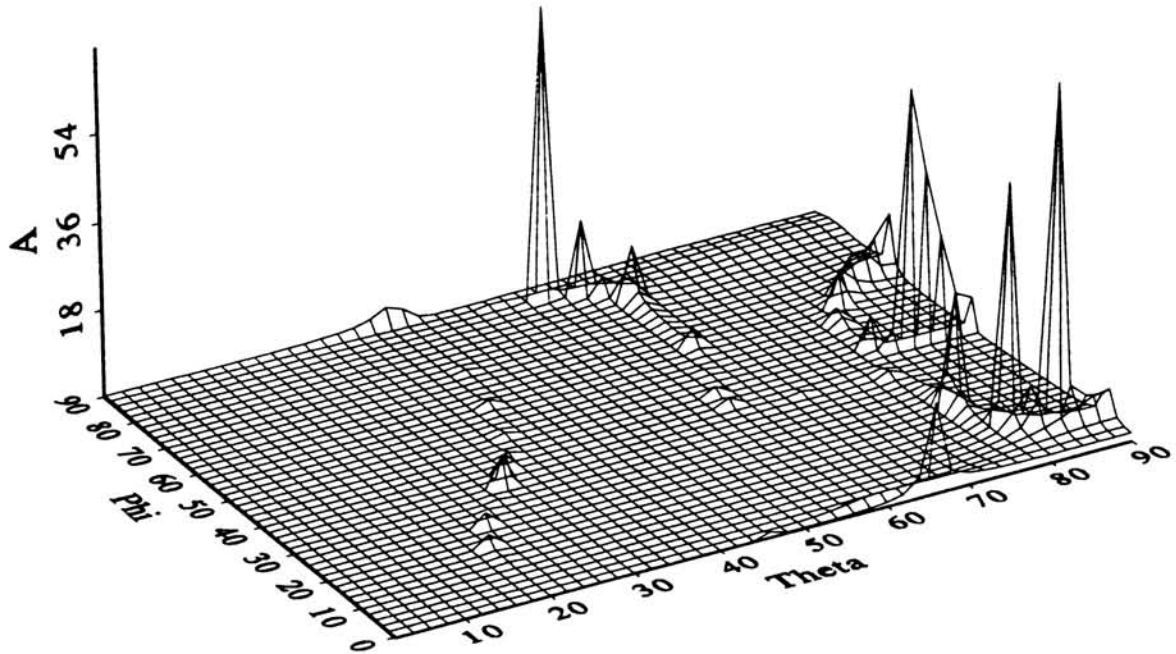


Fig. 7.4(c)

Pseudo 3D representation of the distribution of phonon intensity (A) for the quasilongitudinal mode of YBCO at room temperature.

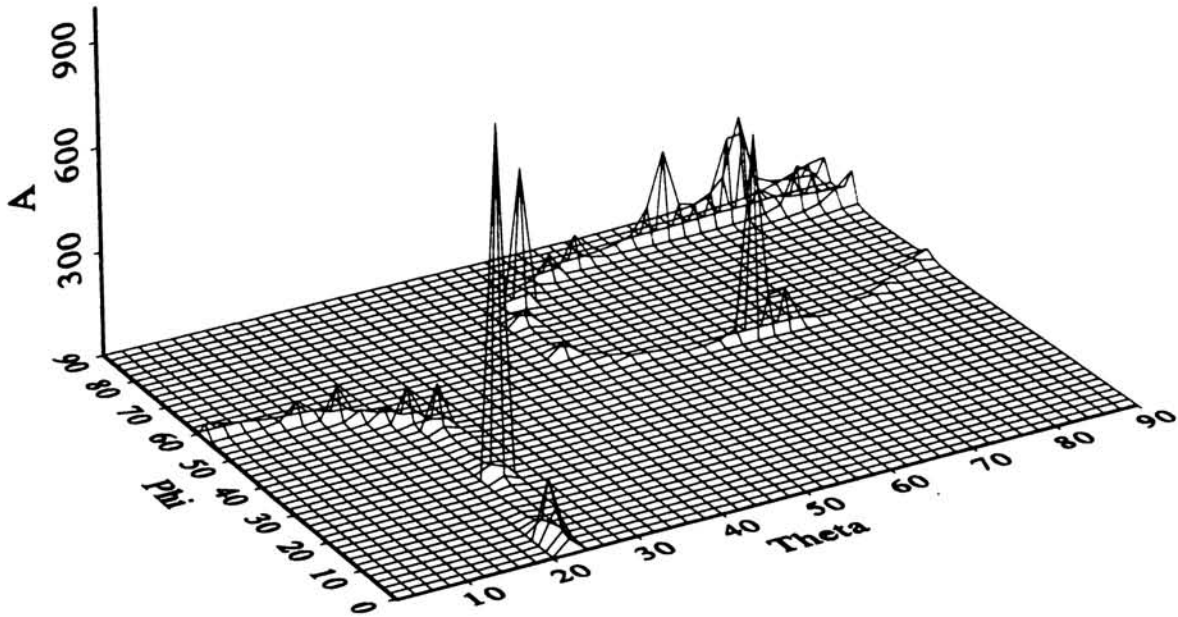


Fig. 7.5(a) Pseudo 3D representation of the distribution of phonon intensity (A) for the shear mode of LSCO at 297 K.

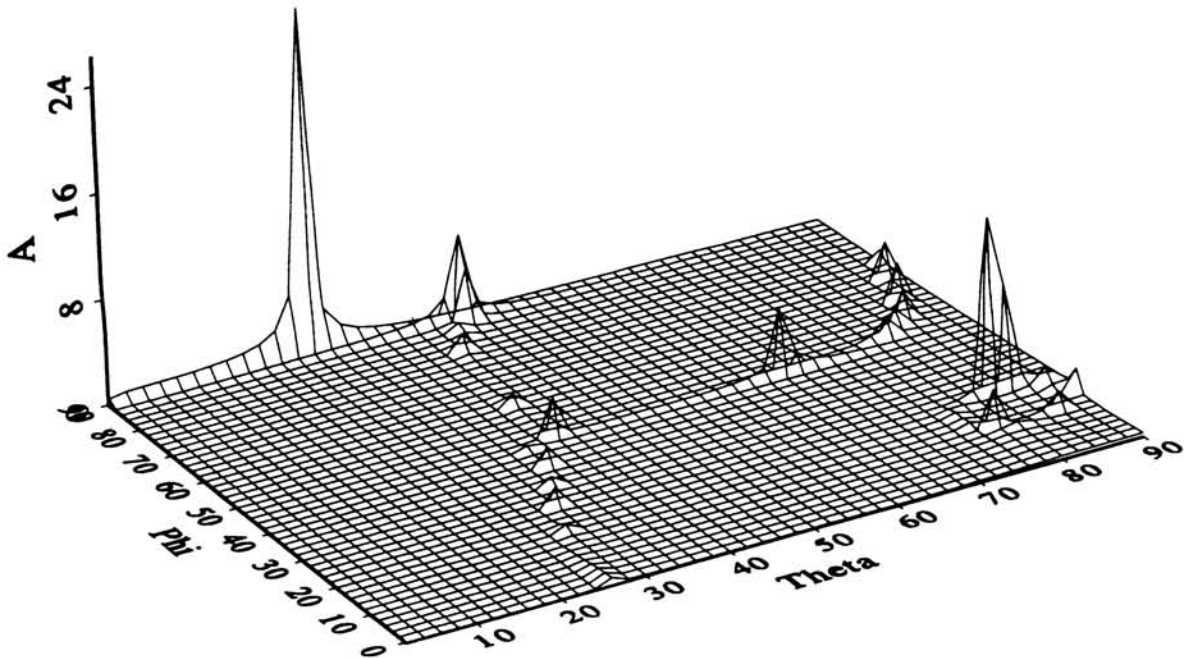


Fig. 7.5(b) Pseudo 3D representation of the distribution of phonon intensity (A) for the quasishear mode of LSCO at 297 K.

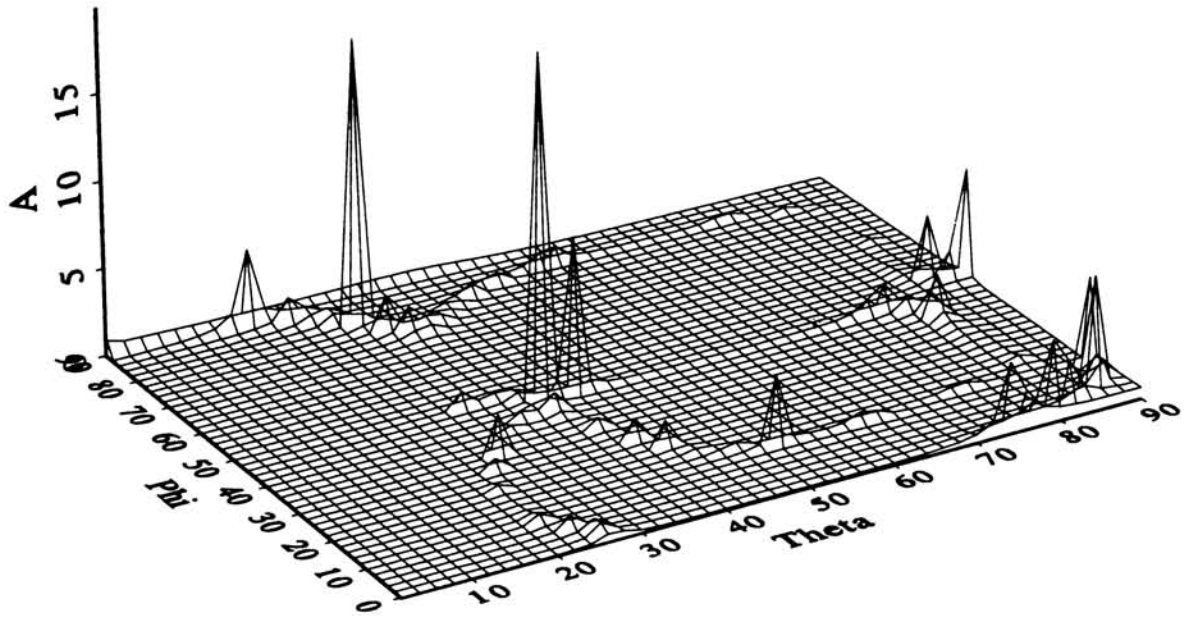


Fig. 7.5(c)

Pseudo 3D representation of the distribution of phonon intensity (A) for the quasilongitudinal mode of LSCO at 297 K.

certain directions. For example, the pure shear mode of YBCO exhibit a very sharp peak at $(\theta_k, \phi_k) = (20, 12)$, whose value run in to several thousands as is clear from Fig. 7.4(a). All the superconductors investigated here are found to possess such exceedingly high values in certain directions, at least for one mode of wave propagation. However, these high intensities cannot be attributed to the real focussing of phonons along these directions, since these values are physically unrealistic. These peaks are interpreted as caused by caustics, which is discussed in detail in the following section.

7.4 Phonon focussing catastrophes

Many previous workers have shown that striking differences occur in the magnitude of phonon intensities along various directions of an anisotropic crystal for the three modes of propagation. An interpretation of these rather complex behaviours of the phonon beams in the ballistic regime should be made by means of the basic theory of phonon focussing. The traditional phonon focussing theory is constructed on the focussing factor introduced by Maris [4] as a ratio of the solid angles occupied by the phonons in the wave vector and real spaces. However, the focussing factor defined in this way is based on a trajectory picture for the phonons or geometrical acoustics approximation [27], and its analytical expression has been recognised to yield infinities, though integrable, along certain crystal axes. Taborek *et al.* [18, 19] have remarked that vectors parallel to such crystallographic directions form conical surfaces, called caustic surfaces or simply caustics in classical wave theories. According to their analysis, the correct phonon intensity obtained by solving the wave equation of the lattice is finite along these directions, though still enhanced heavily [18, 19, 28]. This means that geometrical acoustics approximation breaks down on the caustics.

Considerable efforts have been made to understand the origins of sharp enhancements of the observed phonon flux in connection with the infinities of the focussing factor and the underlying geometry of constant frequency surfaces of the phonons in the wave vector space. Tamura *et al.* [20] have shown that the sharp focussing of the phonon flux are deeply connected with topological properties of the ω surfaces. A similar conclusion has been reached by Northrop *et al.* [11].

Taborek *et al.* [19] have shown that the directions of high focussing are associated with small curvature on the slowness surface and that points of zero curvature yield an infinity in the field amplitude. The possible forms of regions of zero curvature can be investigated by considering perturbations of the slowness surface of an isotropic solid, which is a sphere. The effect of elastic anisotropy is to deform the spheres slightly, leading to regions of negative curvature. Regions of positive and negative curvatures are separated by smooth curves along which the curvature vanishes. Vectors normal to the slowness surface along such a closed curve correspond to Poynting vectors which sweep out a conical surface emanating from the point source on which the field is intense but cannot be computed using geometrical acoustics. These surfaces are the caustics in classical theory mentioned earlier, and higher order approximations to the wave equations must be used to analyse the field in their vicinity. A thorough analysis including complete mathematical treatment of this effect is rather lengthy and not attempted.

Considering the slowness and ray surfaces plotted for the high T_c superconductors in chapter 6, it is clear that the ray surfaces for the pure shear and quasilongitudinal modes do not contain any folds or cusps. The only mode in which cusps appear is the quasishear mode, and this is the case for all the three high T_c superconductors investigated. And, it has been suggested by many authors that phonon energy is focussed along the directions in which cusps occur in the ray velocity surface. So the only mode for which we can expect to see interesting features in phonon enhancement is the quasishear mode for all the superconductors. This aspect is further discussed in the following section.

7.5 Phonon enhancement along fold directions for the quasishear mode

After having identified the directions in which folds or cusps occur in the ray surfaces for the quasishear mode in different high T_c superconductors, we have computed the phonon enhancement factors along these directions for this mode. The general program developed to compute phonon enhancement factors along general directions has been

modified to compute phonon enhancement factors along the directions in which cusps are found to occur in the ray velocity surface. The computation has been performed on BSCCO at 290 K and 20 K, and on YBCO and LSCO at room temperature. Figs. 7.6(a) and (b) represent the curves for BSCCO at 290 K and 20 K respectively in the ab plane; Figs. 7.7(a) and (b) depict those for YBCO in the ab and ac planes respectively and Fig. 7.8 gives the curve for LSCO in the ab plane.

All these figures show peaks in phonon intensity along specific directions. The position of these peaks in these figures corresponds to the points at which the caustics intersect the group velocity surface. A qualitative analysis of the positions of these peaks in comparison with the directions in which cusps occur indicate that these are the directions along which the phonon intensity is getting amplified. It should be noted that the values of the phonon enhancement factors are not abnormally high along these cusp directions. So the sharp peaks in the pure shear and quasilongitudinal modes, present for all the superconductors, can be interpreted as due to caustics.

However, it must be remembered that the ray surfaces have been plotted only in selected symmetry planes of the crystals. A three dimensional view of the group velocity surfaces is necessary to find out the exact positions where the Gaussian curvature of the corresponding slowness surface tends to zero. Moreover, a one to one mapping of the group velocity surface with the corresponding slowness surface will reveal the points where the caustics will meet the group velocity surface. Such points for the quasishear mode will give the directions along which phonon intensities will be more compared to those in an isotropic medium. Such a detailed analysis and mapping are not attempted here since such an analysis for orthorhombic crystals is very involved and lengthy. But a qualitative picture of the physical effects involved can be obtained from the figures 7.6, 7.7 and 7.8. Detailed mapping and analysis have been done for cubic crystals by Tamura [25] and Every [26]. A comparison of the results presented here with the detailed analysis done for cubic crystals aids to obtain an idea about phonon focussing effects in high T_c superconductor crystals.

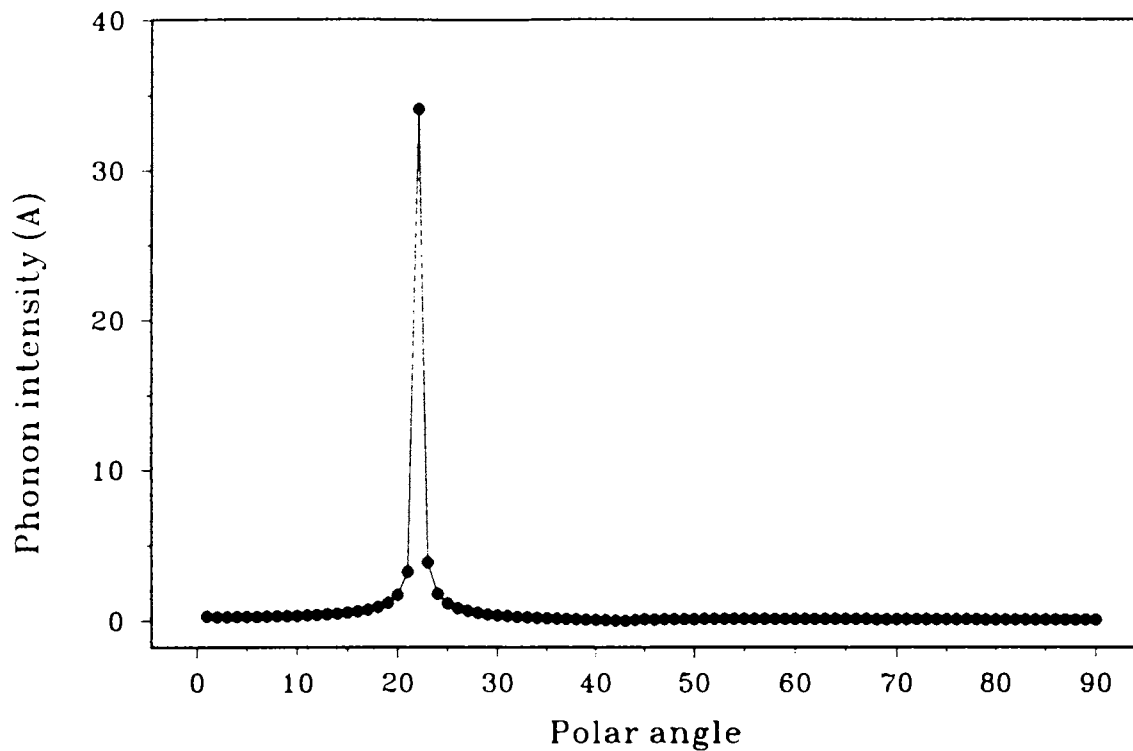


Fig. 7.6(a) Variation of phonon intensity with the polar angle (θ_k) for the propagation of quasishear mode in the *ac* plane of BSCCO at 290 K.

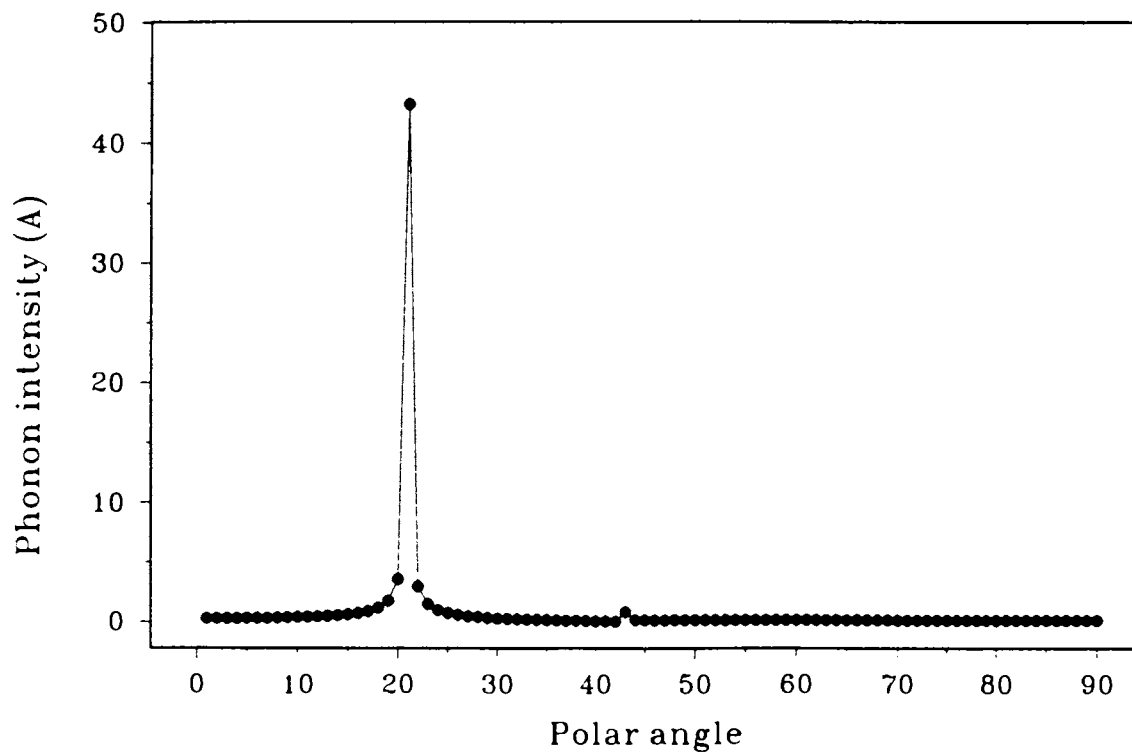


Fig. 7.6(b) Variation of phonon intensity with the polar angle (θ_k) for the propagation of quasishear mode in the *ac* plane of BSCCO at 20 K.

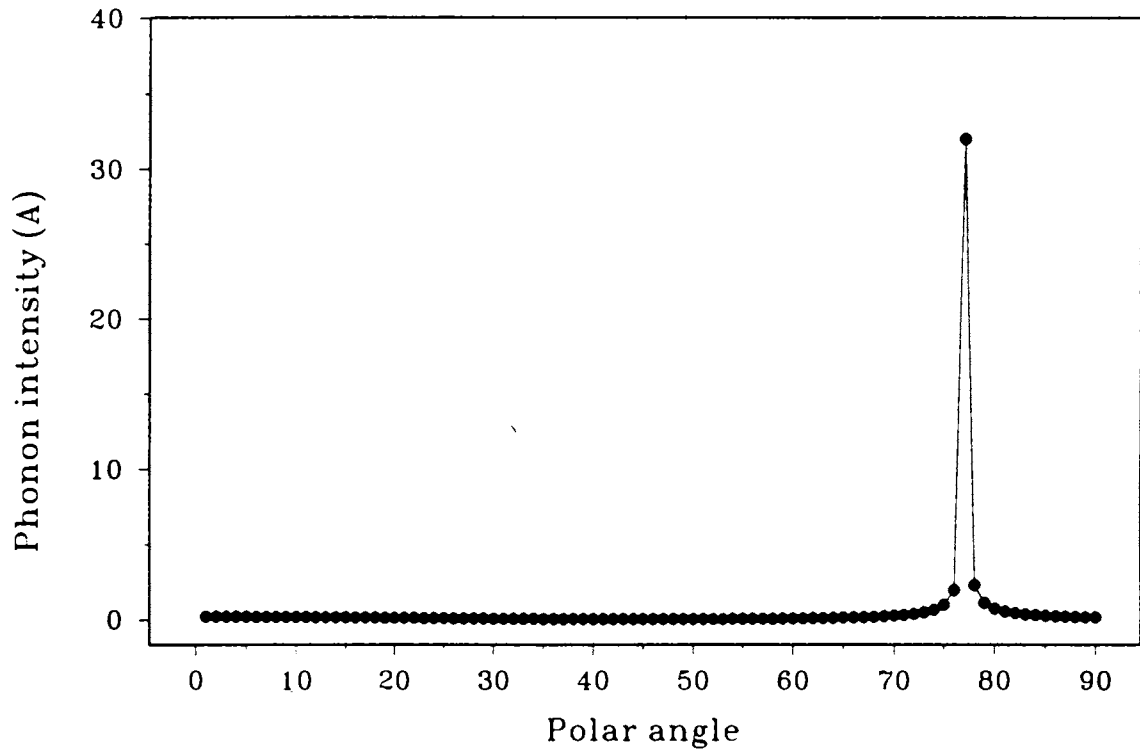


Fig. 7.7(a)

Variation of phonon intensity with the polar angle (θ_k) for the propagation of quasishear mode in the ab plane of YBCO at room temperature.

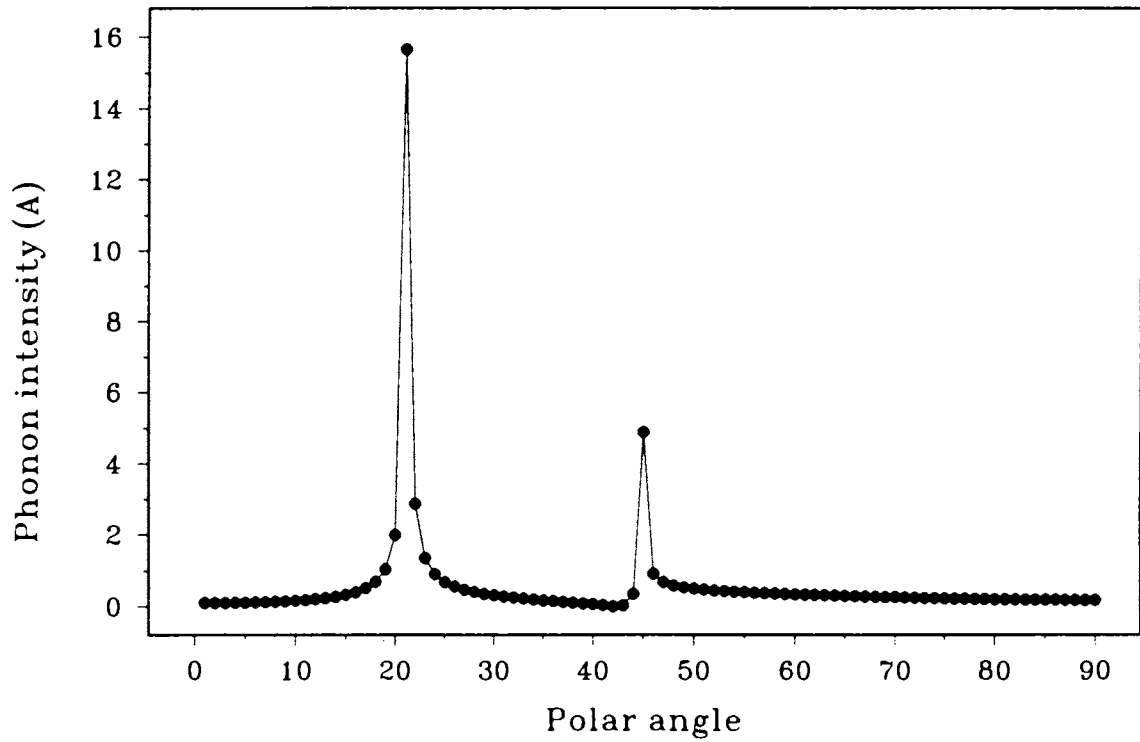


Fig. 7.7(b)

Variation of phonon intensity with the polar angle (θ_k) for the propagation of quasishear mode in the ac plane of YBCO at room temperature.

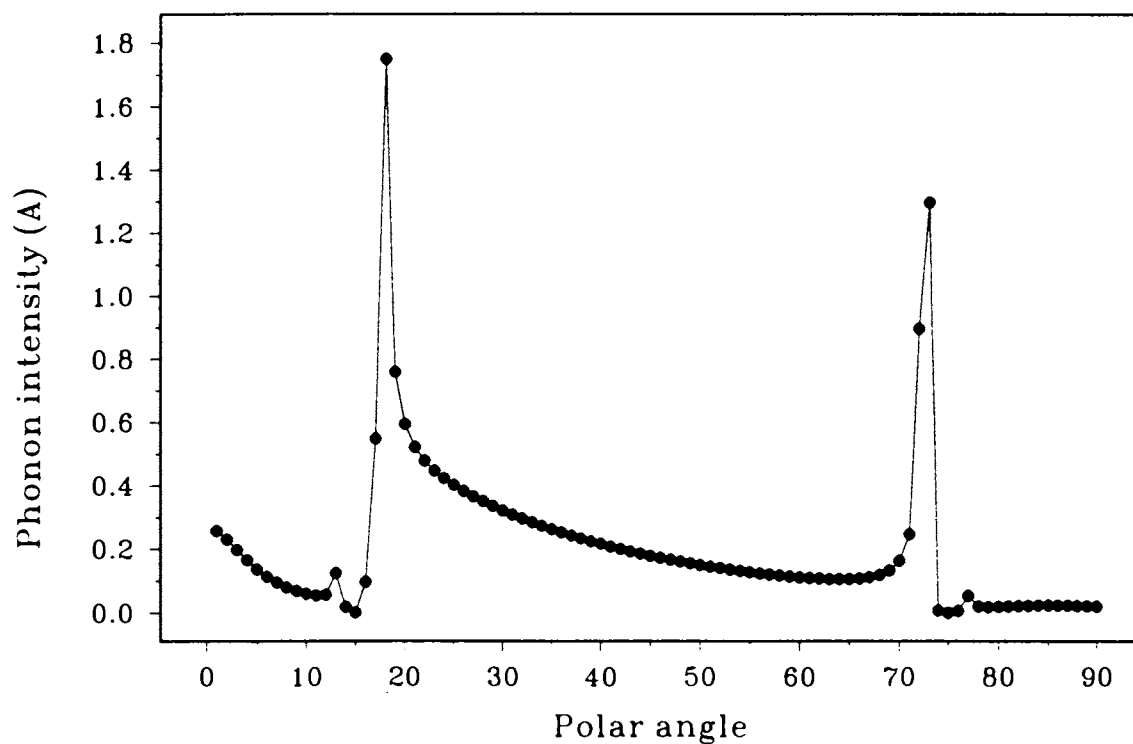


Fig. 7.8

Variation of phonon intensity with the polar angle (θ_k) for the propagation of quasishear mode in the ab plane of LSCO at room temperature.

7.6 Conclusions

The phonon enhancement factors have been computed for the superconductors BSCCO, YBCO and LSCO along different directions and the results are presented. It is found that the phonon intensities plotted in three dimensions take physically unrealistic values in certain directions for all the superconductors. These are interpreted as not due to the real focussing of phonons, but due to the singularities occurring in the mathematical formulation. The phonon intensities have been calculated along directions where phonon amplification is expected for the quasishear mode from the nature of the ray surfaces and found that the values are not abnormally high verifying the predictions of the theory.

It is not suggested that phonon focussing has any direct bearing on superconducting transition. Figs. 7.6(a) and 7.6(d) give the peaks in phonon intensities at the same angle above and below T_c . All one sees is a change in the magnitude of the phonon intensity above and below T_c . This change merely reflects the changes that elastic constants undergo over this temperature range. Interestingly, the positions of the caustics shift with temperature, which again is a consequence of the change in the value of the elastic constants.

Ballistic phonon imaging experiments need to be done on ultrapure single crystals of high T_c materials to verify these results.

7.7 References

- [1] R. J. von Gutfeld and A. H. Nethercot Jr., *Phys. Rev. Lett.* **17**, 868 (1966).
- [2] B. Taylor, H. J. Maris and C. Elbaum, *Phys. Rev. Lett.* **23**, 416 (1969).
- [3] B. Taylor, H. J. Maris and C. Elbaum, *Phys. Rev.* **B3**, 1462 (1971).
- [4] H. J. Maris, *J. Acoust. Soc. Am.* **50**, 812 (1971).
- [5] A. K. McCurdy, H.J.Maris and C.Elbaum, *Phys. Rev.* **B2**, 4077 (1970).
- [6] A. K. McCurdy, *Phys. Rev.* **B9**, 466 (1974).
- [7] F. Rosch and O. Weiss, *Z. Phys.* **B25**, 101 ; **B25**, 115 (1976).
- [8] J. Philip and K. S. Viswanathan, *Phys. Rev.* **B17**, 4969 (1978).
- [9] C. G. Winterheimer and A. K. McCurdy, *Phys. Rev.* **B18**, 6576 (1978).
- [10] G. A. Northorp and J. P. Wolfe, *Phys. Rev. Lett.* **43**, 1424 (1979).
- [11] G. A. Northorp and J. P. Wolfe, *Phys. Rev.* **B22**, 6196 (1980).
- [12] J. C. Hensel and R. C. Dynes, *Phys. Rev. Lett.* **43**, 1033 (1979).
- [13] S. Tamura, *Phys. Rev.* **B25**, 1415 (1982).
- [14] R. G. Ulbrich, V. Narayanamurti and M. A. Chin, *Phys. Rev. Lett.* **45**, 1432 (1980).
- [15] W. Eisenmenger, in *Proc. of the third International Conference on Phonon Scattering in Condensed Matter*, (ed. H. J. Maris), Plenum, New York (1980), p.303.
- [16] R. E. Horstman, *Phys. Lett.* **79A**, 229 (1980).
- [17] M. A. Weilert, M. E. Msall, A. C. Anderson and J. P. Wolfe, *Phys. Rev. Lett.* **71**, 735 (1993).

- [18] P. Taborek and D. L. Goodstein, *Solid State Commun.* **33**, 1191 (1980).
- [19] P. Taborek and D. L. Goodstein, *Phys. Rev.* **B22**, 1550 (1980).
- [20] S. Tamura and Y. Nakane, *Phys. Rev.* **B24**, 4317 (1981).
- [21] M. Abramowitz and I. A. Stegun, in *Handbook of Mathematical Functions*, Dover, New York (1972).
- [22] G. A. Saunders, C. Fanggao, L. Jiaqiang, Q. Wang, M. Cankurtaran, E. F. Lambson, P. J. Ford and D. P. Almond, *Phys. Rev.* **B49**, 9862 (1994).
- [23] Ming Lei, J. L. Sarrao, W. M. Visscher, T. M. Bell, J. D. Thompson and A. Migliori, *Phys. Rev.* **B 47**, 6154 (1993).
- [24] A. Migliori, W. M. Visscher, S. Wong, S. E. Brown, I. Tanaka, H. Kojima and P. B. Allen *Phys. Rev. Lett.* **64**, 2458 (1990).
- [25] S. Tamura, *Phys. Rev.* **28**, 897 (1983).
- [26] A. G. Every, *Phys. Rev* **B24**, 3456 (1981).
- [27] L. D. Landau and E. M. Lifshitz, in *Fluid Mechanics*, Pergamon, New York (1959).
- [28] V. T. Buchwald, *Proc. R. Soc. London. Ser.* **A253**, 563 (1959).

Chapter 8

Summary and conclusions

This thesis is the result of our attempts to study certain thermal and elastic properties of selected high T_c superconductors, which have been motivated by the enormous possibilities offered by these exotic materials not only to the scientific community, but also to the whole mankind due to their applications. This concluding chapter is aimed to provide a summary of the work done as well as to discuss the scope for doing further work in this field.

The thermal and elastic properties of high T_c cuprates have attracted almost as much attention as their superconducting properties ever since the discovery of these materials, not only because of the technological importance of these types of investigations, but also due to the valuable information provided by these studies for the understanding of the mechanism behind superconductivity in these materials.

The thermal properties such as thermal diffusivity, specific heat and thermal conductivity of a set of $\text{YBa}_2\text{Cu}_3\text{O}_{7-\delta}$ - SnO_2 composites have been investigated in which the concentration of SnO_2 was varied from 0 - 8 wt.%. The temperature dependence of thermal diffusivity have been measured for four samples using the photoacoustic technique while the specific heats have been measured using differential scanning calorimetry. Combining these data with density, the thermal conductivity of the samples have been determined. The results obtained are found to support the phonon mediated BCS mechanism as responsible for superconductivity in these materials.

The effect of Ga doping on the elastic properties of $\text{GdBa}_2\text{Cu}_3\text{O}_{7-\delta}$ samples have been studied using the ultrasonic technique. Ultrasonic velocity and attenuation have been measured as a function of temperature on four samples with varying Ga

doping levels, employing the pulse echo overlap technique and pulse comparison technique respectively. Apart from the anomalies observed near T_c , anomalous features are found to occur at temperatures well above T_c , which have been explained as due to the structural changes taking place in the material with Ga doping.

The anisotropy in elastic wave propagation in single crystals of high T_c superconductors have been investigated by computing and plotting the phase and group velocities in three major superconducting systems - BSCCO, YBCO and LSCO - taking elastic constant data from literature. The velocities plotted as a function of the propagation direction for the pure shear, quasishear and quasilongitudinal modes in different symmetry planes give a clear picture of the elastic anisotropy in these materials. The quasishear group velocity surfaces of all superconductors investigated exhibit cuspidal edges, at least in one symmetry plane, in specific directions. A comparison of the phase velocity surfaces for these materials and an analysis of the results have been attempted, based on the structure of these materials. Further, it is seen from the surfaces plotted at temperatures above and below T_c that the nature of anisotropy do not change significantly upon the material undergoing superconducting transition.

Another remarkable consequence of elastic anisotropy, *viz.*, the phonon focussing has also been studied in single crystals of high T_c materials for the first time. The phonon enhancement factors have been computed for the superconductors BSCCO, YBCO and LSCO for the three modes of wave propagation and plotted in spherical polar coordinates. The sharp peaks in phonon enhancement observed at various points of the plots are interpreted as not due to real focussing of phonons, but as due to caustics which are nonphysical and arise from the singularities occurring in the mathematical formulation.

The overall goal of this work has been to study some of the thermal and elastic properties of selected high T_c superconductors which are very important from the theoretical as well as technological viewpoints as has been mentioned already. Eventhough the results do not support any of the well established theoretical models completely, these investigations serve as a test for the validity of the various models. For example, the investigations of the thermal properties of $\text{YBa}_2\text{Cu}_3\text{O}_{7-\delta}$ indicate that the phonon

mediated electron pairing is adequate to explain the phenomenon. From the technological side also, these sort of studies are very valuable. For example, it is likely that these materials would be the basis for many commercial applications in the foreseeable future. Hence, there is a need for a comprehensive experimental description of the material properties of these high T_c materials, including the extent to which their elastic, thermal and transport properties can be anisotropic.

Every possible experimental technique has been applied to study the high T_c materials and innumerable theoretical models have been proposed to explain the superconducting mechanism, ever since the discovery of these materials and many workers feel that this field is a saturated area of research. However, in spite of the intense research centred around these materials, many factors still remain mysterious even after nearly ten years of their discovery and there is much scope for doing further work in the area of high temperature superconductivity.

Though the maximum value of T_c of the 'high temperature superconductors' have been raised to 135 K from the 30 K range within a few years, the realisation of room temperature superconductivity still remains an unreachable goal for the scientific community. Further, these materials could not be used for various applications because of a number of reasons. The brittle behaviour of these materials, for example, is one of the major disadvantages that restrict their engineering applications. The high reactivity of some of these compounds prevents them from using in various applications. The fabrication of various devices and components using these materials is one of the challenges faced by the researchers in technical field. These are a few examples and many more problems remain unsolved for experimentalists in the field.

Since the discovery of these materials, many theories have been proposed to explain the properties exhibited by these systems, as mentioned earlier. While some of the properties can be explained by phonon mediated electron pairing, the extremely small isotope effect and many other unusual electronic properties have led to the belief that the electron - phonon interaction by itself cannot be the dominant mechanism responsible for superconductivity. The occurrence of antiferromagnetic correlations in the copper oxides seem to support the notion that superconductivity in these compounds

may be due to magnetic interactions, while the presence of oxygen breathing mode distortion suggests an alternate pairing mechanism due to charge fluctuations. Again, these are only a few examples of the proposed models and many more theories have been proposed. Unfortunately none of them do clearly explain the mechanism behind superconductivity in these materials, again leaving the field open to further investigations for a theorist.

Appendix A

Computer program to calculate Phonon enhancement factor

C Program - Phonon Focussing

```
REAL JX,JY,JZ,KX,KY, KZ, KXY, KXZ, KYZ
DIMENSION T(50),P(50),T1(45),P1(46)
DIMENSION C(6,6),C1(6,6),X1(50,50),X2(50,50),X3(50,50)
DOUBLE PRECISION LX,LY,LZ ,LXY,LXZ,LYX,LYZ,LZX,LZY,LXYZ
DOUBLE PRECISION A2(50,50),A1(50,50),A0(50,50)
DOUBLE PRECISION G,Q,B,R,S,DX,DY,DZ
DOUBLE PRECISION DDXT,DDYT,DDZT,DDXP,DDYP,DDZP,DA2T,DA2P
DOUBLE PRECISION DA1T,DA1P,DA0T,DA0P,DTST,DTSP,DPST
DOUBLE PRECISION DPSP,RJ,TS
REAL A ,AS(50,50),AQS(50,50),AQL(50,50)
```

C Elastic onstant matrix

```
PRINT *, 'Give the Matrix elements'
READ (*,5) ((C1(I,J), J = 1,6), I = 1,6)
5 FORMAT(6F6.2)
DO 7 I = 1,6
DO 7 J = 1,6
C(I,J) = C1(I,J)*1E9
7 CONTINUE
```

C Coefficients J,K,L

```
JX = C(1,1)+C(5,5)+C(6,6)
JY = C(2,2)+C(4,4)+C(6,6)
JZ = C(3,3)+C(4,4)+C(5,5)
KX = C(1,1)*C(6,6) + C(1,1)*C(5,5) + C(5,5)*C(6,6)
KY = C(2,2)*C(6,6) + C(4,4)*C(6,6) + C(2,2)*C(4,4)
KZ = C(3,3)*C(4,4) + C(3,3)*C(5,5) + C(4,4)*C(5,5)
KXY = C(1,1)*C(2,2) + C(1,1)*C(4,4) + C(5,5)*C(6,6)+
1 C(4,4)*C(6,6) + C(2,2)*C(5,5) - (C(1,2))**2 - 2*C(1,2)*C(6,6)
KXZ = C(1,1)*C(4,4) + C(1,1)*C(3,3) + C(5,5)*C(6,6) +
1 C(3,3)*C(6,6) + C(4,4)*C(5,5) - (C(1,3))**2 - 2*C(1,3)*C(5,5)
KYZ = C(2,2)*C(3,3) + C(2,2)*C(5,5) + C(3,3)*C(6,6)+
```

```

1      C(4,4)*C(6,6) +C(4,4)*C(5,5) - (C(2,3))**2 - 2*C(2,3)*C(4,4)
LX = C(1,1)*C(5,5)*C(6,6)
LY = C(2,2)*C(4,4)*C(6,6)
LZ = C(3,3)*C(4,4)*C(5,5)
LXY = C(1,1)*C(2,2)*C(5,5) + C(1,1)*C(4,4)*C(6,6) -
1      C(5,5)*(C(1,2))**2 - 2*C(1,2)*C(5,5)*C(6,6)
LXZ = C(1,1)*C(4,4)*C(5,5) + C(1,1)*C(3,3)*C(6,6) -
1      C(6,6)*(C(1,3))**2 - 2*C(1,3)*C(5,5)*C(6,6)
LYX = C(2,2)*C(5,5)*C(6,6) + C(1,1)*C(2,2)*C(4,4) -
1      C(4,4)*(C(1,2))**2 - 2*C(1,2)*C(4,4)*C(6,6)
LYZ = C(2,2)*C(4,4)*C(5,5) + C(2,2)*C(3,3)*C(6,6) -
1      C(6,6)*(C(2,3))**2 - 2*C(2,3)*C(4,4)*C(6,6)
LZX = C(1,1)*C(3,3)*C(4,4) + C(3,3)*C(5,5)*C(6,6) -
1      C(4,4)*(C(1,3))**2 - 2*C(1,3)*C(4,4)*C(5,5)
LZY = C(3,3)*C(4,4)*C(6,6) + C(2,2)*C(3,3)*C(5,5) -
1      C(5,5)*(C(2,3))**2 - 2*C(2,3)*C(4,4)*C(5,5)
LXYZ = 4*C(4,4)*C(5,5)*C(6,6) + C(1,1)*C(2,2)*C(3,3) -
1      C(1,1)*(C(2,3))**2 - C(3,3)*(C(1,2))**2 - C(2,2)*(C(1,3))**2
1      + 2*C(1,2)*C(1,3)*C(4,4) + 2*C(1,2)*C(1,3)*C(2,3) +
1      2*C(1,3)*C(2,3)*C(6,6) + 2*C(1,2)*C(4,4)*C(5,5) +
1      2*C(1,2)*C(2,3)*C(5,5) + 2*C(1,3)*C(4,4)*C(6,6) +
1      2*C(2,3)*C(5,5)*C(6,6) - 2*C(1,1)*C(4,4)*C(2,3) -
1      2*C(1,2)*C(3,3)*C(6,6) - 2*C(1,3)*C(2,2)*C(5,5)

```

C Theta, Phi-Definition

```

      PRINT *, 'Give the values of Theta'
      DO 10 I = 1,45
      READ *, T1
      T(I) = (T1(I) * 3.14)/180
10    CONTINUE
      PRINT *, 'Give the values of Phi'
      DO 20 J = 1,46
      READ * , P1
      P(J) = (P1(J) * 3.14)/180
20    CONTINUE

```

C A2, A1, A0 - Calculation

```

DO 30 J = 1,46
DO 30 I = 1,45
A2(I,J) = -(JX * ( SIN (T(I)) )**2 * (COS (P(J)) )**2 +
1          JY * ( SIN (T(I)) )**2 * (SIN (P(J)) )**2 +
1          JZ * ( COS (T(I)) )**2)
A1(I,J) = KX * ( SIN (T(I)) )**4 * (COS (P(J)) )**4 +
1          KY * ( SIN (T(I)) )**4 * (SIN (P(J)) )**4 +
1          KZ * ( COS (T(I)) )**4 +
1          KXY * ( SIN (T(I)) )**4 * (COS (P(J)) )**2 * ( SIN (P(J)) )**2
1 + KXZ * ( SIN (T(I)) )**2 * (COS (T(I)) )**2 * ( COS (P(J)) )**2
1 + KYZ * ( SIN (T(I)) )**2 * (COS (T(I)) )**2 * ( SIN (P(J)) )**2
A0(I,J) = -(LX * ( SIN (T(I)) )**6 * (COS (P(J)) )**6 +
1          LY * ( SIN (T(I)) )**6 * (SIN (P(J)) )**6 +
1          LZ * ( COS (T(I)) )**6 +
1          LXY * (SIN (T(I)) )**6 * (SIN (P(J)) )**2 * ( COS (P(J)) )**4
1 + LXZ * (SIN (T(I)) )**4 * (COS (T(I)) )**2 * ( COS (P(J)) )**4
1 + LYX * (SIN (T(I)) )**6 * (SIN (P(J)) )**4 * ( COS (P(J)) )**2
1 + LYZ * (SIN (T(I)) )**4 * (COS (T(I)) )**2 * ( SIN (P(J)) )**4
1 + LZX * (SIN (T(I)) )**2 * (COS (T(I)) )**4 * ( COS (P(J)) )**2
1 + LZY * (SIN (T(I)) )**2 * (COS (T(I)) )**4 * ( SIN (P(J)) )**2
1 +LXYZ * (SIN (T(I)) )**4 * (COS (T(I)) )**2 *
1 (SIN (P(J)) )**2*(COS (P(J)))**2)

```

C Solution of the cubic equation

```

Q = A1(I,J) /3 - A2(I,J) ** 2 /9
G = ( A1(I,J)*A2(I,J) - 3*A0(I,J))/6 - A2(I,J)**3/27
B = ABS ( Q**3 + G**2 )
R = SQRT ( G**2 + B )
S = ATAN (SQRT(B) / G )
X1(I,J) = -A2(I,J)/3 - 2* R** (1.0/3.0) * COS (S/3)
X2(I,J) = -A2(I,J) / 3 - R ** (1.0/3.0) * COS (S/3) -
1          SQRT(3.0) * R** (1.0/3.0) * SIN(S/3)
X3(I,J) = -A2(I,J) / 3 - R ** (1.0/3.0) * COS (S/3) +
1          SQRT(3.0) * R** (1.0/3.0) * SIN(S/3)

```

```

30 CONTINUE
35 WRITE (*,*) 'Select the mode (0,1,2 or 3)'
   WRITE (*,*) ' 1. For Pure shear'
   WRITE (*,*) ' 2. For Quasi shear'
   WRITE (*,*) ' 3. For Quasi longitudinal'
   WRITE (*,*) ' 0. To print the result'
   WRITE (*,*) ' Any other key to end the program '
   READ *,MODE
   DO 40 J = 1,46
   DO 40 I = 1,45
   IF ( MODE .EQ. 1) THEN
   X = X1(I,J)
   ELSEIF ( MODE .EQ. 2) THEN
   X = X2(I,J)
   ELSEIF ( MODE .EQ. 3) THEN
   X = X3(I,J)
   ELSEIF ( MODE .EQ. 0) THEN
   GO TO 50
   ELSE
   GO TO 100
   ENDIF

```

C Derivatives of A2, A1 and A0

```

DA2T = -2* SIN( T(I))* COS( T(I))* (JX* (COS( P(J)) )**2
1      + JY* (SIN( P(J)) )**2 - JZ)
DA2P = 2*(SIN(T(I))**2 *SIN(P(J))*COS(P(J))* (JX - JY)
DA1T = 4*(SIN(T(I))**3 *COS( T(I))* (KX* (COS( P(J)) )**4
1      + KY* (SIN( P(J)) )**4) -
1      4*KZ* SIN( T(I)) * (COS ( T(I)) )**3 +
1 4* KXY * ( SIN (T(I)) )**3 * COS ( T(I))* (COS (P(J)) )**2 *
1 ( SIN (P(J)) )**2 + 2*KXZ * (COS ( P(J)) )**2 * SIN ( T(I))*
1 COS ( T(I)) * ( (COS ( T(I)) )** 2 - (SIN ( T(I)) )** 2)
1 + 2 * KYZ * (SIN ( P(J)) )**2 * SIN ( T(I)) *
1 COS ( T(I)) * ( (COS ( T(I)) )** 2 - (SIN ( T(I)) )** 2)
DA1P = 4*(SIN ( T(I)) ) **4 *SIN ( P(J)) *COS ( P(J)) *
1      ( KY * (SIN ( P(J)) )**2 - KX * (COS (P(J)) )**2 ) +

```

```

1      2 * KXY * ( SIN ( T(I) ) ) ** 4 * SIN ( P(J) ) *
1      COS( P(J) ) * ( ( COS ( P(J) ) ) ** 2 - ( SIN ( P(J) ) ) ** 2 )
1      + 2 * ( SIN ( T(I) ) ) ** 2 * ( COS ( T(I) ) ) ** 2 *
1      SIN ( P(J) ) * COS ( P(J) ) * ( KYZ - KXZ )
      DAOT = -6 * SIN ( T(I) ) * COS ( T(I) ) * (
1      LX * ( SIN ( T(I) ) ) ** 4 * ( COS ( P(J) ) ) ** 6 +
1      LY * ( SIN ( T(I) ) ) ** 4 * ( SIN ( P(J) ) ) ** 6 -
1      LZ * ( COS ( T(I) ) ) ** 4 + LXY *
1      ( SIN ( T(I) ) ) ** 4 * ( SIN ( P(J) ) ) ** 2 * ( COS ( P(J) ) ) ** 4 )
1      - 2 * LXZ * ( SIN ( T(I) ) ) ** 3 * COS ( T(I) ) * ( COS ( P(J) ) ) ** 4
1      * ( 2 * ( COS ( T(I) ) ) ** 2 - ( SIN ( T(I) ) ) ** 2 ) - 6 * LYX *
1      ( SIN ( T(I) ) ) ** 5 * COS ( T(I) ) * ( SIN ( P(J) ) ) ** 4 *
1      ( COS ( P(J) ) ) ** 2 - 2 * ( SIN ( P(J) ) ) ** 2 * ( SIN ( T(I) ) ) ** 3
1      * COS ( T(I) ) * ( 2 * ( COS ( T(I) ) ) ** 2 - ( SIN ( T(I) ) ) ** 2 )
1      * ( LYZ * ( SIN ( P(J) ) ) ** 2 + LXZY * ( COS ( P(J) ) ) ** 2 ) -
1      2 * SIN ( T(I) ) * ( COS ( T(I) ) ) ** 3 *
1      ( ( COS ( T(I) ) ) ** 2 - 2 * ( SIN ( T(I) ) ) ** 2 ) *
1      ( LZX * ( COS ( P(J) ) ) ** 2 + LZY * ( SIN ( P(J) ) ) ** 2 )
      DAOP = -2 * ( SIN ( T(I) ) ) ** 6 * SIN ( P(J) ) * COS ( P(J) )
1      * ( 3 * LY * ( SIN ( P(J) ) ) ** 4 - ( 3 * LX - LXY ) *
1      ( COS ( P(J) ) ) ** 4 - 2 * LXY * ( SIN ( P(J) ) ) ** 2 *
1      ( COS ( P(J) ) ) ** 2 - LYX * ( SIN ( P(J) ) ) ** 4 + 2 *
1      LYX * ( SIN ( P(J) ) ) ** 2 * ( COS ( P(J) ) ) ** 2 ) - 2 *
1      ( SIN ( T(I) ) ) ** 4 * ( COS ( T(I) ) ) ** 2 * SIN ( P(J) ) *
1      COS ( P(J) ) * ( ( LXZY - 2 * LXZ ) * ( COS ( P(J) ) ) ** 2 +
1      ( 2 * LYZ - LXYZ ) * ( SIN ( P(J) ) ) ** 2 ) + 2 * ( SIN ( T(I) ) ) ** 2
1      * ( COS ( T(I) ) ) ** 4 * SIN ( P(J) ) * COS ( P(J) ) * ( LZY - LZX )
      DXT = -1 * ( X ** 2 * DA2T + X * DA1T + DAOT )
1      / ( 3 * X ** 2 + 2 * A2(I,J) * X + A1(I,J) )
      DXP = -1 * ( X ** 2 * DA2P + X * DA1P + DAOP )
1      / ( 3 * X ** 2 + 2 * A2(I,J) * X + A1(I,J) )

```

C DX, DY, DZ - Calculation

```

      DX = -2 * ( X ** 2 ) * JX * SIN ( T(I) ) * COS ( P(J) ) + 2 * X *
1      ( 2 * KX * ( SIN ( T(I) ) ) ** 3 * ( COS ( P ( J ) ) ) ** 3 +
1      KXY * ( SIN ( T(I) ) ) ** 3 * COS ( P ( J ) ) * ( SIN ( P(J) ) ) ** 2

```

```

1      + KXZ * SIN ( T(I)) * (COS ( T (I)) )** 2 * COS ( P(J)) ) -
1      2* ( 3* LX * (SIN ( T(I)) ) ** 5 * (COS ( P (J)) ) ** 5 + 2*
1      LXY*(SIN (T(I)) )**5 * (COS(P(J)) )**3 * (SIN( P(J)) ) **2 + 2*
1      LXZ * (SIN (T(I)) )**3 * (COS (T(I)) )**2 * (COS( P(J)) ) **3 +
1      LYX * (SIN (T(I)) )**5 * (SIN (P(J)) )**4 * COS( P(J)) +
1      LZX * SIN (T(I)) * (COS (T(I)) )**4 * COS( P(J)) + LXYZ *
1      (SIN (T(I)) )**3 * (COS (T(I)) )**2 * (SIN( P(J)) ) **2
1      * COS (P(J)) )

```

```

      DY = -2 *(X **2) *JY * SIN (T(I)) * SIN (P(J)) + 2* X *
1      ( 2 * KY * (SIN ( T(I)) ) ** 3 * (SIN ( P (J)) ) ** 3 +
1      KXY * (SIN ( T(I)) ) ** 3 * SIN ( P (J)) * (COS ( P(J)) ) **2
1      + KYZ * SIN ( T(I)) * SIN ( P (J)) * (COS (T(I)) )** 2)-
1      2* ( 3* LY * (SIN ( T(I)) ) ** 5 * (SIN (P (J)) ) ** 5 +
1      LXY*(SIN (T(I)) )**5 * (COS(P(J)) )**4 * SIN( P(J)) + 2*
1      LYX*(SIN (T(I)) )**5 * (SIN(P(J)) )**3 * (COS(P(J)) )**2 + 2*
1      LYZ * (SIN (T(I)) )**3 * (COS (T(I)) )**2 * (SIN( P(J)) ) **3 +
1      LZY * SIN (T(I)) * (COS (T(I)) )**4 * SIN( P(J)) + LXYZ *
1      (SIN (T(I)) )**3 * (COS (T(I)) )**2 * SIN( P(J))
1      * (COS (P(J)) ) ** 2 )

```

```

      DZ = -2 *(X **2) *JZ * COS (T(I)) + 2* X *
1      ( 2 * KZ * (COS ( T(I)) ) ** 3 +
1      KXZ * (SIN ( T(I)) ) ** 2 * COS ( T (I)) * (COS ( P(J)) ) **2
1      + KYZ* (SIN (T(I)) ) **2 * COS (T(I)) * (SIN (P(J)) ) **2) -
1      2* ( 3* LZ * (COS ( T(I)) ) ** 5 + LXZ *
1      (SIN (T(I)) )**4 * COS(T(I)) * (COS ( P(J)) ) **4 + LYZ *
1      (SIN (T(I)) )**4 * COS(T(I)) * (SIN( P(J)) ) **4 + 2 * LZX *
1      (SIN(T(I)) )**2 * (COS (T(I)) )**3 * (COS(P(J)) ) **2 + 2* LZY*
1      (SIN (T(I)) )**2 * (COS (T(I)) )**3 * (SIN( P(J)) ) **2 + LXYZ *
1      (SIN (T(I)) )**4 * COS (T(I)) * (SIN( P(J)) ) **2
1      * (COS (P(J)) ) ** 2 )

```

C Derivatives of DX, DY and DZ

```

      DDXT = -2 * X * JX * COS ( P(J)) * ( X * COS ( T(I)) +
1      2* SIN ( T(I)) * DXT) + 2* X* COS ( T(I)) * COS ( P(J))
1      * ( 6 * KX * (SIN ( T(I)) ) ** 2 * (COS ( P(J)) ) ** 2 +
1      3 * KXY * (SIN ( T(I)) ) ** 2 * (SIN ( P(J)) ) ** 2 +

```

```

1  KXZ * ( (COS ( T(I)) ) ** 2 - 2 * (SIN ( T(I)) ) ** 2 )
1  + 2 * DXT * SIN ( T(I)) * COS ( P (J)) * ( 2 * KX *
1  (SIN ( T(I)) ) ** 2 * (COS ( P(J)) ) ** 2 + KXY *
1  (SIN (T(I)) ) **2 *(SIN (P(J)) ) **2 + KXZ* (COS (T(I)) ) **2 )
1  -2 * SIN ( T(I)) * COS ( T(I)) * COS ( P(J)) * ( 15 * LX *
1  (SIN ( T(I)) ) ** 3 * (COS ( P(J)) ) ** 4 + 10 * LXY *
1  (SIN ( T(I)) ) **3 * (COS ( P(J)) ) **2 * (SIN ( P(J)) )**2 +
1  6* LXZ* SIN ( T(I)) * (COS ( T(I)) ) **2 * (COS ( P(J)) ) **2
1  - 4 * LXZ * (SIN ( T(I)) ) ** 3 * (COS ( P(J)) ) ** 2 +
1  5 * LYX * (SIN ( T(I)) ) ** 3 * (SIN ( P(J)) ) ** 4 ) +
1  2* COS ( T(I)) * COS ( P(J)) * ( LZX * (COS ( T(I)) ) **4
1  - 4* LZX * (SIN ( T(I)) ) ** 2 * (COS ( T(I)) ) ** 2 + 3*
1  LXYZ* (SIN (T(I)) ) **2 *(COS (T(I)) )**2 *(SIN (P(J)) )**2
1  - 2 * LXYZ * (SIN ( T(I)) ) ** 4 * (SIN ( P(J)) ) ** 2 )
DDXP = 2 * X * JX * SIN ( T(I)) * ( X * SIN ( P(J)) -
1  2* COS (P(J)) * DXP ) - 2* X* SIN ( T(I)) * SIN ( P(J))
1  * ( 6 * KX * (SIN ( T(I)) ) ** 2 * (COS ( P(J)) ) ** 2 +
1  KXY * (SIN ( T(I)) ) ** 2 * (SIN ( P(J)) ) ** 2 - 2 * KXY *
1  (SIN ( T(I)) ) **2 * COS ( P(J)) + KXZ* (COS ( T(I)) ) **2 )
1  + 2 * DXP * SIN ( T(I)) * COS ( P (J)) * ( 2 * KX *
1  (SIN ( T(I)) ) ** 2 * (COS ( P(J)) ) ** 2 + KXY *
1  (SIN (T(I)) ) **2 *(SIN (P(J)) ) **2 + KXZ* (COS (T(I)) ) **2 )
1  -2 * SIN ( T(I)) * SIN ( P(J)) * COS ( P(J)) * ( -15 * LX *
1  (SIN ( T(I)) ) ** 4 * (COS ( P(J)) ) ** 3 + 4 * LXY *
1  (SIN ( T(I)) ) **4 * (COS ( P(J)) ) **3 - 6 * LXY *
1  (SIN ( T(I)) ) ** 4 * COS ( P(J)) * (SIN ( P(J)) ) **2 - 6 *
1  LXZ* (SIN ( T(I)) )** 2 * (COS ( T(I)) ) ** 2 * COS ( P(J)) +
1  4* LYX *(SIN ( T(I)) ) **4 *(SIN ( P(J)) ) **2 * COS ( P(J)) -
1  LYX* (SIN ( T(I)) ) **4* (SIN ( P(J)) )**4 ) - 2* SIN (T(I)) *
1  SIN ( P(J)) * ( -LZX * (COS ( T(I)) ) ** 4 + 2*
1  LXYZ* (SIN (T(I)) ) **2 *(COS (T(I)) )**2 * (COS (P(J)) )**2 -
1  LXYZ* (SIN (T(I)) ) **2 *(COS (T(I)) ) **2 *(SIN (P(J)) ) **2)
DDYT = -2 * X * JY * SIN ( P(J)) * ( X * COS ( T(I)) +
1  2* SIN ( T(I)) * DXT ) + 2* X* COS ( T(I)) * SIN ( P(J))
1  * ( 6 * KY * (SIN ( T(I)) ) ** 2 * (SIN ( P(J)) ) ** 2 +

```

```

1  3 * KXY * ( SIN ( T(I) ) ) ** 2 * SIN ( P(J) ) * COS ( P(J) ) +
1  KYZ * ( ( COS ( T(I) ) ) ** 2 - 2 * ( SIN ( T(I) ) ) ** 2 ) )
1  + 2 * DXT * SIN ( T(I) ) * SIN ( P ( J) ) * ( 2 * KY *
1  ( SIN ( T(I) ) ) ** 2 * ( SIN ( P(J) ) ) ** 2 + KXY *
1  ( SIN ( T(I) ) ) **2 *(COS ( P(J) ) ) **2 + KYZ* ( COS ( T(I) ) ) **2 )
1  -2 * COS ( T(I) ) * SIN ( P(J) ) * ( 15 * LY *
1  ( SIN ( T(I) ) ) ** 4 * ( SIN ( P(J) ) ) ** 4 + 5 * LXY *
1  ( SIN ( T(I) ) ) **4 * ( COS ( P(J) ) ) **4 + 10 * LYX *
1  ( SIN ( T(I) ) ) **4 * ( SIN ( P(J) ) ) **2 *(COS ( P(J) ) ) **2 +
1  6 * LYZ* ( SIN ( T(I) ) )**2 * ( COS ( T(I) ) )**2 * ( SIN ( P(J) ) )**2
1  -4*LYZ* ( SIN(T(I) ) )**4 *(SIN(P(J) ) )**2 + LZY*(COS(T(I) ) )**4)
1  -2* COS ( T(I) ) * SIN ( T(I) ) * SIN ( P(J) ) * ( -4 * LZY *
1  SIN ( T(I) ) * ( COS ( T(I) ) ) ** 2 + 3 * LXYZ *
1  SIN ( T(I) ) * ( COS ( T(I) ) ) **2 * ( COS ( P(J) ) ) **2
1  - 2 * LXYZ * ( SIN ( T(I) ) ) ** 3 * ( COS ( P(J) ) ) ** 2 )
DDYP = -2 * X * JY * SIN ( T(I) ) * ( X * COS ( P(J) ) +
1  2* SIN ( P(J) ) * DXP ) + 2* X* SIN ( T(I) ) * COS ( P(J) )
1  * ( 6 * KY * ( SIN ( T(I) ) ) ** 2 * ( SIN ( P(J) ) ) ** 2 +
1  KXY * ( SIN ( T(I) ) ) ** 2 * ( COS ( P(J) ) ) ** 2 - 2 * KXY *
1  ( SIN ( T(I) ) ) **2 * ( SIN(P(J) ) )**2 + KYZ* ( COS(T(I) ) )**2 )
1  - 2 * DXP * SIN ( T(I) ) * SIN ( P ( J) ) * ( 2 * KY *
1  ( SIN ( T(I) ) ) ** 2 * ( SIN ( P(J) ) ) ** 2 + KXY *
1  ( SIN ( T(I) ) ) **2 *(COS ( P(J) ) ) **2 + KYZ* ( COS ( T(I) ) ) **2 )
1  -2 * SIN ( T(I) ) * COS ( P(J) ) * ( 15 * LY *
1  ( SIN ( T(I) ) ) ** 4 * ( SIN ( P(J) ) ) ** 4 + LXY *
1  ( SIN ( T(I) ) ) **4 * ( COS ( P(J) ) ) **4 - 4 * LXY *
1  ( SIN ( T(I) ) ) ** 4 * ( SIN ( P(J) ) ) **2 *
1  ( COS ( P(J) ) ) ** 2 + 6 * LYX* ( SIN ( T(I) ) ) ** 4 *
1  ( SIN ( P(J) ) ) **2 * ( COS ( P(J) ) ) **2 - 4 * LYX *
1  ( SIN ( T(I) ) )**4* ( SIN ( P(J) ) )**4 + 6* LYZ* ( SIN(T(I) ) )**2*
1  ( COS ( T(I) ) )**2 * ( SIN ( P(J) ) )** 2 + LZY * ( COS(T(I) ) )**4
1  + LXYZ* ( SIN ( T(I) ) )**2 *(COS(T(I) ) )**2 * ( COS(P(J) ) )**2 -
1  2* LXYZ* ( SIN ( T(I) ) )**2 *(COS(T(I) ) )**2 *(SIN(P(J) ) )**2 )
DDZT = 2 * X * JZ * ( X * SIN ( T(I) ) -
1  2* COS ( T(I) ) * DXT ) + 2* X* SIN ( T(I) ) *

```



```

1      (-6 * KZ * (COS ( T(I)) ) ** 2 + KXZ * (COS ( P(J)) ) **2 *
1      ( 2 * (COS ( T(I)) ) ** 2 - (SIN ( T(I)) ) ** 2 ) + KYZ *
1      (SIN (P(J)) )**2 *(2* (COS (T(I)) )**2 - (SIN( T(I)) )**2) )
1      + 2 * DXT * COS ( T(I)) * ( 2 * KZ * (COS ( T(I)) ) **2
1      + KXZ * (SIN ( T(I)) ) ** 2 * (COS ( P(J)) ) ** 2 +
1      KYZ * (SIN (T(I)) ) ** 2 * (SIN (P(J)) ) **2 )
1      -2 * SIN ( T(I)) * ( -15 * LZ * (COS ( T(I))) **4 + LXZ *
1      (SIN (T(I)) ) **2 *(COS (P(J)) ) **4 * (4* (COS (T(I)) ) **2
1      - (SIN ( T(I)) )**2 ) + LYZ* (SIN(T(I)) )**2 * (SIN(P(J)) )**4
1      * (4* (COS ( T(I)) ) **2 - (SIN ( T(I)) ) **2 ) + 2 * LZX *
1      (COS ( T(I)) ) **2 * (COS ( P(J)) ) **2 *( 2*(COS(T(I)) )**2
1      - 3* (SIN ( T(I)) ) ** 2 ) + 2* LZY * (SIN ( P(J)) ) **2 *
1      (COS(T(I)) )**2 *(2 *(COS (T(I)) )**2 - 3* (SIN (T(I)) )**2 )
1      + LXYZ *(SIN (T(I)) ) **2 *(COS (P(J)) )**2 *(SIN (P(J)) )**2
1      * ( 4* (COS ( T(I)) ) ** 2 - (SIN ( T(I)) ) ** 2 ))
DDZP = -4 * X * JZ * COS ( T(I))
1      * DXP + 4* X* (SIN(T(I)) )** 2 *COS (T(I)) * SIN (P(J))
1      * COS ( P(J)) * ( KYZ - KXZ ) + 2 * DXP * COS ( T(I)) *
1      (2* KZ * (COS ( T(I)) ) ** 2 + KXZ * (SIN ( T(I)) ) ** 2 *
1      (COS ( P(J)) ) **2 + KYZ * (SIN ( T(I)) ) **2 ) *
1      (SIN ( P(J)) **2 ) - 2 * (SIN ( T(I)) )** 2 * COS ( T(I)) *
1      SIN ( P(J)) * COS ( P(J)) * ( -4 * LXZ *
1      (SIN (T(I)) )**2 *(COS (P(J)) )**2 + 4* LYZ* (SIN (T(I)) )**2
1      * (SIN ( P(J)) )**2 - 4* LZX * (COS ( T(I)) )** 2 + 4* LZY *
1      (COS ( T(I)) ) ** 2 - 2 * LXYZ * (SIN ( T(I)) ) ** 2 *
1      ((COS ( P(J)) ) **2 - ( SIN ( P(J)) ) **2 ) )

```

C Derivatives of (Theta)s and (Phi)s

```

DTST = ( DZ * ( DY * DDYT + DX * DDXT)
1      - ( DX **2 + DY **2 ) * DDZT ) /
1      ( SQRT( DX **2 + DY **2 ) * ( DX **2 +
1      DY **2 + DZ **2 ) )
DTSP = ( DZ * ( DY * DDYP + DX * DDXP)
1      - ( DX **2 + DY **2 ) * DDZP ) /
1      ( SQRT( DX **2 + DY **2 ) * ( DX **2 +

```

```

1      DY **2 + DZ **2 ) )
      DPST = ( DX * DDYT - DY * DDXT ) / ( DX **2 + DY **2)
      DPSP = ( DX* DDYP - DY * DDXP ) / ( DX **2 + DY **2)
      RJ = DTST * DPSP - DTSP * DPST
      TS =ATAN(( sqrt(DX **2 + DY **2)) / DZ)
      A = (SIN ( TS ) * RJ ) / SIN ( T(I) )
      WRITE (*,*) ABS(1/A)
      IF ( MODE .EQ. 1) THEN
      AS1 = ABS(1/A)
      AS(I,J) = AS1
      ELSEIF ( MODE .EQ. 2) THEN
      AQS1 = ABS(1/A)
      AQS(I,J) = AQS1
      ELSEIF ( MODE .EQ. 3) THEN
      AQL1 = ABS(1/A)
      AQL(I,J) = AQL1
      ELSEIF (MODE .EQ. 0) THEN
      GO TO 50
      ELSE
      GO TO 100
      ENDIF
40     CONTINUE
      GO TO 35
      WRITE (6,55)
55     FORMAT(1X, 'Phi', 3X, 'Theta', 8X, 'Shear', 15X, 'Q.Shear', 17X, 'Q.Long. ')
      DO 60 J = 1,46
      DO 60 I = 1,45
      THETA = (T(I)*180)/3.14
      PHI = (P(J)*180)/3.14
      WRITE (6,80) PHI, THETA, AS(I, J), AQS(I, J), AQL(I, J)
60     CONTINUE
80     FORMAT ( 1X,F3.0,4X,F3.0,6X,F11.5,8X,F11.5,11X,F11.5)
100    STOP
      END

```